

Syracuse University

SURFACE

Dissertations - ALL

SURFACE

May 2014

DYADIC GREEN'S FUNCTIONS FOR LAYERED GENERAL ANISOTROPIC MEDIA AND THEIR APPLICATION TO RADIATION OF DIPOLE ANTENNAS

Ying Huang
Syracuse University

Follow this and additional works at: <https://surface.syr.edu/etd>



Part of the [Engineering Commons](#)

Recommended Citation

Huang, Ying, "DYADIC GREEN'S FUNCTIONS FOR LAYERED GENERAL ANISOTROPIC MEDIA AND THEIR APPLICATION TO RADIATION OF DIPOLE ANTENNAS" (2014). *Dissertations - ALL*. 99.

<https://surface.syr.edu/etd/99>

This Dissertation is brought to you for free and open access by the SURFACE at SURFACE. It has been accepted for inclusion in Dissertations - ALL by an authorized administrator of SURFACE. For more information, please contact surface@syr.edu.

ABSTRACT

In this dissertation, the dyadic Green's functions (DGFs) for unbounded and layered anisotropic media, with no restriction imposed on the medium property, are derived. Utilizing the obtained DGFs, the radiation problems of a Hertzian dipole and a microstrip antenna in the presence of an anisotropic substrate are solved.

After a brief introduction, the eigenvector dyadic Green's functions (E-DGFs) for an unbounded general anisotropic medium through the eigen-decomposition method are derived. The E-DGFs of a layered anisotropic geometry are then constructed based on the derivation of the unbounded E-DGFs using two different approaches. One is through the symmetrical property of the DGFs and the other is through the direct construction method. Rigorous proof and detailed derivation of the formulation for the E-DGFs are presented. The usage and limitation of each approach as well as the relationships between the corresponding E-DGFs are discussed.

Applying the method of stationary phase to the associated E-DGFs, we formulate the radiation fields of an arbitrarily oriented Hertzian dipole located either above or inside the layered anisotropic medium. The important new findings include the analysis of the radiation field in terms of the reflection coefficients as a function of incidence angle, and the use of the biasing magnetic field to improve the broadside directivity for a z-directed source when a gyroelectric medium is involved.

In addition to solving the radiation of a Hertzian dipole in the presence of a layered anisotropic medium, the layered E-DGFs derived here are also utilized to solve the more practical problem of a microstrip dipole printed on an anisotropic substrate. A method of

moment solution is formulated with the E-DGF in the spectral domain. To demonstrate the feasibility of this method applicable to a general anisotropic medium, the current distribution, input impedances, and radiation patterns are numerically calculated for a microstrip dipole printed on various anisotropic substrates. Furthermore, a detailed parametric study of the effect of frequency, and direction and magnitude of the biasing magnetic field is provided for a dipole printed on a gyroelectric substrate. The parametric analysis in this dissertation may lead to a method whereby the additional freedom introduced by the gyroelectric medium can be utilized effectively to adjust the resonant length and radiation pattern of a printed dipole antenna.

**DYADIC GREEN'S FUNCTIONS FOR LAYERED GENERAL ANISOTROPIC
MEDIA AND THEIR APPLICATION TO RADIATION OF DIPOLE ANTENNAS**

by

Ying Huang

B.S., Nanjing University, 2005

M.S., Nanjing University, 2008

Dissertation

Submitted in partial fulfillment of the requirements for the degree
of Doctor of Philosophy in Electrical and Computer Engineering in the Graduate School
of Syracuse University

May 2014

Copyright © Ying Huang 2014
All Rights Reserved

ACKNOWLEDGEMENTS

Foremost, I would like to express my sincere gratitude to my advisor Professor Jay Kyoong Lee for the continuous support of my PhD study and research, for his patience, motivation, enthusiasm, and immense knowledge. His guidance helped me in all the time of research and writing of this dissertation. I could not have imagined having a better advisor and mentor for my PhD study.

I would also like to thank Professor Ercument Arvas, Professor Qi Wang Song, Professor Amit Agrawal, Professor Prasanta Ghosh, and Professor Thong Quoc Dang for serving as members of the oral examination committee.

I would like to acknowledge the support from the Graduate Editing Center of Syracuse University and its staff for proofreading the chapters. I also thank my colleague Dr. Jennifer Graham for spending her time and effort in proofreading Chapter 3.

Last, but by no means least, I thank my family for their support and encouragement throughout.

CONTENTS

Abstract.....	i
Acknowledgements.....	v
List of Figures.....	xi
List of Tables.....	xxii
1 INTRODUCTION.....	1
1.1 Anisotropic Materials and Applications	1
1.2 Previous Work.....	4
1.2.1 Dyadic Green’s Functions and Radiation of a Hertzian Dipole	5
1.2.2 A Printed Dipole in the Presence of an Anisotropic Substrate	8
1.3 Chapter Outlines.....	10
2 DYADIC GREEN’S FUNCTIONS FOR AN UNBOUNDED GENERAL ANISOTROPIC MEDIUM.....	13
2.1 Eigen-decomposition of DGF for a General Anisotropic Medium.....	13
2.2 DGFs of an Unbounded Uniaxial Medium	23
2.3 DGFs of an Unbounded Gyrotropic Medium	34

2.3.1	DGFs of a Gyroelectric Medium	34
2.3.2	DGFs of a Gyromagnetic Medium	44
3	DYADIC GREEN'S FUNCTIONS FOR HALF-SPACE AND TWO-LAYER GEOMETRIES	48
3.1	Dyadic Green's Functions with Source inside the Isotropic Region	48
3.1.1	DGF for the Region of $z < z'$	49
3.2	Modified Symmetrical Property for $\overline{\overline{G}}^{(0,0)}(\underline{r}, \underline{r}')$ of the Region $z > z'$ and $0 < z < z'$	57
3.2.1	Proof of Modified Symmetrical Property of $\overline{\overline{G}}^{(0,0)}(\underline{r}, \underline{r}')$	58
3.2.2	DGF for the Region of $z > z'$	66
3.3	Modified Symmetrical Property for $\overline{\overline{G}}^{(1,0)}(\underline{r}, \underline{r}')$ and $\overline{\overline{G}}^{(0,1)}(\underline{r}, \underline{r}')$	69
3.3.1	Proof of the Modified Symmetrical Property	69
3.3.2	Usage and Limitation of the Modified Symmetrical Property.....	79
3.4	DGFs of a Two-Layer Geometry with a Source inside the Anisotropic Region	85
3.4.1	Direct Construction Method to Obtain the DGFs for All the Regions	86
3.4.2	Discussion of DGF $\overline{\overline{G}}^{(0,1)}(\underline{r}, \underline{r}')$ Obtained Using Two Approaches.....	93
4	RADIATION OF A HERTZIAN DIPOLE IN THE PRESENCE OF A LAYERED ANISOTROPIC MEDIUM.....	97

4.1 Radiation of a Hertzian Dipole for a Half-Space Problem	97
4.1.1 The Source Embedded in the Isotropic Region	99
4.1.2 The Source Embedded in the Anisotropic Region.....	102
4.2 Radiation of a Hertzian Dipole for a Two-Layer Problem	104
4.2.1 The Source Embedded in the Isotropic Region	105
4.2.2 The Source Embedded in the Anisotropic Region.....	112
4.3 Analytic and Numerical Validation.....	114
4.3.1 Case I: Self-check of $\overline{G}^{(0,0)}$ and $\overline{G}^{(0,1)}$	114
4.3.2 Case II: Unbounded Isotropic Medium and Layered Biaxial Medium.....	118
4.3.3 The Anisotropic Region Filled with Gyroelectric and Gyromagnetic Media	122
4.4 Radiation of a Hertzian Dipole in the Presence of Gyroelectric Medium	125
4.4.1 Radiation of a Vertical Dipole on Top of a Half-space Gyroelectric Medium.....	125
4.4.1.1 Parametric Effect of Frequency and Biasing Magnetic Field.....	128
4.4.1.2 Relation of Directive Radiation with Total Internal Reflection.....	130
4.4.2 The Two-Layer Problem with a Source above the Anisotropic Region.....	136
4.4.3 The Two-Layer Problem with a Source Embedded in the Anisotropic Region	139
4.4.3.1 Radiation of a Horizontal Dipole inside a Grounded Isotropic Plasma Slab.....	140
4.4.3.2 Radiation of a Horizontal Dipole inside the Grounded Gyroelectric Slab	144
4.4.3.3 Radiation of a Vertical Dipole inside the Grounded Gyroelectric Slab.....	149

5 RADIATION OF A MICROSTRIP DIPOLE PRINTED ON AN ANISOTROPIC SUBSTRATE.....	157
5.1 Formulation of Method of Moment (MOM)	158
5.1.1 Basis Function.....	159
5.1.2 Excitation	161
5.1.3 Symmetry Analysis for Impedance Matrix.....	165
5.1.3.1 Z_{im} and Z_{mi}	166
5.1.3.2 Symmetry of Integrand for Z_{im}	167
5.1.3.3 Integration Path.....	171
5.1.3.4 Sampling Rate and Integration Range	172
5.2 Properties of the Dyadic Green's Function	172
5.2.1 Integration Path to Avoid the Singularity of $\underline{\underline{G}}^{(0,0)}$	175
5.2.2 Surface Wave Pole.....	179
5.2.2.1 A Grounded Isotropic Slab	179
5.2.2.2 A Grounded Uniaxial Slab.....	184
5.2.2.3 A Grounded Biaxial Slab.....	191
5.2.2.4 A Grounded Gyroelectric Slab.....	195
5.3 Current Distribution of a Microstrip Dipole.....	202
5.3.1 Current Distribution of a Microstrip Dipole on a Grounded Biaxial Slab.....	202
5.3.2 Current Distribution for a Microstrip Dipole on a Grounded Gyroelectric Slab	204

5.4 Antenna Parameters	207
5.4.1 Formulations of Input Impedance and Radiated field.....	207
5.4.1.1 Input Impedance.....	207
5.4.1.2 Radiation Behavior	209
5.4.1.3 Antenna Gain	211
5.4.2 Numerical Validation with Printed Dipoles on Various Media.....	211
5.4.2.1 A Printed Dipole on an Isotropic Slab	211
5.4.2.2 A Printed Dipole on a Grounded Biaxial Slab.....	214
5.4.2.3 A Printed Dipole on a Grounded Ferrite Slab.....	218
5.4.3 A Printed Dipole on a Grounded Gyroelectric Slab	221
5.4.3.1 Input Impedance and Resonant Length.....	221
5.4.3.2 Radiation Behavior	227
 6 CONCLUSIONS	 232
 BIBLIOGRAPHY	 236
 VITA.....	 246

LIST OF FIGURES

Fig. 2-1:	Two different polarizations of plane waves in uniaxial medium: (a) Type I (ordinary wave) and (b) Type II (extraordinary wave).....	31
Fig. 2-2:	Arbitrary biasing magnetic field in the xyz coordinate	35
Fig. 3-1:	Geometry of (a) half-space and (b) two-layer problem.	49
Fig. 3-2:	Amplitude vectors of waves in the two-layered geometry.	54
Fig. 3-3:	Two different geometries for the proof of modified symmetrical property.....	58
Fig. 3-4:	Two different geometries constructed here for the proof of symmetrical property when the source are in different regions.	71
Fig. 3-5:	Geometry of the two-layer problem with source inside the anisotropic region....	88
Fig. 4-1:	Geometry for the half-space problem with a Hertzian dipole placed at a certain distance away from the boundary separating the isotropic and anisotropic regions. (a) Dipole in Region 0 (isotropic region) and (b) dipole in Region 1 (anisotropic region).	98
Fig. 4-2:	Two-layer geometry: (a) The dipole is located in Region 0 (isotropic medium) and (b) The dipole is located in Region 1 (anisotropic medium).	104
Fig. 4-3:	Geometry of Case I with (a) DGF $\overline{\overline{G}}^{(0,0)}$ (b) DGF $\overline{\overline{G}}^{(0,1)}$	114
Fig. 4-4:	Radiated fields calculated using (a) DGF of $\overline{\overline{G}}^{(0,0)}$ and (b) DGF of $\overline{\overline{G}}^{(0,1)}$	117
Fig. 4-5:	Geometry of unbounded isotropic medium.	119
Fig. 4-6:	Radiation pattern of the x, y and z-directed Hertzian dipole in unbounded medium in the XZ plane.....	119

Fig. 4-7:	$ E_\theta $ vs. θ in the $\varphi = 45^\circ$ plane for a z-directed Hertzian dipole in Region 0 (free space) with $h_d = 0.1\lambda_0$ and $\bar{\varepsilon} = (\varepsilon_x, 2, 3)$, $\varepsilon_x = 2, 5, 9$	120
Fig. 4-8:	$ E_\theta $ vs. h_d in the $\varphi = 45^\circ$ plane for a z-directed Hertzian dipole in Region 1 with $(\varepsilon_x, \varepsilon_y, \varepsilon_z) = (2, 8, 4)$, $(\alpha, \beta, \gamma) = (30^\circ, 20^\circ, 0^\circ)$	121
Fig. 4-9:	$ E_\theta $ vs. θ in the $\varphi = 90^\circ$ plane for various values of h_d for a z-directed Hertzian dipole positioned in region 0 of a two-layer problem. Region 1 is biaxial with $(\varepsilon_x, \varepsilon_y, \varepsilon_z) = (2, 8, 4)$, $(\alpha, \beta, \gamma) = (0, 0, 0)$ and slab thickness is $0.4\lambda_0$	121
Fig. 4-10:	$ E_\varphi $ vs. θ in the $\varphi = 0^\circ$ plane for various values of α (rotation angle) and an x-directed Hertzian dipole positioned in Region 1 of a two-layer problem. Region 1 is biaxial with $(\varepsilon_x, \varepsilon_y, \varepsilon_z) = (2, 8, 4)$, $(\alpha, \beta, \gamma) = (0^\circ, 70^\circ, 0^\circ)$ and with $h_d = 0.3\lambda_0$, $d = 0.4\lambda_0$	121
Fig. 4-11:	Geometry of the grounded gyroelectric slab in [46].	122
Fig. 4-12:	$ E_\theta $ vs. θ in the plane of $\varphi = 0^\circ$ for a z-directed Hertzian dipole located in Region 0, with $h_d = 0.55\lambda_0$ away from the interface of free space and gyroelectric slab. (a) Result from Wu [46] and (b) Radiated field using the formula in this chapter.....	123
Fig. 4-13:	Geometry of a two-layer problem filled with gyromagnetic medium.	123
Fig. 4-14:	$ E_\theta $ and $ E_\varphi $ vs. θ in the plane of $\varphi = 0^\circ, 90^\circ$ with the source in Region 0 and the field in Region 2.....	124

- Fig. 4-15:** $|E_\theta|$ vs. θ in the plane of $\varphi = 0^\circ$ for a z-directed Hertzian dipole located in Region 0 with $h_d = 0$ away from the interface of free space and gyroelectric medium. The biasing magnetic field is along the (a) z and (b) y directions. 128
- Fig. 4-16:** Field pattern for a z-directed Hertzian dipole located in Region 0 with $h_d = 0$ away from the interface of free space and gyroelectric medium. The biasing magnetic field is along $\theta_B = 20^\circ, 40^\circ, 60^\circ, 80^\circ, \varphi_B = 0^\circ$ and the frequency of the incidence wave is $1.01\omega_1$. (a) $|E_\theta|$ and (b) $|E_\varphi|$ vs. θ in the plane of $\varphi = 0^\circ$; (c) $|E_\theta|$ and (d) $|E_\varphi|$ vs. θ in the plane of $\varphi = 90^\circ$ 129
- Fig. 4-17:** Normalized wave vector surface of an isotropic medium and these for Type I and Type II waves of a gyroelectric medium vs. θ in the plane of $\varphi = 0^\circ$ 131
- Fig. 4-18:** Magnitude and phase of reflection coefficients R_{vv}^{01}, R_{hv}^{01} vs. different incidence angles for an incidence plane of $\varphi = 0^\circ$ 133
- Fig. 4-19:** (a) E_θ and (b) $|E_\varphi|$ vs. θ in the plane of $\varphi = 0^\circ$ for a z-directed Hertzian dipole located in region 0 with $h_d = 0$ away from the interface of free space and gyroelectric medium with the direction of biasing magnetic field along $\theta_B = 0^\circ$.
- $\omega_p = 2\pi 10^9, \omega_b = 1.9\omega_p, \omega = 1.01\omega_1, \omega_1 = \frac{\omega_b}{2} + \sqrt{\frac{\omega_b^2}{4} + \omega_p^2}$ 134
- Fig. 4-20:** (a) $|E_\theta|$ and (b) $|E_\varphi|$ vs. θ in the plane of $\varphi = 0^\circ$ for a z-directed Hertzian dipole located in Region 0 with $h_d = 0$ away from the interface of free space and a

gyroelectric medium with $\omega = 1.01\omega_1$ and the biasing magnetic field along

$\theta_B = 90^\circ, \varphi_B = 90^\circ$ 135

Fig. 4-21: (a) $|E_\theta|$ and (b) $|E_\varphi|$ vs. θ in the plane of $\varphi = 90^\circ$ for a z-directed Hertzian dipole in Region 0 with $h_d = 0$ away from the interface of half-space gyroelectric medium with the biasing magnetic field along $\theta_B = 90^\circ, \varphi_B = 90^\circ$ 136

Fig. 4-22: Normalized radiated field E_θ for an x-directed dipole located at the interface of the grounded gyroelectric slab and air in the xz-plane for different frequency regions of the gyroelectric medium. 137

Fig. 4-23: Normalized radiated field patterns E_θ for an x-directed dipole located at an air-gyroelectric medium interface of a grounded slab as a function of different biasing magnetic field directions 138

Fig. 4-24: Geometry of a horizontal dipole located inside a grounded gyroelectric slab with a distance h_d away from the air-slab interface. 140

Fig. 4-25: Power density (dB) of (a) θ component and (b) φ component as a function of the slab thickness. 142

Fig. 4-26: Power density (dB) of φ component as a function of the slab thickness. $h_d = 0.25\lambda_\epsilon$ and $f = 1.1f_p$ 143

Fig. 4-27: Power density of (a) θ component and (b) φ component radiated in broadside direction by a unit current moment y-directed Hertzian dipole placed at the center

of a grounded gyroelectric slab as a function of the slab thickness with

$\omega_b = 0.001\omega_p$, $f = 1.1f_p$ 145

Fig. 4-28: (a) Power density and (b) phase difference of $P_\theta(0)$ and $P_\varphi(0)$ for a unit current moment y-directed Hertzian dipole placed in the middle of a grounded gyroelectric slab as a function of the slab thickness with $\omega_b = \omega_p$, $f = 1.1f_p$.. 146

Fig. 4-29: Normalized radiated field for a y-directed dipole located in the middle of the isotropic plasma slab in the XZ-plane as a function of observation angle which is measured from the z-axis..... 148

Fig. 4-30: Radiation patterns for a y-oriented dipole located in the middle of the anisotropic gyroelectric slab vs. different slab thicknesses. 149

Fig. 4-31: Geometry of a vertical dipole located inside the grounded anisotropic slab with a distance of h_d away from the air-slab interface..... 149

Fig. 4-32: Normalized field pattern of $|E_\theta|$ vs. θ in the plane of $\varphi = 0^\circ$ with vertical dipole located in the middle of the grounded gyroelectric slab of thickness of $0.05\lambda_0$. 150

Fig. 4-33: (a) The angle of the maximum radiation of the vertical dipole inside the grounded gyroelectric slab vs. different frequencies. (b) The difference of the radiated power along the maximum radiation direction of the Hertzian dipole inside the slab and in free space vs. different frequencies. 151

Fig. 4-34: Normalized field pattern of $|E_\theta|$ and $|E_\varphi|$ (xz plane) for a vertical dipole located in the middle of a grounded gyroelectric slab of thickness $0.05\lambda_0$ (free space

wavelength) with different direction of the biasing magnetic field.

$\omega_p = 2\pi 10^9, \omega_b = 0.8\omega_p, \omega = 1.1\omega_p$ 153

Fig. 4-35: Normalized field pattern of $|E_\theta|$ (XZ plane) for the vertical dipole located in the middle of the grounded gyroelectric slab with the biasing magnetic field perpendicular to the observation plane as a function of different thickness.

$\omega_p = 2\pi 10^9, \omega_b = 0.8\omega_p, \omega = 1.1\omega_p$ 154

Fig. 4-36: Normalized field pattern of $|E_\theta|$ (XZ plane) for a vertical dipole located in the middle of a grounded isotropic slab of $\epsilon = 1$ vs. different slab thickness. 154

Fig. 5-1: Geometry of the microstrip dipole problem..... 158

Fig. 5-2: Locations of the subdomain basis functions $J_x(x)$ and $J_x(y)$ along x-direction.
..... 160

Fig. 5-3: Integration in the $k_x - k_y$ plane. Area over (a) the entire $k_x - k_y$ plane, (b) the upper half-space, and (c) the first quadrant of $k_x - k_y$ plane..... 168

Fig. 5-4: Symmetry relation for the dyadic Green's function elements of $\tilde{G}_{xx}^{(0,0)}(k_x, k_y)$ for a reciprocal medium..... 169

Fig. 5-5: Integration regions in the $k_x - k_y$ plane: (a) Region 1 (b) Region 2 and (c) Region 3..... 175

Fig. 5-6: Region 1 integration paths in the k_x and k_y planes: (a) k_x plane, (b) k_y plane. ... 176

Fig. 5-7: Region 2A integration paths in the k_x and k_y planes: (a) k_x plane, (b) k_y plane. 177

Fig. 5-8:	Region 2B integration paths in the k_x and k_y planes: (a) k_x plane, (b) k_y plane..	177
Fig. 5-9:	Region 2C integration paths in the k_x and k_y planes: (a) k_x plane, (b) k_y plane.	178
Fig. 5-10:	Effect of the magnitude of δ on the calculation of $\text{Re}\left(\tilde{G}_{xx}^{(0,0)}\right)$ in the region 2A. (a) $\delta = 0.05k_0$, (b) $\delta = 0.6k_0$. $(\varepsilon_x, \varepsilon_y, \varepsilon_z) = (5, 3, 4)$, $(\alpha, \beta, \gamma) = (0^\circ, 0^\circ, 0^\circ)$, and $h = 0.1\lambda_0$.	179
Fig. 5-11:	Geometry of the grounded isotropic slab.....	180
Fig. 5-12:	Graphical determination of $k_{1z}d$ for (a) TM and (b) TE modes.....	183
Fig. 5-13:	Surface wave propagation constants for a grounded dielectric slab with $\varepsilon_{1r} = 2.55$, for $d / \lambda_0 = 0$ to 1.2	183
Fig. 5-14:	Geometry of the grounded uniaxial slab with the optic axis along z-direction. .	184
Fig. 5-15:	Graphical method to obtain the surface wave modes for a grounded uniaxial slab of $(\varepsilon_1 \ \varepsilon_1 \ \varepsilon_{1z}) = (2.55 \ 2.55 \ 4)$. The slab thickness is (a) $0.63\lambda_0$ and (b) $1.2\lambda_0$	189
Fig. 5-16:	The value of (a) $\text{Re}\left(\tilde{G}_{xx}^{00}\right)$ and (b) the determinant $\left \begin{matrix} \bar{I} & \bar{R} \\ \bar{R} & \bar{R} \end{matrix} \right $ vs. k_ρ for the propagation angle of $\varphi = \tan^{-1}(k_y/k_x) = 45^\circ$	192
Fig. 5-17:	The determinant $\left \begin{matrix} \bar{I} & \bar{R} \\ \bar{R} & \bar{R} \end{matrix} \right $ vs. k_ρ for the different propagation angles $\varphi = \tan^{-1}(k_y/k_x)$ of the surface wave from 0° to 90°	193

- Fig. 5-18:** Surface wave poles and branch point loci for a grounded biaxial slab of $(\varepsilon_x, \varepsilon_y, \varepsilon_z) = (3, 5, 4)$ with $d = 0.3\lambda_0$. (a) in all the four quadrants of the $k_x - k_y$ plane, and (b) in the first quadrant of the $k_x - k_y$ plane. 194
- Fig. 5-19:** The propagating constant $k_{x,sw}$ (a) (with $k_y = 0$) and (b) $k_{y,sw}$ (with $k_x = 0$) versus the thickness of a biaxial slab for various surface wave modes present in a conductor backed biaxial slab with $(\varepsilon_x, \varepsilon_y, \varepsilon_z) = (3, 5, 4)$ 195
- Fig. 5-20:** $k_{x,sw}$ obtained with $k_y = 0$ versus the thickness of the gyroelectric slab for various surface wave modes present in a conductor backed gyroelectric slab with the biasing magnetic field along (a) y-direction, and (b) z-direction. 201
- Fig. 5-21:** $k_{y,sw}$ obtained with $k_x = 0$ versus the thickness of the gyroelectric slab for various surface wave modes present in a conductor backed gyroelectric slab with biasing magnetic field along (a) y-direction, and (b) z-direction. 201
- Fig. 5-22:** Current distributions of a λ dipole on (a) a unrotated biaxial medium of $(\varepsilon_x, \varepsilon_y, \varepsilon_z) = (5, 3, 4)$ and (b) a rotated biaxial medium with $(\alpha, \beta, \gamma) = (10^\circ, 20^\circ, 30^\circ)$ 203
- Fig. 5-23:** Current distribution of $\text{Re}(J(x))$ for a $\lambda/2$ dipole on gyroelectric medium with $\omega = 2\pi \times 1.059 \times 10^9 \text{ rad/s}$, $\omega_p = 2\pi 10^9 \text{ rad/s}$, $\omega_b = 0.5\omega_p$ and the biasing magnetic field along x-direction ($\theta_B = 90^\circ, \varphi_B = 0^\circ$). $h = 0.1\lambda_0, W = 0.01\lambda_0$. $N=6, N=12$ and $N=16$ 205

- Fig. 5-24:** Current distribution of $\text{Re}(J(x))$ and $\text{Imag}(J(x))$ for a $\lambda/2$ dipole on a gyroelectric medium with $\omega = 2\pi \times 1.059 \times 10^9 \text{ rad/s}$, $\omega_p = 2\pi 10^9 \text{ rad/s}$, $\omega_b = 0.5\omega_p$ and the biasing magnetic field along (a) the z-direction ($\theta_B = 0^\circ$) and (b) the y-direction ($\theta_B = 90^\circ, \varphi_B = 90^\circ$). $h = 0.1\lambda_0$, $W = 0.01\lambda_0$. $N=12$ 206
- Fig. 5-25:** (a) Real and (b) imaginary parts of the input impedance of a printed dipole on an isotropic substrate of $(\epsilon_x, \epsilon_y, \epsilon_z) = (3.25, 3.25, 3.251)$ with the dipole width of $0.01\lambda_0$. The height of the slab is $0.0796\lambda_0$ 212
- Fig. 5-26:** Input impedance for gap-fed dipole with width of $0.001\lambda_0$ printed on an isotropic substrate with $(\epsilon_x, \epsilon_y, \epsilon_z) = (2.45, 2.45, 2.451)$. The height is $0.2\lambda_0$ 213
- Fig. 5-27:** (a) Real and (b) imaginary parts of the input impedance vs. dipole length of a microstrip dipole on an unrotated biaxially anisotropic medium of $(\epsilon_x, \epsilon_y, \epsilon_z) = (5, 3, 4)$. The the dipole width is $0.01\lambda_0$ 215
- Fig. 5-28:** Effect of rotation angle β to the input impedance and the resonant length with $\alpha = 0^\circ$ and $\gamma = 0^\circ$. (a1) and (a2) are from Pettis [37]..... 216
- Fig. 5-29:** Effect of rotation angle α to the input impedance and the resonant length with $\beta = 0^\circ$ and $\gamma = 0^\circ$. (a1) and (a2) are from Pettis [37]..... 217
- Fig. 5-30:** Directive gain of a λ resonant dipole on a conductor backed slab filled with an unrotated biaxial medium of $(\epsilon_x, \epsilon_y, \epsilon_z) = (5, 3, 4)$. (a) from Pettis [37]..... 218

- Fig. 5-31:** Center-fed dipole resonant length versus frequency of printed dipole on a ferrite substrate of $\epsilon_r = 12.6$, $\mu_0 H_0 = 0.225$ [T], $\mu_0 M_s = 0.25$ [T] and an isotropic substrate of $\epsilon_r = 12.6$. The direction of the biasing magnetic field is along the direction of the dipole axis, i.e., x-direction ($\theta_B = 90^\circ, \phi_B = 0^\circ$). 219
- Fig. 5-32:** Wave vector surfaces of Type I and Type II waves for the gyroelectric medium with $\omega = 2\pi \times 1.059 \times 10^9$ rad/s, $\omega_p = 2\pi 10^9$ rad/s, $\omega_b = 2\omega_p$, and the biasing magnetic field is along z-direction ($\theta_B = 0^\circ$). 222
- Fig. 5-33:** (a) Real and (b) imaginary parts of the input impedance of the printed dipole on gyroelectric substrate with different directions of the biasing magnetic field. $\omega = 2\pi \times 1.059 \times 10^9$ rad/s, $\omega_p = 2\pi 10^9$ rad/s, $\omega_b = 2\omega_p$, the dipole width is $0.01\lambda_0$ and the substrate thickness is $0.1\lambda_0$ 223
- Fig. 5-34:** (a) Real and (b) imaginary parts of input impedance vs. various dipole length for a microstrip dipole printed on a gyroelectric substrate with gyrofrequency $\omega_b = 0.5\omega_p$, $\omega_b = 1.5\omega_p$, and $\omega_b = 2\omega_p$ 225
- Fig. 5-35:** Co-polarized and cross polarized radiation pattern of printed dipole for (a) E-plane and (b) H-plane with the direction of the biasing magnetic field along x-direction. 227
- Fig. 5-36:** Co-polarized and cross polarized radiation pattern of printed dipole for (a) E-plane and (b) H-plane with the direction of the biasing magnetic field along y-direction. 228

Fig. 5-37: Co-polarized and cross polarized radiation pattern of printed dipole for (a) E-plane and (b) H-plane with the direction of the biasing magnetic field along z-direction. 228

Fig. 5-38: (a) Co-polarized field pattern and (b) cross-polarized field pattern in E-plane with gyrofrequency $\omega_b = 0.5\omega_p, \omega_b = 1.5\omega_p, \omega_b = 2\omega_p$, when the biasing magnetic field is along x direction. 230

Fig. 5-39: (a) Co-polarized field pattern and (b) cross-polarized field pattern in H-plane with gyrofrequency $\omega_b = 0.5\omega_p, \omega_b = 1.5\omega_p, \omega_b = 2\omega_p$, when the biasing magnetic field is along x direction. 231

LIST OF TABLES

Table 4-1: Frequency bands with different propagating waves for a gyroelectric medium. .	126
Table 5-1: k_p versus the thickness of the slab for various surface wave modes in a grounded uniaxial slab with (a) $(\epsilon_1, \epsilon_1, \epsilon_{1z}) = (2.55, 2.55, 2.55)$, (b) $(2.55, 2.55, 0.5)$, (c) $(0.5, 0.5, 2.55)$, (d) $(2.55, 2.55, 4)$	190
Table 5-2: Propagating modes for different choices of permittivity	191
Table 5-3: Wave vector surfaces of all the frequency regions for Case I with the choice of $\omega_b = 0.5\omega_p$	197
Table 5-4: Wave vector surfaces of all the frequency regions for Case II with the choice of $\omega_b = 1.9\omega_p$	198
Table 5-5: (a) E-plane and (b) H-plane directivity for a center-fed dipole on a ferrite substrate.	220
Table 5-6: Resonant lengths for microstrip dipoles on a gyroelectric substrate.	226

1 INTRODUCTION

1.1 Anisotropic Materials and Applications

Dielectric and magnetic anisotropic effects often exist within many materials that are used as the substrate for integrated microwave circuits and printed-circuit antennas [1]. Two different types of anisotropic effects are usually observed: reciprocal and non-reciprocal anisotropies. Sapphire and boron nitride [2-4] are uniaxially anisotropic, while PTFE cloth and glass cloth [5-7] are biaxially anisotropic. Both uniaxial and biaxial properties belong to reciprocal anisotropies. Some of these reciprocal anisotropic effects are unintentional and occur naturally in the material, while others are introduced during the manufacturing process. Non-reciprocal anisotropic effects (magnetic or dielectric) are usually introduced by applying the external magnetic field to the ferrite, plasma or semiconductors.

The frequency-dependent permeability of ferrite reveals interesting applications in antennas, including the adjustment of radiation patterns and the reduction of radar cross-sections [8-10]. The freedom of controlling the non-reciprocal behavior of the ferrite, by applying the external magnetic field, uncovers wide applications for microwave devices such as isolators, circulators and phase shifters [11-14]. However, there are some limitations for the ferrite material.

First, relative bandwidth decreases in the operating frequency beyond 40 GHz due to material limitations. Secondly, it is difficult to achieve the full integration for the microwave integrated circuits (MIC) due to the incompatibility of the ferrite and semiconductor processing technology [15-16]. To overcome these drawbacks of ferrite, semiconductor devices based on the

gyroelectric property described by the tensor permittivity have been extensively researched in the last decade.

Under the influence of a constant magnetic field applied to the semiconductors, the gyroelectric effect arises from the cyclotron motion of nearly free electrons, in accordance with the Drude model. The behavior of magnetized semiconductors can then be characterized by a frequency-dependent permittivity tensor [17], as illustrated in the equation below.

$$\varepsilon(\omega) = \begin{bmatrix} \xi & 0 & -j\eta \\ 0 & \zeta & 0 \\ j\eta & 0 & \xi \end{bmatrix}$$

where

$$\xi = \varepsilon^{(0)} - \frac{\omega_p^2(\omega - j\nu)}{\omega[(\omega - j\nu)^2 - \omega_c^2]}, \quad \eta = \frac{-\omega_p^2\omega_c}{\omega[(\omega - j\nu)^2 - \omega_c^2]}, \quad \zeta = \varepsilon^{(0)} - \frac{\omega_p^2}{\omega(\omega - j\nu)}$$

ω_c is the gyrofrequency (or cyclotron frequency) calculated using $-eB_0/m$, where m represents the mass of each electron with charge e (a negative number) and B_0 is the constant magnetic field applied to the medium. $\varepsilon^{(0)}$ is the static dielectric constant of the material. Collision frequency $\nu = 1/\tau$ is included in the expression of the dielectric tensor, which models the losses in the semiconducting material. τ is the momentum relaxation time, which is equivalent to the mobility of the semiconductor. ω_p is the plasma frequency decided by carrier concentration as $(N_0e^2/m\varepsilon_0)^{1/2}$, where N_0 is the number of free electrons per unit volume.

Common semiconductor materials associated with magnetoplasma devices are InSb, Te, GaAs, Si, and Hg_{1-x}MnxTe. The properties of these materials are provided in Table 1 of [18].

For example, a high-quality, moderately-doped GaAs with a carrier concentration of $n = 2.1 \times 10^{15} \text{ cm}^{-3}$ is equivalent to a gyroelectric medium with plasma frequency $\omega_p = 10^{13} \text{ rad/s}$.

With a magnetic field of 3810 G, the cyclotron frequency is given as $\omega_c = 10^{12} \text{ rad/s}$.

Due to the non-reciprocal gyroelectric characteristics of the semiconductor, wide application of the semiconductors to circulators [19-24] and resonators [25] are developed. Propagation for semiconductor waveguides has also been of interest for researchers. A multilayer gyrotropic thin-film semiconductor waveguide comprising S-I GaAs/AlAs/n-GaAs/AlGaAs in a static magnetic field of 0.15 T has been analyzed over the frequency range of 0–200 GHz [26]. Surprisingly, while extensive research is performed on the microwave devices, very few works is found for the application of the gyroelectric medium (especially magnetized semiconductors) to the printed dipole antenna.

In addition to the anisotropic materials presented above, recent advances in material technology allow the production and control of material with the anisotropic property that does not naturally occur. The so-called metamaterial is gaining more and more attention due to its novel characteristics. A significant amount of research has been done for applications to antennas, waveguide miniaturization [27-28], and transmission lines [29]. Especially, the strong gyrotropy [30-33], introduced by the artificial materials, has started to attract attention as a potential candidate for applications in microwave and optoelectronic devices.

As presented above, an anisotropic effect either occurs naturally or is intentionally introduced for specific applications. In both cases, accurate analysis of different types of anisotropic effects is required for the full understanding of the electromagnetic wave's interaction with the anisotropic medium. For the planar layered geometry commonly used in

today's transmission and radiation applications, one of the well-established tools for the analysis of electromagnetic propagation, radiation and scattering problems is the method of Green's function [34]. In this dissertation, the approach of the Green's function is utilized to analyze the radiation properties of a Hertzian dipole and printed dipole on top of an anisotropic substrate. In particular, the research objectives primarily include the following:

- 1) To formulate Green's function solutions with the source placed inside an unbounded general anisotropic medium with no restriction imposed on the property of the medium.
- 2) To formulate Green's function solutions for the cases with the source placed either above or below the interface of a single-layer or two-layer geometry filled with a general anisotropic medium.
- 3) To develop numerically efficient asymptotic techniques for the analysis of the radiated fields of a Hertzian dipole placed above and below the interface of a single-layer or two-layer geometry filled with a general anisotropic medium. Especially, detailed numerical analysis is focused on the layered geometry filled with a gyroelectric medium.
- 4) To apply Green's function solving for the properties of microstrip dipole antennas printed at the interface of a conductor-backed, general anisotropic slab. Especially, detailed numerical analysis here is focused on the layered geometry filled with a gyroelectric medium.

1.2 Previous Work

In this section, we will briefly review the previous work on the Green's function involved with the anisotropic medium and the radiation of a Hertzian dipole in the presence of an

anisotropic medium. Also, previous work is summarized here on the application of the Green's function to solve the radiation of a printed dipole on top of an anisotropic substrate. Finally, through the complete literature survey on the previous work, it is demonstrated how the major contributions are made by achieving our research objectives.

1.2.1 Dyadic Green's Functions and Radiation of a Hertzian Dipole

Several different approaches have been proposed to obtain the Green's function of layered structure, including Fourier transform method, which is equivalent to the eigen-decomposition method [35-40]; the transition matrix method proposed by Krowne [41]; the equivalent boundary method by Mesa et al. [42]; and the cylindrical vector wave function method by Li et al. [43-44]. The transmission line method, proposed in [45], obtains the Green's function of an isotropic medium based upon the decomposition of fields into TE and TM modes. This method can actually be treated as a special case of the eigen-decomposition method.

The eigen-decomposition method was first introduced by Lee and Kong [35] to obtain the Green's function of layered geometry filled with a uniaxial medium with an arbitrarily oriented optic axis. The same method was then extended to obtain the dyadic Green's function of a layered biaxial anisotropic medium [36-37], an unbounded gyroelectric medium [38-39], and a gyromagnetic medium [40]. The basic feature of the eigen-decomposition method is based on the calculation of the corresponding eigenvectors of the electric field from the adjoint matrix of the electric wave matrix. This matrix is derived from the second-order differential equation of the electric field in the spectral-domain by applying a 3D Fourier transform. The eigenvectors can be calculated either analytically [35-40] or numerically. Different from the eigen-decomposition method, the transition matrix method applies 2D Fourier transform and utilizes a matrix

exponential approach method. It reduces the 6 Maxwell's equations in the Cartesian coordinate to four equations in which tangential electric and magnetic fields are expressed in terms of the normal electric field and magnetic field components. For the sake of brevity, the E-DGFs correspond to the DGFs obtained using the eigen-decomposition method, while the T-DGFs refer to the DGFs obtained using the transition matrix method through the dissertation.

The third method employed for the multi-layer structure is the equivalent boundary method (EBM) [42]. One of the main features of the EBM is its objective to obtain not the bi-dimensional spectral DGF, but its inverse. It is claimed that the EBM method leads to a compact and stable algorithm. The EBM method is suitable for the calculation of the propagation characteristics of the slot line, parallel plate waveguide, and the coplanar waveguide since this method is constructed for a geometry with upper-electric and lower-electric walls.

Another method to construct the DGF is the cylindrical vector wave function method. The scattering dyadic Green's function for each layer is constructed in terms of the cylindrical vector wave functions by applying the method of scattering superposition. This method has been applied to find the DGF of the layered isotropic medium [43] and the unbounded gyrotropic [44] medium.

Out of so many different methods, the E-DGFs and the T-DGFs are the two most commonly used techniques to construct the dyadic Green's function for the planar stratified anisotropic geometry. Both of the DGFs are suitable for the propagation and radiation problems. Comparing the E-DGFs with the T-DGFs, each has its merits. Derivation of the T-DGFs are more complex in mathematics, and only the elements of the DGFs relating the tangential currents and tangential sources can be obtained directly from the solution to a 4 by 4 linear equation. However, the E-DGFs are expressed in terms of coordinate tensors and therefore make

the integral of the electromagnetic field straightforward and succinct. In addition, all the nine elements of the E-DGFs which correlate the electromagnetic fields with an arbitrary current distribution are obtained one time with no further work required. The T-DGFs are suitable for the problem with tangential current at the interface and are widely applied for the numerical analysis of transmission lines and patch antenna problems. The E-DGFs are suitable for problems with arbitrary current distribution.

With the DGFs obtained, the radiated fields of a Hertzian dipole can then be formulated. In the last few decades, researchers have extensively studied the radiation of a Hertzian dipole in the presence of an unbounded and layered anisotropic substrate.

With the assumption of the biasing magnetic field along the z direction, the radiation of a dipole in unbounded and layered gyroelectric media is treated in [46-47]. The radiation of a Hertzian dipole involved with a gyromagnetic medium is considered in [48-49]. Extensive work for the radiation of the dipole over and inside the layered uniaxial slab can be found in [50-54] due to the simple tensor form of the uniaxial medium. For the more complicated case of biaxial slab, formulation and analysis are available in [37]. It is noted here that radiated fields available in [37, 54] are derived from the E-DGFs for the corresponding geometry and medium. The radiated fields of a dipole for the general anisotropic layers characterized by arbitrarily oriented axes of anisotropy are considered in [55-57], which is closely related to the derivation of the T-DGFs.

Unlike the expressions of a radiated field derived from the T-DGF (as in [55-57]), which apply to general anisotropic geometry, formulations for the radiated field derived from the E-DGFs in previous work are usually solved for only one specific type of an anisotropic medium. The radiated field for the general anisotropic geometry is not currently available. According to

the literature survey above, the reason for this is due to the lack of the E-DGFs for a layered geometry filled with a general anisotropic medium. To overcome this limitation of former E-DGFs and also to fill the gap, it is essential to develop the E-DGFs for a layered general anisotropic geometry, which requires the availability of the E-DGFs for an unbounded general anisotropic medium. This directly corresponds to the first and second research objectives of the current study, as proposed in Section 1.1.

The third research objective is to formulate the radiated fields of a Hertzian dipole in the presence of a general anisotropic medium with no restrictions imposed on the permittivity or permeability. This goal can be achieved using the E-DGFs available after the first research objective is accomplished. It is also indicated in the current literature survey that numerical results for the radiated field of a Hertzian dipole above or inside the gyroelectric slab with an arbitrary biasing magnetic field are not available. One special case investigated in [46-47] is about the radiation of a Hertzian dipole in the presence of a gyroelectric medium with the biasing magnetic field along the z-direction. However, the effect of the biasing magnetic field on the radiation is not taken into account. Thus, in addition to developing the general formulation, studying the radiation behavior of the dipole in the presence of a gyroelectric medium with arbitrarily directed biasing magnetic field becomes the second part of the third research objective.

1.2.2 A Printed Dipole in the Presence of an Anisotropic Substrate

Currently, there is an increasing interest in complete monolithic systems which combine antenna elements or antenna arrays on the same substrate as the integrated RF/IF front end network. One of the most popular antenna elements is the printed antenna due to its

characteristics of low-cost, low-profile, conformability, and ease of manufacturing. Typical methods used to analyze the printed circuits include the method of moments (MoM), the finite difference time domain method (FDTD), and the finite element method (FEM).

The initial research employing the method of moments (MoM) utilized a combination of spatial and spectral techniques in order to analyze microstrip dipole and microstrip patch antennas on a single layer grounded isotropic medium [58] – [64]. In [58-60], the Green's functions are formulated in the spectral domain and the reaction formulation is applied in the spatial domain. Soon after, authors such as Deshpande and Bailey [61] following Itoh and Menzel's analysis technique [62] applied the reaction formulation entirely in the spectral domain. Many authors, including Pozar [63-64], followed this approach. Later on, this approach was extended to solve the radiation problem of the microstrip dipole on the grounded anisotropic substrate, which included uniaxial [4], biaxial [37] and ferrite [8-9] substrates.

It is worth noting here that most current numerical analyses of transmission lines and patch antenna problems on anisotropic substrates [4, 8-9, 37] are involving the application of the T-DGFs, while very little research has been performed on the numerical application of the E-DGF. One relevant and available study is [65], which applies the E-DGFs to solve the microstrip antenna on an arbitrarily oriented biaxially anisotropic medium. However, it is again noted here that the E-DGF used in [65] restricts its application to a layered biaxial medium only.

The survey of microstrip antennas above naturally leads to the fourth research objective proposed in Section 1.1, that is, to apply the E-DGFs solving for the properties of microstrip dipole antennas printed at the interface of a conductor-backed, general anisotropic slab. Since the E-DGFs are developed in the spectral domain, this dissertation will follow Itoh and Menzel's analysis technique [62] – applying the reaction formulation entirely in the spectral domain to

determine the current distribution of microstrip antennas on a single layer, arbitrarily oriented general anisotropic medium. The singularity analysis of the E-DGF is also performed to accurately calculate the numerical integral for the printed dipole on a layered biaxial slab. With the current distribution obtained, all other antenna parameters (including resonant length, input impedance, and radiation patterns) can be obtained. In particular, detailed numerical analyses will be focused on the printed dipole on a layered gyroelectric medium since there is very little such work found from literature survey.

1.3 Chapter Outlines

The major contributions of this dissertation include the development of the E-DGFs for a layered general anisotropic medium and the numerical applications of the corresponding E-DGFs to the radiation of a Hertzian dipole and a printed dipole on a layered geometry. With extensive numerical results and detailed analyses, it demonstrates the feasibility and validity of applying the E-DGFs to a general layered anisotropic medium with no restriction imposed on the property of the medium. This dissertation is organized as follows according to the research objective outlined in Section 1.1.

In Chapter 2, the eigenvector dyadic Green's functions (E-DGFs) for an unbounded general anisotropic medium including both reciprocal and non-reciprocal media are derived using the eigen-decomposition method. The E-DGFs for the unbounded uniaxial and gyrotropic media are presented in Section 2.2 and Section 2.3, respectively. It is discovered that modification to the initial E-DGF of an unbounded gyroelectric medium derived in [38] is required to fully represent the non-reciprocal behavior of the medium.

Chapter 3 presents the complete formulations of the E-DGF of each region for the half-space and two-layer anisotropic problems. The E-DGFs with a source inside the isotropic region is presented in Section 3.1. In Section 3.2, the modified symmetrical property is derived to obtain the DGFs above the source point when the source is inside the isotropic region. Particularly, it is pointed out that original symmetrical property, from which the E-DGFs above the source point can be obtained from E-DGFs below the source point, needs modifications when the anisotropic region is filled with a non-reciprocal medium. In Section 3.3, the modified symmetrical property for the DGFs with source and field points in two different regions is derived for a layered non-reciprocal medium. The usage and limitation of this modified symmetrical property is discussed. In Section 3.4, the direct construction method is proposed to obtain the complete E-DGFs with a source located in the anisotropic region. A comparison of the E-DGFs obtained through these two different approaches (modified symmetrical property and direct construction method) is presented and interesting relationship is discovered.

In Chapter 4, the E-DGF constructed in Chapter 3 is applied to solve the problem of radiation of a Hertzian dipole located above and inside the anisotropic region using the method of steepest descent. Compared with the results obtained in [55-57], the concise expressions for the radiated fields consisting of the reflection and transmission coefficients provide a straightforward physical insight to the radiated field when the dipole is located either above or inside the anisotropic layer. In Section 4.1, the focus is on the half-space geometry with a source located either in an isotropic or an anisotropic region. In Section 4.2 the formulation of the radiated field is presented for a Hertzian dipole embedded either inside an isotropic or an anisotropic region of two-layer geometry. In Section 4.3, the explicit formulas obtained in previous sections are validated numerically with the available results from current literature. In

Section 4.4, numerical analysis is presented in detail for the radiation of a Hertzian dipole placed both above and inside the layered gyroelectric slab, and a potential application for the enhanced radiation of a dipole using the grounded gyroelectric slab is proposed.

In Chapter 5, the problems of the microstrip dipole on a grounded substrate filled with various anisotropic media are solved using the Fourier transform domain method of moment employing Galerkin's method. Section 5.1 presents the formulation of method of moment. In Section 5.2, the properties of E-DGFs are studied in detail to facilitate the numerical integration obtained from Section 5.1. The current distributions of a printed dipole over the different grounded substrates, including uniaxial, biaxial, ferrite (gyromagnetic) and gyroelectric media, are presented in Section 5.3. The input impedance, resonant length, and radiation patterns of the microstrip dipole over a grounded isotropic slab, a grounded biaxial slab, and a grounded ferrite slab are calculated and compared with the previous results in Section 5.4. Also, in this section, numerical discussions will be presented in detail to illustrate the effect of the magnitude and direction of the biasing magnetic field to the input impedance, resonant length, and radiation pattern of the microstrip dipole on a gyroelectric medium.

Finally, conclusions are drawn and discussed in Chapter 6. As demonstrated in the previous chapters, since the E-DGF developed in this dissertation is for the general anisotropic medium with no restrictions imposed on the type of the medium, it has wide applications for a Hertzian dipole or a printed dipole on general anisotropic substrates. Future works are also briefly discussed.

2 DYADIC GREEN'S FUNCTIONS FOR AN UNBOUNDED GENERAL ANISOTROPIC MEDIUM

In this chapter, the approach in [35] is extended so it can be applied to obtain the eigenvector dyadic Green's functions (E-DGFs) of an unbounded general anisotropic medium with no restriction imposed on the property of the medium. This approach will be called the *eigen-decomposition method*. The basic feature of the eigen-decomposition method is based on the calculation of the corresponding eigenvectors from the specific adjoint wave matrix, which is obtained from the second-order differential equation in the spectral domain.

This chapter is organized as follows. In Section 2.1, the eigen-decomposition method is applied to obtain the electric type E-DGF of a general anisotropic medium due to an electric current source. In Section 2.2, the eigen-decomposition method is applied to obtain the analytic formula of the E-DGF for a uniaxial medium and an isotropic medium. Exact agreement is obtained with the previous results. In Section 2.3, E-DGFs of the gyrotropic media are derived using the same method. Particularly, it is discovered that the formulations of the E-DGFs for the unbounded non-reciprocal medium and reciprocal medium are different and modifications to the formulas proposed in [38] are required.

2.1 Eigen-decomposition of DGF for a General Anisotropic Medium

A medium is considered *anisotropic* when its electrical and/or magnetic properties depend upon the directions of field vectors. The relations between fields can be written in the following form.

$$\bar{D} = \epsilon_0 \bar{\epsilon}_r \cdot \bar{E} \quad \bar{B} = \mu_0 \bar{\mu}_r \cdot \bar{H} \quad (2.1-1)$$

In the equation above, ϵ_0 and μ_0 are the free space permittivity and permeability, while $\bar{\epsilon}_r$ and $\bar{\mu}_r$ are the relative permittivity and permeability tensors. For a general anisotropic medium, the permittivity and permeability tensors are of the following form.

$$\bar{\epsilon}_r = \begin{bmatrix} \epsilon_{xx} & \epsilon_{xy} & \epsilon_{xz} \\ \epsilon_{yx} & \epsilon_{yy} & \epsilon_{yz} \\ \epsilon_{zx} & \epsilon_{zy} & \epsilon_{zz} \end{bmatrix} \quad \bar{\mu}_r = \begin{bmatrix} \mu_{xx} & \mu_{xy} & \mu_{xz} \\ \mu_{yx} & \mu_{yy} & \mu_{yz} \\ \mu_{zx} & \mu_{zy} & \mu_{zz} \end{bmatrix} \quad (2.1-2)$$

For reciprocal media such as uniaxial and biaxial media, $\bar{\epsilon}_r$ and $\bar{\mu}_r$ are symmetric matrices. In the principal coordinate system (where the coordinate axes are aligned with the principal axes of the permittivity tensor), only the diagonal elements of $\bar{\epsilon}_r$ are non-zero.

For non-reciprocal media, such as gyroelectric and gyromagnetic media, the matrices for $\bar{\epsilon}_r$ and $\bar{\mu}_r$ are antisymmetric. Even in the principal coordinate system (where the coordinate axis is aligned along the direction of the biasing magnetic field), the off-diagonal elements of the permittivity and permeability matrices are non-zero and are complex conjugate to each other for the lossless media.

The complete set of DGFs for a general anisotropic medium with the electric and magnetic current sources (\bar{J} and \bar{M}) located at $z = z'$ in the unbounded region has been derived in [39]. In this dissertation, the electric type E-DGF which correlates the electric current source and electric field as in Eq. (2.1-3) is only utilized.

$$\bar{E} = \int_{v'} \bar{G}(\bar{r}, \bar{r}') \cdot \bar{J}(\bar{r}') d^3 \bar{r}' \quad (2.1-3)$$

Thus, this section will present the eigen-decomposition method only for the electric type E-DGF. Through the analysis, time variation of $e^{-i\omega t}$ is assumed. Eq. (2.1-4) shows the electric type DGF for an unbounded anisotropic medium derived in [39], which is expressed as a 3D Fourier transform of $adj\overline{\overline{W}}_E$ (adjoint of the electric wave matrix $\overline{\overline{W}}_E$).

$$\overline{\overline{G}}(\overline{r}, \overline{r}') = \frac{-i\omega\mu_0}{(2\pi)^3} \int_{-\infty}^{\infty} \overline{\overline{W}}_E^{-1} e^{i\overline{k}\cdot(\overline{r}-\overline{r}')} d^3\overline{k} \quad \text{or} \quad \overline{\overline{G}}(\overline{r}, \overline{r}') = \frac{-i\omega\mu_0}{(2\pi)^3} \int_{-\infty}^{\infty} \frac{adj\overline{\overline{W}}_E}{|\overline{\overline{W}}_E|} e^{i\overline{k}\cdot(\overline{r}-\overline{r}')} d^3\overline{k} \quad (2.1-4)$$

$$\overline{\overline{W}}_E = \overline{\overline{k}} \overline{\overline{\mu}}_r \overline{\overline{k}} + k_0^2 \overline{\overline{\epsilon}}_r, \quad \overline{\overline{k}} = \begin{bmatrix} 0 & -k_z & k_y \\ k_z & 0 & -k_x \\ -k_y & k_x & 0 \end{bmatrix}, \quad \overline{k} = \hat{x}k_x + \hat{y}k_y + \hat{z}k_z \quad (2.1-5)$$

k_x, k_y and k_z are the x, y, z components of the wave vector in the Cartesian coordinate system.

The application of the eigen-decomposition method starts with reducing the 3D integration of Eq. (2.1-4) to a 2D integration over k_x and k_y by integrating the integrand of $\overline{\overline{G}}(\overline{r}, \overline{r}')$ over k_z . To address how this is performed, the analysis of the determinant of electric wave matrix $|\overline{\overline{W}}_E|$ is required. It is easy to derive that $|\overline{\overline{W}}_E|$ can be expanded as a fourth order polynomial in terms of k_z with the coefficients of the polynomial as the functions of k_x and k_y . Generally, with given k_x and k_y , there exist four different values of k_z to let the determinant of wave matrix (e.g., $|\overline{\overline{W}}_E|$) to be zero, which appear as four poles of the integrand of DGF $\overline{\overline{G}}(\overline{r}, \overline{r}')$.

Denoting the four solutions for k_z to the equation of $|\overline{\overline{W}}_E| = 0$ as k_{zp}^q ($p = I, II; q = d, u$), the

determinant $|\overline{\overline{W}}_E|$ can be written as Booker quartic equation below.

$$\left| \overline{W}_E \right| = a_4 (k_z - k_{zI}^u)(k_z - k_{zI}^d)(k_z - k_{zII}^u)(k_z - k_{zII}^d) \quad (2.1-6)$$

where a_4 is a constant dependent on the permittivity and permeability matrix. For a gyroelectric medium with z-directed biasing magnetic field, a_4 is derived in [38]. The notations of k_{zp}^q ($p = I, II$; $q = d, u$) are explained here. According to the location of k_{zp}^q on the wave vector surface, the subscript p indicates the type of the characteristic wave for a general anisotropic medium with $p = I$ and $p = II$ corresponding to the Type I and Type II waves, respectively. The superscript q indicates the direction of power flow. For propagating waves, the superscripts ‘ u ’ and ‘ d ’ indicate the waves carrying power away from the interface in the upward and the downward directions, respectively. For evanescent waves (where there exists no power flow away from the interface in either upward or downward directions or where the z-component of time average Poynting vector is zero), the superscripts of ‘ u ’ and ‘ d ’ indicate the wave amplitudes decaying away from the interface along the upward and downward directions, respectively.

For a lossless medium (for which permittivity and permeability matrices are hermitian matrices), the four distinct solutions of k_z can be categorized into the following three cases: two pairs of complex conjugate solutions, two real and two complex conjugate solutions or four real solutions. The propagating waves are characterized with k_z being the real solutions and evanescent waves are characterized with k_z being complex or pure imaginary solutions. It needs to be noted here that the wave with a positive real number of k_{zp}^q usually indicates an upward propagating wave. However, this is not always the case. Due to the existence of the backward wave, the direction of power flow and phase advance can be opposite to each other.

As discussed earlier, solutions of $k_{zI}^u, k_{zI}^d, k_{zII}^u, k_{zII}^d$ pose singularity to the integrand of $\overline{\overline{G}}(\bar{r}, \bar{r}')$ shown in Eq. (2.1-4). These singularity poles can be extracted from the integration by integrating over k_z using residue theorem and the radiation boundary condition at infinity. With the assumption of the medium to be slightly lossy, i.e., $\text{Im } k_{zI}^u \ll \text{Re } k_{zI}^u, \text{Im } k_{zI}^u > 0, \text{Im } k_{zII}^u \ll \text{Re } k_{zII}^u, \text{Im } k_{zII}^u > 0$, the following DGF in the 2D integral form is obtained by performing the contour integration over k_z .

For $z > z'$

$$\overline{\overline{G}}(\bar{r}, \bar{r}') = \frac{\omega\mu_0}{(2\pi)^2} \int_{-\infty}^{\infty} \int_{-\infty}^{\infty} \left(\frac{\text{adj}\overline{\overline{W}}_E(k_{zI}^u)}{a_4(k_{zI}^u - k_{zI}^d)(k_{zI}^u - k_{zII}^u)(k_{zI}^u - k_{zII}^d)} e^{ik_{zI}^u \cdot (\bar{r} - \bar{r}')} + \frac{\text{adj}\overline{\overline{W}}_E(k_{zII}^u)}{a_4(k_{zII}^u - k_{zI}^d)(k_{zII}^u - k_{zI}^u)(k_{zII}^u - k_{zII}^d)} e^{ik_{zII}^u \cdot (\bar{r} - \bar{r}')} \right) dk_x dk_y \quad (2.1-7)$$

For $z < z'$

$$\overline{\overline{G}}(\bar{r}, \bar{r}') = -\frac{\omega\mu_0}{(2\pi)^2} \int_{-\infty}^{\infty} \int_{-\infty}^{\infty} \left(\frac{\lambda(k_{zI}^d) \hat{e}(k_{zI}^d) \hat{e}(k_{zI}^d)}{a_4(k_{zI}^d - k_{zI}^u)(k_{zI}^d - k_{zII}^u)(k_{zI}^d - k_{zII}^d)} e^{ik_{zI}^d \cdot (\bar{r} - \bar{r}')} + \frac{\lambda(k_{zII}^d) \hat{e}(k_{zII}^d) \hat{e}(k_{zII}^d)}{a_4(k_{zII}^d - k_{zI}^d)(k_{zII}^d - k_{zI}^u)(k_{zII}^d - k_{zII}^u)} e^{ik_{zII}^d \cdot (\bar{r} - \bar{r}')} \right) dk_x dk_y \quad (2.1-8)$$

where the wave vectors are defined as

$$\overline{k}_I^u = \hat{x}k_x + \hat{y}k_y + \hat{z}k_{zI}^u \quad \overline{k}_I^d = \hat{x}k_x + \hat{y}k_y + \hat{z}k_{zI}^d; \quad \overline{k}_{II}^u = \hat{x}k_x + \hat{y}k_y + \hat{z}k_{zII}^u \quad \overline{k}_{II}^d = \hat{x}k_x + \hat{y}k_y + \hat{z}k_{zII}^d$$

Applying the eigen-decomposition technique, the adjoint electric wave matrix

$\text{adj}\overline{\overline{W}}_E(k_{zp}^q)$ ($p = I, II; q = d, u$) in the integrand of $\overline{\overline{G}}(\bar{r}, \bar{r}')$ shown in Eq. (2.1-7) and Eq.

(2.1-8) can be decomposed into a single dyad. Details will be presented below.

It is shown by H. Chen [66, p. 29] that if the determinant of a matrix is zero and the adjoint matrix is a non-zero matrix, this matrix may be expressed as a sum of two dyads and the adjoint matrix as a single dyad. Thus, for an electric wave matrix, if k_z is taken as the value such that the determinant of electric wave matrix $\overline{\overline{W}}_E$ is 0, then the adjoint electric wave matrix $adj\overline{\overline{W}}_E$ can always be decomposed into the form of a single dyad as follows.

$$adj\overline{\overline{W}}_E = \lambda \overline{u} \overline{v} \quad (2.1-9)$$

For now, λ is chosen as the eigenvalue of $adj\overline{\overline{W}}_E$ and no constraint has been put on the vectors of \overline{u} and \overline{v} in the above dyadic form. It will be shown below that the matrix of $adj\overline{\overline{W}}_E$ has only one non-zero eigenvalue as long as $|\overline{\overline{W}}_E| = 0$. As for the choice of vectors of \overline{u} and \overline{v} , it is dependent on the property of the adjoint electric wave matrix $adj\overline{\overline{W}}_E$. The property is affected by the solutions for k_z of the Booker quartic equation for specific k_x and k_y , since k_z can be taken as any value due to the integration over the infinite range of k_x and k_y .

For a non-magnetic general anisotropic medium ($\overline{\overline{\mu}}_r = \overline{\overline{I}}$) with the permittivity matrix shown in Eq. (2.1-2), the electric wave matrix is expressed as follows.

$$\overline{\overline{W}}_E = \overline{\overline{k}}k + k_0^2 \overline{\overline{\epsilon}}_r = \begin{bmatrix} k_0^2 \epsilon_{xx} - k_z^2 - k_y^2 & k_0^2 \epsilon_{xy} + k_x k_y & k_0^2 \epsilon_{xz} + k_x k_z \\ k_0^2 \epsilon_{yx} + k_x k_y & k_0^2 \epsilon_{yy} - k_z^2 - k_x^2 & k_0^2 \epsilon_{yz} + k_y k_z \\ k_0^2 \epsilon_{zx} + k_x k_z & k_0^2 \epsilon_{zy} + k_y k_z & k_0^2 \epsilon_{zz} - k_x^2 - k_y^2 \end{bmatrix} \quad (2.1-10)$$

With the anisotropic medium being either reciprocal or non-reciprocal, the property of the electric wave matrix is different. Thus, to demonstrate the difference in the formulation of DGF using the eigen-decomposition method, these two cases are considered here.

A. Reciprocal Medium

For a lossless reciprocal medium, the permittivity tensor $\overline{\overline{\varepsilon_r}}$ is a symmetric matrix. It is straightforward to derive from Eq. (2.1-10) that $\overline{\overline{W_E}}$ is always a symmetric matrix. Thus, the adjoint matrix of $\overline{\overline{W_E}}$ ($adj\overline{\overline{W_E}}$) is also a symmetric matrix. If k_z is real, then $adj\overline{\overline{W_E}}$ is a real symmetric matrix, and if k_z is not real, then $adj\overline{\overline{W_E}}$ will be a complex symmetric matrix. k_z is the solution to the Booker quartic equation for given k_x and k_y . The following analysis will show that $adj\overline{\overline{W_E}}(k_z)$ has only one non-zero eigenvalue when $k_z = k_{zI}^u, k_{zII}^u, k_{zI}^d, k_{zII}^d$. To obtain the eigenvalues, the characteristic equation for $adj\overline{\overline{W_E}}(k_z)$ is first derived.

$$\begin{aligned} f(\lambda) &= \left| \lambda \overline{\overline{I}} - adj\overline{\overline{W_E}}(k_z) \right| \\ &= \lambda^3 - tr(adj\overline{\overline{W_E}}(k_z))\lambda^2 + tr(adjadj(\overline{\overline{W_E}}(k_z)))\lambda - \left| adj\overline{\overline{W_E}}(k_z) \right| = 0 \end{aligned} \quad (2.1-11)$$

where tr stands for the trace of a matrix.

Applying the following identities, [65, p. 13]

$$\left| adj\overline{\overline{W_E}} \right| = \left| \overline{\overline{W_E}} \right|^2 \quad (2.1-12)$$

$$adj(adj\overline{\overline{W_E}}) = \left| \overline{\overline{W_E}} \right| \overline{\overline{W_E}} \quad (2.1-13)$$

when $k_z = k_{zI}^u, k_{zII}^u, k_{zI}^d, k_{zII}^d$, $\left| \overline{\overline{W_E}} \right| = 0$, the characteristic equation of Eq. (2.1-11) reduces to the

following form.

$$f(\lambda) = \lambda^3 - tr(adj\overline{\overline{W_E}}(k_z))\lambda^2 \quad (2.1-14)$$

Thus, the eigenvalues for $adj\overline{\overline{W_E}}(k_z)$ are

$$\lambda_1 = \text{tr}(\overline{\overline{\text{adj}W_E}}(k_z)), \quad \lambda_2 = \lambda_3 = 0 \quad (2.1-15)$$

It is known that the unitary diagonalization exists for a real symmetric matrix $\overline{\overline{\text{adj}W_E}}$ and dyadic decomposition takes the form as [67].

$$\overline{\overline{\text{adj}W_E}} = \lambda_1 \bar{u}_1 \bar{u}_1 + \lambda_2 \bar{u}_2 \bar{u}_2 + \lambda_3 \bar{u}_3 \bar{u}_3 \quad (2.1-16)$$

Since only one non-zero eigenvalue exists, then

$$\overline{\overline{\text{adj}W_E}}(k_{zp}^q) = \lambda_p^q \hat{e}_p^q \hat{e}_p^q, \quad p = I, II; \quad q = d, u \quad (2.1-17)$$

where λ_p^q is the non-zero eigenvalue of the matrix $\overline{\overline{\text{adj}W_E}}(k_{zp}^q)$ and \hat{e}_p^q is the corresponding eigenvector.

A comparison of Eq. (2.1-17) with Eq. (2.1-9) reveals that if the matrix $\overline{\overline{\text{adj}W_E}}$ is real and symmetric, then both of the vectors \bar{u}, \bar{v} will be taken as the eigenvectors corresponding to the only one non-zero eigenvalue.

However, if $k_z = k_{zI}^u, k_{zII}^u, k_{zI}^d, k_{zII}^d$ is complex (including the case of being pure imaginary), then $\overline{\overline{\text{adj}W_E}}$ is a complex symmetric matrix. It will be shown below a complex symmetric matrix can still be decomposed into a dyad composed of two identical vectors.

A non-defective matrix is a matrix which has a full linearly independent set of eigenvectors. Since $\overline{\overline{\text{adj}W_E}}$ is a non-defective matrix [67, p. 186], which can be proved by showing that $\overline{\overline{W_E}}$ has three distinct eigenvalues, $\overline{\overline{\text{adj}W_E}}$ can be factorized in the following diagonal form.

$$adj\overline{\overline{W}}_E(k_z) = \overline{\overline{X}}\overline{\overline{\Lambda}}\overline{\overline{X}}^{-1}$$

$$\overline{\overline{X}} = \begin{bmatrix} \overline{u}_1 & \overline{u}_2 & \overline{u}_3 \end{bmatrix}, \overline{\overline{\Lambda}} = \begin{bmatrix} \lambda_1 & 0 & 0 \\ 0 & \lambda_2 & 0 \\ 0 & 0 & \lambda_3 \end{bmatrix}, \overline{\overline{X}}^{-1} = \begin{bmatrix} -\overline{v}_1^T \\ -\overline{v}_2^T \\ -\overline{v}_3^T \end{bmatrix} \quad (2.1-18)$$

\overline{u}_j is the j th column of $\overline{\overline{X}}$, which corresponds to an eigenvector of $adj\overline{\overline{W}}_E$ and λ_j is the j th diagonal entry of $\overline{\overline{\Lambda}}$, which is the associated eigenvalue. $-\overline{v}_j^T$ is the j th row of $\overline{\overline{X}}^{-1}$.

It is proved earlier that $adj\overline{\overline{W}}_E$ has only one non-zero eigenvalue when $k_z = k_{zp}^q$; thus,

$$adj\overline{\overline{W}}_E(k_{zp}^q) = \lambda_p^q \widehat{e}_p^q \left(\widehat{v}_p^q \right)^T \quad (2.1-19)$$

where \widehat{v}_p^q satisfies

$$\left(\widehat{v}_p^q \right)^T \widehat{e}_p^q = 1, \quad p = I, II; q = d, u \quad (2.1-20)$$

An inspection of Eq. (2.1-19) with Eq. (2.1-9) reveals that vector \overline{u} is actually the eigenvector of $adj\overline{\overline{W}}_E(k_{zp}^q)$ which corresponds to the non-zero eigenvalue, and the vector \overline{v} has to satisfy the condition $-\overline{v}^T \overline{u} = 1$. Combining Eq. (2.1-17) and Eq. (2.1-19) shows the complete eigen-decomposition for the matrix $adj\overline{\overline{W}}_E(k_{zp}^q)$ according to the different ranges of k_{zp}^q .

If k_{zp}^q is real, $adj\overline{\overline{W}}_E$ is a real symmetric matrix.

$$adj\overline{\overline{W}}_E(k_{zp}^q) = \lambda_p^q \widehat{e}_p^q \left(\widehat{e}_p^q \right)^T, \quad p = I, II; q = d, u \quad (2.1-21)$$

If k_{zp}^q is complex, $adj\overline{\overline{W}}_E$ is a complex symmetric matrix.

$$adj\overline{\overline{W}}_E(k_{zp}^q) = \lambda_p^q \widehat{e}_p^q \left(\widehat{v}_p^q \right)^T, \quad \left(\widehat{v}_p^q \right)^T \widehat{e}_p^q = 1, \quad p = I, II; q = d, u$$

Especially if the eigenvector is taken such that $(e_{px}^q)^2 + (e_{py}^q)^2 + (e_{pz}^q)^2 = 1$, then it is seen that $\hat{v}_p^q = \hat{e}_p^q$. Thus, for a reciprocal medium (both for lossless and lossy cases), the adjoint electric wave matrix can always be decomposed into the form of a single dyad which is composed of the eigenvector corresponding to the only one non-zero eigenvalue. However, this is not the case if the medium is non-reciprocal.

B. Non-reciprocal Medium

If the medium is lossless and non-reciprocal, which indicates that the dielectric permittivity tensor is a hermitian matrix, then it is seen from Eq. (2.1-10) that, if k_{zp}^q is real, the matrix $\overline{\overline{W}}_E$ and its adjoint matrix $\overline{\overline{adjW}}_E(k_z)$ are hermitian matrices, and if k_{zp}^q is complex, the matrix $\overline{\overline{W}}_E$ and its adjoint matrix $\overline{\overline{adjW}}_E(k_z)$ are non-hermitian matrices. It is known that the unitary diagonalization can be applied to a hermitian matrix. For a non-hermitian matrix, similar diagonalization can be applied if the matrix is non-defective. With $\overline{\overline{adjW}}_E(k_z)$ being a hermitian matrix or a non-hermitian and non-defective matrix under the different conditions of k_{zp}^q , the corresponding eigen-decomposition for a non-reciprocal medium is shown as follows.

If k_{zp}^q is real, $\overline{\overline{adjW}}_E$ is a hermitian matrix.

$$\overline{\overline{adjW}}_E(k_{zp}^q) = \lambda_p^q \hat{e}_p^q (\hat{e}_p^q)^*, \quad p = I, II; q = d, u \quad (2.1-22)$$

If k_{zp}^q is complex, $\overline{\overline{adjW}}_E$ is a non-hermitian and non-defective matrix.

$$\overline{\overline{adjW}}_E(k_{zp}^q) = \lambda_p^q \hat{e}_p^q (\hat{v}_p^q)^T, \quad (\hat{v}_p^q)^T \hat{e}_p^q = 1, \quad p = I, II; q = d, u$$

If the medium is lossy and non-reciprocal, which indicates that the matrix $\overline{\overline{W}}_E$ is not a hermitian matrix even if k_{zp}^q is real, and then the eigenvalue decomposition for a lossy medium always takes the form of

$$adj\overline{\overline{W}}_E(k_{zp}^q) = \lambda_p^q \widehat{e}_p^q \left(\widehat{v}_p^q \right)^T, \quad \left(\widehat{v}_p^q \right)^T \widehat{e}_p^q = 1, \quad p = I, II; q = d, u \quad (2.1-23)$$

Discussion above shows that Eq. (2.1-24) or the statement in [68] by A. Eroglu – “*that for unbounded gyroelectric medium the adjoint electric wave matrix in the dyadic Green’s function of 2D integration form ($adj\overline{\overline{W}}_E(k_{zp}^q)$) ($p = I, II; q = d, u$) can always be decomposed into a single dyad form as follows by assuming $adj\overline{\overline{W}}_E$ is a hermitian matrix*” – is not correct.

$$adj\overline{\overline{W}}_E(k_{zp}^q) = \lambda_p^q \widehat{e}_p^q \left(\widehat{e}_p^q \right)^*, \quad p = I, II; q = d, u \quad (2.1-24)$$

where λ_p^q is the non-zero eigenvalue of $adj\overline{\overline{W}}_E(k_{zp}^q)$.

It has been shown that that $adj\overline{\overline{W}}_E$ is always a linear matrix and can be decomposed into a single dyad form. A careful treatment is required to obtain the dyadic form of DGFs when the eigen-decomposition method is used if the medium is gyrotropic or a lossy anisotropic medium. Detailed discussions about using the eigen-decomposition method to obtain the DGFs of uniaxial and gyrotropic media will be presented in the following sections.

2.2 DGFs of an Unbounded Uniaxial Medium

DGFs of uniaxial and isotropic media are considered in this section. To simplify the analysis, we consider the electric type Green’s function for a uniaxial medium with the optic axis

aligned along the z-axis, which is characterized by the relative permittivity and permeability tensors of the following form.

$$\overline{\overline{\mu}}_r = \overline{\overline{I}}, \quad \overline{\overline{\varepsilon}}_r = \begin{bmatrix} \varepsilon_1 & 0 & 0 \\ 0 & \varepsilon_1 & 0 \\ 0 & 0 & \varepsilon_{1z} \end{bmatrix} \quad (2.2-1)$$

As shown in previous section, to obtain the electric type DGF, it requires solving the inverse of electric wave matrix, which can be obtained using $\overline{\overline{W}}_E^{-1} = \frac{adj \overline{\overline{W}}_E}{|\overline{\overline{W}}_E|}$. Substituting Eq.

(2.2-1) into Eq. (2.1-5), the determinant of $\overline{\overline{W}}_E$ can be expressed in terms of k_x, k_y, k_z as follows.

$$|\overline{\overline{W}}_E| = |\overline{\overline{k}}\overline{\overline{k}} + k_0^2 \overline{\overline{\varepsilon}}| = k_0^2 \varepsilon_{1z} (k_z^2 - k_{zI}^2)(k_z^2 - k_{zII}^2) \quad (2.2-2)$$

$$k_{zI} = \sqrt{k_0^2 \varepsilon_1 - k_\rho^2} \quad k_{zII} = \sqrt{k_0^2 \varepsilon_1 - k_\rho^2 \frac{\varepsilon_1}{\varepsilon_{1z}}} \quad (2.2-3)$$

where $k_\rho^2 = k_x^2 + k_y^2$. We note that

$$\begin{aligned} k_{zI}^u &= k_{zI}, & k_{zI}^d &= -k_{zI} \\ k_{zII}^u &= k_{zII}, & k_{zII}^d &= -k_{zII} \end{aligned} \quad (2.2-4)$$

The adjoint electric wave matrix is given as

$$adj W_E = \begin{bmatrix} A_{11} & A_{12} & A_{13} \\ A_{21} & A_{22} & A_{23} \\ A_{31} & A_{32} & A_{33} \end{bmatrix} \quad (2.2-5)$$

The elements of the matrix in Eq. (2.2-5) are listed as follows.

$$\begin{aligned}
A_{11} &= (k_\rho^2 + k_z^2)k_x^2 - k_0^2 [\varepsilon_1 k_\rho^2 + \varepsilon_{1z}(k_x^2 + k_z^2)] + k_0^4 \varepsilon_1 \varepsilon_{1z} \\
A_{12} &= (k_\rho^2 + k_z^2 - k_0^2 \varepsilon_{1z})k_x k_y \\
A_{13} &= (k_\rho^2 + k_z^2 - k_0^2 \varepsilon_1)k_x k_z \\
A_{21} &= A_{12} = (k_\rho^2 + k_z^2 - k_0^2 \varepsilon_{1z})k_x k_y \\
A_{22} &= (k_\rho^2 + k_z^2)k_y^2 - k_0^2 [\varepsilon_1 k_\rho^2 + \varepsilon_{1z}(k_y^2 + k_z^2)] + k_0^4 \varepsilon_1 \varepsilon_{1z} \\
A_{23} &= (k_\rho^2 + k_z^2 - k_0^2 \varepsilon_1)k_y k_z \\
A_{31} &= A_{13} = (k_\rho^2 + k_z^2 - k_0^2 \varepsilon_1)k_x k_z \\
A_{32} &= A_{23} = (k_\rho^2 + k_z^2 - k_0^2 \varepsilon_1)k_y k_z \\
A_{33} &= (k_\rho^2 + k_z^2)k_z^2 - k_0^2 \varepsilon_1 (k_\rho^2 + 2k_z^2) + k_0^4 \varepsilon_1^2
\end{aligned} \tag{2.2-6}$$

Applying Eq. (2.2-2) to Eq. (2.1-4) and then Eq. (2.1-4) can be written as follows.

$$\overline{\overline{G}}(\vec{r}, \vec{r}') = \frac{-i\omega\mu_0}{(2\pi)^3} \int_{-\infty}^{\infty} \int_{-\infty}^{\infty} \int_{-\infty}^{\infty} \frac{\overline{\overline{adjW}}_E}{k_0^2 \varepsilon_{1z} (k_z^2 - k_{zl}^2)(k_z^2 - k_{zll}^2)} e^{i\vec{k} \cdot (\vec{r} - \vec{r}')} dk_x dk_y dk_z \tag{2.2-7}$$

It is seen from Eq. (2.2-2) that for each specific k_x, k_y , four poles of the integrand exist when $k_z = \pm k_{zl}, \pm k_{zll}$, which are given in Eq. (2.2-3) and Eq. (2.2-4). If the optic axis of the medium is not aligned along the z-axis, all the nine elements of the permittivity matrix are non-zero. In this case, four distinct poles will exist, and Eq. (2.2-7) can be written in a more general form as follows.

$$\overline{\overline{G}}(\vec{r}, \vec{r}') = \frac{-i\omega\mu_0}{(2\pi)^3} \int_{-\infty}^{\infty} \int_{-\infty}^{\infty} \int_{-\infty}^{\infty} \frac{\overline{\overline{adjW}}_E}{k_0^2 \varepsilon_{1z} (k_z - k_{zl}^u)(k_z - k_{zl}^d)(k_z - k_{zll}^u)(k_z - k_{zll}^d)} e^{i\vec{k} \cdot (\vec{r} - \vec{r}')} dk_x dk_y dk_z \tag{2.2-8}$$

Assuming the medium to be slightly lossy, (i.e., $\text{Im } k_{zl}^u \ll \text{Re } k_{zl}^u, \text{Im } k_{zl}^d > 0$,

$\text{Im } k_{zll}^u \ll \text{Re } k_{zll}^u, \text{Im } k_{zll}^d > 0$), when performing the contour integration over k_z using the residue theorem and the radiation boundary condition at infinity, the DGFs for the regions above and below the source point can be written as follows.

For $z > z'$

$$\overline{\overline{G}}(\vec{r}, \vec{r}') = \frac{\omega\mu_0}{(2\pi)^2} \int_{-\infty}^{\infty} \int_{-\infty}^{\infty} \left(\frac{\overline{\overline{adjW}}_E(k_{zl}^u)}{k_0^2 \varepsilon_{1z} (k_{zl}^u - k_{zl}^d)(k_{zl}^u - k_{zll}^u)(k_{zl}^u - k_{zll}^d)} e^{ik_{zl}^u \cdot (\vec{r} - \vec{r}')} + \frac{\overline{\overline{adjW}}_E(k_{zll}^u)}{k_0^2 \varepsilon_{1z} (k_{zll}^u - k_{zl}^d)(k_{zll}^u - k_{zl}^u)(k_{zll}^u - k_{zll}^d)} e^{ik_{zll}^u \cdot (\vec{r} - \vec{r}')} \right) dk_x dk_y \quad (2.2-9)$$

For $z < z'$

$$\overline{\overline{G}}(\vec{r}, \vec{r}') = -\frac{\omega\mu_0}{(2\pi)^2} \int_{-\infty}^{\infty} \int_{-\infty}^{\infty} \left(\frac{\overline{\overline{adjW}}_E(k_{zl}^d)}{k_0^2 \varepsilon_{1z} (k_{zl}^d - k_{zl}^u)(k_{zl}^d - k_{zll}^u)(k_{zl}^d - k_{zll}^d)} e^{ik_{zl}^d \cdot (\vec{r} - \vec{r}')} + \frac{\overline{\overline{adjW}}_E(k_{zll}^d)}{k_0^2 \varepsilon_{1z} (k_{zll}^d - k_{zl}^u)(k_{zll}^d - k_{zl}^d)(k_{zll}^d - k_{zll}^u)} e^{ik_{zll}^d \cdot (\vec{r} - \vec{r}')} \right) dk_x dk_y$$

For a uniaxial medium with the optic axis aligned along the z-direction, applying Eq.

(2.2-3) and Eq. (2.2-4) into Eq. (2.2-9), then it can be simplified as follows.

For $z > z'$

$$\overline{\overline{G}}(\vec{r}, \vec{r}') = \frac{\omega\mu_0}{8\pi^2} \int_{-\infty}^{\infty} \int_{-\infty}^{\infty} \left(\frac{\overline{\overline{adjW}}_E(k_{zl}^u)}{k_0^2 \varepsilon_{1z} k_{zl}^u (k_{zl}^2 - k_{zll}^2)} e^{ik_{zl}^u \cdot (\vec{r} - \vec{r}')} + \frac{\overline{\overline{adjW}}_E(k_{zll}^u)}{k_0^2 \varepsilon_{1z} k_{zll}^u (k_{zll}^2 - k_{zl}^2)} e^{ik_{zll}^u \cdot (\vec{r} - \vec{r}')} \right) dk_x dk_y \quad (2.2-10)$$

For $z < z'$

$$\overline{\overline{G}}(\vec{r}, \vec{r}') = \frac{\omega\mu_0}{8\pi^2} \int_{-\infty}^{\infty} \int_{-\infty}^{\infty} \left(\frac{\overline{\overline{adjW}}_E(k_{zl}^d)}{k_0^2 \varepsilon_{1z} k_{zl}^d (k_{zl}^2 - k_{zll}^2)} e^{ik_{zl}^d \cdot (\vec{r} - \vec{r}')} + \frac{\overline{\overline{adjW}}_E(k_{zll}^d)}{k_0^2 \varepsilon_{1z} k_{zll}^d (k_{zll}^2 - k_{zl}^2)} e^{ik_{zll}^d \cdot (\vec{r} - \vec{r}')} \right) dk_x dk_y$$

The DGFs given by Eq. (2.2-10) can also be represented in a dyadic form by finding the eigenvalues and eigenvectors of the adjoint matrix $\overline{\overline{adjW}}_E$. For the uniaxial medium with the optic axis aligned along the z-axis, the eigenvalues are obtained as follows.

$$\lambda_l^u = \lambda_l^d = k_\rho^2 k_0^2 (\varepsilon_{1z} - \varepsilon_1) \quad (2.2-11)$$

$$\lambda_{ll}^u = \lambda_{ll}^d = k_\rho^2 k_0^2 (\varepsilon_1 - \varepsilon_{1z}) + k_\rho^4 (1 - \varepsilon_1 / \varepsilon_{1z})^2 \quad (2.2-12)$$

We also note that

$$k_o^2 \varepsilon_{1z} ((k_{zl}^u)^2 - (k_{zll}^u)^2) = k_o^2 \varepsilon_{1z} ((k_{zl}^d)^2 - (k_{zll}^d)^2) = k_\rho^2 k_0^2 (\varepsilon_1 - \varepsilon_{1z}) \quad (2.2-13)$$

It is seen from Eq. (2.2-11) and Eq. (2.2-12) that for both Type I and Type II waves, the eigenvalues of upward and downward waves are the same. It will be shown below that eigenvectors are the same for Type I upward and downward waves. However, for Type II waves, eigenvectors are different for upward and downward waves. When substituting Eq. (2.2-11) and Eq. (2.2-12) into Eq. (2.2-10), the DGFs are obtained as follows.

For $z > z'$

$$\bar{\bar{G}}(\bar{r}, \bar{r}') = -\frac{\omega\mu_0}{8\pi^2} \int_{-\infty}^{\infty} \int_{-\infty}^{\infty} dk_x dk_y \left(\frac{\hat{e}_l^u \hat{e}_l^u e^{i\bar{k}_l \cdot (\bar{r} - \bar{r}')}}{k_{zl}^u} + \frac{\left(k_0^2 + k_\rho^2 \frac{\varepsilon_1 - \varepsilon_{1z}}{(\varepsilon_{1z})^2} \right) \hat{e}_{ll}^u \hat{e}_{ll}^u e^{i\bar{k}_{ll} \cdot (\bar{r} - \bar{r}')}}}{k_0^2 k_{zll}^u} \right) \quad (2.2-14)$$

For $z < z'$

$$\bar{\bar{G}}(\bar{r}, \bar{r}') = -\frac{\omega\mu_0}{8\pi^2} \int_{-\infty}^{\infty} \int_{-\infty}^{\infty} dk_x dk_y \left(\frac{\hat{e}_l^d \hat{e}_l^d e^{i\bar{k}_l \cdot (\bar{r} - \bar{r}')}}{k_{zl}^d} + \frac{\left(k_0^2 + k_\rho^2 \frac{\varepsilon_1 - \varepsilon_{1z}}{(\varepsilon_{1z})^2} \right) \hat{e}_{ll}^d \hat{e}_{ll}^d e^{i\bar{k}_{ll} \cdot (\bar{r} - \bar{r}')}}}{k_0^2 k_{zll}^d} \right)$$

The eigenvectors can then be obtained from the characteristic equation with the corresponding eigenvalues substituted into the equation. The detailed derivation is given below. First, it is shown that the adjoint matrices for Type I upward and downward waves are the same and take the following form.

$$\overline{\overline{\text{adj}W_E}}(k_{zl}^d) = \overline{\overline{\text{adj}W_E}}(k_{zl}^u) = \begin{bmatrix} A_{11} & A_{12} & 0 \\ A_{21} & A_{22} & 0 \\ 0 & 0 & 0 \end{bmatrix} \quad (2.2-15)$$

where

$$A_{11} = k_0^2(\varepsilon_{1z} - \varepsilon_1)k_y^2, A_{12} = A_{21} = k_0^2(\varepsilon_1 - \varepsilon_{1z})k_x k_y, A_{22} = k_0^2(\varepsilon_{1z} - \varepsilon_1)k_x^2$$

The adjoint matrix can be simplified by extracting $k_0^2(\varepsilon_{1z} - \varepsilon_1)$ as follows.

$$\overline{\overline{\text{adj}W_E}}(k_{zl}^d) = \overline{\overline{\text{adj}W_E}}(k_{zl}^u) = k_0^2(\varepsilon_{1z} - \varepsilon_1) \begin{bmatrix} k_y^2 & -k_x k_y & 0 \\ -k_x k_y & k_x^2 & 0 \\ 0 & 0 & 0 \end{bmatrix} \quad (2.2-16)$$

Also, it is known from Eq. (2.2-11) that the eigenvalues are the same for both the upward and downward adjoint wave matrices. The eigenvectors $\hat{e}_l^u = \hat{e}_l^d$ can be solved from the following equation and it is easily seen that the eigenvectors for upward and downward propagating waves are the same.

$$\begin{aligned} \text{Step 1: } & \overline{\overline{\text{adj}W_E}}(k_{zl}^u)\hat{e}_l^u = \lambda_{zl}^u \hat{e}_l^u \\ \text{Step 2: } & k_0^2(\varepsilon_{1z} - \varepsilon_1) \begin{bmatrix} k_y^2 & -k_x k_y & 0 \\ -k_x k_y & k_x^2 & 0 \\ 0 & 0 & 0 \end{bmatrix} \begin{bmatrix} e_{lx}^u \\ e_{ly}^u \\ e_{lz}^u \end{bmatrix} = k_\rho^2 k_0^2(\varepsilon_{1z} - \varepsilon_1) \begin{bmatrix} e_{lx}^u \\ e_{ly}^u \\ e_{lz}^u \end{bmatrix} \\ \text{Step 3: } & e_{lx}^u = \frac{k_y}{k_\rho}, e_{ly}^u = -\frac{k_x}{k_\rho}, e_{lz}^u = 0 \end{aligned} \quad (2.2-17)$$

When denoting $\bar{k}_l^u = \hat{x}k_x + \hat{y}k_y + \hat{z}k_{zl}^u$, $\bar{k}_l^d = \hat{x}k_x + \hat{y}k_y + \hat{z}k_{zl}^d$, it is easily verified that the vectors of Type I waves agree with the formulations of vectors shown in [35].

$$\hat{e}_l^u = \frac{\hat{z} \times \bar{k}_l^u}{\sqrt{(\hat{z} \times \bar{k}_l^u)^2}}, \quad \hat{e}_l^d = \hat{e}_l^u = \frac{\hat{z} \times \bar{k}_l^d}{\sqrt{(\hat{z} \times \bar{k}_l^d)^2}} \quad (2.2-18)$$

It's easy to observe from Eq. (2.2-18) that the Type I wave is polarized along the direction that is perpendicular to the optic axis and the wave vector, which is denoted as an *ordinary wave*.

Now, let's consider the Type II wave. Different from the Type I wave, the adjoint matrices for the upward and downward Type II waves exhibit two different forms, though the eigenvalues for both waves are the same as seen from Eq. (2.2-12). The adjoint matrices are first derived here for both of the Type II upward and downward waves.

$$\overline{\overline{adjW}}_E(k_{zII}^{d(u)}) = \begin{bmatrix} A_{11}(k_{zII}^{d(u)}) & A_{12}(k_{zII}^{d(u)}) & A_{13}(k_{zII}^{d(u)}) \\ A_{21}(k_{zII}^{d(u)}) & A_{22}(k_{zII}^{d(u)}) & A_{23}(k_{zII}^{d(u)}) \\ A_{31}(k_{zII}^{d(u)}) & A_{32}(k_{zII}^{d(u)}) & A_{33}(k_{zII}^{d(u)}) \end{bmatrix}$$

where

$$\begin{aligned} A_{11}(k_{zII}^d) &= A_{11}(k_{zII}^u) = -\frac{\varepsilon_{1z}}{\varepsilon_1} \left(1 - \frac{\varepsilon_1}{\varepsilon_{1z}}\right) k_{zII}^2 k_x^2 \\ A_{22}(k_{zII}^d) &= A_{22}(k_{zII}^u) = -\frac{\varepsilon_{1z}}{\varepsilon_1} \left(1 - \frac{\varepsilon_1}{\varepsilon_{1z}}\right) k_{zII}^2 k_y^2 \\ A_{33}(k_{zII}^d) &= A_{33}(k_{zII}^u) = k_\rho^2 \left(1 - \frac{\varepsilon_1}{\varepsilon_{1z}}\right) \left(-\frac{\varepsilon_1}{\varepsilon_{1z}} k_\rho^2\right) \\ A_{12}(k_{zII}^d) &= A_{21}(k_{zII}^d) = A_{12}(k_{zII}^u) = A_{21}(k_{zII}^u) = -\frac{\varepsilon_{1z}}{\varepsilon_1} \left(1 - \frac{\varepsilon_1}{\varepsilon_{1z}}\right) (k_{zII}^d)^2 k_x k_y \\ A_{13}(k_{zII}^d) &= A_{31}(k_{zII}^d) = -A_{12}(k_{zII}^u) = -A_{21}(k_{zII}^u) = \left(1 - \frac{\varepsilon_1}{\varepsilon_{1z}}\right) k_\rho^2 k_x k_{zII}^d \\ A_{23}(k_{zII}^d) &= A_{32}(k_{zII}^d) = -A_{23}(k_{zII}^u) = -A_{32}(k_{zII}^u) = \left(1 - \frac{\varepsilon_1}{\varepsilon_{1z}}\right) k_\rho^2 k_y k_{zII}^d \end{aligned} \tag{2.2-19}$$

Then the eigenvectors for the upward and downward Type II waves derived from the adjoint matrix are shown below.

$$\hat{e}_{II}^d = \begin{bmatrix} e_{IIx}^d \\ e_{IIy}^d \\ e_{IIz}^d \end{bmatrix} = \begin{bmatrix} \frac{k_x k_{zII}^d}{k_\rho \sqrt{(k_{zII}^d)^2 + \varepsilon_1^2 k_\rho^2 / \varepsilon_{1z}^2}} \\ \frac{k_y k_{zII}^d}{k_\rho \sqrt{(k_{zII}^d)^2 + \varepsilon_1^2 k_\rho^2 / \varepsilon_{1z}^2}} \\ -\frac{\varepsilon_1}{\varepsilon_{1z}} \frac{k_\rho}{\sqrt{(k_{zII}^d)^2 + \varepsilon_1^2 k_\rho^2 / \varepsilon_{1z}^2}} \end{bmatrix}, \quad \hat{e}_{II}^u = \begin{bmatrix} e_{IIx}^u \\ e_{IIy}^u \\ e_{IIz}^u \end{bmatrix} = \begin{bmatrix} \frac{k_x k_{zII}^u}{k_\rho \sqrt{(k_{zII}^u)^2 + \varepsilon_1^2 k_\rho^2 / \varepsilon_{1z}^2}} \\ \frac{k_y k_{zII}^u}{k_\rho \sqrt{(k_{zII}^u)^2 + \varepsilon_1^2 k_\rho^2 / \varepsilon_{1z}^2}} \\ -\frac{\varepsilon_1}{\varepsilon_{1z}} \frac{k_\rho}{\sqrt{(k_{zII}^u)^2 + \varepsilon_1^2 k_\rho^2 / \varepsilon_{1z}^2}} \end{bmatrix} \quad (2.2-20)$$

It is easily observed from Eq. (2.2-20) that the eigenvectors for the upward and the downward propagating waves satisfy the following relations when the optic axis of the uniaxial medium is along the z-axis.

$$e_{IIx}^d = -e_{IIx}^u, \quad e_{IIy}^d = -e_{IIy}^u, \quad e_{IIz}^d = e_{IIz}^u \quad (2.2-21)$$

Eq. (2.2-21) agrees with the result obtained in [35]. Also, when denoting wave vectors

$\bar{k}_{II}^u = \hat{x}k_x + \hat{y}k_y + \hat{z}k_{zII}^u$ and $\bar{k}_{II}^d = \hat{x}k_x + \hat{y}k_y + \hat{z}k_{zII}^d$, multiplying the wave vectors \bar{k}_{II}^u and \bar{k}_{II}^d for the upward and downward waves with the corresponding electric field vectors of Eq. (2.2-20) shows that,

$$\begin{aligned} \hat{e}_{II}^u \cdot \bar{k}_{II}^u &\neq 0 & \hat{e}_{II}^d \cdot \bar{k}_{II}^d &\neq 0 \\ \bar{\varepsilon} \hat{e}_{II}^u \cdot \bar{k}_{II}^u &= 0 & \bar{\varepsilon} \hat{e}_{II}^d \cdot \bar{k}_{II}^d &= 0 \end{aligned} \quad (2.2-22)$$

As shown in Eq. (2.2-22) that the displacement vector \bar{D} instead of the electric field is perpendicular to the wave vector for Type II wave, which is denoted as an *extraordinary wave*. The polarizations of both ordinary (Type I) and extraordinary (Type II) waves are shown in Fig. 2-1. For Type I wave (ordinary wave), the \bar{E} field is polarized perpendicular to the plane formed by the optic axis and the wave vector as shown in Fig. 2-1(a). For Type II wave (extraordinary

wave), the \vec{E} field is polarized in the plane formed by the optic axis and the wave vector as shown in Fig. 2-1(b).

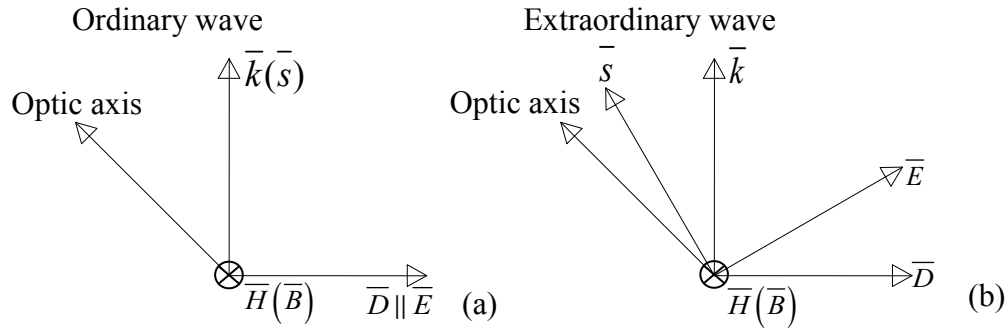


Fig. 2-1: Two different polarizations of plane waves in uniaxial medium: (a) Type I (ordinary wave) and (b) Type II (extraordinary wave).

Limiting Case of Isotropic Medium:

If $\varepsilon_1 = \varepsilon_{1z} = 1$, then the uniaxial medium reduces to an isotropic medium. From the dispersion relation of the isotropic medium, it is easily seen that the z component of the wave vector will satisfy the following equation.

$$k_{zl}^d = k_{zll}^d = -k_{0z}, \quad k_{zl}^u = k_{zll}^u = k_{0z} \quad (2.2-23)$$

When $\vec{k}_0^u = \hat{x}k_x + \hat{y}k_y + \hat{z}k_{0z}$, $\vec{k}_0^d = \hat{x}k_x + \hat{y}k_y - \hat{z}k_{0z}$ (2.2-24)

the adjoint matrix for an isotropic medium becomes zero:

$$\overline{\overline{adjW}}_E = 0 \quad (2.2-25)$$

Thus, the dyadic Green's function can no longer be obtained from the adjoint matrix directly. However, it can be obtained by letting $\varepsilon_1 = \varepsilon_{1z} = 1$ into the dyadic Green's function of Eq. (2.2-14) for the uniaxial medium. They can be rewritten for the isotropic case as follows.

For $z > z'$

$$\overline{\overline{G}}(\vec{r}, \vec{r}') = -\frac{\omega\mu_0}{8\pi^2} \int_{-\infty}^{\infty} \int_{-\infty}^{\infty} dk_x dk_y \left(\frac{\hat{e}_I^u \hat{e}_I^u}{k_{0z}} + \frac{\hat{e}_{II}^u \hat{e}_{II}^u}{k_{0z}} \right) e^{ik_0^u \cdot (\vec{r} - \vec{r}')} \quad (2.2-26)$$

For $z < z'$

$$\overline{\overline{G}}(\vec{r}, \vec{r}') = -\frac{\omega\mu_0}{8\pi^2} \int_{-\infty}^{\infty} \int_{-\infty}^{\infty} dk_x dk_y \left(\frac{\hat{e}_I^d \hat{e}_I^d}{k_{0z}} + \frac{\hat{e}_{II}^d \hat{e}_{II}^d}{k_{0z}} \right) e^{ik_0^d \cdot (\vec{r} - \vec{r}')} \quad (2.2-27)$$

In the equations above, the eigenvectors $\hat{e}_I^d, \hat{e}_I^u, \hat{e}_{II}^d, \hat{e}_{II}^u$ are defined below.

$$\begin{aligned} \hat{e}_I^d &= \hat{e}_I^u = \frac{\hat{z} \times \overline{\hat{k}}_0^d}{\sqrt{(\hat{z} \times \overline{\hat{k}}_0^d)^2}} \\ \hat{e}_{II}^d &= \hat{x}e_{IIx}^d + \hat{y}e_{IIy}^d + \hat{z}e_{IIz}^d, \quad \hat{e}_{II}^u = \hat{x}e_{IIx}^u + \hat{y}e_{IIy}^u + \hat{z}e_{IIz}^u, \end{aligned} \quad (2.2-28)$$

where

$$e_{IIx}^u = -e_{IIx}^d = \frac{k_x k_{0z}}{k_\rho k_0}, \quad e_{IIy}^u = -e_{IIy}^d = \frac{k_y k_{0z}}{k_\rho k_0}, \quad e_{IIz}^u = e_{IIz}^d = -\frac{k_\rho}{k_0}$$

Defining

$$\begin{aligned} \hat{h}_0^\pm &= \hat{h}_0(\pm k_{0z}) = \frac{\hat{z} \times \overline{\hat{k}}_0^u}{k_\rho} = \frac{\hat{y}k_x - \hat{x}k_y}{\sqrt{k_x^2 + k_y^2}} \\ \hat{v}_0^+ &= \hat{v}_0(+k_{0z}) = \frac{\hat{h}_0(+k_{0z}) \times \overline{\hat{k}}_0^u}{k_0}, \quad \hat{v}_0^- = \hat{v}_0(-k_{0z}) = \frac{\hat{h}_0(-k_{0z}) \times \overline{\hat{k}}_0^d}{k_0} \end{aligned} \quad (2.2-29)$$

it is easily verified that

$$\hat{e}_I^d = \hat{e}_I^u = \hat{h}_0^+ = \hat{h}_0^-, \quad \hat{v}_0^+ = \hat{e}_{II}^u, \hat{v}_0^- = \hat{e}_{II}^d \quad (2.2-30)$$

As shown in the equation above, the $\overline{\overline{E}}$ field of Type I wave is perpendicular to the plane of incidence indicating *horizontally polarized* wave in an isotropic medium, and the $\overline{\overline{E}}$ field of

Type II wave is parallel to the plane of incidence and perpendicular to the wave vector, indicating *vertically polarized* wave in an isotropic medium. It is noted here that in this case $\overline{\overline{D}}$ and $\overline{\overline{E}}$ are in the same direction. The dyadic Green's function for an isotropic medium can be obtained as follows with \hat{h} and \hat{v} defined in Eq. (2.2-29). This result is consistent with the result shown in [69], which is repeated in Eq. (2.2-31).

For $z < z'$

$$\overline{\overline{G}}(\vec{r}, \vec{r}') = -\frac{\omega\mu_0}{8\pi^2} \int_{-\infty}^{\infty} \int_{-\infty}^{\infty} \frac{1}{k_{0z}} dk_x dk_y \left(\hat{h}_0^- \hat{h}_0^- e^{i\vec{k}_0^d \cdot (\vec{r} - \vec{r}')} + \hat{v}_0^- \hat{v}_0^- e^{i\vec{k}_0^d \cdot (\vec{r} - \vec{r}')} \right)$$

For $z > z'$

$$\overline{\overline{G}}(\vec{r}, \vec{r}') = -\frac{\omega\mu_0}{8\pi^2} \int_{-\infty}^{\infty} \int_{-\infty}^{\infty} \frac{1}{k_{0z}} dk_x dk_y \left(\hat{h}_0^+ \hat{h}_0^+ e^{i\vec{k}_0^u \cdot (\vec{r} - \vec{r}')} + \hat{v}_0^+ \hat{v}_0^+ e^{i\vec{k}_0^u \cdot (\vec{r} - \vec{r}')} \right) \quad (2.2-31)$$

The derivation in this section analytically shows that the eigen-decomposition of $\overline{\overline{adjW}}_E$ into a single dyad holds for the uniaxial medium. The dyads in the DGFs are composed of two eigenvectors corresponding to the ordinary and extraordinary waves, respectively.

As stated in Section 2.1, $\overline{\overline{adjW}}_E$ can always be decomposed into a single dyad composed of the eigenvector corresponding to the non-zero eigenvalue of $\overline{\overline{adjW}}_E$ since the adjoint electric wave matrix is always symmetric for an unbounded uniaxial medium or biaxial medium with an arbitrarily rotated optic axis. Thus, the DGFs are expressed in Eq. (2.2-32). In Eq. (2.2-32), $\lambda(k_{zp}^q)$ and $\hat{e}(k_{zp}^q)$ stand for the eigenvalue and eigenvectors of the adjoint matrix $\overline{\overline{adjW}}_E(k_{zp}^q)$, where $q = u, d$, $p = I, II$. a_4 stands for the coefficient of the fourth order polynomial of k_z in the expansion of $\left| \overline{\overline{W}}_E \right|$. It is expected that for a biaxial medium $\hat{e}(k_{zI}^u)$ and $\hat{e}(k_{zI}^d)$ correspond to

the upward and downward ‘a’ waves, and $\hat{e}(k_{z1}^u)$ and $\hat{e}(k_{z1}^d)$ correspond to the upward and downward ‘b’ waves in [36-37].

For $z < z'$

$$\bar{\bar{G}}(\bar{r}, \bar{r}') = -\frac{\omega\mu_0}{(2\pi)^2} \int_{-\infty}^{\infty} \int_{-\infty}^{\infty} \left(\frac{\lambda(k_{z1}^d)\hat{e}(k_{z1}^d)\hat{e}(k_{z1}^d)}{a_4(k_{z1}^d - k_{z1}^u)(k_{z1}^d - k_{z1}^u)(k_{z1}^d - k_{z1}^d)} e^{ik_{z1}^d \cdot (\bar{r} - \bar{r}')} + \frac{\lambda(k_{z1}^d)\hat{e}(k_{z1}^d)\hat{e}(k_{z1}^d)}{a_4(k_{z1}^d - k_{z1}^d)(k_{z1}^d - k_{z1}^u)(k_{z1}^d - k_{z1}^u)} e^{ik_{z1}^d \cdot (\bar{r} - \bar{r}')} \right) dk_x dk_y$$

For $z > z'$

(2.2-32)

$$\bar{\bar{G}}(\bar{r}, \bar{r}') = \frac{\omega\mu_0}{(2\pi)^2} \int_{-\infty}^{\infty} \int_{-\infty}^{\infty} \left(\frac{\lambda(k_{z1}^u)\hat{e}(k_{z1}^u)\hat{e}(k_{z1}^u)}{a_4(k_{z1}^u - k_{z1}^d)(k_{z1}^u - k_{z1}^u)(k_{z1}^u - k_{z1}^d)} e^{ik_{z1}^u \cdot (\bar{r} - \bar{r}')} + \frac{\lambda(k_{z1}^u)\hat{e}(k_{z1}^u)\hat{e}(k_{z1}^u)}{a_4(k_{z1}^u - k_{z1}^d)(k_{z1}^u - k_{z1}^u)(k_{z1}^u - k_{z1}^d)} e^{ik_{z1}^u \cdot (\bar{r} - \bar{r}')} \right) dk_x dk_y$$

2.3 DGFs of an Unbounded Gyrotropic Medium

2.3.1 DGFs of a Gyroelectric Medium

If the medium is characterized by the relative permittivity tensor in the following form, it is called a gyroelectric medium.

$$\bar{\bar{\varepsilon}} = \varepsilon_{\perp} (\bar{I} - \hat{b}_0 \hat{b}_0) + i\varepsilon_g (\hat{b}_0 \times \bar{I}) + \varepsilon_{//} \hat{b}_0 \hat{b}_0 \quad (2.3-1)$$

where \hat{b}_0 shows the direction of the applied constant (dc) magnetic field

When the biasing magnetic field direction is along \hat{z} direction, i.e., $\hat{b}_0 = \hat{z}$, the above tensor form can be written in the following matrix form.

$$\underline{\underline{\varepsilon}}_p = \begin{bmatrix} \varepsilon_{\perp} & -i\varepsilon_g & 0 \\ i\varepsilon_g & \varepsilon_{\perp} & 0 \\ 0 & 0 & \varepsilon_{//} \end{bmatrix} \quad (2.3-2)$$

For example, if the medium is cold plasma which is a gyroelectric medium, then the relative permittivity tensor parameters are given as

$$\varepsilon_{\perp} = 1 - \frac{\omega_p^2}{\omega^2 - \omega_b^2}, \quad \varepsilon_g = -\frac{\omega_b \omega_p^2}{\omega(\omega^2 - \omega_b^2)}, \quad \varepsilon_{//} = 1 - \frac{\omega_p^2}{\omega^2}$$

$$\omega_b = -\frac{eB_0}{m}, \quad \omega_p = \sqrt{\frac{N_0 e^2}{m\varepsilon_0}} \quad (2.3-3)$$

ω_b is called the gyrofrequency or cyclotron frequency and ω_p is called the plasma frequency.

N_0 shows the number of free electrons per unit volume, and m represents the mass of each electron with charge e (a negative number).

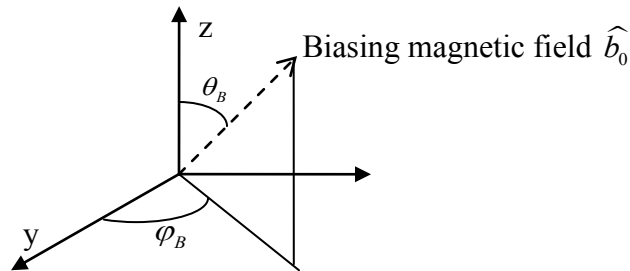


Fig. 2-2: Arbitrary biasing magnetic field in the xyz coordinate

However, if the biasing magnetic field is rotated by θ_B with respect to the z -axis and φ_B with respect to the x -axis in the Cartesian coordinate system as shown in Fig. 2-2, the permittivity tensor will have nine non-zero elements. The matrix elements ε_{mn} ($m, n = x, y, z$) are derived according to the transformation matrix as follows.

$$\overline{\overline{\varepsilon}}_c = T^{-1} \overline{\overline{\varepsilon}}_p T = \begin{bmatrix} \varepsilon_{xx} & \varepsilon_{xy} & \varepsilon_{xz} \\ \varepsilon_{yx} & \varepsilon_{yy} & \varepsilon_{yz} \\ \varepsilon_{zx} & \varepsilon_{zy} & \varepsilon_{zz} \end{bmatrix}, \quad T = \begin{bmatrix} \sin \varphi_B & -\cos \varphi_B & 0 \\ \cos \theta_B \cos \varphi_B & \cos \theta_B \sin \varphi_B & -\sin \theta_B \\ \sin \theta_B \cos \varphi_B & \sin \theta_B \sin \varphi_B & \cos \theta_B \end{bmatrix} \quad (2.3-4)$$

The DGFs for the two different cases – one with the biasing magnetic field along the z-direction and one with an arbitrary direction of θ_B and φ_B are derived in this section.

A. Z-oriented Biasing Magnetic Field

First, we consider the case when the biasing magnetic field is along the z-axis. Then, the relative permittivity takes the form of Eq. (2.3-3). The determinant of the electric wave matrix is written as follows.

$$\left| \overline{\overline{W}}_E \right| = \begin{vmatrix} k_o^2 \varepsilon_{\perp} - k_y^2 - k_z^2 & k_x k_y - i \varepsilon_g k_o^2 & k_x k_z \\ k_x k_y + i \varepsilon_g k_o^2 & k_o^2 \varepsilon_{\perp} - k_x^2 - k_z^2 & k_y k_z \\ k_x k_z & k_y k_z & k_o^2 \varepsilon_{\parallel} - k_x^2 - k_y^2 \end{vmatrix} = 0 \quad (2.3-5)$$

Expansion of $\left| \overline{\overline{W}}_E \right|$ leads to the fourth order equation in k_z as follows.

$$\begin{aligned} \left| \overline{\overline{W}}_E \right| &= a k_z^4 + b k_z^2 + c \\ a &= k_o^2 \varepsilon_{\parallel} \\ b &= k_o^2 (k_x^2 + k_y^2) (\varepsilon_{\perp} + \varepsilon_{\parallel}) - 2 k_o^4 \varepsilon_{\perp} \varepsilon_{\parallel} \\ c &= k_o^6 \varepsilon_{\parallel} (\varepsilon_{\perp}^2 - \varepsilon_g^2) - k_o^4 (k_x^2 + k_y^2) (\varepsilon_{\perp}^2 - \varepsilon_g^2 + \varepsilon_{\perp} \varepsilon_{\parallel}) + k_o^2 (k_x^2 + k_y^2)^2 \varepsilon_{\perp} \end{aligned} \quad (2.3-6)$$

When the biasing magnetic field is along the z-axis, two distinct sets of k_z exist to make the determinant of the electric wave matrix to be zero as shown in Eq. (2.3-7).

$$k_{zI} = \pm \sqrt{\frac{-b + \sqrt{b^2 - 4ac}}{2a}}, \quad k_{zII} = \pm \sqrt{\frac{-b - \sqrt{b^2 - 4ac}}{2a}} \quad (2.3-7)$$

Then the determinant of the electric wave matrix can be written as follows.

$$\left| \overline{\overline{W}}_E \right| = a(k_z^2 - k_{zI}^2)(k_z^2 - k_{zII}^2) = k_0^2 \varepsilon_{//} (k_z^2 - k_{zI}^2)(k_z^2 - k_{zII}^2) \quad (2.3-8)$$

Following the same procedure as described in Section 1.2, the DGF for the unbounded gyroelectric medium can be expressed as the dyad form which is obtained from the eigenvalue and eigenvectors of the adjoint matrix $adj(\overline{\overline{W}}_E)$ as follows.

$$adj \overline{\overline{W}}_E (\pm k_{zI}) = \begin{bmatrix} A_{11} & A_{12} & A_{13} \\ A_{21} & A_{22} & A_{23} \\ A_{31} & A_{32} & A_{33} \end{bmatrix}, \quad (2.3-9)$$

$$\begin{aligned} A_{11} &= k_I^2 k_x^2 - k_0^2 \left[\varepsilon_{\perp} (k_x^2 + k_y^2) + \varepsilon_{//} (k_x^2 + k_z^2) \right] + k_0^4 \varepsilon_{\perp} \varepsilon_{//} \\ A_{12} &= k_I^2 k_x k_y - k_0^2 \left[i \varepsilon_g (k_x^2 + k_y^2) + \varepsilon_{//} k_x k_y \right] + i k_0^4 \varepsilon_g \varepsilon_{//} \\ A_{13} &= k_I^2 k_x k_z - k_0^2 \left[\varepsilon_{\perp} k_x k_z + i \varepsilon_g k_y k_z \right] \\ A_{21} &= k_I^2 k_x k_y - k_0^2 \left[-i \varepsilon_g (k_x^2 + k_y^2) + \varepsilon_{//} k_x k_y \right] - i k_0^4 \varepsilon_g \varepsilon_{//} \\ A_{22} &= k_I^2 k_y^2 - k_0^2 \left[\varepsilon_{\perp} (k_x^2 + k_y^2) + \varepsilon_{//} (k_y^2 + k_z^2) \right] + k_0^4 \varepsilon_{\perp} \varepsilon_{//} \\ A_{23} &= k_I^2 k_y k_z - k_0^2 \left[\varepsilon_{\perp} k_y k_z - i \varepsilon_g k_x k_z \right] \\ A_{31} &= k_I^2 k_x k_z - k_0^2 \left[\varepsilon_{\perp} k_x k_z - i \varepsilon_g k_y k_z \right] \\ A_{32} &= k_I^2 k_y k_z - k_0^2 \left[\varepsilon_{\perp} k_y k_z + i \varepsilon_g k_x k_z \right] \\ A_{33} &= k_I^2 k_z^2 - k_0^2 \left[\varepsilon_{\perp} (k_x^2 + k_y^2 + 2k_z^2) \right] + k_0^4 \left[\varepsilon_{\perp}^2 - \varepsilon_g^2 \right] \end{aligned}$$

In Eq. (2.3-9), $k_I^2 = k_{\rho}^2 + k_{zI}^2$ and it represents the wave number of the Type I wave.

Substituting k_I^2 with k_{II}^2 will give the adjoint wave matrix for Type II wave. It needs to be noted

here that $A_{21} = A_{12}^*$ always holds as long as k_x and k_y are real. However, relation of

$A_{31} = A_{13}^*$, $A_{32} = A_{23}^*$ does not necessary hold and it depends on the choice of k_z . According to

Section 1.2, the adjoint wave matrix can be decomposed into the following dyad form if the matrix is a hermitian matrix.

$$\begin{aligned}
adj\overline{\overline{W}}_E(\pm k_{zI}) &= \lambda_I \left[\hat{e}_{nI}(\pm k_{zI}) \hat{e}_{nI}^*(\pm k_{zI}) \right], & adj\overline{\overline{W}}_E(\pm k_{zII}) &= \lambda_{II} \left[\hat{e}_{nII}(\pm k_{zII}) \hat{e}_{nII}^*(\pm k_{zII}) \right] \\
\lambda_I &= k_I^4 - k_I^2 k_0^2 (3\varepsilon_{\perp} + \varepsilon_{//}) - k_{zI}^2 k_0^2 (\varepsilon_{//} - \varepsilon_{\perp}) + k_0^4 (\varepsilon_{\perp}^2 - \varepsilon_g^2 + 2\varepsilon_{\perp} \varepsilon_{//}) \\
\lambda_{II} &= k_{II}^4 - k_{II}^2 k_0^2 (3\varepsilon_{\perp} + \varepsilon_{//}) - k_{zII}^2 k_0^2 (\varepsilon_{//} - \varepsilon_{\perp}) + k_0^4 (\varepsilon_{\perp}^2 - \varepsilon_g^2 + 2\varepsilon_{\perp} \varepsilon_{//})
\end{aligned} \tag{2.3-10}$$

Derivation of the eigenvector is shown below.

$$\begin{bmatrix} A_{11} & A_{12} & A_{13} \\ A_{21} & A_{22} & A_{23} \\ A_{31} & A_{32} & A_{33} \end{bmatrix} \begin{bmatrix} e_1 \\ e_2 \\ e_3 \end{bmatrix} = \lambda \begin{bmatrix} e_1 \\ e_2 \\ e_3 \end{bmatrix} \longrightarrow \begin{cases} (A_{11} - \lambda)e_1 + A_{12}e_2 + A_{13}e_3 = 0 \rightarrow (a) \\ A_{21}e_1 + (A_{22} - \lambda)e_2 + A_{23}e_3 = 0 \rightarrow (b) \\ A_{31}e_1 + A_{32}e_2 + (A_{33} - \lambda)e_3 = 0 \rightarrow (c) \end{cases} \tag{2.3-11}$$

Eliminating e_3 from (a) and (b) in Eq. (2.3-11), we obtain

$$p_1 e_1 + p_2 e_2 = 0, \quad p_1 = (A_{11} - \lambda)A_{23} - A_{21}A_{13}, \quad p_2 = A_{11}A_{23} - (A_{22} - \lambda)A_{13}, \tag{2.3-12}$$

Eliminating e_1 from (b) and (c) in Eq. (2.3-11), we obtain

$$q_1 e_2 + q_2 e_3 = 0, \quad q_1 = (A_{22} - \lambda)A_{31} - A_{32}A_{21}, \quad q_2 = A_{31}A_{23} - (A_{33} - \lambda)A_{21} \tag{2.3-13}$$

Eliminating e_2 from (a) and (c) in Eq. (2.3-11), we obtain

$$s_1 e_1 + s_2 e_3 = 0, \quad s_1 = (A_{11} - \lambda)A_{32} - A_{31}A_{12}, \quad s_2 = A_{13}A_{32} - (A_{33} - \lambda)A_{12} \tag{2.3-14}$$

Four different cases should be considered here in calculating e_1, e_2, e_3 .

$$\text{Case I: } \begin{cases} p_1 = 0 \ \& \ p_2 \neq 0 \\ e_2 = 0, \quad \frac{e_1}{e_3} = -\frac{s_2}{s_1} \end{cases} \tag{2.3-15}$$

$$\text{Case II: } \begin{cases} p_1 \neq 0 \ \& \ p_2 = 0 \\ e_1 = 0, \quad \frac{e_2}{e_3} = -\frac{q_2}{q_1} \end{cases} \tag{2.3-16}$$

$$\text{Case III: } \begin{cases} p_1 \neq 0 \& p_2 \neq 0 \& q_1 = 0 \& q_2 \neq 0 \\ e_3 = 0, \quad \frac{e_1}{e_2} = -\frac{p_2}{p_1} \end{cases} \quad (2.3-17)$$

$$\text{Case IV: } \begin{cases} p_1 \neq 0 \& p_2 \neq 0 \& q_1 \neq 0 \& q_2 \neq 0 \\ e_1 = 1, \quad e_2 = -\frac{p_1}{p_2}, \quad e_3 = -\frac{s_1}{s_2}, \end{cases} \quad (2.3-18)$$

Substituting p_1, p_2, s_1, s_2 in Eqs. (2.3-12) and (2.3-14) gives the normalized $\hat{e}_{nl}(\pm k_{z_l})$ for case IV below.

$$\hat{e}_{nl}(\pm k_{z_l}) = \frac{\bar{e}_l(\pm k_{z_l})}{\text{norm}(\bar{e}_l(\pm k_{z_l}))}, \quad \bar{e}_l(\pm k_{z_l}) = \begin{bmatrix} 1 \\ \frac{A_{13}A_{21} + A_{23}\lambda_l - A_{23}A_{11}}{A_{23}A_{12} + A_{13}\lambda_l - A_{13}A_{22}} \\ -\frac{A_{12}}{A_{13}} \left[\frac{A_{13}A_{21} + A_{23}\lambda_l - A_{23}A_{11}}{A_{23}A_{12} + A_{13}\lambda_l - A_{13}A_{22}} \right] + \frac{\lambda_l - A_{11}}{A_{13}} \end{bmatrix} \quad (2.3-19)$$

$\text{norm}(\bar{e}_l(\pm k_{z_l})) = \sqrt{\text{conj}(\bar{e}_l(\pm k_{z_l}))^T \cdot \bar{e}_l(\pm k_{z_l})}$ is the square root of the inner product of the vector $\bar{e}_l(\pm k_{z_l})$ and itself.

Then the adjoint electric wave matrix can be expressed in terms of single dyad below.

$$\text{adj}\overline{\overline{W}}_E = \lambda_p \hat{e}_{np} \hat{v}_p, \quad p = I, II \quad (2.3-20)$$

If k_{zp} is real, then $\text{adj}\overline{\overline{W}}_E$ is a hermitian matrix.

$$\hat{v}_p = (\hat{e}_{np})^* \quad (2.3-21)$$

It is noted here that Eq. (2.3-19) and Eq. (2.3-21) agree with the results obtained in Eroglu and Lee [38]. However, the results obtained in [38] state that the DGF for a gyroelectric medium

always take the form of Eq. (2.3-21), which is not true. As discussed in detail in Section 2.1, if

k_{zp} is real, then $\overline{\overline{adjW}}_E$ is no longer a hermitian matrix, and the vector \hat{v}_p in Eq. (2.3-20) takes

the following form.

$$\hat{v}_p = [v_{p1} \quad v_{p2} \quad v_{p3}], \quad v_{p1} = \frac{A_{11}}{\lambda_p e_{p1}}, \quad v_{p2} = \frac{A_{12}}{\lambda_p e_{p1}}, \quad v_{p3} = \frac{A_{13}}{\lambda_p e_{p1}} \quad (2.3-22)$$

Substituting Eq. (2.3-8) into Eq. (2.1-4) gives

$$\overline{\overline{G}}(\bar{r}, \bar{r}') = \frac{-i\omega\mu_0}{(2\pi)^3} \int_{-\infty}^{\infty} \frac{\overline{\overline{adjW}}_E}{k_0^2 \varepsilon_{//} (k_z^2 - k_{z1}^2)(k_z^2 - k_{z11}^2)} e^{i\bar{k} \cdot (\bar{r} - \bar{r}')} d^3 \bar{k} \quad (2.3-23)$$

Applying the residue theorem and the radiation boundary condition at infinity, the 3D integration can be reduced to 2D integration by integrating over k_z . Thus in each region, the DGF is obtained as follows.

For $z > z'$

$$\overline{\overline{G}}(\bar{r}, \bar{r}') = \frac{\omega\mu_0}{8\pi^2} \int_{-\infty}^{\infty} \int_{-\infty}^{\infty} dk_x dk_y \left\{ \frac{1}{k_0^2 \varepsilon_{//} (k_{z1}^2 - k_{z11}^2)} \left[\frac{\lambda_I \left[\hat{e}_{nI}(k_{z1}) \hat{e}_{nI}^*(k_{z1}) \right]}{k_{z1}} e^{i\bar{k}_I \cdot (\bar{r} - \bar{r}')} \right. \right. \\ \left. \left. - \frac{\lambda_{II} \left[\hat{e}_{nII}(k_{z11}) \hat{e}_{nII}^*(k_{z11}) \right]}{k_{z11}} e^{i\bar{k}_{II} \cdot (\bar{r} - \bar{r}')} \right] \right\}$$

For $z < z'$

$$\overline{\overline{G}}(\bar{r}, \bar{r}') = \frac{-\omega\mu_0}{8\pi^2} \int_{-\infty}^{\infty} \int_{-\infty}^{\infty} dk_x dk_y \left\{ \frac{1}{k_0^2 \varepsilon_{//} (k_{z1}^2 - k_{z11}^2)} \left[\frac{\lambda_I \left[\hat{e}_{nI}(-k_{z1}) \hat{e}_{nI}^*(-k_{z1}) \right]}{k_{z1}} e^{i\bar{k}_I \cdot (\bar{r} - \bar{r}')} \right. \right. \\ \left. \left. - \frac{\lambda_{II} \left[\hat{e}_{nII}(-k_{z11}) \hat{e}_{nII}^*(-k_{z11}) \right]}{k_{z11}} e^{i\bar{k}_{II} \cdot (\bar{r} - \bar{r}')} \right] \right\} \quad (2.3-24)$$

In the above formulas, the wave propagation vectors are defined as follows.

$$\begin{aligned} \overline{k}_I &= \hat{x}k_x + \hat{y}k_x + \hat{z}k_{zI} & \overline{\kappa}_I &= \hat{x}k_x + \hat{y}k_x - \hat{z}k_{zI} \\ \overline{k}_{II} &= \hat{x}k_x + \hat{y}k_x + \hat{z}k_{zII} & \overline{\kappa}_{II} &= \hat{x}k_x + \hat{y}k_x - \hat{z}k_{zII} \end{aligned} \quad (2.3-25)$$

It is seen from above formula that if the biasing magnetic field is along the z-axis, the Type I upward and downward waves will have z component of wave vectors of the same magnitude and opposite sign. If the biasing magnetic field is oriented along an arbitrary direction, then this will be no longer the case.

B. Arbitrarily Directed Biasing Magnetic Field

Assuming the biasing magnetic field is along an arbitrary direction of θ_B and φ_B , the permittivity takes the form of Eq. (2.3-4). $\left| \overline{W}_E \right|$ can then be expanded in terms of k_z as follows.

$$\begin{aligned} \left| \overline{W}_E \right| &= a_4 k_z^4 + a_3 k_z^3 + a_2 k_z^2 + a_1 k_z + a_0, \\ a_4 &= k_0^2 (\varepsilon_{\perp} \sin^2 \theta_B + \varepsilon_{//} \cos^2 \theta_B) \\ a_3 &= 2k_0^2 (\varepsilon_{//} - \varepsilon_{\perp}) (k_x \cos \varphi_B + k_y \sin \varphi_B) \sin \theta_B \cos \theta_B \\ a_2 &= k_0^2 (\varepsilon_{\perp} [k_{\rho}^2 \cos^2 \theta_B + (k_x \sin \varphi_B - k_y \cos \varphi_B)^2 \sin^2 \theta_B] \\ &\quad + \varepsilon_{//} [(k_x \cos \varphi_B + k_y \sin \varphi_B)^2 \sin^2 \theta_B] \\ &\quad + [\varepsilon_{\perp} k_{\rho}^2 + (\varepsilon_g^2 - \varepsilon_{\perp}^2 - \varepsilon_{\perp} \varepsilon_{//}) k_o^2] \sin^2 \theta_B + \varepsilon_{//} (k_{\rho}^2 - 2\varepsilon_{\perp} k_o^2) \cos^2 \theta_B) \\ a_1 &= 2k_0^2 [(\varepsilon_{//} - \varepsilon_{\perp}) k_{\rho}^2 + (\varepsilon_{\perp}^2 - \varepsilon_g^2 - \varepsilon_{\perp} \varepsilon_{//}) k_o^2] (k_x \cos \varphi_B + k_y \sin \varphi_B) \sin \theta_B \cos \theta_B \\ a_0 &= k_0^2 [(\varepsilon_{//} - \varepsilon_{\perp}) k_{\rho}^2 + (\varepsilon_{\perp}^2 - \varepsilon_g^2 - \varepsilon_{\perp} \varepsilon_{//}) k_o^2] (k_x \cos \varphi_B + k_y \sin \varphi_B)^2 \sin^2 \theta_B \\ &\quad + (k_{\rho}^2 - \varepsilon_{//} k_o^2) [\varepsilon_{\perp} k_{\rho}^2 - (\varepsilon_{\perp}^2 - \varepsilon_x^2) k_o^2] \end{aligned} \quad (2.3-26)$$

Four distinct solutions of $k_{zI}^u, k_{zII}^u, k_{zI}^d, k_{zII}^d$ exist for a given set of k_x and k_y . The wave vectors with k_{zI}^u, k_{zII}^u correspond to upward Type I and Type II waves, while k_{zI}^d, k_{zII}^d correspond to downward Type I and Type II waves. Then the determinant of the electric wave matrix is written as

$$\left| \overline{\overline{W}}_E \right| = k_o^2 (\varepsilon_{\perp} \sin^2 \theta_B + \varepsilon_{//} \cos^2 \theta_B) (k_z - k_{z'}^u) (k_z - k_{z''}^u) (k_z - k_{z'}^d) (k_z - k_{z''}^d) \quad (2.3-27)$$

With k_z obtained, the electric wave matrix is given below.

$$\overline{\overline{W}}_E = \begin{bmatrix} k_o^2 \varepsilon_{xx} - k_y^2 - k_z^2 & k_x k_y + k_o^2 \varepsilon_{xy} & k_x k_z + k_o^2 \varepsilon_{xz} \\ k_x k_y + k_o^2 \varepsilon_{xy}^* & k_o^2 \varepsilon_{yy} - k_x^2 - k_z^2 & k_y k_z + k_o^2 \varepsilon_{yz} \\ k_x k_z + k_o^2 \varepsilon_{xz}^* & k_y k_z + k_o^2 \varepsilon_{yz}^* & k_o^2 \varepsilon_{zz} - k_x^2 - k_y^2 \end{bmatrix} \quad (2.3-28)$$

The adjoint matrix of the electric wave matrix takes the following form.

$$\text{adj} \overline{\overline{W}}_E = \begin{bmatrix} A_{11} & A_{12} & A_{13} \\ A_{21} & A_{22} & A_{23} \\ A_{31} & A_{32} & A_{33} \end{bmatrix} \quad (2.3-29)$$

where

$$\begin{aligned} A_{11} &= (k_{\rho}^2 + k_z^2) k_x^2 - k_o^2 \left[\varepsilon_{zz} (k_x^2 + k_z^2) + \varepsilon_{yy} (k_x^2 + k_y^2) \right] + k_o^4 (\varepsilon_{yy} \varepsilon_{zz} - \varepsilon_{yz} \varepsilon_{yz}^*) - k_y k_z k_o^2 (\varepsilon_{yz} + \varepsilon_{yz}^*) \\ A_{12} &= (k_{\rho}^2 + k_z^2) k_x k_y + k_o^2 \left[\varepsilon_{xy} (k_x^2 + k_y^2) - \varepsilon_{zz} k_x k_y \right] + k_o^2 (k_x k_z \varepsilon_{yz}^* + k_y k_z \varepsilon_{xz} + k_o^2 \varepsilon_{xz} \varepsilon_{yz}^*) - k_o^4 \varepsilon_{xy} \varepsilon_{zz} \\ A_{13} &= (k_{\rho}^2 + k_z^2) k_x k_z + k_o^2 \left[\varepsilon_{xy} k_y k_z - \varepsilon_{yy} k_x k_z \right] + k_o^2 \varepsilon_{yz} (k_x k_y + \varepsilon_{xy} k_o^2) + k_o^2 \varepsilon_{xz} (k_x^2 + k_z^2 - \varepsilon_{yy} k_o^2) \\ A_{21} &= (k_{\rho}^2 + k_z^2) k_x k_y + k_o^2 \left[\varepsilon_{xy}^* (k_x^2 + k_y^2) - \varepsilon_{zz} k_x k_y \right] + k_o^2 (k_x k_z \varepsilon_{yz} + k_y k_z \varepsilon_{xz}^* + k_o^2 \varepsilon_{xz}^* \varepsilon_{yz}) - k_o^4 \varepsilon_{xy}^* \varepsilon_{zz} \\ A_{22} &= (k_{\rho}^2 + k_z^2) k_y^2 - k_o^2 \left[\varepsilon_{zz} (k_y^2 + k_z^2) + \varepsilon_{xx} (k_x^2 + k_y^2) \right] + k_o^4 (\varepsilon_{xx} \varepsilon_{zz} - \varepsilon_{xz} \varepsilon_{xz}^*) - k_x k_z k_o^2 (\varepsilon_{xz} + \varepsilon_{xz}^*) \\ A_{23} &= (k_{\rho}^2 + k_z^2) k_y k_z - k_o^2 \left[\varepsilon_{xx} k_y k_z - \varepsilon_{xy}^* k_x k_z \right] + k_o^2 (\varepsilon_{xz} k_x k_y + \varepsilon_{yz} (k_y^2 + k_z^2)) + k_o^4 (\varepsilon_{xz} \varepsilon_{xy}^* - \varepsilon_{xx} \varepsilon_{yz}^*) \\ A_{31} &= (k_{\rho}^2 + k_z^2) k_x k_z + k_o^2 \left[\varepsilon_{xy}^* k_y k_z - \varepsilon_{yy} k_x k_z \right] + k_o^2 \varepsilon_{yz}^* (k_x k_y + \varepsilon_{xy}^* k_o^2) + k_o^2 \varepsilon_{xz}^* (k_x^2 + k_z^2 - \varepsilon_{yy} k_o^2) \\ A_{32} &= (k_{\rho}^2 + k_z^2) k_y k_z - k_o^2 \left[\varepsilon_{xx} k_y k_z - \varepsilon_{xy} k_x k_z \right] + k_o^2 (\varepsilon_{xz}^* k_x k_y + \varepsilon_{yz}^* (k_y^2 + k_z^2)) + k_o^4 (\varepsilon_{xz}^* \varepsilon_{xy} - \varepsilon_{xx} \varepsilon_{yz}^*) \\ A_{33} &= (k_{\rho}^2 + k_z^2) k_z^2 - k_o^2 \left[(\varepsilon_{xx} + \varepsilon_{yy}) k_z^2 + \varepsilon_{xx} k_x^2 + \varepsilon_{yy} k_y^2 \right] + k_o^4 (\varepsilon_{xx} \varepsilon_{yy} - \varepsilon_{xy} \varepsilon_{xy}^*) - k_x k_y k_o^2 (\varepsilon_{xy} + \varepsilon_{xy}^*) \end{aligned}$$

Applying Eq. (2.3-27) to the DGF of Eq. (2.1-4) gives the 3D integration form of the DGF.

$$\begin{aligned} \overline{\overline{G}}(\vec{r}, \vec{r}') &= \frac{-i\omega\mu_0}{(2\pi)^3} \int_{-\infty}^{\infty} \int_{-\infty}^{\infty} \int_{-\infty}^{\infty} \frac{\text{adj} \overline{\overline{W}}_E}{c(k_z - k_{z'}^u)(k_z - k_{z''}^u)(k_z - k_{z'}^d)(k_z - k_{z''}^d)} e^{i\vec{k} \cdot (\vec{r} - \vec{r}')} dk_x dk_y dk_z \\ c &= k_o^2 (\varepsilon_{\perp} \sin^2 \theta_B + \varepsilon_{//} \cos^2 \theta_B) \end{aligned} \quad (2.3-30)$$

Integrating Eq. (2.3-30) over k_z and applying residue theorem gives the DGF.

For $z < z'$

$$\overline{\overline{G}}(\bar{r}, \bar{r}') = -\frac{\omega\mu_0}{4\pi^2} \int_{-\infty}^{\infty} \int_{-\infty}^{\infty} dk_x dk_y \frac{1}{k_o^2 (\varepsilon_{\perp} \sin^2 \theta_B + \varepsilon_{//} \cos^2 \theta_B) (k_{zI}^d - k_{zII}^d)} \begin{pmatrix} \text{adj}(\overline{\overline{W}}_E(k_{zI}^d)) e^{i\bar{\kappa}_I \cdot (\bar{r} - \bar{r}')} \\ (k_{zI}^d - k_{zI}^u)(k_{zI}^d - k_{zII}^u) \\ \text{adj}(\overline{\overline{W}}_E(k_{zII}^d)) e^{i\bar{\kappa}_{II} \cdot (\bar{r} - \bar{r}')} \\ (k_{zII}^d - k_{zI}^u)(k_{zII}^d - k_{zII}^u) \end{pmatrix} \quad (2.3-31)$$

For $z > z'$

$$\overline{\overline{G}}(\bar{r}, \bar{r}') = \frac{\omega\mu_0}{4\pi^2} \int_{-\infty}^{\infty} \int_{-\infty}^{\infty} dk_x dk_y \frac{1}{k_o^2 (\varepsilon_{\perp} \sin^2 \theta_B + \varepsilon_{//} \cos^2 \theta_B) (k_{zI}^u - k_{zII}^u)} \begin{pmatrix} \text{adj}(\overline{\overline{W}}_E(k_{zI}^u)) e^{i\bar{\kappa}_I \cdot (\bar{r} - \bar{r}')} \\ (k_{zI}^u - k_{zI}^d)(k_{zI}^u - k_{zII}^d) \\ \text{adj}(\overline{\overline{W}}_E(k_{zII}^u)) e^{i\bar{\kappa}_{II} \cdot (\bar{r} - \bar{r}')} \\ (k_{zII}^u - k_{zI}^d)(k_{zII}^u - k_{zII}^d) \end{pmatrix} \quad (2.3-32)$$

$$\bar{k}_I = \hat{x}k_x + \hat{y}k_y + \hat{z}k_{zI}^u \quad \bar{\kappa}_I = \hat{x}k_x + \hat{y}k_y + \hat{z}k_{zI}^d; \quad \bar{k}_{II} = \hat{x}k_x + \hat{y}k_y + \hat{z}k_{zII}^u \quad \bar{\kappa}_{II} = \hat{x}k_x + \hat{y}k_y + \hat{z}k_{zII}^d$$

Again the adjoint matrix can be represented in the following dyadic form if k_{zp}^q is real.

$$\begin{aligned} \text{adj}\overline{\overline{W}}_E(k_{zI}^u) &= \lambda_I^u \left[\hat{e}_{nI}(k_{zI}^u) \hat{e}_{nI}^*(k_{zI}^u) \right], & \text{adj}\overline{\overline{W}}_E(k_{zII}^u) &= \lambda_{II}^u \left[\hat{e}_{nII}(k_{zII}^u) \hat{e}_{nII}^*(k_{zII}^u) \right] \\ \text{adj}\overline{\overline{W}}_E(k_{zI}^d) &= \lambda_I^d \left[\hat{e}_{nI}(k_{zI}^d) \hat{e}_{nI}^*(k_{zI}^d) \right], & \text{adj}\overline{\overline{W}}_E(k_{zII}^d) &= \lambda_{II}^d \left[\hat{e}_{nII}(k_{zII}^d) \hat{e}_{nII}^*(k_{zII}^d) \right] \end{aligned} \quad (2.3-33)$$

$$\lambda_p^q = (k_{\rho}^2 + (k_{zp}^q)^2)^2 - (k_{\rho}^2 + (k_{zp}^q)^2) k_o^2 (3\varepsilon_{\perp} + \varepsilon_{//}) - (k_{3p}^q)^2 k_o^2 (\varepsilon_{//} - \varepsilon_{\perp}) + k_o^4 (\varepsilon_{\perp}^2 - \varepsilon_{\rho}^2 + 2\varepsilon_{\perp} \varepsilon_{//})$$

$$k_{3p}^q = k_x \sin \theta_B \cos \varphi_B + k_y \sin \theta_B \sin \varphi_B + k_{zp}^q \cos \theta_B$$

The eigenvectors are shown below.

$$\hat{e}_n(k_{zp}^q) = \frac{\bar{e}(k_{zp}^q)}{\text{norm}(\bar{e}(k_{zp}^q))}, \quad \bar{e}(k_{zp}^q) = \begin{bmatrix} 1 \\ \frac{A_{13}A_{21} + A_{23}\lambda_p^q - A_{23}A_{11}}{A_{23}A_{12} + A_{13}\lambda_p^q - A_{13}A_{22}} \\ -\frac{A_{12}}{A_{13}} \left[\frac{A_{13}A_{21} + A_{23}\lambda_p^q - A_{23}A_{11}}{A_{23}A_{12} + A_{13}\lambda_p^q - A_{13}A_{22}} \right] + \frac{\lambda_p^q - A_{11}}{A_{13}} \end{bmatrix} \quad (2.3-34)$$

$$p = I, II, q = u, d,$$

It is noted here that the above eigenvectors are valid only for the case IV discussed previously.

2.3.2 DGFs of a Gyromagnetic Medium

A gyromagnetic medium is the medium characterized by the relative permittivity of ϵ_r and the relative permeability tensor $\overline{\overline{\mu}}_r$ in the following form.

$$\overline{\overline{\mu}}_r = \mu_{\perp} \left(\overline{\overline{I}} - \widehat{b}_0 \widehat{b}_0 \right) + i\mu_g (\widehat{b}_0 \times \overline{\overline{I}}) + \mu_{//} \widehat{b}_0 \widehat{b}_0 \quad (2.3-35)$$

When the biasing magnetic field direction is along \hat{z} direction, i.e., $\widehat{b}_0 = \hat{z}$ the above tensor form can be written in the following matrix form of $\overline{\overline{\mu}}_p$, which indicates the relative permeability in the principal coordinate system.

$$\overline{\overline{\mu}}_r = \overline{\overline{\mu}}_p = \begin{bmatrix} \mu_{\perp} & i\mu_g & 0 \\ -i\mu_g & \mu_{\perp} & 0 \\ 0 & 0 & \mu_{//} \end{bmatrix} \quad (2.3-36)$$

$$\mu_{\perp} = 1 - \frac{\omega_0 \omega_m}{\omega^2 - \omega_0^2}, \quad \mu_g = -\frac{\omega \omega_m}{\omega^2 - \omega_0^2}, \quad \mu_{//} = 1, \quad \omega_m = \gamma M_0, \quad \omega_0 = \gamma H_0$$

ω_m is defined as the Larmor precession frequency of the electron in the applied magnetic field H_0 and ω_0 is defined as the resonant frequency. M_0 is the saturated magnetization vector and is in the same direction as the applied magnetic field H_0 . γ is the gyromagnetic ratio and its value is given as $\gamma = 2.21 * 10^5 \left(\frac{rad}{s} \right) \left(\frac{m}{A \cdot turns} \right)$. If the biasing magnetic field is along an arbitrary direction, the permeability matrix will take the following form.

$$\overline{\overline{\mu}}_r = T^{-1} \overline{\overline{\mu}}_p T = \begin{bmatrix} \mu_{xx} & \mu_{xy} & \mu_{xz} \\ \mu_{yx} & \mu_{yy} & \mu_{yz} \\ \mu_{zx} & \mu_{zy} & \mu_{zz} \end{bmatrix}, \quad T = \begin{bmatrix} \sin \varphi_B & -\cos \varphi_B & 0 \\ \cos \theta_B \cos \varphi_B & \cos \theta_B \sin \varphi_B & -\sin \theta_B \\ \sin \theta_B \cos \varphi_B & \sin \theta_B \sin \varphi_B & \cos \theta_B \end{bmatrix} \quad (2.3-37)$$

With the permeability matrix of Eq. (2.3-37), the electric wave matrix is derived below.

$$\overline{\overline{W}}_E = \overline{\overline{\mu}}_r^{-1} \overline{\overline{k}} + k_0^2 \varepsilon_{1r} \overline{\overline{I}} =$$

$$\begin{bmatrix} a_{11} & a_{12} & a_{13} \\ a_{21} & a_{22} & a_{23} \\ a_{31} & a_{32} & a_{33} \end{bmatrix} = \begin{bmatrix} 0 & -k_z & k_y \\ k_z & 0 & -k_x \\ -k_y & k_x & 0 \end{bmatrix} \begin{bmatrix} \mu_{xx} & \mu_{xy} & \mu_{xz} \\ \mu_{yx} & \mu_{yy} & \mu_{yz} \\ \mu_{zx} & \mu_{zy} & \mu_{zz} \end{bmatrix}^{-1} \begin{bmatrix} 0 & -k_z & k_y \\ k_z & 0 & -k_x \\ -k_y & k_x & 0 \end{bmatrix} + k_0^2 \varepsilon_{1r} \overline{\overline{I}} \quad (2.3-38)$$

The determinant of the electric wave matrix $\overline{\overline{W}}_E$ can then be expanded in terms of k_z .

$$\left| \overline{\overline{W}}_E \right| = \frac{1}{\left| \overline{\overline{\mu}}_r \right|} (a_4 k_z^4 + a_3 k_z^3 + a_2 k_z^2 + a_1 k_z + a_0) \quad (2.3-39)$$

$$a_4 = k_0^2 \varepsilon_r (\mu_{\perp} \sin^2 \theta_B + \mu_{//} \cos^2 \theta_B)$$

$$a_3 = 2k_0^2 \varepsilon_r (\mu_{//} - \mu_{\perp}) (k_x \cos \varphi_B + k_y \sin \varphi_B) \sin \theta_B \cos \theta_B$$

$$a_2 = k_0^2 \varepsilon_r \{ \mu_{\perp} [k_{\rho}^2 \cos^2 \theta_B + (k_x \sin \varphi_B - k_y \cos \varphi_B)^2 \sin^2 \theta_B] + \mu_{//} [(k_x \cos \varphi_B + k_y \sin \varphi_B)^2 \sin^2 \theta_B] \\ + [\mu_{\perp} k_{\rho}^2 + (\mu_x^2 - \mu_{\perp}^2 - \mu_{\perp} \mu_{//}) k_0^2 \varepsilon_r] \sin^2 \theta_B + \mu_{//} (k_{\rho}^2 - 2\mu_{\perp} k_0^2 \varepsilon_r) \cos^2 \theta_B \}$$

$$a_1 = 2k_0^2 \varepsilon_r [(\mu_{//} - \mu_{\perp}) k_{\rho}^2 + (\mu_{\perp}^2 - \mu_g^2 - \mu_{\perp} \mu_{//}) k_0^2 \varepsilon_r] (k_x \cos \varphi_B + k_y \sin \varphi_B) \sin \theta_B \cos \theta_B$$

$$a_0 = k_0^2 \varepsilon_r \{ [(\mu_{//} - \mu_{\perp}) k_{\rho}^2 + (\mu_{\perp}^2 - \mu_z^2 - \mu_{\perp} \mu_{//}) k_0^2 \varepsilon_r] (k_x \cos \varphi_B + k_y \sin \varphi_B)^2 \sin^2 \theta_B \\ + (k_{\rho}^2 - \mu_{//} k_0^2 \varepsilon_r) [\mu_{\perp} k_{\rho}^2 - (\mu_{\perp}^2 - \mu_g^2) k_0^2] \}$$

It is easily seen that Eq. (2.3-39) has four distinct solutions of k_{z}^u , k_{z}^u , k_{z}^d , k_{z}^d .

$$\left| \overline{\overline{W}}_E \right| = \frac{1}{\left| \overline{\overline{\mu}}_r \right|} k_0^2 \varepsilon_r (\mu_{\perp} \sin^2 \theta_B + \mu_{//} \cos^2 \theta_B) (k - k_{z}^u) (k - k_{z}^u) (k - k_{z}^d) (k - k_{z}^d) \quad (2.3-40)$$

Comparison of the coefficients of the dispersion equation [Eq. (2.3-39)] for gyromagnetic medium with the coefficients of the dispersion equation for a gyroelectric medium [Eq. (2.3-26)]

shows that except the factor $\frac{1}{\left| \overline{\overline{\mu}}_r \right|}$ (determinant of the relative permeability matrix) being added

to each term, duality relation exists between Eq. (2.3-39) and Eq. (2.3-26). Substituting each

term of ε_r in Eq. (2.3-26) with the corresponding matrix elements of $\overline{\overline{\mu}}_r$ gives Eq. (2.3-39).

Then following the same procedure used to obtain the DGF for the gyroelectric medium, the electric type dyadic Green's function for a gyromagnetic medium is obtained as follows.

For $z > z'$

$$\overline{\overline{G}}(\vec{r}, \vec{r}') = \frac{\omega\mu_0}{4\pi^2} \int_{-\infty}^{\infty} \int_{-\infty}^{\infty} dk_x dk_y \frac{|\overline{\mu}_r|}{k_o^2 \varepsilon_r (\mu_{\perp} \sin^2 \theta_B + \mu_{\parallel} \cos^2 \theta_B) (k_{z'}^u - k_{z''}^u)} \begin{pmatrix} \frac{adj(\overline{\overline{W}}_E(k_{z'}^u)) e^{i\vec{k}_l \cdot (\vec{r} - \vec{r}')}}{(k_{z'}^u - k_{z'}^d)(k_{z'}^u - k_{z''}^d)} \\ \frac{adj(\overline{\overline{W}}_E(k_{z''}^u)) e^{i\vec{k}_{ll} \cdot (\vec{r} - \vec{r}')}}{(k_{z''}^u - k_{z'}^d)(k_{z''}^u - k_{z''}^d)} \end{pmatrix} \quad (2.3-41)$$

For $z < z'$

$$\overline{\overline{G}}(\vec{r}, \vec{r}') = -\frac{\omega\mu_0}{4\pi^2} \int_{-\infty}^{\infty} \int_{-\infty}^{\infty} dk_x dk_y \frac{|\overline{\mu}_r|}{k_o^2 \varepsilon_r (\mu_{\perp} \sin^2 \theta_B + \mu_{\parallel} \cos^2 \theta_B) (k_{z'}^d - k_{z''}^d)} \begin{pmatrix} \frac{adj(\overline{\overline{W}}_E(k_{z'}^d)) e^{i\vec{k}_l \cdot (\vec{r} - \vec{r}')}}{(k_{z'}^d - k_{z'}^u)(k_{z'}^d - k_{z''}^u)} \\ \frac{adj(\overline{\overline{W}}_E(k_{z''}^d)) e^{i\vec{k}_{ll} \cdot (\vec{r} - \vec{r}')}}{(k_{z''}^d - k_{z'}^u)(k_{z''}^d - k_{z''}^u)} \end{pmatrix} \quad (2.3-42)$$

Again the adjoint matrix can be represented in the following dyadic form if k_{zp}^q is real.

$$\begin{aligned} adj\overline{\overline{W}}_E(k_{z'}^u) &= \lambda_l^u \left[\hat{e}_{nl}(k_{z'}^u) \hat{e}_{nl}^*(k_{z'}^u) \right], & adj\overline{\overline{W}}_E(k_{z''}^u) &= \lambda_{ll}^u \left[\hat{e}_{nl}(k_{z''}^u) \hat{e}_{nl}^*(k_{z''}^u) \right] \\ adj\overline{\overline{W}}_E(k_{z'}^d) &= \lambda_l^d \left[\hat{e}_{nl}(k_{z'}^d) \hat{e}_{nl}^*(k_{z'}^d) \right], & adj\overline{\overline{W}}_E(k_{z''}^d) &= \lambda_{ll}^d \left[\hat{e}_{nl}(k_{z''}^d) \hat{e}_{nl}^*(k_{z''}^d) \right] \\ \lambda_p^q &= \begin{pmatrix} (k_{\rho}^2 + (k_{zp}^q)^2)^2 - (k_{\rho}^2 + (k_{zp}^q)^2) k_0^2 (3\mu_{\perp} + \mu_{\parallel}) \\ -(k_{3p}^q)^2 k_0^2 (\mu_{\parallel} - \mu_{\perp}) + k_0^4 (\mu_{\perp}^2 - \mu_g^2 + 2\mu_{\perp} \mu_{\parallel}) \end{pmatrix} \end{aligned} \quad (2.3-43)$$

where

$$k_{3p}^q = k_x \sin \theta_B \cos \varphi_B + k_y \sin \theta_B \sin \varphi_B + k_{zp}^q \cos \theta_B$$

The eigenvectors can be obtained using Eq. (2.3-34) with an appropriate substitution. The DGF of Eq. (2.3-43) agrees with what's obtained in Park [40]. However, it is noted here that the DGF of the unbounded gyromagnetic medium obtained in [40] is only valid for the case when

the adjoint wave matrix is a hermitian matrix with k_{zp}^q being a real number. Combining all the special cases considered in this chapter, the DGFs of an unbounded general anisotropic medium can be summarized in the following form.

For $z < z'$

$$\overline{\overline{G}}(\vec{r}, \vec{r}') = \frac{i}{(2\pi)^2} \int_{-\infty}^{\infty} \int_{-\infty}^{\infty} \left(\frac{\lambda(k_{zl}^d) \hat{e}(k_{zl}^d) \hat{v}(k_{zl}^d)}{a_4(k_{zl}^d - k_{zl}^u)(k_{zl}^d - k_{zll}^u)(k_{zl}^d - k_{zll}^d)} e^{i\vec{k}_l^d \cdot (\vec{r} - \vec{r}')} + \frac{\lambda(k_{zll}^d) \hat{e}(k_{zll}^d) \hat{v}(k_{zll}^d)}{a_4(k_{zll}^d - k_{zl}^d)(k_{zll}^d - k_{zl}^u)(k_{zll}^d - k_{zll}^u)} e^{i\vec{k}_{ll}^d \cdot (\vec{r} - \vec{r}')} \right) dk_x dk_y \quad (2.3-44)$$

For $z > z'$

$$\overline{\overline{G}}(\vec{r}, \vec{r}') = -\frac{i}{(2\pi)^2} \int_{-\infty}^{\infty} \int_{-\infty}^{\infty} \left(\frac{\lambda(k_{zl}^u) \hat{e}(k_{zl}^u) \hat{v}(k_{zl}^u)}{a_4(k_{zl}^u - k_{zl}^d)(k_{zl}^u - k_{zll}^u)(k_{zl}^u - k_{zll}^d)} e^{i\vec{k}_l^u \cdot (\vec{r} - \vec{r}')} + \frac{\lambda(k_{zll}^u) \hat{e}(k_{zll}^u) \hat{v}(k_{zll}^u)}{a_4(k_{zll}^u - k_{zl}^d)(k_{zll}^u - k_{zl}^u)(k_{zll}^u - k_{zll}^d)} e^{i\vec{k}_{ll}^u \cdot (\vec{r} - \vec{r}')} \right) dk_x dk_y \quad (2.3-45)$$

3 DYADIC GREEN'S FUNCTIONS FOR HALF-SPACE AND TWO-LAYER GEOMETRIES

In this chapter, the electric type eigenvector dyadic Green's functions (E-DGFs) for the half-space and two-layer problems with a source located either in the isotropic or anisotropic region are obtained. In Section 3.1, the DGFs for the regions below the source point when it is located in the isotropic region are derived. In Section 3.2, the modified symmetrical property applicable to the DGFs with source and field points in the same region (Region 0) is derived to obtain the DGFs above the source point when the anisotropic region is non-reciprocal. In Section 3.3, the modified symmetrical property for the DGFs with source and field points in two different regions is derived for a layered geometry with a non-reciprocal medium. The usage and limitation of the modified symmetrical property is discussed. To overcome the limitation of the modified symmetrical property in Section 3.3, the direct construction method is proposed to obtain the complete DGFs with a source located in the anisotropic region in Section 3.4. A comparison of the DGF for the isotropic region with a source located in the anisotropic region derived using two different approaches is presented and interesting relationship is discovered.

3.1 Dyadic Green's Functions with Source inside the Isotropic Region

In this section, the DGFs of half-space and two-layer problems are given for each region below the source point when a source is located in the isotropic region. The half-space and two-layer geometries are shown in Fig. 3-1(a) and (b), respectively. For both half-space and two-layer geometries, Region 0 is an isotropic region with relative permittivity and permeability

denoted as ε_{0r} and μ_{0r} , while Region 1 is an electrically anisotropic region with relative permittivity tensor $\bar{\varepsilon}_{1r}$ and relative permeability μ_{1r} . For a two-layer geometry, the thickness of the anisotropic region is denoted as ‘ d ’, and Region 2 is an isotropic region with relative permittivity and permeability of ε_{2r} and μ_{2r} . For both problems, the source is located at $z = z'$ in Region 0.

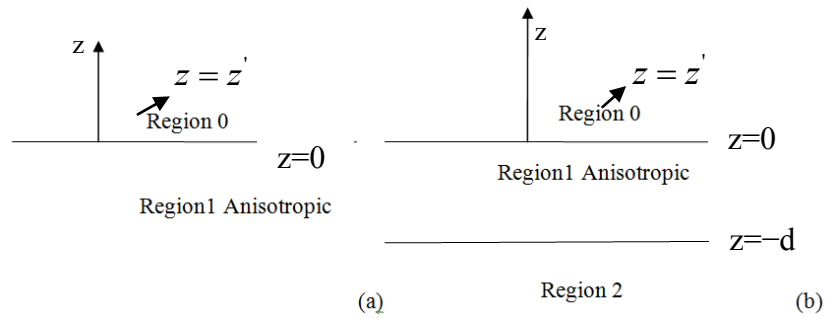


Fig. 3-1: Geometry of (a) half-space and (b) two-layer problem.

3.1.1 DGF for the Region of $z < z'$

For the half-space problem shown in Fig. 3-1(a), the DGFs of interest are $\bar{G}^{(0,0)}(\bar{r}, \bar{r}')$ and $\bar{G}^{(1,0)}(\bar{r}, \bar{r}')$. The first and second indices of superscript of the DGFs are used to indicate the region of the field and source points, respectively, while \bar{r} and \bar{r}' indicate the field and the source points. $\bar{G}^{(0,0)}(\bar{r}, \bar{r}')$ refers to the DGF of Region 0 with source in Region 1, and $\bar{G}^{(1,0)}(\bar{r}, \bar{r}')$ corresponds to the DGF of Region 1 with source in Region 0. When considering the two-layer geometry shown in Fig. 3-1(b), the DGF for Region 2 is denoted as $\bar{G}^{(2,0)}(\bar{r}, \bar{r}')$ in addition to the DGFs of $\bar{G}^{(0,0)}(\bar{r}, \bar{r}')$ and $\bar{G}^{(1,0)}(\bar{r}, \bar{r}')$. With DGFs for each region of a two-layer

problem assigned, the Maxwell's equations for the DGFs of the two-layer geometry are written below.

$$\begin{aligned}
\left[\nabla \times \nabla \times \bar{I} - k_0^2 \bar{\epsilon}_{0r} \bar{\mu}_{0r} \right] \cdot \bar{G}^{(0,0)}(\bar{r}, \bar{r}') &= \bar{I} \delta(\bar{r} - \bar{r}') \\
\left[\nabla \times \nabla \times \bar{I} - k_0^2 \bar{\epsilon}_{1r} \bar{\mu}_{1r} \right] \cdot \bar{G}^{(1,0)}(\bar{r}, \bar{r}') &= 0 \\
\left[\nabla \times \nabla \times \bar{I} - k_0^2 \bar{\epsilon}_{2r} \bar{\mu}_{2r} \right] \cdot \bar{G}^{(2,0)}(\bar{r}, \bar{r}') &= 0
\end{aligned} \tag{3.1-1}$$

The continuity conditions of the tangential electric and magnetic fields require the two-layer DGFs to satisfy the following boundary conditions.

At $z = 0$

$$\begin{aligned}
\hat{z} \times \bar{G}^{(0,0)}(\bar{r}, \bar{r}') &= \hat{z} \times \bar{G}^{(1,0)}(\bar{r}, \bar{r}') \\
\frac{1}{\mu_{0r}} \hat{z} \times \nabla \times \bar{G}^{(0,0)}(\bar{r}, \bar{r}') &= \frac{1}{\mu_{1r}} \hat{z} \times \nabla \times \bar{G}^{(1,0)}(\bar{r}, \bar{r}')
\end{aligned} \tag{3.1-2}$$

At $z = -d$

$$\begin{aligned}
\hat{z} \times \bar{G}^{(1,0)}(\bar{r}, \bar{r}') &= \hat{z} \times \bar{G}^{(2,0)}(\bar{r}, \bar{r}') \\
\frac{1}{\mu_{1r}} \hat{z} \times \nabla \times \bar{G}^{(1,0)}(\bar{r}, \bar{r}') &= \frac{1}{\mu_{2r}} \hat{z} \times \nabla \times \bar{G}^{(2,0)}(\bar{r}, \bar{r}')
\end{aligned} \tag{3.1-3}$$

It is noted here that for a half-space problem, the DGFs have to satisfy Eq. (3.1-2) only.

By applying the same matrix method used in [35] to the DGFs of the unbounded anisotropic region obtained in Chapter 1, the DGFs for each region of a half-space problem can be expressed in the dyadic form below.

For $0 < z < z'$

$$\overline{\overline{G}}^{(0,0)}(\vec{r}, \vec{r}') = \frac{i}{8\pi^2} \int_{-\infty}^{\infty} dk_x dk_y \frac{1}{k_{0z}} \left\{ \begin{array}{l} \left[\begin{array}{l} \hat{h}_0(-k_{0z}) e^{i\bar{\kappa}_0 \cdot \vec{r}} \\ + R_{hh}^{01} \hat{h}_0(k_{0z}) e^{i\bar{\kappa}_0 \cdot \vec{r}} \\ + R_{hv}^{01} \hat{v}_0(k_{0z}) e^{i\bar{\kappa}_0 \cdot \vec{r}} \end{array} \right] \hat{h}_0(-k_{0z}) \\ + \left[\begin{array}{l} \hat{v}_0(-k_{0z}) e^{i\bar{\kappa}_0 \cdot \vec{r}} \\ + R_{vh}^{01} \hat{h}_0(k_{0z}) e^{i\bar{\kappa}_0 \cdot \vec{r}} \\ + R_{vv}^{01} \hat{v}_0(k_{0z}) e^{i\bar{\kappa}_0 \cdot \vec{r}} \end{array} \right] \hat{v}_0(-k_{0z}) \end{array} \right\} e^{-i\bar{\kappa}_0 \cdot \vec{r}'} \quad (3.1-4)$$

For $z < 0$

$$\overline{\overline{G}}^{(1,0)}(\vec{r}, \vec{r}') = \frac{i}{8\pi^2} \int_{-\infty}^{\infty} dk_x dk_y \frac{1}{k_{0z}} \left\{ \begin{array}{l} \left[\begin{array}{l} X_{he_l^d}^{01} \hat{e}_l(k_{zl}^d) e^{i\bar{\kappa}_l \cdot \vec{r}} \\ + X_{he_{ll}^d}^{01} \hat{e}_{ll}(k_{zll}^d) e^{i\bar{\kappa}_{ll} \cdot \vec{r}} \end{array} \right] \hat{h}_0(-k_{0z}) \\ + \left[\begin{array}{l} X_{ve_l^d}^{01} \hat{e}_l(k_{zl}^d) e^{i\bar{\kappa}_l \cdot \vec{r}} \\ + X_{ve_{ll}^d}^{01} \hat{e}_{ll}(k_{zll}^d) e^{i\bar{\kappa}_{ll} \cdot \vec{r}} \end{array} \right] \hat{v}_0(-k_{0z}) \end{array} \right\} e^{-i\bar{\kappa}_0 \cdot \vec{r}'} \quad (3.1-5)$$

It is noted here to be consistent with the notations of DGFs derived in [37]; the constant coefficient $i\omega\mu_0$ is extracted out from Green's function of Eq. (3.1-4) and Eq. (3.1-5). Through all the following discussions, $i\omega\mu_0$ is not included in the DGFs.

In Eq. (3.1-4) and Eq. (3.1-5), $\bar{\kappa}_0$ and $\bar{\kappa}_0$ denote the wave vectors of upward and downward propagating (or decaying) waves along the z-direction in Region 0, respectively.

$$\bar{\kappa}_0 = \hat{x}k_x + \hat{y}k_y + \hat{z}k_{0z}, \quad \bar{\kappa}_0 = \hat{x}k_x + \hat{y}k_y - \hat{z}k_{0z} \quad (3.1-6)$$

The components of the wave vector in Eq. (3.1-6) have to satisfy the dispersion relation of the Region 0 filled with the isotropic medium as follows.

$$k_x^2 + k_y^2 + k_{0z}^2 = k_0^2 \mu_{0r} \varepsilon_{0r}, \quad k_0^2 = \omega^2 \mu_0 \varepsilon_0 \quad (3.1-7)$$

$\widehat{h}_0(\pm k_{0z})$ and $\widehat{v}_0(\pm k_{0z})$ correspond to the two different polarized electric fields in Region 0 with the propagating direction being either upward or downward indicated by the sign of k_{0z} . It has been discussed in Chapter 2 that $\widehat{h}_0(\pm k_{0z})$ denotes the wave polarized perpendicular to the incidence plane, while $\widehat{v}_0(\pm k_{0z})$ denotes the wave polarized parallel to the incidence plane and perpendicular to the wave vector. For convenience, the four different polarized electric fields in the isotropic regions for a two-layer geometry are simplified as $\widehat{h}_n^+, \widehat{h}_n^-, \widehat{v}_n^+, \widehat{v}_n^-$ with the subscript $n = 0$ corresponding to Region 0 and $n = 2$ corresponding to Region 2. The expressions of the electric fields are given below.

$$\widehat{h}_n^+ = \widehat{h}_n^- = \frac{\widehat{z} \times \overline{k}_n}{k_\rho} = \frac{\widehat{y}k_x - \widehat{x}k_y}{\sqrt{k_x^2 + k_y^2}}, \quad k_\rho = \sqrt{k_x^2 + k_y^2} \quad (3.1-8)$$

$$\widehat{v}_n^+ = \frac{\widehat{h}_n^+(+k_{nz}) \times \overline{k}_n}{k_n} = \frac{1}{k_0 \sqrt{\mu_{nr} \epsilon_{nr}}} \frac{\widehat{x}k_x k_{nz} + \widehat{y}k_y k_{nz} - \widehat{z}(k_x^2 + k_y^2)}{\sqrt{k_x^2 + k_y^2}} \quad (3.1-9)$$

$$\widehat{v}_n^- = \frac{\widehat{h}_n^-(-k_{nz}) \times \overline{\kappa}_n}{k_n} = \frac{1}{k_0 \sqrt{\mu_{nr} \epsilon_{nr}}} \frac{-\widehat{x}k_x k_{nz} - \widehat{y}k_y k_{nz} - \widehat{z}(k_x^2 + k_y^2)}{\sqrt{k_x^2 + k_y^2}} \quad (3.1-10)$$

\overline{k}_m and $\overline{\kappa}_m$ denote the wave vectors of Region 1 for upward and downward propagating characteristic waves of Type m ($m = I, II$), respectively.

$$\begin{aligned} \overline{k}_I &= \widehat{x}k_x + \widehat{x}k_y + \widehat{z}k_{zI}^u, & \overline{k}_{II} &= \widehat{x}k_x + \widehat{y}k_y + \widehat{z}k_{zII}^u \\ \overline{\kappa}_I &= \widehat{x}k_x + \widehat{y}k_y + \widehat{z}k_{zI}^d, & \overline{\kappa}_{II} &= \widehat{x}k_x + \widehat{y}k_y + \widehat{z}k_{zII}^d \end{aligned} \quad (3.1-11)$$

As shown in Chapter 2, the four different values k_{zm}^n ($m = I, II$ and $n=u, d$), indicating the z component of wave vector for Region 1, can be obtained by setting the determinant of electric wave matrix to be zero with given tangential components of wave vector.

The normalized electric field vectors for the upward and downward characteristic waves of Type m are denoted as $\hat{e}_m^u(k_{zm}^u)$ and $\hat{e}_m^d(k_{zm}^d)$ ($m = I, II$), respectively. As described in Chapter 2, these vectors can be obtained using the eigen-decomposition method.

The terms of $R_{\alpha\beta}^{01}$ and $X_{\alpha\beta}^{01}$ indicate the half-space reflection and transmission coefficients when the wave is incident from Region 0 to Region 1. The first and second indices of the subscript indicate the polarizations of the incident wave and transmitted wave, respectively.

For a two-layer problem, the dyadic Green's functions in each region can be expressed in dyadic forms as follows.

For $0 < z < z'$

$$\overline{\overline{G}}^{(0,0)}(\vec{r}, \vec{r}') = \frac{i}{8\pi^2} \int_{-\infty}^{\infty} dk_x dk_y \frac{1}{k_{0z}} \left\{ \begin{array}{l} \left[\begin{array}{l} \hat{h}_0(-k_{0z}) e^{i\vec{k}_0 \cdot \vec{r}} \\ + R_{hh} \hat{h}_0(k_{0z}) e^{i\vec{k}_0 \cdot \vec{r}} \\ + R_{hv} \hat{v}_0(k_{0z}) e^{i\vec{k}_0 \cdot \vec{r}} \end{array} \right] \hat{h}_0(-k_{0z}) \\ + \left[\begin{array}{l} \hat{v}_0(-k_{0z}) e^{i\vec{k}_0 \cdot \vec{r}} \\ + R_{vh} \hat{h}_0(k_{0z}) e^{i\vec{k}_0 \cdot \vec{r}} \\ + R_{vv} \hat{v}_0(k_{0z}) e^{i\vec{k}_0 \cdot \vec{r}} \end{array} \right] \hat{v}_0(-k_{0z}) \end{array} \right\} e^{-i\vec{k}_0 \cdot \vec{r}'} \quad (3.1-12)$$

For $-d < z < 0$

$$\overline{\overline{G}}^{(1,0)}(\vec{r}, \vec{r}') = \frac{i}{8\pi^2} \int_{-\infty}^{\infty} dk_x dk_y \frac{1}{k_{0z}} \left\{ \begin{array}{l} \left[\begin{array}{l} A_{hel} \hat{e}_I(k_{zI}^d) e^{i\vec{k}_{I1} \cdot \vec{r}} \\ + B_{hel} \hat{e}_I(k_{zI}^u) e^{i\vec{k}_{I1} \cdot \vec{r}} \\ + A_{hell} \hat{e}_{II}(k_{zII}^d) e^{i\vec{k}_{II} \cdot \vec{r}} \\ + B_{hell} \hat{e}_{II}(k_{zII}^u) e^{i\vec{k}_{II} \cdot \vec{r}} \end{array} \right] \hat{h}_0(-k_{0z}) \\ + \left[\begin{array}{l} A_{vel} \hat{e}_I(k_{zI}^d) e^{i\vec{k}_{I1} \cdot \vec{r}} \\ + B_{vel} \hat{e}_I(k_{zI}^u) e^{i\vec{k}_{I1} \cdot \vec{r}} \\ + A_{vell} \hat{e}_{II}(k_{zII}^d) e^{i\vec{k}_{II} \cdot \vec{r}} \\ + B_{vell} \hat{e}_{II}(k_{zII}^u) e^{i\vec{k}_{II} \cdot \vec{r}} \end{array} \right] \hat{v}_0(-k_{0z}) \end{array} \right\} e^{-i\vec{k}_0 \cdot \vec{r}'} \quad (3.1-13)$$

For $z < -d$

$$\overline{\overline{G}}^{(2,0)}(\vec{r}, \vec{r}') = \frac{i}{8\pi^2} \int_{-\infty}^{\infty} dk_x dk_y \frac{1}{k_{0z}} \left\{ \begin{array}{l} \left[\begin{array}{l} X_{hh} \hat{h}_2(-k_{2z}) e^{i\vec{\kappa}_2 \cdot \vec{r}} \\ + X_{hv} \hat{v}_2(-k_{2z}) e^{i\vec{\kappa}_2 \cdot \vec{r}} \end{array} \right] \hat{h}_0(-k_{0z}) \\ + \left[\begin{array}{l} X_{vh} \hat{h}_2(-k_{2z}) e^{i\vec{\kappa}_2 \cdot \vec{r}} \\ + X_{vv} \hat{v}_2(-k_{2z}) e^{i\vec{\kappa}_2 \cdot \vec{r}} \end{array} \right] \hat{v}_0(-k_{0z}) \end{array} \right\} e^{-i\vec{\kappa}_0 \cdot \vec{r}} \quad (3.1-14)$$

In Eq. (3.1-12), $R_{\alpha\beta}$ stands for the two-layer reflection coefficients of the reflected wave with β polarization from the incident α polarized wave. In Eq. (3.1-13), $A_{\alpha\beta}$ and $B_{\alpha\beta}$ stand for the coefficients of the downward and upward waves with β polarization converted from incident wave with α polarization inside the anisotropic medium. In Eq. (3.1-14), $X_{\alpha\beta}$ stands for the two-layer transmission coefficients of the transmitted wave with β polarization from the incident α polarized wave.

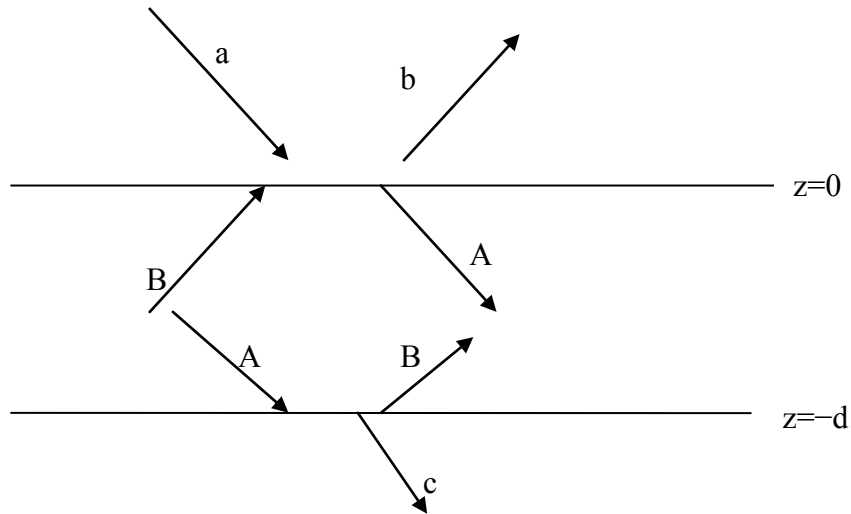


Fig. 3-2: Amplitude vectors of waves in the two-layered geometry.

The total 16 reflection and transmission coefficients for the two-layer problem can be calculated applying the boundary conditions at $z=0$ and $z=-d$. The procedure of obtaining the coefficients can be significantly simplified by decomposing the two-layer problem into two half-

space problems as shown in [35]. This approach is briefly reviewed here since the similar approach will be utilized to obtain complete DGFs of all the regions when the source is located in the anisotropic region in Section 3.4.1. As shown in Fig. 3-2, “a” stands for the amplitude vectors of the downward waves generated by the source in Region 0. “b” stands for the amplitude vectors of the total reflected waves along the upward direction due to the boundary at $z=0$ in Region 0. “A” stands for the amplitude vectors of the total downward waves in Region 1 and “B” stands for the amplitude vectors of the total upward waves in Region 1. “c” stands for the amplitude vectors of the total transmitted downward waves in Region 2.

From the discussion in Chapter 2, it is known that in an anisotropic medium, two different polarized characteristic waves exist along a specific direction described by k_x, k_y, k_z . The two polarizations in Region 1 are assigned as the Type I and Type II polarized waves, which can be obtained using the eigen-decomposition method described in Chapter 2. For an isotropic medium as in Region 0 and Region 2, the two polarizations correspond to the h - and v - polarized waves as shown in Eq.(3.1-8) - Eq. (3.1-10). Thus, all the waves (including the incidence wave “a” and reflected wave “b” in Region 0, the downward and upward propagating waves (“A” and “B”) in Region 1, and the transmitted wave “c” in Region 2) can all be expressed as a 2 by 1 vectors, which corresponds to the coefficients for the normalized electric field vectors of two different polarizations in the given region. Then, all the waves in each region can be related through the half-space reflection and transmission matrices as follows.

$$\begin{bmatrix} b \\ A \end{bmatrix} = \begin{bmatrix} \overline{\overline{R}}^{01} & \overline{\overline{X}}^{10} \\ \overline{\overline{X}}^{01} & \overline{\overline{R}}^{10} \end{bmatrix} \begin{bmatrix} a \\ B \end{bmatrix}, \quad \begin{bmatrix} B \\ c \end{bmatrix} = \begin{bmatrix} \overline{\overline{R}}^{12} \\ \overline{\overline{X}}^{12} \end{bmatrix} A \quad (3.1-15)$$

In Eq. (3.1-15), $\overline{\overline{R}}^{pq}$ ($p, q=0, I, 2$) is a 2 by 2 matrix which gives the half-space reflection coefficients of waves incident from Region p to Region q . $\overline{\overline{X}}^{pq}$ is a 2 by 2 matrix which gives the half-space transmission coefficients of waves incident from Region p to Region q . The half-space reflection and transmission matrices are expressed in the form below.

$$\overline{\overline{R}}^{01} = \begin{bmatrix} R_{hh}^{01} & R_{vh}^{01} \\ R_{hv}^{01} & R_{vv}^{01} \end{bmatrix}, \quad \overline{\overline{X}}^{01} = \begin{bmatrix} X_{hh}^{01} & X_{vh}^{01} \\ X_{hv}^{01} & X_{vv}^{01} \end{bmatrix} \quad (3.1-16)$$

$$\begin{aligned} \overline{\overline{R}}^{12} &= \begin{bmatrix} R_{eIeI}^{12} \exp[i(-k_{zI}^d + k_{zI}^u)d] & R_{eIIeI}^{12} \exp[i(-k_{zII}^d + k_{zI}^u)d] \\ R_{eIeII}^{12} \exp[i(-k_{zI}^d + k_{zII}^u)d] & R_{eIIeII}^{12} \exp[i(-k_{zII}^d + k_{zII}^u)d] \end{bmatrix} \\ &= \begin{bmatrix} e_{I,I} & e_{II,I} \\ e_{I,II} & e_{II,II} \end{bmatrix} \end{aligned} \quad (3.1-17)$$

$$\begin{aligned} \overline{\overline{X}}^{12} &= \begin{bmatrix} X_{eIh}^{12} \exp[i(-k_{zI}^d - k_{2z})d] & R_{eIIh}^{12} \exp[i(-k_{zII}^d - k_{2z})d] \\ R_{eIv}^{12} \exp[i(-k_{zI}^d - k_{2z})d] & R_{eIIv}^{12} \exp[i(-k_{zII}^d - k_{2z})d] \end{bmatrix} \\ &= \begin{bmatrix} X_{I,h} & X_{II,h} \\ X_{I,v} & X_{II,v} \end{bmatrix} \end{aligned} \quad (3.1-18)$$

It is noted here that R_{eIeI}^{12} is reflection coefficient with reference plane at $z=0$, the phase shift at $z=-d$ is taken into account by the multiplication of the exponential terms as shown in Eq. (3.1-17). Rearranging Eq. (3.1-14) gives the following matrix relationships.

$$\begin{aligned} b &= \overline{\overline{R}}a, & \overline{\overline{R}} &= \overline{\overline{R}}^{01} + \overline{\overline{X}} \overline{\overline{R}}^{10} \overline{\overline{R}}^{12} (I - \overline{\overline{R}}^{10} \overline{\overline{R}}^{12})^{-1} \overline{\overline{X}}^{01} \\ A &= \overline{\overline{D}}a, & \overline{\overline{D}} &= (I - \overline{\overline{R}}^{10} \overline{\overline{R}}^{12})^{-1} \overline{\overline{X}}^{01} \\ B &= \overline{\overline{U}}a, & \overline{\overline{U}} &= \overline{\overline{R}}^{12} (I - \overline{\overline{R}}^{10} \overline{\overline{R}}^{12})^{-1} \overline{\overline{X}}^{01} \\ c &= \overline{\overline{X}}a, & \overline{\overline{X}} &= \overline{\overline{X}}^{12} (I - \overline{\overline{R}}^{10} \overline{\overline{R}}^{12})^{-1} \overline{\overline{X}}^{01} \end{aligned} \quad (3.1-19)$$

Substituting the half-space reflection and transmission coefficients into Eq. (3.1-19) gives all the coefficients of the DGFs shown in Eq. (3.1-12)–Eq. (3.1-14) as follows.

$$\begin{aligned}
 R_{\beta\alpha} &= R_{\beta\alpha}^{01} + X_{\beta e_I}^{01} (e_{I,I} L_1 + e_{II,I} M_2) X_{e_I\alpha}^{10} + X_{\beta e_{II}}^{01} (e_{I,II} L_1 + e_{II,II} M_2) X_{e_{II}\alpha}^{10} \\
 &\quad + X_{\beta e_I}^{01} (e_{I,I} L_2 + e_{II,I} M_1) X_{e_I\alpha}^{10} + X_{\beta e_{II}}^{01} (e_{I,II} L_2 + e_{II,II} M_1) X_{e_{II}\alpha}^{10} \\
 A_{\beta e_I} &= L_1 X_{\beta e_I}^{01} + L_2 X_{\beta e_{II}}^{01} \\
 A_{\beta e_{II}} &= M_2 X_{\beta e_I}^{01} + M_1 X_{\beta e_{II}}^{01}
 \end{aligned} \tag{3.1-20}$$

$$\begin{aligned}
 B_{\beta n} &= (e_{I,n} L_1 + e_{II,n} M_2) X_{\beta e_I}^{01} + (e_{I,n} L_2 + e_{II,n} M_1) X_{\beta e_{II}}^{01} \\
 X_{\beta\alpha} &= (X_{I,\alpha} L_1 + X_{II,\alpha} M_2) X_{\beta e_I}^{01} + (X_{I,\alpha} L_2 + X_{II,\alpha} M_1) X_{\beta e_{II}}^{01} \\
 \left(\begin{array}{cc} I & -R \\ -R & R \end{array} \right)^{-1} &= \begin{bmatrix} L_1 & L_2 \\ M_2 & M_1 \end{bmatrix}
 \end{aligned} \tag{3.1-21}$$

where β, α, I, II stand for the polarizations of the wave.

The procedure described in this section provides the DGFs for all the regions below the source point when the source is located in Region 0 regardless of Region 1 being either a reciprocal or non-reciprocal medium. The DGF above the source point can be directly obtained from the transpose of the DGF below the source point if Region 1 is filled with a reciprocal medium as shown in [37]. However, existing symmetrical property does not work for the case with Region 1 being a non-reciprocal medium, which is of the main interest in the next section.

3.2 Modified Symmetrical Property for $\overline{\overline{G}}^{(0,0)}(r, r')$ of the Region $z > z'$ and $0 < z < z'$

In this section, a modified symmetrical property is proposed to correlate the DGFs for the regions above and below the source point when Region 1 is filled with a non-reciprocal medium.

Applying the modified symmetrical property, the DGF above the source point is further obtained to facilitate the formulation of the radiated field which will be demonstrated in Chapter 4.

3.2.1 Proof of Modified Symmetrical Property of $\overline{\overline{G}}^{(0,0)}(\underline{r}, \underline{r}')$

In this section, it is proven that when the source point and field point are both located in Region 0, the symmetrical property of the dyadic Green's function in Eq. (3.2-1) is always valid, even for the anisotropic region filled with a non-reciprocal medium.

$$\overline{\overline{G}}^{(0,0)}(\underline{r}, \underline{r}') = \left[\overline{\overline{G}}^{(0,0)}(\underline{r}', \underline{r}) \right]_{\overline{\overline{\epsilon}}_{1r} = \overline{\overline{\epsilon}}_{1r}^T}^T \quad (3.2-1)$$

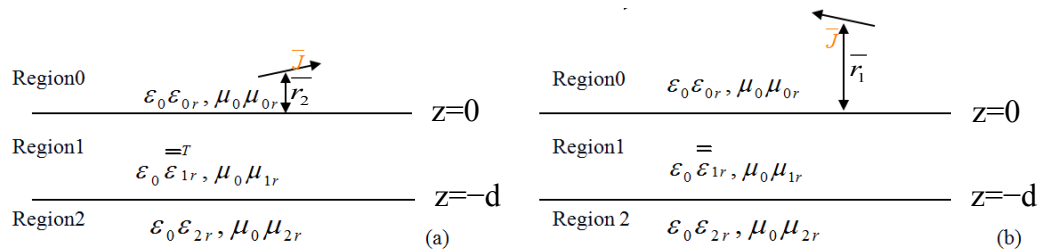


Fig. 3-3: Two different geometries for the proof of modified symmetrical property.

Two different geometries as shown in Fig. 3-3 are considered here to facilitate the proof of the modified symmetrical property. In both Fig. 3-3(a) and (b), Region 0 and Region 2 are denoted as the isotropic regions. The relative permeability and permittivity for Region 0 and Region 2 are denoted as μ_{0r}, ϵ_{0r} and μ_{2r}, ϵ_{2r} . However, the media in Region 1 are different for Fig. 3-3(a) and (b). Region 1 is denoted as the anisotropic medium with relative permeability and permittivity of $\mu_{1r}, \overline{\overline{\epsilon}}_{1r}^T$ for the geometry shown in Fig. 3-3(a), while in Fig. 3-3(b), Region 1 is denoted as the anisotropic medium with relative permeability and permittivity of $\mu_{1r}, \overline{\overline{\epsilon}}_{1r}$. In

addition to the different media assigned for Region 1, the source locations are also different for Fig. 3-3(a) and (b). In Fig. 3-3(a), the source is located at \bar{r}_2 and in Fig. 3-3(b), the source is located at \bar{r}_1 in Region 0.

In order to prove Eq. (3.2-1), the dyadic-dyadic Green's theorem of the second kind given by Tai [34] is used, which is shown below.

$$\begin{aligned} & \iiint_V \left\{ \left[\nabla \times \nabla \times \bar{Q} \right]^T \cdot \bar{P} - \bar{Q} \cdot \left[\nabla \times \nabla \times \bar{P} \right] \right\} dv \\ &= \oiint_S \left\{ \left[\hat{n} \times \bar{Q} \right]^T \cdot \left(\nabla \times \bar{P} \right) - \left[\nabla \times \bar{Q} \right]^T \cdot \left(\hat{n} \times \bar{P} \right) \right\} ds \end{aligned} \quad (3.2-2)$$

Step 1: Let $\bar{P} = \bar{G}^{(0,0)}(\bar{r}, \bar{r}_1)$, $\bar{Q} = \bar{G}^{(0,0)}(\bar{r}, \bar{r}_2)$

It is noted here \bar{Q} and \bar{P} represent the DGFs of Region 0 for the geometries shown in Fig. 3-3(a) and (b), respectively. Thus, for the region of $z > 0$, \bar{Q} and \bar{P} satisfy the following wave equations.

$$\begin{aligned} \nabla \times \nabla \times \bar{Q} - k_0^2 \mu_{0r} \epsilon_{0r} \bar{Q} &= \bar{I} \delta(\bar{r} - \bar{r}_2) \rightarrow \nabla \times \nabla \times \bar{Q} = k_0^2 \mu_{0r} \epsilon_{0r} \bar{Q} + \bar{I} \delta(\bar{r} - \bar{r}_2) \\ \nabla \times \nabla \times \bar{P} - k_0^2 \mu_{0r} \epsilon_{0r} \bar{P} &= \bar{I} \delta(\bar{r} - \bar{r}_1) \rightarrow \nabla \times \nabla \times \bar{P} = k_0^2 \mu_{0r} \epsilon_{0r} \bar{P} + \bar{I} \delta(\bar{r} - \bar{r}_1) \end{aligned} \quad (3.2-3)$$

Substituting Eq. (3.2-3) into Eq. (3.2-2) gives

$$\iiint_V \left\{ \begin{aligned} & \left[k_0^2 \mu_{0r} \epsilon_{0r} \bar{Q} + \bar{I} \delta(\bar{r} - \bar{r}_2) \right]^T \cdot \bar{P} \\ & - \bar{Q} \cdot \left[k_0^2 \mu_{0r} \epsilon_{0r} \bar{P} + \bar{I} \delta(\bar{r} - \bar{r}_1) \right] \end{aligned} \right\} dv = \oiint_S \left\{ \begin{aligned} & \left[\hat{n} \times \bar{Q} \right]^T \cdot \left(\nabla \times \bar{P} \right) \\ & - \left[\nabla \times \bar{Q} \right]^T \cdot \left(\hat{n} \times \bar{P} \right) \end{aligned} \right\} ds \quad (3.2-4)$$

The volume integral is for Region 0 and the closed surface integral is for the surface bounding the volume of Region 0. With \bar{Q} and \bar{P} substituted, Eq. (3.2-4) is equivalent to

$$\begin{aligned}
& \iiint_V \left\{ \begin{aligned} & \left[k_0^2 \mu_{0r} \varepsilon_{0r} \overline{\overline{G}}^{(0,0)}(\bar{r}, \bar{r}_2) + \overline{I} \delta(\bar{r} - \bar{r}_2) \right]^T \cdot \overline{\overline{G}}^{(0,0)}(\bar{r}, \bar{r}_1) \\ & - \overline{\overline{G}}^{(0,0)}(\bar{r}, \bar{r}_2)^T \cdot \left[k_0^2 \mu_{0r} \varepsilon_{0r} \overline{\overline{G}}^{(0,0)}(\bar{r}, \bar{r}_1) + \overline{I} \delta(\bar{r} - \bar{r}_1) \right] \end{aligned} \right\} dv \\
& = \oint_S \left\{ \begin{aligned} & \left[\hat{n} \times \overline{\overline{G}}^{(0,0)}(\bar{r}, \bar{r}_2) \right]^T \cdot \left(\nabla \times \overline{\overline{G}}^{(0,0)}(\bar{r}, \bar{r}_1) \right) \\ & - \left[\nabla \times \overline{\overline{G}}^{(0,0)}(\bar{r}, \bar{r}_2) \right]^T \cdot \left(\hat{n} \times \overline{\overline{G}}^{(0,0)}(\bar{r}, \bar{r}_1) \right) \end{aligned} \right\} ds
\end{aligned} \tag{3.2-5}$$

Simplifying Eq. (3.2-5) gives

$$\overline{\overline{G}}^{(0,0)}(\bar{r}_2, \bar{r}_1) - \overline{\overline{G}}^{(0,0)}(\bar{r}_1, \bar{r}_2)^T = \oint_S \left\{ \begin{aligned} & \left[\hat{n} \times \overline{\overline{G}}^{(0,0)}(\bar{r}, \bar{r}_2) \right]^T \cdot \left(\nabla \times \overline{\overline{G}}^{(0,0)}(\bar{r}, \bar{r}_1) \right) \\ & - \left[\nabla \times \overline{\overline{G}}^{(0,0)}(\bar{r}, \bar{r}_2) \right]^T \cdot \left(\hat{n} \times \overline{\overline{G}}^{(0,0)}(\bar{r}, \bar{r}_1) \right) \end{aligned} \right\} ds \tag{3.2-6}$$

The closed surface integral can be reduced to a surface integral about the $z=0$ plane by employing the radiation boundary condition as $z \rightarrow \infty$. In this case, Eq. (3.2-6) reduces to

$$\overline{\overline{G}}^{(0,0)}(\bar{r}_2, \bar{r}_1) - \overline{\overline{G}}^{(0,0)}(\bar{r}_1, \bar{r}_2)^T = - \iint_{z=0 \text{ plane}} ds \left\{ \begin{aligned} & \left[\hat{z} \times \overline{\overline{G}}^{(0,0)}(\bar{r}, \bar{r}_2) \right]^T \cdot \left(\nabla \times \overline{\overline{G}}^{(0,0)}(\bar{r}, \bar{r}_1) \right) \\ & - \left[\nabla \times \overline{\overline{G}}^{(0,0)}(\bar{r}, \bar{r}_2) \right]^T \cdot \left(\hat{z} \times \overline{\overline{G}}^{(0,0)}(\bar{r}, \bar{r}_1) \right) \end{aligned} \right\} \tag{3.2-7}$$

It is noted that the negative sign is due to the fact that $\hat{n} = -\hat{z}$.

The continuity conditions of the electric field and magnetic field at $z = 0$ for the geometry shown in Fig. 3-3(a) require the DGFs to satisfy the following boundary conditions.

$$\begin{aligned}
& \hat{z} \times \overline{\overline{G}}^{(0,0)}(\bar{r}, \bar{r}_1) = \hat{z} \times \overline{\overline{G}}^{(1,0)}(\bar{r}, \bar{r}_1), \\
& \frac{1}{\mu_{0r}} \hat{z} \times \nabla \times \overline{\overline{G}}^{(0,0)}(\bar{r}, \bar{r}_1) = \frac{1}{\mu_{1r}} \hat{z} \times \nabla \times \overline{\overline{G}}^{(1,0)}(\bar{r}, \bar{r}_1)
\end{aligned} \tag{3.2-8}$$

The continuity conditions of the electric field and magnetic field at $z=0$ for geometry shown in Fig. 3-3(b) require the DGFs to satisfy the following equations.

$$\begin{aligned} \hat{z} \times \overline{\overline{G}}^{(0,0)}(\bar{r}, \bar{r}_2) &= \hat{z} \times \overline{\overline{G}}^{(1,0)}(\bar{r}, \bar{r}_2), \\ \frac{1}{\mu_{0r}} \hat{z} \times \nabla \times \overline{\overline{G}}^{(0,0)}(\bar{r}, \bar{r}_2) &= \frac{1}{\mu_{1r}} \hat{z} \times \nabla \times \overline{\overline{G}}^{(1,0)}(\bar{r}, \bar{r}_2) \end{aligned} \quad (3.2-9)$$

The following identity is also useful.

$$\left(\hat{z} \times \overline{\overline{I}} \right)^T = -\hat{z} \times \overline{\overline{I}} \quad (3.2-10)$$

Applying the boundary conditions of Eq. (3.2-8) and Eq. (3.2-9) together with the identity of Eq. (3.2-10) to Eq.(3.2-7), it reduces to

$$\begin{aligned} \overline{\overline{G}}^{(0,0)}(\bar{r}_2, \bar{r}_1) - \overline{\overline{G}}^{(0,0)}(\bar{r}_1, \bar{r}_2)^T &= - \iint_{z=0 \text{ plane}} ds \left\{ \begin{aligned} &\left[\hat{z} \times \overline{\overline{G}}^{(1,0)}(\bar{r}, \bar{r}_2) \right]^T \cdot \left(\nabla \times \overline{\overline{G}}^{(0,0)}(\bar{r}, \bar{r}_1) \right) \\ &- \left[\nabla \times \overline{\overline{G}}^{(0,0)}(\bar{r}, \bar{r}_2) \right]^T \cdot \left(\hat{z} \times \overline{\overline{G}}^{(1,0)}(\bar{r}, \bar{r}_1) \right) \end{aligned} \right\} \\ &= - \iint_{z=0 \text{ plane}} ds \left\{ \begin{aligned} &\left[\overline{\overline{G}}^{(1,0)}(\bar{r}, \bar{r}_2) \right]^T \left(\hat{z} \times \overline{\overline{I}} \right)^T \cdot \left(\nabla \times \overline{\overline{G}}^{(0,0)}(\bar{r}, \bar{r}_1) \right) - \\ &\left[\left(\overline{\overline{G}}^{(1,0)}(\bar{r}, \bar{r}_1) \right)^T \left(\hat{z} \times \overline{\overline{I}} \right)^T \cdot \nabla \times \overline{\overline{G}}^{(0,0)}(\bar{r}, \bar{r}_2) \right]^T \end{aligned} \right\} \\ &= - \iint_{z=0 \text{ plane}} ds \left\{ \begin{aligned} &- \left[\overline{\overline{G}}^{(1,0)}(\bar{r}, \bar{r}_2) \right]^T \cdot \hat{z} \times \left(\nabla \times \overline{\overline{G}}^{(0,0)}(\bar{r}, \bar{r}_1) \right) \\ &+ \left[\left(\overline{\overline{G}}^{(1,0)}(\bar{r}, \bar{r}_1) \right)^T \cdot \hat{z} \times \left(\nabla \times \overline{\overline{G}}^{(0,0)}(\bar{r}, \bar{r}_2) \right) \right]^T \end{aligned} \right\} \\ &= - \frac{\mu_{0r}}{\mu_{1r}} \iint_{z=0 \text{ plane}} ds \left\{ \begin{aligned} &- \left[\overline{\overline{G}}^{(1,0)}(\bar{r}, \bar{r}_2) \right]^T \cdot \hat{z} \times \nabla \times \overline{\overline{G}}^{(1,0)}(\bar{r}, \bar{r}_1) \\ &+ \left[\left(\overline{\overline{G}}^{(1,0)}(\bar{r}, \bar{r}_1) \right)^T \cdot \hat{z} \times \nabla \times \overline{\overline{G}}^{(1,0)}(\bar{r}, \bar{r}_2) \right]^T \end{aligned} \right\} \end{aligned} \quad (3.2-11)$$

Step 2: Let $\overline{\overline{P}} = \overline{\overline{G}}^{(1,0)}(\overline{r}, \overline{r}_1)$, $\overline{\overline{Q}} = \overline{\overline{G}}^{(1,0)}(\overline{r}, \overline{r}_2)$

It is noted here $\overline{\overline{Q}}$ and $\overline{\overline{P}}$ represent the DGFs of Region 1 for the geometries shown in Fig. 3-3(a) and (b), respectively. With $\overline{\overline{Q}}$ and $\overline{\overline{P}}$ substituted in Eq. (3.2-2), the volume integral in Eq. (3.2-2) is for Region 1 and the closed surface integral is for the surface bounding the volume of Region 1. Thus for Region 1, $\overline{\overline{Q}}$ and $\overline{\overline{P}}$ satisfy the following wave equations.

$$\begin{aligned} \nabla \times \nabla \times \overline{\overline{Q}} - k_0^2 \overline{\overline{\epsilon}}_{1r} \overline{\overline{\mu}}_{1r} \overline{\overline{Q}} &= 0 \rightarrow \nabla \times \nabla \times \overline{\overline{Q}} = k_0^2 \overline{\overline{\epsilon}}_{1r} \overline{\overline{\mu}}_{1r} \overline{\overline{Q}} \\ \nabla \times \nabla \times \overline{\overline{P}} - k_0^2 \overline{\overline{\epsilon}}_{1r} \overline{\overline{\mu}}_{1r} \overline{\overline{P}} &= 0 \rightarrow \nabla \times \nabla \times \overline{\overline{P}} = k_0^2 \overline{\overline{\epsilon}}_{1r} \overline{\overline{\mu}}_{1r} \overline{\overline{P}} \end{aligned} \quad (3.2-12)$$

Substituting Eq. (3.2-12) together with defined $\overline{\overline{Q}}$ and $\overline{\overline{P}}$ into Eq. (3.2-2) and replacing the closed surface integral with a surface integral about the $z=0$ plane gives

$$\begin{aligned} & \iiint_V \left\{ \left[k_0^2 \overline{\overline{\epsilon}}_{1r} \overline{\overline{\mu}}_{1r} \overline{\overline{G}}^{(1,0)}(\overline{r}, \overline{r}_2) \right]^T \cdot \overline{\overline{G}}^{(1,0)}(\overline{r}, \overline{r}_1) \right. \\ & \left. - \left[\overline{\overline{G}}^{(1,0)}(\overline{r}, \overline{r}_2) \right]^T \cdot \left[k_0^2 \overline{\overline{\epsilon}}_{1r} \overline{\overline{\mu}}_{1r} \overline{\overline{G}}^{(1,0)}(\overline{r}, \overline{r}_1) \right] \right\} dv \\ &= \iiint_V \left\{ k_0^2 \overline{\overline{G}}^{(1,0)}(\overline{r}, \overline{r}_2)^T \overline{\overline{\epsilon}}_{1r} \overline{\overline{\mu}}_{1r} \cdot \overline{\overline{G}}^{(1,0)}(\overline{r}, \overline{r}_1) \right. \\ & \left. - \left[\overline{\overline{G}}^{(1,0)}(\overline{r}, \overline{r}_2) \right]^T \cdot \left[k_0^2 \overline{\overline{\epsilon}}_{1r} \overline{\overline{\mu}}_{1r} \overline{\overline{G}}^{(1,0)}(\overline{r}, \overline{r}_1) \right] \right\} dv \\ &= 0 = \iint_{z=0 \text{ plane}} ds \left\{ \left[\hat{z} \times \overline{\overline{G}}^{(1,0)}(\overline{r}, \overline{r}_2) \right]^T \cdot \left(\nabla \times \overline{\overline{G}}^{(1,0)}(\overline{r}, \overline{r}_1) \right) \right. \\ & \left. - \left[\nabla \times \overline{\overline{G}}^{(1,0)}(\overline{r}, \overline{r}_2) \right]^T \cdot \left(\hat{z} \times \overline{\overline{G}}^{(1,0)}(\overline{r}, \overline{r}_1) \right) \right\} \\ & - \iint_{z=-d \text{ plane}} ds \left\{ \left[\hat{z} \times \overline{\overline{G}}^{(1,0)}(\overline{r}, \overline{r}_2) \right]^T \cdot \left(\nabla \times \overline{\overline{G}}^{(1,0)}(\overline{r}, \overline{r}_1) \right) \right. \\ & \left. - \left[\nabla \times \overline{\overline{G}}^{(1,0)}(\overline{r}, \overline{r}_2) \right]^T \cdot \left(\hat{z} \times \overline{\overline{G}}^{(1,0)}(\overline{r}, \overline{r}_1) \right) \right\} \end{aligned} \quad (3.2-13)$$

It should be noted that $\hat{n} = \hat{z}$ for the $z = 0$ plane and $\hat{n} = -\hat{z}$ for the $z = -d$ plane. Applying the identity of Eq. (3.2-10), Eq. (3.2-13) can be written as

$$\begin{aligned}
0 &= \left(\iint_{z=0 \text{ plane}} - \iint_{z=-d \text{ plane}} \right) ds \left\{ \begin{aligned} &\left[\hat{z} \times \overline{\overline{G}}^{(1,0)}(\bar{r}, \bar{r}_2) \right]^T \cdot \left(\nabla \times \overline{\overline{G}}^{(1,0)}(\bar{r}, \bar{r}_1) \right) \\ &- \left[\nabla \times \overline{\overline{G}}^{(1,0)}(\bar{r}, \bar{r}_2) \right]^T \cdot \left(\hat{z} \times \overline{\overline{G}}^{(1,0)}(\bar{r}, \bar{r}_1) \right) \end{aligned} \right\} \\
&= \left(\iint_{z=0 \text{ plane}} - \iint_{z=-d \text{ plane}} \right) ds \left\{ \begin{aligned} &\overline{\overline{G}}^{(1,0)}(\bar{r}, \bar{r}_2)^T \left(\hat{z} \times \bar{I} \right)^T \cdot \left(\nabla \times \overline{\overline{G}}^{(1,0)}(\bar{r}, \bar{r}_1) \right) \\ &- \left[\overline{\overline{G}}^{(1,0)}(\bar{r}, \bar{r}_1)^T \left(\hat{z} \times \bar{I} \right)^T \cdot \left(\nabla \times \overline{\overline{G}}^{(1,0)}(\bar{r}, \bar{r}_2) \right) \right]^T \end{aligned} \right\} \\
&= \left(\iint_{z=0 \text{ plane}} - \iint_{z=-d \text{ plane}} \right) ds \left\{ \begin{aligned} &-\overline{\overline{G}}^{(1,0)}(\bar{r}, \bar{r}_2)^T \cdot \hat{z} \times \nabla \times \overline{\overline{G}}^{(1,0)}(\bar{r}, \bar{r}_1) \\ &+ \left[\overline{\overline{G}}^{(1,0)}(\bar{r}, \bar{r}_1)^T \cdot \hat{z} \times \nabla \times \overline{\overline{G}}^{(1,0)}(\bar{r}, \bar{r}_2) \right]^T \end{aligned} \right\}
\end{aligned} \tag{3.2-14}$$

Step 3: Let $\overline{\overline{P}} = \overline{\overline{G}}^{(2,0)}(\bar{r}, \bar{r}_1)$, $\overline{\overline{Q}} = \overline{\overline{G}}^{(2,0)}(\bar{r}, \bar{r}_2)$

It is noted here $\overline{\overline{Q}}$ and $\overline{\overline{P}}$ represent the DGFs of Region 2 for the geometries shown in Fig.

3-3(a) and (b), respectively. Thus, for the region of $z < -d$, $\overline{\overline{Q}}$ and $\overline{\overline{P}}$ satisfy the following wave equations.

$$\begin{aligned}
\nabla \times \nabla \times \overline{\overline{Q}} - k_0^2 \mu_{2r} \varepsilon_{2r} \overline{\overline{Q}} &= 0 \rightarrow \nabla \times \nabla \times \overline{\overline{Q}} = k_0^2 \mu_{2r} \varepsilon_{2r} \overline{\overline{Q}} \\
\nabla \times \nabla \times \overline{\overline{P}} - k_0^2 \mu_{2r} \varepsilon_{2r} \overline{\overline{P}} &= 0 \rightarrow \nabla \times \nabla \times \overline{\overline{P}} = k_0^2 \mu_{2r} \varepsilon_{2r} \overline{\overline{P}}
\end{aligned} \tag{3.2-15}$$

Substituting Eq. (3.2-15) into Eq. (3.2-2) gives

$$\iiint_V \left\{ \begin{aligned} &\left[k_0^2 \mu_{2r} \varepsilon_{2r} \overline{\overline{Q}} \right]^T \cdot \overline{\overline{P}} \\ &-\overline{\overline{Q}}^T \cdot \left[k_0^2 \mu_{2r} \varepsilon_{2r} \overline{\overline{P}} \right] \end{aligned} \right\} dv = \oint_S \left\{ \begin{aligned} &\left[\hat{n} \times \overline{\overline{Q}} \right]^T \cdot \left(\nabla \times \overline{\overline{P}} \right) \\ &- \left[\nabla \times \overline{\overline{Q}} \right]^T \cdot \left(\hat{n} \times \overline{\overline{P}} \right) \end{aligned} \right\} ds \tag{3.2-16}$$

The volume integral is for Region 2 and the closed surface integral is for the surface bounding the volume of Region 2. With $\overline{\overline{Q}}$ and $\overline{\overline{P}}$ substituted, Eq. (3.2-26) is equivalent to

$$\begin{aligned} & \iiint_V \left\{ \left[k_0^2 \mu_{2r} \varepsilon_{2r} \overline{\overline{G}}^{(2,0)}(\overline{r}, \overline{r}_2) \right]^T \cdot \overline{\overline{G}}^{(2,0)}(\overline{r}, \overline{r}_1) \right. \\ & \left. - \overline{\overline{G}}^{(2,0)}(\overline{r}, \overline{r}_2) \cdot \left[k_0^2 \mu_{2r} \varepsilon_{2r} \overline{\overline{G}}^{(2,0)}(\overline{r}, \overline{r}_1) \right] \right\} dv = \\ & \oint_S \left\{ \left[\hat{n} \times \overline{\overline{G}}^{(2,0)}(\overline{r}, \overline{r}_2) \right]^T \cdot \left(\nabla \times \overline{\overline{G}}^{(2,0)}(\overline{r}, \overline{r}_1) \right) \right. \\ & \left. - \left[\nabla \times \overline{\overline{G}}^{(2,0)}(\overline{r}, \overline{r}_2) \right]^T \cdot \left(\hat{n} \times \overline{\overline{G}}^{(2,0)}(\overline{r}, \overline{r}_1) \right) \right\} ds \end{aligned} \quad (3.2-17)$$

Simplifying Eq. (3.2-17) gives

$$0 = \oint_S \left\{ \left[\hat{n} \times \overline{\overline{G}}^{(2,0)}(\overline{r}, \overline{r}_2) \right]^T \cdot \left(\nabla \times \overline{\overline{G}}^{(2,0)}(\overline{r}, \overline{r}_1) \right) \right. \\ \left. - \left[\nabla \times \overline{\overline{G}}^{(2,0)}(\overline{r}, \overline{r}_2) \right]^T \cdot \left(\hat{n} \times \overline{\overline{G}}^{(2,0)}(\overline{r}, \overline{r}_1) \right) \right\} ds \quad (3.2-18)$$

The closed surface integral can be reduced to a surface integral about the $z = -d$ plane by employing the radiation boundary condition as $z \rightarrow -\infty$. In this case, Eq. (3.2-6) reduces to

$$0 = \iint_{z=-d \text{ plane}} ds \left\{ \left[\hat{z} \times \overline{\overline{G}}^{(2,0)}(\overline{r}, \overline{r}_2) \right]^T \cdot \left(\nabla \times \overline{\overline{G}}^{(2,0)}(\overline{r}, \overline{r}_1) \right) \right. \\ \left. - \left[\nabla \times \overline{\overline{G}}^{(2,0)}(\overline{r}, \overline{r}_2) \right]^T \cdot \left(\hat{z} \times \overline{\overline{G}}^{(2,0)}(\overline{r}, \overline{r}_1) \right) \right\} \quad (3.2-19)$$

The continuity of the electric field and magnetic field at $z = -d$ for the geometry shown in Fig. 3-3(a) requires the DGFs to satisfy the following boundary conditions.

$$\begin{aligned}\hat{z} \times \overline{\overline{G}}^{(2,0)}(\bar{r}, \bar{r}_1) &= \hat{z} \times \overline{\overline{G}}^{(1,0)}(\bar{r}, \bar{r}_1), \\ \frac{1}{\mu_{2r}} \hat{z} \times \nabla \times \overline{\overline{G}}^{(2,0)}(\bar{r}, \bar{r}_1) &= \frac{1}{\mu_{1r}} \hat{z} \times \nabla \times \overline{\overline{G}}^{(1,0)}(\bar{r}, \bar{r}_1)\end{aligned}\quad (3.2-20)$$

The continuity of the electric field and magnetic field at $z = -d$ for geometry shown in

Fig. 3-3(b) requires the DGFs to satisfy the following boundary conditions.

$$\begin{aligned}\hat{z} \times \overline{\overline{G}}^{(2,0)}(\bar{r}, \bar{r}_2) &= \hat{z} \times \overline{\overline{G}}^{(1,0)}(\bar{r}, \bar{r}_2), \\ \frac{1}{\mu_{2r}} \hat{z} \times \nabla \times \overline{\overline{G}}^{(2,0)}(\bar{r}, \bar{r}_2) &= \frac{1}{\mu_{1r}} \hat{z} \times \nabla \times \overline{\overline{G}}^{(1,0)}(\bar{r}, \bar{r}_2)\end{aligned}\quad (3.2-21)$$

Applying the boundary conditions of Eq. (3.2-20) and Eq. (3.2-21) together with the identity of Eq. (3.2-10) to Eq. (3.2-19), it reduces to

$$\begin{aligned}0 &= \iint_{z=-d \text{ plane}} ds \left\{ \begin{aligned} &\left[\hat{z} \times \overline{\overline{G}}^{(1,0)}(\bar{r}, \bar{r}_2) \right]^T \cdot \left(\nabla \times \overline{\overline{G}}^{(2,0)}(\bar{r}, \bar{r}_1) \right) \\ &- \left[\nabla \times \overline{\overline{G}}^{(2,0)}(\bar{r}, \bar{r}_2) \right]^T \cdot \left(\hat{z} \times \overline{\overline{G}}^{(1,0)}(\bar{r}, \bar{r}_1) \right) \end{aligned} \right\} \\ &= \iint_{z=-d \text{ plane}} ds \left\{ \begin{aligned} &\left[\overline{\overline{G}}^{(1,0)}(\bar{r}, \bar{r}_2) \right]^T \left(\hat{z} \times \bar{I} \right)^T \cdot \left(\nabla \times \overline{\overline{G}}^{(2,0)}(\bar{r}, \bar{r}_1) \right) \\ &- \left[\left(\overline{\overline{G}}^{(1,0)}(\bar{r}, \bar{r}_1) \right)^T \left(\hat{z} \times \bar{I} \right)^T \cdot \nabla \times \overline{\overline{G}}^{(2,0)}(\bar{r}, \bar{r}_2) \right]^T \end{aligned} \right\} \\ &= \iint_{z=-d \text{ plane}} ds \left\{ \begin{aligned} &- \left[\overline{\overline{G}}^{(1,0)}(\bar{r}, \bar{r}_2) \right]^T \cdot \hat{z} \times \left(\nabla \times \overline{\overline{G}}^{(2,0)}(\bar{r}, \bar{r}_1) \right) \\ &+ \left[\left(\overline{\overline{G}}^{(1,0)}(\bar{r}, \bar{r}_1) \right)^T \cdot \hat{z} \times \left(\nabla \times \overline{\overline{G}}^{(2,0)}(\bar{r}, \bar{r}_2) \right) \right]^T \end{aligned} \right\} \\ &= \frac{\mu_{2r}}{\mu_{1r}} \iint_{z=-d \text{ plane}} ds \left\{ \begin{aligned} &- \left[\overline{\overline{G}}^{(1,0)}(\bar{r}, \bar{r}_2) \right]^T \cdot \hat{z} \times \nabla \times \overline{\overline{G}}^{(1,0)}(\bar{r}, \bar{r}_1) \\ &+ \left[\left(\overline{\overline{G}}^{(1,0)}(\bar{r}, \bar{r}_1) \right)^T \cdot \hat{z} \times \nabla \times \overline{\overline{G}}^{(1,0)}(\bar{r}, \bar{r}_2) \right]^T \end{aligned} \right\}\end{aligned}\quad (3.2-22)$$

Eq. (3.2-22) is equivalent to

$$\iint_{z=-d \text{ plane}} ds \left\{ \begin{array}{l} - \left[\overline{\overline{G}}^{(1,0)}(\bar{r}, \bar{r}_2) \right]^T \cdot \hat{z} \times \nabla \times \overline{\overline{G}}^{(1,0)}(\bar{r}, \bar{r}_1) \\ + \left[\left(\overline{\overline{G}}^{(1,0)}(\bar{r}, \bar{r}_1) \right)^T \cdot \hat{z} \times \nabla \times \overline{\overline{G}}^{(1,0)}(\bar{r}, \bar{r}_2) \right]^T \end{array} \right\} = 0 \quad (3.2-23)$$

Substituting Eq. (3.2-33) into Eq. (3.2-14) leads to

$$\iint_{z=0 \text{ plane}} ds \left\{ \begin{array}{l} - \overline{\overline{G}}^{(1,0)}(\bar{r}, \bar{r}_2)^T \cdot \hat{z} \times \nabla \times \overline{\overline{G}}^{(1,0)}(\bar{r}, \bar{r}_1) \\ + \left[\overline{\overline{G}}^{(1,0)}(\bar{r}, \bar{r}_1)^T \cdot \hat{z} \times \nabla \times \overline{\overline{G}}^{(1,0)}(\bar{r}, \bar{r}_2) \right]^T \end{array} \right\} = 0 \quad (3.2-24)$$

With Eq. (3.2-24) substituted into Eq. (3.2-11), the following symmetry property is obtained.

$$\begin{aligned} \overline{\overline{G}}^{(0,0)}(\bar{r}_2, \bar{r}_1) - \overline{\overline{G}}^{(0,0)}(\bar{r}_1, \bar{r}_2)^T &= 0 \\ \Rightarrow \overline{\overline{G}}^{(0,0)}(\bar{r}_2, \bar{r}_1) \Big|_{\varepsilon_{1r}} &= \overline{\overline{G}}^{(0,0)}(\bar{r}_1, \bar{r}_2)^T \Big|_{\varepsilon_{1r}^T} \end{aligned} \quad (3.2-25)$$

3.2.2 DGF for the Region of $z > z'$

The DGFs for the region of $0 < z < z'$ in Region 0 of the half-space problem is already obtained in Section 3.1.1, which is repeated below.

For $0 < z < z'$

$$\overline{\overline{G}}^{(0,0)}(\bar{r}, \bar{r}') = \frac{i}{8\pi^2} \int_{-\infty}^{\infty} dk_x dk_y \frac{1}{k_{0z}} \left\{ \begin{array}{l} \left[\hat{h}_0(-k_{0z}) e^{i\bar{k}_0 \cdot \bar{r}} + R_{hh}^{01} \hat{h}_0(k_{0z}) e^{i\bar{k}_0 \cdot \bar{r}} \right] \hat{h}_0(-k_{0z}) \\ + \left[R_{hv}^{01} \hat{v}_0(k_{0z}) e^{i\bar{k}_0 \cdot \bar{r}} \right] \hat{v}_0(-k_{0z}) \end{array} \right\} e^{-i\bar{k}_0 \cdot \bar{r}'} \quad (3.2-26)$$

Using the symmetrical property derived in Eq. (3.2-25), the DGF for the region of $z > z'$ is obtained as follows.

For $z > z'$

$$\begin{aligned} \overline{\overline{G}}^{(0,0)}(\vec{r}, \vec{r}') &= \left[\overline{\overline{G}}^{(0,0)}(\vec{r}', \vec{r}) \right]_{\varepsilon_1}^T = \\ & \frac{i}{8\pi^2} \int_{-\infty}^{\infty} dk_x dk_y \frac{1}{k_{0z}} \left\{ \begin{array}{l} \hat{h}_0(-k_{0z}) e^{-i\vec{k}_0 \cdot \vec{r}} \left[\hat{h}_0(-k_{0z}) e^{i\vec{k}_0 \cdot \vec{r}'} + R_{hh}^{01} \hat{h}_0(k_{0z}) e^{i\vec{k}_0 \cdot \vec{r}'} \right] \\ + R_{hv}^{01} \hat{v}_0(k_{0z}) e^{i\vec{k}_0 \cdot \vec{r}'} \\ \hat{v}_0(-k_{0z}) e^{-i\vec{k}_0 \cdot \vec{r}} \left[\hat{v}_0(-k_{0z}) e^{i\vec{k}_0 \cdot \vec{r}'} + R_{vh}^{01} \hat{h}_0(k_{0z}) e^{i\vec{k}_0 \cdot \vec{r}'} \right] \\ + R_{vv}^{01} \hat{v}_0(k_{0z}) e^{i\vec{k}_0 \cdot \vec{r}'} \end{array} \right\}_{\varepsilon_1}^T \end{aligned} \quad (3.2-27)$$

In order to make the above equation have more clearly physical meaning, the following substitution is applied to the above equation,

$$k_x \rightarrow -k_x, \quad k_y \rightarrow -k_y \quad (3.2-28)$$

Under this transformation, the field vectors in the isotropic Region 0 become as follows.

$$\hat{h}_0(-k_x, -k_y, -k_{0z}) = -\hat{h}_0(k_x, k_y, k_{0z}), \quad \hat{v}_0(-k_x, -k_y) = \hat{v}_0^+(k_x, k_y) \quad (3.2-29)$$

Substituting Eq. (3.2-29) into Eq. (3.2-27), the DGF for the region above the source point ($z > z'$) is written as follows.

$$\begin{aligned} \overline{\overline{G}}^{(0,0)}(\vec{r}, \vec{r}') &= \frac{i}{8\pi^2} \int_{-\infty}^{\infty} dk_x dk_y \frac{1}{k_{0z}} \left\{ \begin{array}{l} \hat{h}_0(+k_{0z}) e^{i\vec{k}_0 \cdot \vec{r}} \left[\hat{h}_0(+k_{0z}) e^{-i\vec{k}_0 \cdot \vec{r}'} \right. \\ \left. + R_{hh}^{01}(-k_x, -k_y) \hat{h}_0(-k_{0z}) e^{-i\vec{k}_0 \cdot \vec{r}'} \right. \\ \left. - R_{hv}^{01}(-k_x, -k_y) \hat{v}_0(-k_{0z}) e^{-i\vec{k}_0 \cdot \vec{r}'} \right] \\ + \hat{v}_0(+k_{0z}) e^{+i\vec{k}_0 \cdot \vec{r}} \left[\hat{v}_0(+k_{0z}) e^{-i\vec{k}_0 \cdot \vec{r}'} \right. \\ \left. - R_{vh}^{01}(-k_x, -k_y) \hat{h}_0(-k_{0z}) e^{-i\vec{k}_0 \cdot \vec{r}'} \right. \\ \left. + R_{vv}^{01}(-k_x, -k_y) \hat{v}_0(-k_{0z}) e^{-i\vec{k}_0 \cdot \vec{r}'} \right] \end{array} \right\}_{\varepsilon_1}^T \end{aligned} \quad (3.2-30)$$

It can be shown numerically that the following relation holds for a biaxial medium.

$$\begin{aligned}
R_{hh}^{01}(-k_x, -k_y) &= R_{hh}^{01}(k_x, k_y) \\
R_{hv}^{01}(-k_x, -k_y) &= -R_{vh}^{01}(k_x, k_y) \\
R_{vh}^{01}(-k_x, -k_y) &= -R_{hv}^{01}(k_x, k_y) \\
R_{vv}^{01}(-k_x, -k_y) &= R_{vv}^{01}(k_x, k_y)
\end{aligned} \tag{3.2-31}$$

For the two-layer geometry, the dyadic Green's function for the region above the source point ($z > z'$) can also be obtained using the symmetrical property of Eq. (3.2-25).

$$\overline{\overline{G}}^{(0,0)}(\vec{r}, \vec{r}') = \frac{i}{8\pi^2} \int_{-\infty}^{\infty} dk_x dk_y \frac{1}{k_{0z}} \left\{ \begin{array}{l} \hat{h}_0(+k_{0z}) e^{i\vec{k}_0 \cdot \vec{r}'} \\ + R_{hh}(-k_x, -k_y) \hat{h}_0(-k_{0z}) e^{-i\vec{k}_0 \cdot \vec{r}'} \\ - R_{hv}(-k_x, -k_y) \hat{v}_0(-k_{0z}) e^{-i\vec{k}_0 \cdot \vec{r}'} \end{array} \right\}_{\varepsilon_1} \tag{3.2-32}$$

$$\left\{ \begin{array}{l} \hat{v}_0(+k_{0z}) e^{-i\vec{k}_0 \cdot \vec{r}'} \\ - R_{vh}(-k_x, -k_y) \hat{h}_0(-k_{0z}) e^{-i\vec{k}_0 \cdot \vec{r}'} \\ + R_{vv}(-k_x, -k_y) \hat{v}_0(-k_{0z}) e^{-i\vec{k}_0 \cdot \vec{r}'} \end{array} \right\}_{\varepsilon_1}$$

Same as the half-space reflection coefficients, it can also be shown numerically that the two-layer reflection coefficients satisfy the following relation for a two-layer problem with the anisotropic region being a biaxial medium.

$$\begin{aligned}
R_{hh}(-k_x, -k_y) &= R_{hh}(k_x, k_y) \\
R_{hv}(-k_x, -k_y) &= -R_{vh}(k_x, k_y) \\
R_{vh}(-k_x, -k_y) &= -R_{hv}(k_x, k_y) \\
R_{vv}(-k_x, -k_y) &= R_{vv}(k_x, k_y)
\end{aligned} \tag{3.2-33}$$

It needs to be noted here no such kind of relationship holds for both the half-space problem and two-layer geometry filled with a non-reciprocal medium. The DGF of $\overline{\overline{G}}^{(0,0)}(\vec{r}, \vec{r}')$ for the region $z > z'$ obtained here has no restriction to the property of the medium. The anisotropic

medium could be either reciprocal or non-reciprocal medium. It is crucial to obtain the DGF of $\overline{\overline{G}}^{(0,0)}(\vec{r}, \vec{r}')$ for the region of $z > z'$ to calculate the radiated field due to a current source in the presence of a layered geometry with arbitrary anisotropic medium involved, which will be shown in detail in Chapter 4.

3.3 Modified Symmetrical Property for $\overline{\overline{G}}^{(1,0)}(\vec{r}, \vec{r}')$ and $\overline{\overline{G}}^{(0,1)}(\vec{r}, \vec{r}')$

In order to obtain the far field in Region 0 when the source is located in Region 1 (anisotropic region), the DGF for region $z > 0$ is usually needed. It is known from [37] that if the source is located in Region 1 (anisotropic medium) instead of Region 0 (isotropic medium), the DGF for the region above the source point can be obtained from the DGF for the anisotropic region below the source point using symmetrical property if the medium is reciprocal. What if the anisotropic region containing the source is non-reciprocal with the permittivity or permeability as a hermitian matrix instead of a symmetric matrix, can the symmetrical property still be applied? The reciprocity relationships for the unbounded gyrotropic media is considered in [70]. However, symmetrical property for a layered geometry with a non-reciprocal medium involved is not investigated previously, which is of primary interest in this section.

3.3.1 Proof of the Modified Symmetrical Property

It will be shown in this section that $\overline{\overline{G}}^{(0,1)}(\vec{r}, \vec{r}')$ can be obtained from $\overline{\overline{G}}^{(1,0)}(\vec{r}, \vec{r}')$ which corresponds to the DGF of Region 1 with the source located in Region 0 for a layered geometry as derived from Section 3.1. In particular, the following relationships hold for a layered geometry with the anisotropic region filled with a reciprocal medium.

Region 1 is reciprocal:

$$\overline{\overline{G}}^{(0,1)}(\overline{r}_2, \overline{r}_1) = \frac{\mu_{0r}}{\mu_{1r}} \overline{\overline{G}}^{(1,0)}(\overline{r}_1, \overline{r}_2)^T \quad (3.3-1)$$

Eq. (3.3-1) states that for the half-space problem or two-layer geometry filled with a reciprocal medium, the DGF in Region 0 (isotropic region) when source is located inside the anisotropic region can be obtained from the transpose of the DGF of Region 1 with source in Region 0. If the source is embedded inside the anisotropic region of a non-reciprocal medium, the modified symmetrical property is given in Eq. (3.3-2).

Region 1 is non-reciprocal:

$$\overline{\overline{G}}^{(0,1)}(\overline{r}_2, \overline{r}_1) \Big|_{\varepsilon(\text{region}1)=\varepsilon_{1r}} = \frac{\mu_{0r}}{\mu_{1r}} \overline{\overline{G}}^{(1,0)}(\overline{r}_1, \overline{r}_2)^T \Big|_{\varepsilon(\text{region}1)=\varepsilon_{1r}^T} \quad (3.3-2)$$

Eq. (3.3-2) states that the DGFs of Region 0 for the both the half-space and two-layer problems can still be obtained from the DGFs of Region 1 with source located in Region 0 under the condition that Region 1 is filled with the medium whose permittivity tensor is the transpose of that of the original medium of Region 1. For the gyrotropic medium, this condition is equivalent to reversing the direction of the biasing magnetic field of Region 1.

Observing Eq. (3.3-1) and Eq. (3.3-2) reveals that Eq. (3.3-1) is actually a special case of Eq. (3.3-2) as the relationship of $\varepsilon_{1r}^T = \varepsilon_{1r}$ holds for a reciprocal medium. Thus, the proof of Eq. (3.3-2) is only presented. Dyadic-dyadic Green's theorem of the second kind (Eq. (3.2-2)), given by Tai [34] is again essential in this proof of the modified symmetrical property.

To facilitate the proof of the modified symmetrical property, two different geometries are considered as shown in Fig. 3-4.

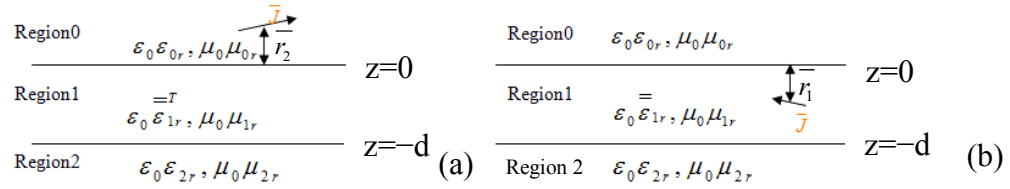


Fig. 3-4: Two different geometries constructed here for the proof of symmetrical property when the source are in different regions.

In both Fig. 3-4(a) and Fig. 3-4(b), Region 0 is denoted as the isotropic region with the relative permittivity and permeability of $\varepsilon_{0r}, \mu_{0r}$, and Region 2 is denoted as the isotropic region with the relative permittivity and permeability of $\varepsilon_{2r}, \mu_{2r}$. However, the source locations and the media for Region 1 are different for the two geometries. In Fig. 3-4(a), Region 1 is filled with the medium characterized by $\varepsilon_{1r}, \mu_{1r}$ and the source is located at \bar{r}_2 in Region 0, while in Fig. 3-4(b), the source is located at \bar{r}_1 in Region 1 with Region 1 filled with the medium of $\varepsilon_{1r}, \mu_{1r}$.

Step 1: $\bar{\bar{Q}}$ and $\bar{\bar{P}}$ are assigned as follows.

$$\bar{\bar{Q}} = \bar{\bar{G}}^{(0,0)}(\bar{r}, \bar{r}_2), \quad \bar{\bar{P}} = \bar{\bar{G}}^{(0,1)}(\bar{r}, \bar{r}_1) \quad (3.3-3)$$

In Eq. (3.3-3), $\bar{\bar{Q}}$ represents the dyadic Green's function of Region 0 when the source is Region 0 for the geometry shown in Fig. 3-4(a), and $\bar{\bar{P}}$ represents the dyadic Green's function of Region 0 when the source is in Region 1 for the geometry shown in Fig. 3-4(b). Thus, for Region 0 the DGFs of $\bar{\bar{Q}}$ and $\bar{\bar{P}}$ satisfy the wave equations shown below.

$$\begin{aligned} \nabla \times \nabla \times \bar{\bar{G}}^{(0,0)}(\bar{r}, \bar{r}_2) - k_0^2 \varepsilon_{0r} \mu_{0r} \bar{\bar{G}}^{(0,0)}(\bar{r}, \bar{r}_2) &= \bar{\bar{I}} \delta(\bar{r} - \bar{r}_2) \\ \nabla \times \nabla \times \bar{\bar{G}}^{(0,1)}(\bar{r}, \bar{r}_1) - k_0^2 \varepsilon_{0r} \mu_{0r} \bar{\bar{G}}^{(0,1)}(\bar{r}, \bar{r}_1) &= 0 \end{aligned} \quad (3.3-4)$$

Substituting Eq. (3.3-3) into Eq. (3.2-2) yields

$$\begin{aligned}
& \iiint_V \left\{ \begin{aligned} & \left[\nabla \times \nabla \times \overline{\overline{G}}^{(0,0)}(\overline{r}, \overline{r}_2) \right]^T \cdot \overline{\overline{G}}^{(0,1)}(\overline{r}, \overline{r}_1) \\ & - \overline{\overline{G}}^{(0,0)}(\overline{r}, \overline{r}_2)^T \cdot \left[\nabla \times \nabla \times \overline{\overline{G}}^{(0,1)}(\overline{r}, \overline{r}_1) \right] \end{aligned} \right\} dv \\
& = \oint_S \left\{ \begin{aligned} & \left[\hat{n} \times \overline{\overline{G}}^{(0,0)}(\overline{r}, \overline{r}_2) \right]^T \cdot \left(\nabla \times \overline{\overline{G}}^{(0,1)}(\overline{r}, \overline{r}_1) \right) \\ & - \left[\nabla \times \overline{\overline{G}}^{(0,0)}(\overline{r}, \overline{r}_2) \right]^T \cdot \left(\hat{n} \times \overline{\overline{G}}^{(0,1)}(\overline{r}, \overline{r}_1) \right) \end{aligned} \right\} ds
\end{aligned} \tag{3.3-5}$$

In the above equation, the volume integration is over Region 0 and the closed surface integration is for the surface bounding the volume of Region 0 as shown in Fig. 3-4. Substituting Eq. (3.3-4) into Eq. (3.3-5) results in

$$\begin{aligned}
& \iiint_V \left\{ \begin{aligned} & \left[k_0^2 \epsilon_{0r} \mu_{0r} \overline{\overline{G}}^{(0,0)}(\overline{r}, \overline{r}_2) + I \delta(\overline{r} - \overline{r}_2) \right]^T \cdot \overline{\overline{G}}^{(0,1)}(\overline{r}, \overline{r}_1) \\ & - \overline{\overline{G}}^{(0,0)}(\overline{r}, \overline{r}_2)^T \cdot \left[k_0^2 \epsilon_{0r} \mu_{0r} \overline{\overline{G}}^{(0,1)}(\overline{r}, \overline{r}_1) \right] \end{aligned} \right\} dv \\
& = \oint_S \left\{ \begin{aligned} & \left[\hat{n} \times \overline{\overline{G}}^{(0,0)}(\overline{r}, \overline{r}_2) \right]^T \cdot \left(\nabla \times \overline{\overline{G}}^{(0,1)}(\overline{r}, \overline{r}_1) \right) \\ & - \left[\nabla \times \overline{\overline{G}}^{(0,0)}(\overline{r}, \overline{r}_2) \right]^T \cdot \left(\hat{n} \times \overline{\overline{G}}^{(0,1)}(\overline{r}, \overline{r}_1) \right) \end{aligned} \right\} ds
\end{aligned} \tag{3.3-6}$$

The closed surface integral in Eq. (3.3-6) can be reduced to a surface integral at $z=0$ plane using the radiation condition at infinity, which is shown below.

$$\overline{\overline{G}}^{(0,1)}(\overline{r}_2, \overline{r}_1) = - \iint_{z=0 \text{ plane}} \left\{ \begin{aligned} & \left[\hat{z} \times \overline{\overline{G}}^{(0,0)}(\overline{r}, \overline{r}_2) \right]^T \cdot \left(\nabla \times \overline{\overline{G}}^{(0,1)}(\overline{r}, \overline{r}_1) \right) \\ & - \left[\nabla \times \overline{\overline{G}}^{(0,0)}(\overline{r}, \overline{r}_2) \right]^T \cdot \left(\hat{z} \times \overline{\overline{G}}^{(0,1)}(\overline{r}, \overline{r}_1) \right) \end{aligned} \right\} ds \tag{3.3-7}$$

Step 2: $\overline{\overline{Q}}$ and $\overline{\overline{P}}$ are assigned as follows.

$$\overline{\overline{Q}} = \overline{\overline{G}}^{(1,0)}(\bar{r}, \bar{r}_2), \quad \overline{\overline{P}} = \overline{\overline{G}}^{(1,1)}(\bar{r}, \bar{r}_1) \quad (3.3-8)$$

In Eq. (3.3-8), $\overline{\overline{Q}}$ represents the dyadic Green's function of Region 1 when the source is in Region 0 for the geometry as shown in Fig. 3-4(a), and $\overline{\overline{P}}$ represents the dyadic Green's function of Region 1 when the source is in Region 1 for the geometry as shown in Fig. 3-4(b).

Thus, for Region 1 the dyadic Green's functions satisfy the wave equations shown below.

$$\begin{aligned} \nabla \times \nabla \times \overline{\overline{G}}^{(1,0)}(\bar{r}, \bar{r}_2) - \varepsilon_{1r} \mu_{1r} k_0^2 \overline{\overline{G}}^{(1,0)}(\bar{r}, \bar{r}_2) &= 0 \\ \nabla \times \nabla \times \overline{\overline{G}}^{(1,1)}(\bar{r}, \bar{r}_1) - \varepsilon_{1r} \mu_{1r} k_0^2 \overline{\overline{G}}^{(1,1)}(\bar{r}, \bar{r}_1) &= \overline{\overline{I}} \delta(\bar{r} - \bar{r}_1) \end{aligned} \quad (3.3-9)$$

Substituting Eq. (3.3-8) into Eq. (3.2-2) yields

$$\begin{aligned} & \iiint_V \left\{ \left[\nabla \times \nabla \times \overline{\overline{G}}^{(1,0)}(\bar{r}, \bar{r}_2) \right]^T \cdot \overline{\overline{G}}^{(1,1)}(\bar{r}, \bar{r}_1) - \overline{\overline{G}}^{(1,0)}(\bar{r}, \bar{r}_2)^T \cdot \left[\nabla \times \nabla \times \overline{\overline{G}}^{(1,1)}(\bar{r}, \bar{r}_1) \right] \right\} dv \\ &= \oiint_S \left\{ \left[\hat{n} \times \overline{\overline{G}}^{(1,0)}(\bar{r}, \bar{r}_2) \right]^T \cdot \left(\nabla \times \overline{\overline{G}}^{(1,1)}(\bar{r}, \bar{r}_1) \right) - \left[\nabla \times \overline{\overline{G}}^{(1,0)}(\bar{r}, \bar{r}_2) \right]^T \cdot \left(\hat{n} \times \overline{\overline{G}}^{(1,1)}(\bar{r}, \bar{r}_1) \right) \right\} ds \end{aligned} \quad (3.3-10)$$

Substituting Eq. (3.3-9) into Eq. (3.3-10) gives

$$\begin{aligned} & \iiint_V \left\{ \left[k_0^2 \varepsilon_{1r} \mu_{1r} \overline{\overline{G}}^{(1,0)}(\bar{r}, \bar{r}_2) \right]^T \cdot \overline{\overline{G}}^{(1,1)}(\bar{r}, \bar{r}_1) \right. \\ & \left. - \overline{\overline{G}}^{(1,0)}(\bar{r}, \bar{r}_2)^T \cdot \left[k_0^2 \varepsilon_{1r} \mu_{1r} \overline{\overline{G}}^{(1,1)}(\bar{r}, \bar{r}_1) + \overline{\overline{I}} \delta(\bar{r} - \bar{r}_1) \right] \right\} dv \\ &= \oiint_S \left\{ \left[\hat{n} \times \overline{\overline{G}}^{(1,0)}(\bar{r}, \bar{r}_2) \right]^T \cdot \left(\nabla \times \overline{\overline{G}}^{(1,1)}(\bar{r}, \bar{r}_1) \right) \right. \\ & \left. - \left[\nabla \times \overline{\overline{G}}^{(1,0)}(\bar{r}, \bar{r}_2) \right]^T \cdot \left(\hat{n} \times \overline{\overline{G}}^{(1,1)}(\bar{r}, \bar{r}_1) \right) \right\} ds \end{aligned} \quad (3.3-11)$$

In Eq. (3.3-11), the volume integral is for Region 1 and the closed surface integral is for the surface bounding the volume of Region 1. Simplifying Eq. (3.3-11) gives

$$\begin{aligned}
& \iiint_V \left\{ \begin{aligned} & \left[k_0^2 \mu_r \overline{\overline{G}}(\overline{r}, \overline{r}_2) \right]^T \cdot (\overline{\varepsilon}_{1r} - \overline{\varepsilon}_{1r}) \overline{\overline{G}}(\overline{r}, \overline{r}_1) \\ & - \overline{\overline{G}}(\overline{r}, \overline{r}_2)^T \cdot \overline{I} \delta(\overline{r} - \overline{r}_1) \end{aligned} \right\} dv \\
& = \oiint_S \left\{ \begin{aligned} & \left[\hat{n} \times \overline{\overline{G}}(\overline{r}, \overline{r}_2) \right]^T \cdot \left(\nabla \times \overline{\overline{G}}(\overline{r}, \overline{r}_1) \right) \\ & - \left[\nabla \times \overline{\overline{G}}(\overline{r}, \overline{r}_2) \right]^T \cdot \left(\hat{n} \times \overline{\overline{G}}(\overline{r}, \overline{r}_1) \right) \end{aligned} \right\} ds
\end{aligned} \tag{3.3-12}$$

This directly leads to

$$\overline{\overline{G}}(\overline{r}_1, \overline{r}_2)^T = - \oiint_S \left\{ \begin{aligned} & \left[\hat{n} \times \overline{\overline{G}}(\overline{r}, \overline{r}_2) \right]^T \cdot \left(\nabla \times \overline{\overline{G}}(\overline{r}, \overline{r}_1) \right) \\ & - \left[\nabla \times \overline{\overline{G}}(\overline{r}, \overline{r}_2) \right]^T \cdot \left(\hat{n} \times \overline{\overline{G}}(\overline{r}, \overline{r}_1) \right) \end{aligned} \right\} ds \tag{3.3-13}$$

Again the closed surface integral consists of the planes located at $z=0$ and $z=-d$ plane, therefore, Eq. (3.3-13) can be expanded as

$$\begin{aligned}
& \overline{\overline{G}}(\overline{r}_1, \overline{r}_2)^T = \\
& - \iint_{z=0 \text{ plane}} ds \left\{ \begin{aligned} & \left[\hat{z} \times \overline{\overline{G}}(\overline{r}, \overline{r}_2) \right]^T \cdot \left(\nabla \times \overline{\overline{G}}(\overline{r}, \overline{r}_1) \right) \\ & - \left[\nabla \times \overline{\overline{G}}(\overline{r}, \overline{r}_2) \right]^T \cdot \left(\hat{z} \times \overline{\overline{G}}(\overline{r}, \overline{r}_1) \right) \end{aligned} \right\} \\
& + \iint_{z=-d \text{ plane}} ds \left\{ \begin{aligned} & \left[\hat{z} \times \overline{\overline{G}}(\overline{r}, \overline{r}_2) \right]^T \cdot \left(\nabla \times \overline{\overline{G}}(\overline{r}, \overline{r}_1) \right) \\ & - \left[\nabla \times \overline{\overline{G}}(\overline{r}, \overline{r}_2) \right]^T \cdot \left(\hat{z} \times \overline{\overline{G}}(\overline{r}, \overline{r}_1) \right) \end{aligned} \right\}
\end{aligned} \tag{3.3-14}$$

It is noted that the normal to the surface at $z=0$ is in the positive z direction and the normal to the surface at $z=-d$ is in the negative z direction.

Step 3: $\overline{\overline{Q}}$ and $\overline{\overline{P}}$ are assigned as follows.

$$\overline{\overline{Q}} = \overline{\overline{G}}^{(2,0)}(\overline{r}, \overline{r}_2), \overline{\overline{P}} = \overline{\overline{G}}^{(2,1)}(\overline{r}, \overline{r}_1) \quad (3.3-15)$$

In Eq. (3.3-15), $\overline{\overline{Q}}$ represents the dyadic Green's function of Region 2 when the source is in Region 0 for the geometry as shown in Fig. 3-4(a), and $\overline{\overline{P}}$ represents the dyadic Green's function of Region 2 when the source is in Region 1 for the geometry as shown in Fig. 3-4(b).

Thus, for Region 2 the dyadic Green's functions satisfy the wave equations shown below.

$$\begin{aligned} \nabla \times \nabla \times \overline{\overline{G}}^{(2,0)}(\overline{r}, \overline{r}_2) - \varepsilon_{2r} \mu_{2r} k_0^2 \overline{\overline{G}}^{(2,0)}(\overline{r}, \overline{r}_2) &= 0 \\ \nabla \times \nabla \times \overline{\overline{G}}^{(2,1)}(\overline{r}, \overline{r}_1) - \varepsilon_{2r} \mu_{2r} k_0^2 \overline{\overline{G}}^{(2,1)}(\overline{r}, \overline{r}_1) &= 0 \end{aligned} \quad (3.3-16)$$

Substituting Eq. (3.3-15) into Eq. (3.2-2) leads to

$$\begin{aligned} & \iiint_V \left\{ \left[\nabla \times \nabla \times \overline{\overline{G}}^{(2,0)}(\overline{r}, \overline{r}_2) \right]^T \cdot \overline{\overline{G}}^{(2,1)}(\overline{r}, \overline{r}_1) - \overline{\overline{G}}^{(2,0)}(\overline{r}, \overline{r}_2)^T \cdot \left[\nabla \times \nabla \times \overline{\overline{G}}^{(2,1)}(\overline{r}, \overline{r}_1) \right] \right\} dV \\ &= \oint_S \left\{ \left[\hat{n} \times \overline{\overline{G}}^{(2,0)}(\overline{r}, \overline{r}_2) \right]^T \cdot \left(\nabla \times \overline{\overline{G}}^{(2,1)}(\overline{r}, \overline{r}_1) \right) - \left[\nabla \times \overline{\overline{G}}^{(2,0)}(\overline{r}, \overline{r}_2) \right]^T \cdot \left(\hat{n} \times \overline{\overline{G}}^{(2,1)}(\overline{r}, \overline{r}_1) \right) \right\} ds \end{aligned} \quad (3.3-17)$$

Substituting Eq. (3.3-17) into Eq. (3.3-17) yields

$$\begin{aligned} & \iiint_V \left\{ \left[k_0^2 \varepsilon_{2r} \mu_{2r} \overline{\overline{G}}^{(2,0)}(\overline{r}, \overline{r}_2) \right]^T \cdot \overline{\overline{G}}^{(2,1)}(\overline{r}, \overline{r}_1) \right. \\ & \quad \left. - \overline{\overline{G}}^{(2,0)}(\overline{r}, \overline{r}_2)^T \cdot \left[k_0^2 \varepsilon_{2r} \mu_{2r} \overline{\overline{G}}^{(2,1)}(\overline{r}, \overline{r}_1) \right] \right\} dV \\ &= \oint_S \left\{ \left[\hat{n} \times \overline{\overline{G}}^{(2,0)}(\overline{r}, \overline{r}_2) \right]^T \cdot \left(\nabla \times \overline{\overline{G}}^{(2,1)}(\overline{r}, \overline{r}_1) \right) \right. \\ & \quad \left. - \left[\nabla \times \overline{\overline{G}}^{(2,0)}(\overline{r}, \overline{r}_2) \right]^T \cdot \left(\hat{n} \times \overline{\overline{G}}^{(2,1)}(\overline{r}, \overline{r}_1) \right) \right\} ds \end{aligned} \quad (3.3-18)$$

Inspecting Eq.(3.3-18) shows that

$$\oint_S \left\{ \begin{aligned} & \left[\hat{n} \times \overline{\overline{G}}^{(2,0)}(\bar{r}, \bar{r}_2) \right]^T \cdot \left(\nabla \times \overline{\overline{G}}^{(2,1)}(\bar{r}, \bar{r}_1) \right) \\ & - \left[\nabla \times \overline{\overline{G}}^{(2,0)}(\bar{r}, \bar{r}_2) \right]^T \cdot \left(\hat{n} \times \overline{\overline{G}}^{(2,1)}(\bar{r}, \bar{r}_1) \right) \end{aligned} \right\} ds = 0 \quad (3.3-19)$$

The closed surface integration is for the surface bounding the volume of Region 2 and the closed surface integral can be reduced to a surface integral at $z=-d$ plane using the radiation condition at negative infinity, which is as follows,

$$0 = \iint_{z=-d \text{ plane}} \left\{ \begin{aligned} & \left[\hat{z} \times \overline{\overline{G}}^{(2,0)}(\bar{r}, \bar{r}_2) \right]^T \cdot \left(\nabla \times \overline{\overline{G}}^{(2,1)}(\bar{r}, \bar{r}_1) \right) \\ & - \left[\nabla \times \overline{\overline{G}}^{(2,0)}(\bar{r}, \bar{r}_2) \right]^T \cdot \left(\hat{z} \times \overline{\overline{G}}^{(2,1)}(\bar{r}, \bar{r}_1) \right) \end{aligned} \right\} ds \quad (3.3-20)$$

At $z = -d$ plane, the continuity of the tangential electrical field and tangential magnetic field requires the DGFs to satisfy the following boundary conditions given in Eq. (3.3-21) and Eq. (3.3-22), corresponding to the geometries shown in Fig. 3-4 (a) and Fig. 3-4 (b), respectively.

$$\begin{aligned} \hat{z} \times \overline{\overline{G}}^{(2,0)}(\bar{r}, \bar{r}_2) &= \hat{z} \times \overline{\overline{G}}^{(1,0)}(\bar{r}, \bar{r}_2) \\ \hat{z} \times \frac{1}{\mu_{2r}} \nabla \times \overline{\overline{G}}^{(2,0)}(\bar{r}, \bar{r}_2) &= \hat{z} \times \frac{1}{\mu_{1r}} \nabla \times \overline{\overline{G}}^{(1,0)}(\bar{r}, \bar{r}_2) \end{aligned} \quad (3.3-21)$$

$$\begin{aligned} \hat{z} \times \overline{\overline{G}}^{(2,1)}(\bar{r}, \bar{r}_1) &= \hat{z} \times \overline{\overline{G}}^{(1,1)}(\bar{r}, \bar{r}_1) \\ \hat{z} \times \frac{1}{\mu_{2r}} \nabla \times \overline{\overline{G}}^{(2,1)}(\bar{r}, \bar{r}_1) &= \hat{z} \times \frac{1}{\mu_{1r}} \nabla \times \overline{\overline{G}}^{(1,1)}(\bar{r}, \bar{r}_1) \end{aligned} \quad (3.3-22)$$

Substituting the boundary conditions of Eq.(3.3-21) and Eq. (3.3-22) into Eq. (3.3-20) gives

$$0 = \iint_{z=-d \text{ plane}} \left\{ \left[\hat{z} \times \overline{\overline{G}}^{(1,0)}(\bar{r}, \bar{r}_2) \right]^T \cdot \left(\nabla \times \overline{\overline{G}}^{(2,1)}(\bar{r}, \bar{r}_1) \right) - \left[\nabla \times \overline{\overline{G}}^{(2,0)}(\bar{r}, \bar{r}_2) \right]^T \cdot \left(\hat{z} \times \overline{\overline{G}}^{(1,1)}(\bar{r}, \bar{r}_1) \right) \right\} ds$$

which can be written in the form below.

$$0 = \iint_{z=-d \text{ plane}} \left\{ \left[\overline{\overline{G}}^{(1,0)}(\overline{r}, \overline{r}_2) \right]^T \left(\hat{z} \times \overline{\overline{I}} \right)^T \cdot \left(\nabla \times \overline{\overline{G}}^{(2,1)}(\overline{r}, \overline{r}_1) \right) - \left[\nabla \times \overline{\overline{G}}^{(2,0)}(\overline{r}, \overline{r}_2) \right]^T \cdot \left(\hat{z} \times \overline{\overline{I}} \right) \left(\overline{\overline{G}}^{(1,1)}(\overline{r}, \overline{r}_1) \right) \right\} ds$$

Applying the identity of $\left(\hat{z} \times \overline{\overline{I}} \right)^T = -\hat{z} \times \overline{\overline{I}}$, we obtain

$$0 = \iint_{z=-d \text{ plane}} \left\{ \left[\overline{\overline{G}}^{(1,0)}(\overline{r}, \overline{r}_2) \right]^T \left(\hat{z} \times \nabla \times \overline{\overline{G}}^{(2,1)}(\overline{r}, \overline{r}_1) \right) - \left[\hat{z} \times \nabla \times \overline{\overline{G}}^{(2,0)}(\overline{r}, \overline{r}_2) \right]^T \cdot \left(\overline{\overline{G}}^{(1,1)}(\overline{r}, \overline{r}_1) \right) \right\} ds$$

Again substituting the boundary conditions of Eq.(3.3-21) and Eq. (3.3-22), it is obtained

$$0 = \frac{\mu_{2r}}{\mu_{1r}} \iint_{z=-d \text{ plane}} \left\{ \left[\overline{\overline{G}}^{(1,0)}(\overline{r}, \overline{r}_2) \right]^T \left(\hat{z} \times \nabla \times \overline{\overline{G}}^{(1,1)}(\overline{r}, \overline{r}_1) \right) - \left[\hat{z} \times \nabla \times \overline{\overline{G}}^{(1,0)}(\overline{r}, \overline{r}_2) \right]^T \cdot \left(\overline{\overline{G}}^{(1,1)}(\overline{r}, \overline{r}_1) \right) \right\} ds$$

which is equivalent to

$$0 = \frac{\mu_{2r}}{\mu_{1r}} \iint_{z=-d \text{ plane}} \left\{ \left[\hat{z} \times \overline{\overline{G}}^{(1,0)}(\overline{r}, \overline{r}_2) \right]^T \cdot \left(\nabla \times \overline{\overline{G}}^{(1,1)}(\overline{r}, \overline{r}_1) \right) - \left[\nabla \times \overline{\overline{G}}^{(1,0)}(\overline{r}, \overline{r}_2) \right]^T \cdot \left(\hat{z} \times \overline{\overline{G}}^{(1,1)}(\overline{r}, \overline{r}_1) \right) \right\} ds \quad (3.3-23)$$

Comparing the second integral in Eq. (3.3-14) and Eq. (3.3-23), it is seen that this second term is 0 and Eq. (3.3-14) can be rewritten as follows.

$$\overline{\overline{G}}^{(1,0)}(\overline{r}_1, \overline{r}_2)^T = - \iint_{z=0 \text{ plane}} \left\{ \left[\hat{z} \times \overline{\overline{G}}^{(1,0)}(\overline{r}, \overline{r}_2) \right]^T \cdot \left(\nabla \times \overline{\overline{G}}^{(1,1)}(\overline{r}, \overline{r}_1) \right) - \left[\nabla \times \overline{\overline{G}}^{(1,0)}(\overline{r}, \overline{r}_2) \right]^T \cdot \left(\hat{z} \times \overline{\overline{G}}^{(1,1)}(\overline{r}, \overline{r}_1) \right) \right\} ds \quad (3.3-24)$$

At $z=0$ plane, the continuity of the tangential electrical field and tangential magnetic field requires the DGFs to satisfy the following boundary conditions given in Eq. (3.3-25) and Eq. (3.3-26), corresponding to the geometries shown in Fig. 3-4(a) and Fig. 3-4(b), respectively.

$$\begin{aligned}\hat{z} \times \overline{\overline{G}}^{(0,0)}(\bar{r}, \bar{r}_2) &= \hat{z} \times \overline{\overline{G}}^{(1,0)}(\bar{r}, \bar{r}_2) \\ \hat{z} \times \frac{1}{\mu_{0r}} \nabla \times \overline{\overline{G}}^{(0,0)}(\bar{r}, \bar{r}_2) &= \hat{z} \times \frac{1}{\mu_{1r}} \nabla \times \overline{\overline{G}}^{(1,0)}(\bar{r}, \bar{r}_2)\end{aligned}\quad (3.3-25)$$

$$\begin{aligned}\hat{z} \times \overline{\overline{G}}^{(0,1)}(\bar{r}, \bar{r}_1) &= \hat{z} \times \overline{\overline{G}}^{(1,1)}(\bar{r}, \bar{r}_1) \\ \hat{z} \times \frac{1}{\mu_{0r}} \nabla \times \overline{\overline{G}}^{(0,1)}(\bar{r}, \bar{r}_1) &= \hat{z} \times \frac{1}{\mu_{1r}} \nabla \times \overline{\overline{G}}^{(1,1)}(\bar{r}, \bar{r}_1)\end{aligned}\quad (3.3-26)$$

Making use of Eq.(3.3-25) and Eq. (3.3-26) in Eq. (3.3-24) and following a similar procedure, it is obtained

$$\overline{\overline{G}}^{(1,0)}(\bar{r}_1, \bar{r}_2)^T = -\frac{\mu_{1r}}{\mu_{0r}} \iint_{z=0 \text{ plane}} \left\{ \begin{aligned} &\left[\hat{z} \times \overline{\overline{G}}^{(0,0)}(\bar{r}, \bar{r}_2) \right]^T \cdot \left(\nabla \times \overline{\overline{G}}^{(0,1)}(\bar{r}, \bar{r}_1) \right) \\ &-\left[\nabla \times \overline{\overline{G}}^{(0,0)}(\bar{r}, \bar{r}_2) \right]^T \cdot \left(\hat{z} \times \overline{\overline{G}}^{(0,1)}(\bar{r}, \bar{r}_1) \right) \end{aligned} \right\} ds \quad (3.3-27)$$

Comparing Eq. (3.3-27) with Eq.(3.3-7) reveals the following relation.

$$\overline{\overline{G}}^{(0,1)}(\bar{r}_2, \bar{r}_1) \Big|_{\varepsilon(\text{region1})=\varepsilon_{1r}} = \frac{\mu_{0r}}{\mu_{1r}} \overline{\overline{G}}^{(1,0)}(\bar{r}_1, \bar{r}_2)^T \Big|_{\varepsilon(\text{region1})=\varepsilon_{1r}} \quad (3.3-28)$$

If the anisotropic region is filled with a reciprocal medium with the permittivity satisfying

$\varepsilon_{1r}^T = \varepsilon_{1r}$, then the above symmetrical property reduces to the following form.

$$\overline{\overline{G}}^{(0,1)}(\bar{r}_2, \bar{r}_1) = \frac{\mu_{0r}}{\mu_{1r}} \overline{\overline{G}}^{(1,0)}(\bar{r}_1, \bar{r}_2)^T \quad (3.3-29)$$

It is noted here that the symmetrical property is derived based on the two-layer geometry, however it also applies to the half-space anisotropic geometry, which is treated as one special case of the layered geometry.

3.3.2 Usage and Limitation of the Modified Symmetrical Property

According to the discussion presented in Section 3.3.1, to obtain the DGF of Region 0 (isotropic region) above the source point with source located inside Region 1 (anisotropic region), the modified symmetrical property of Eq. (3.3-28) can be used for a layered geometry with the anisotropic region being non-reciprocal media as a gyrotropic media, and symmetrical property of Eq.(3.3-29) can be used for a layered geometry with the anisotropic region filled with reciprocal media such as uniaxial and biaxial media. In this section, the symmetrical property of Eq. (3.3-28) is applied to obtain the DGFs of Region 0 with source located in Region 1 for both the half-space and two-layer problems with the anisotropic Region 1 filled with either the reciprocal or non-reciprocal medium. In addition to the usage of the symmetrical property, the limitation of the modified symmetrical property is also briefly reviewed in this section.

First, the modified symmetrical property of Eq. (3.3-28) is applied to the half-space DGF of $\overline{\overline{G}}^{(1,0)}(\vec{r}', r)$ obtained in Eq. (3.1-5), and the dyadic Green's function for the region of $z > z'$ with source in Region 1 is obtained as follows (assuming non-magnetic medium).

$$\overline{\overline{G}}^{(0,1)}(\vec{r}, \vec{r}') = \overline{\overline{G}}^{(1,0)}(\vec{r}', \vec{r})^T = \frac{i}{8\pi^2} \int_{-\infty}^{\infty} dk_x dk_y \frac{1}{k_{0z}} \left\{ \begin{array}{l} \hat{h}_0(-k_{0z}) e^{-i\vec{k}_0 \cdot \vec{r}} \left[\begin{array}{l} X_{hel}^{01} \hat{e}_I^d(k_{zI}^d) e^{i\vec{k}_{I1} \cdot \vec{r}'} \\ + X_{hel}^{01} \hat{e}_{II}^d(k_{zII}^d) e^{i\vec{k}_{II1} \cdot \vec{r}'} \end{array} \right] \\ + \hat{v}_0(-k_{0z}) e^{-i\vec{k}_0 \cdot \vec{r}} \left[\begin{array}{l} X_{vel}^{01} \hat{e}_I^d(k_{zI}^d) e^{i\vec{k}_{I1} \cdot \vec{r}'} \\ + X_{vell}^{01} \hat{e}_{II}^d(k_{zII}^d) e^{i\vec{k}_{II1} \cdot \vec{r}'} \end{array} \right] \end{array} \right\} \quad (3.3-30)$$

In order to have the DGF shown in Eq. (3.3-30) above give more straightforward physical meaning, the transformation shown in Eq.(3.3-31) is applied to the above formula.

$$k_x \rightarrow -k_x, \quad k_y \rightarrow -k_y \quad (3.3-31)$$

Then, it's straightforward to get

For $z > 0$

$$\begin{aligned} \overline{\overline{G}}^{(0,1)}(\vec{r}, \vec{r}') &= \frac{i}{8\pi^2} \int_{-\infty}^{\infty} dk_x dk_y \frac{1}{k_{0z}} \\ &\left\{ \begin{aligned} &\hat{h}_0(-k_{0z}, -k_x, -k_y) e^{-i\vec{k}_0 \cdot \vec{r}} \left[\begin{aligned} &X_{hel}^{01}(-k_x, -k_y) \hat{e}_I^d(k_{zI}^d, -k_x, -k_y) e^{i\vec{k}_I \cdot \vec{r}'} \\ &+ X_{hel}^{01}(-k_x, -k_y) \hat{e}_{II}^d(k_{zII}^d, -k_x, -k_y) e^{i\vec{k}_{II} \cdot \vec{r}'} \end{aligned} \right] \\ &+ \hat{v}_0(-k_{0z}, -k_x, -k_y) e^{-i\vec{k}_0 \cdot \vec{r}} \left[\begin{aligned} &X_{vel}^{01}(-k_x, -k_y) \hat{e}_I^d(k_{zI}^d, -k_x, -k_y) e^{i\vec{k}_I \cdot \vec{r}'} \\ &+ X_{vel}^{01}(-k_x, -k_y) \hat{e}_{II}^d(k_{zII}^d, -k_x, -k_y) e^{i\vec{k}_{II} \cdot \vec{r}'} \end{aligned} \right] \end{aligned} \right\} \quad (3.3-32) \end{aligned}$$

It can be shown that the propagation vector and field vector of the isotropic region (Region 0) satisfy the following relation.

$$\begin{aligned} \vec{k}_0(-k_x, -k_y, -k_{0z}) &= -\vec{k}_0(k_x, k_y) \\ \hat{h}_0(-k_x, -k_y, -k_{0z}) &= -\hat{h}_0(k_x, k_y, k_{0z}), \quad \hat{v}_0(-k_x, -k_y) = \hat{v}_0^+(k_x, k_y) \end{aligned} \quad (3.3-33)$$

Then Eq. (3.3-32) reduces to the following form.

For $z > 0$

$$\begin{aligned} \overline{\overline{G}}^{(0,1)}(\vec{r}, \vec{r}') &= \frac{i}{8\pi^2} \int_{-\infty}^{\infty} dk_x dk_y \frac{1}{k_{0z}} \\ &\left\{ \begin{aligned} &-\hat{h}_0^+ e^{i\vec{k}_0 \cdot \vec{r}} \left[\begin{aligned} &X_{hel}^{01}(-k_x, -k_y) \hat{e}_I^d(k_{zI}^d, -k_x, -k_y) e^{i\vec{k}_I(-k_x, -k_y) \cdot \vec{r}'} \\ &+ X_{hel}^{01}(-k_x, -k_y) \hat{e}_{II}^d(k_{zII}^d, -k_x, -k_y) e^{i\vec{k}_{II}(-k_x, -k_y) \cdot \vec{r}'} \end{aligned} \right] \\ &+ \hat{v}_0^+ e^{i\vec{k}_0 \cdot \vec{r}} \left[\begin{aligned} &X_{vel}^{01}(-k_x, -k_y) \hat{e}_I^d(k_{zI}^d, -k_x, -k_y) e^{i\vec{k}_I(-k_x, -k_y) \cdot \vec{r}'} \\ &+ X_{vel}^{01}(-k_x, -k_y) \hat{e}_{II}^d(k_{zII}^d, -k_x, -k_y) e^{i\vec{k}_{II}(-k_x, -k_y) \cdot \vec{r}'} \end{aligned} \right] \end{aligned} \right\} \quad (3.3-34) \end{aligned}$$

It is noted here that for half-space reciprocal medium, the coefficients, wave vectors and eigenvectors shown in Eq. (3.3-34) are calculated for the anisotropic medium of $\bar{\epsilon}_{1r}$, while for the half-space non-reciprocal medium, they are calculated for the anisotropic medium of $\bar{\epsilon}_{1r}^T$.

If Region 1 is filled with a biaxial medium, the propagation vectors and field vectors of Region 1 satisfy the following relation, which is proved in Appendix M of [37].

$$\begin{aligned}\bar{\kappa}_I(-k_x, -k_y, k_{zI}^d) &= -\bar{\kappa}_I(k_x, k_y), & \bar{\kappa}_{II}(-k_x, -k_y, k_{zII}^d) &= -\bar{\kappa}_{II}(k_x, k_y) \\ \hat{e}_I^d(-k_x, -k_y) &= -\hat{e}_I^u(k_x, k_y), & \hat{e}_{II}^d(-k_x, -k_y) &= \hat{e}_{II}^u(k_x, k_y)\end{aligned}\quad (3.3-35)$$

It needs to be noted here that the relationship between the eigenvectors of Region 1 are chosen such that it is consistent with the notation used by Pettis [37]. Substituting Eq. (3.3-35) into Eq.(3.3-34) gives

For $z > 0$

$$\bar{G}^{(0,1)}(\bar{r}, \bar{r}') = \frac{i}{8\pi^2} \int_{-\infty}^{\infty} dk_x dk_y \frac{1}{k_{0z}} \left\{ \begin{array}{l} \hat{h}_0^+ e^{i\bar{k}_0 \cdot \bar{r}} \left[\begin{array}{l} X_{hel}^{01}(-k_x, -k_y) \hat{e}_I^u(k_{zI}^u) e^{-i\bar{k}_I \cdot \bar{r}'} \\ -X_{hel}^{01}(-k_x, -k_y) \hat{e}_{II}^u(k_{zII}^u) e^{-i\bar{k}_{II} \cdot \bar{r}'} \end{array} \right] \\ + \hat{v}_0^+ e^{i\bar{k}_0 \cdot \bar{r}} \left[\begin{array}{l} -X_{vel}^{01}(-k_x, -k_y) \hat{e}_I^u(k_{zI}^u) e^{-i\bar{k}_I \cdot \bar{r}'} \\ +X_{vel}^{01}(-k_x, -k_y) \hat{e}_{II}^u(k_{zII}^u) e^{-i\bar{k}_{II} \cdot \bar{r}'} \end{array} \right] \end{array} \right\} \quad (3.3-36)$$

It was given in Eq. 5.2.26 of [37] that the following relationships hold for a layered biaxial medium.

$$\begin{aligned}
X_{hel}^{01}(-k_x, -k_y) &= \gamma(k_x, k_y, \bar{\varepsilon}) X_{elh}^{10}(k_x, k_y) \\
X_{vel}^{01}(-k_x, -k_y) &= -\gamma(k_x, k_y, \bar{\varepsilon}) X_{elv}^{10}(k_x, k_y) \\
X_{hell}^{01}(-k_x, -k_y) &= -\eta(k_x, k_y, \bar{\varepsilon}) X_{ellh}^{10}(k_x, k_y) \\
X_{vell}^{01}(-k_x, -k_y) &= \eta(k_x, k_y, \bar{\varepsilon}) X_{ellv}^{10}(k_x, k_y)
\end{aligned} \tag{3.3-37}$$

It is claimed in [37] that the exact functional relationship of $\gamma(k_x, k_y, \bar{\varepsilon})$, $\eta(k_x, k_y, \bar{\varepsilon})$ is unknown. Here we show that $\gamma(k_x, k_y, \bar{\varepsilon})$, $\eta(k_x, k_y, \bar{\varepsilon})$ are related with the amplitude coefficients of the dyad in Green's function of the unbounded medium filled in Region 1. This will be shown in Section 3.4.2, where the direct construction method of dyadic Green's function is discussed when the source is located in Region 1.

Symmetrical property is also applied to the dyadic Green's function of the two-layer problem in Eq. (3.1-13) as follows.

$$\begin{aligned}
\bar{\bar{G}}^{(0,1)}(\bar{r}, \bar{r}') &= \left[\bar{\bar{G}}^{(1,0)}(\bar{r}', \bar{r}) \right]^T = \frac{i}{8\pi^2} \int_{-\infty}^{\infty} dk_x dk_y \frac{1}{k_{0z}} \\
&\left\{ \hat{h}_0(-k_{0z}) e^{-i\bar{k}_0 \cdot \bar{r}} \left[\begin{aligned} &A_{hel} \hat{e}_I(k_{zI}^d) e^{i\bar{k}_I \cdot \bar{r}'} + B_{hel} \hat{e}_I(k_{zI}^u) e^{i\bar{k}_I \cdot \bar{r}'} \\ &+ A_{hell} \hat{e}_{II}(k_{zII}^d) e^{i\bar{k}_{II} \cdot \bar{r}'} + B_{hell} \hat{e}_{II}(k_{zII}^u) e^{i\bar{k}_{II} \cdot \bar{r}'} \end{aligned} \right] \right. \\
&\left. + \hat{v}_0(-k_{0z}) e^{-i\bar{k}_0 \cdot \bar{r}} \left[\begin{aligned} &A_{vel} \hat{e}_I(k_{zI}^d) e^{i\bar{k}_I \cdot \bar{r}'} + B_{vel} \hat{e}_I(k_{zI}^u) e^{i\bar{k}_I \cdot \bar{r}'} \\ &+ A_{vell} \hat{e}_{II}(k_{zII}^d) e^{i\bar{k}_{II} \cdot \bar{r}'} + B_{vell} \hat{e}_{II}(k_{zII}^u) e^{i\bar{k}_{II} \cdot \bar{r}'} \end{aligned} \right] \right\} \tag{3.3-38}
\end{aligned}$$

Applying the transformation as shown in Eq. (3.3-31) and Eq.(3.3-33), Eq. (3.3-38) can be written as follows.

$$\begin{aligned}
\overline{G}^{(0,1)}(\vec{r}, \vec{r}') &= \frac{i}{8\pi^2} \int_{-\infty}^{\infty} dk_x dk_y \frac{1}{k_{0z}} \\
&\left\{ \begin{array}{l}
-\hat{h}_0(k_{0z}) e^{i\vec{k}_0 \cdot \vec{r}} \left[\begin{array}{l}
A_{hel}(-k_x, -k_y) \hat{e}_I^d(-k_x, -k_y) e^{i\vec{k}_I^d(-k_x, -k_y) \cdot \vec{r}} \\
+B_{hel}(-k_x, -k_y) \hat{e}_I^u(-k_x, -k_y) e^{i\vec{k}_I^u(-k_x, -k_y) \cdot \vec{r}} \\
A_{hell}(-k_x, -k_y) \hat{e}_{II}^d(-k_x, -k_y) e^{i\vec{k}_{II}^d(-k_x, -k_y) \cdot \vec{r}} \\
+B_{hell}(-k_x, -k_y) \hat{e}_{II}^u(-k_x, -k_y) e^{i\vec{k}_{II}^u(-k_x, -k_y) \cdot \vec{r}}
\end{array} \right] \\
+\hat{v}_0(k_{0z}) e^{i\vec{k}_0 \cdot \vec{r}} \left[\begin{array}{l}
A_{vel}(-k_x, -k_y) \hat{e}_I^d(-k_x, -k_y) e^{i\vec{k}_I^d(-k_x, -k_y) \cdot \vec{r}} \\
+B_{vel}(-k_x, -k_y) \hat{e}_I^u(-k_x, -k_y) e^{i\vec{k}_I^u(-k_x, -k_y) \cdot \vec{r}} \\
+A_{vell}(-k_x, -k_y) \hat{e}_{II}^d(-k_x, -k_y) e^{i\vec{k}_{II}^d(-k_x, -k_y) \cdot \vec{r}} \\
+B_{vell}(-k_x, -k_y) \hat{e}_{II}^u(-k_x, -k_y) e^{i\vec{k}_{II}^u(-k_x, -k_y) \cdot \vec{r}}
\end{array} \right]
\end{array} \right\} \quad (3.3-39)
\end{aligned}$$

Eq. (3.3-39) can be applied for a two-layer problem filled with either a reciprocal or a non-reciprocal medium. It is noted here that for a two-layer reciprocal medium, the coefficients, wave vectors and eigenvectors shown in Eq. (3.3-39) are calculated for the anisotropic medium of $\overline{\epsilon}_{1r}$, while for a two-layer non-reciprocal medium, they are calculated for the anisotropic medium of

$\overline{\epsilon}_{1r}^T$.

As was shown in the half-space case, if Region 1 is filled with a reciprocal medium, the propagation vectors and field vectors satisfy the relation shown in Eq. (3.3-35). Then, the above formula of Eq. (3.3-39) for the DGF reduces to a simplified form shown below.

$$\hat{G}^{(0,1)}(\vec{r}, \vec{r}') = \frac{i}{8\pi^2} \int_{-\infty}^{\infty} dk_x dk_y \frac{1}{k_{0z}} \left\{ \begin{array}{l} \hat{h}_0(k_{0z}) e^{i\vec{k}_0 \cdot \vec{r}} \left[\begin{array}{l} A_{hel}(-k_x, -k_y) \hat{e}_I(k_{zI}^u) e^{-i\vec{k}_I^u \cdot \vec{r}'} \\ + B_{hel}(-k_x, -k_y) \hat{e}_I(k_{zI}^d) e^{-i\vec{k}_I^d \cdot \vec{r}'} \\ - A_{hell}(-k_x, -k_y) \hat{e}_{II}(k_{zII}^u) e^{-i\vec{k}_{II}^u \cdot \vec{r}'} \\ - B_{hell}(-k_x, -k_y) \hat{e}_{II}(k_{zII}^d) e^{-i\vec{k}_{II}^d \cdot \vec{r}'} \end{array} \right] \\ + \hat{v}_0(k_{0z}) e^{i\vec{k}_0 \cdot \vec{r}} \left[\begin{array}{l} -A_{vel}(-k_x, -k_y) \hat{e}_I(k_{zI}^u) e^{-i\vec{k}_I^u \cdot \vec{r}'} \\ - B_{vel}(-k_x, -k_y) \hat{e}_I(k_{zI}^d) e^{-i\vec{k}_I^d \cdot \vec{r}'} \\ + A_{vell}(-k_x, -k_y) \hat{e}_{II}(k_{zII}^u) e^{-i\vec{k}_{II}^u \cdot \vec{r}'} \\ + B_{vell}(-k_x, -k_y) \hat{e}_{II}(k_{zII}^d) e^{-i\vec{k}_{II}^d \cdot \vec{r}'} \end{array} \right] \end{array} \right\} \quad (3.3-40)$$

Eq. (3.3-40) can only be applied to the geometry filled with a reciprocal medium, and the amplitude coefficients of the formula will have the same relationship of Eq. (3.3-37) as for the half-space problem if the reciprocal medium is a biaxial medium, which will be discussed in detail in Section 3.4.2. In the integrand of Eq. (3.3-40), the wave vectors $\vec{k}_{I,II}^{u,d}$, the Region 0 field vectors \hat{h}_0 , \hat{v}_0 and the characteristic field vectors for the anisotropic region $\hat{e}_{I,II}^{d,u}$ are obtained for a specific set of (k_x, k_y) . However, the amplitude coefficients A, B are calculated from the half-space reflection and transmission coefficients that are calculated for the incidence wave with tangential wave vector $(-k_x, -k_y)$ at the interface. This is different from Eq. (3.3-39), which shows that except the field vectors \hat{h}_0 , and \hat{v}_0 for the isotropic Region 0, all other field vectors, wave vectors and amplitude coefficients are calculated for given $(-k_x, -k_y)$ with the permittivity of the matrix of anisotropic medium as the transpose of the permittivity matrix of the original medium.

As shown in this section, applying the modified symmetrical property can give the DGF $\overline{\overline{G}}^{(0,1)}(\overline{r}, \overline{r}')$ directly from a known DGF of $\overline{\overline{G}}^{(1,0)}(\overline{r}, \overline{r}')$. Similarly, the DGF of $\overline{\overline{G}}^{(0,2)}(\overline{r}, \overline{r}')$ can also be obtained by applying the modified symmetrical property to the DGF of $\overline{\overline{G}}^{(2,0)}(\overline{r}, \overline{r}')$. This property is extremely useful if the medium is reciprocal as it does not require any additional calculations, as long as the DGFs of a layered anisotropic geometry with the anisotropic medium characterized by $\overline{\overline{\varepsilon}}_{1r}$ are already solved.

However, if the medium is non-reciprocal, even if the DGFs of a layered anisotropic geometry with the anisotropic medium characterized by $\overline{\overline{\varepsilon}}_{1r}$ is already provided, to apply the modified symmetrical property, additional calculations of the DGFs of a layered anisotropic geometry with the anisotropic medium characterized by $\overline{\overline{\varepsilon}}_{1r}^T$ is unavoidable. In addition, if the DGF of $\overline{\overline{G}}^{(1,1)}(\overline{r}, \overline{r}')$ is of interest, then this symmetrical property will not help. In this case, to get the complete set of DGFs for the layered geometry with the source located in the anisotropic region, the direct construction method needs to be used. It will be shown in Section 3.4 that in addition to providing the complete set of DGFs of all the regions including the anisotropic region where the source is located, a straightforward physical insight can be obtained from the DGFs derived using the direct construction method.

3.4 DGFs of a Two-Layer Geometry with a Source inside the Anisotropic Region

As demonstrated in the previous section, applying the modified symmetrical property to the DGF of $\overline{\overline{G}}^{(1,0)}(\overline{r}, \overline{r}')$ with the source inside Region 0 is only to provide the DGF of $\overline{\overline{G}}^{(0,1)}(\overline{r}, \overline{r}')$.

To obtain the DGFs of all the regions for a layered geometry with a source inside the anisotropic region, the direction construction method is discussed in detail in this section.

3.4.1 Direct Construction Method to Obtain the DGFs for All the Regions

The first step to utilize the direct construction method is to obtain the DGFs for the unbounded anisotropic medium. As presented in Section 2.2, the dyadic Green's functions for an unbounded anisotropic medium are given in Eq. (2.2-32), which are repeated here again with $i\omega\mu_0$ extracted out.

For $z < z'$

$$\overline{\overline{G}}(\vec{r}, \vec{r}') = \frac{i}{(2\pi)^2} \int_{-\infty}^{\infty} \int_{-\infty}^{\infty} \left(\begin{array}{l} \frac{\lambda(k_{z1}^d) \hat{e}(k_{z1}^d) \hat{v}(k_{z1}^d)}{a_4(k_{z1}^d - k_{z1}^u)(k_{z1}^d - k_{z11}^u)(k_{z1}^d - k_{z11}^d)} e^{i\vec{k}_1^d \cdot (\vec{r} - \vec{r}')} \\ + \frac{\lambda(k_{z11}^d) \hat{e}(k_{z11}^d) \hat{v}(k_{z11}^d)}{a_4(k_{z11}^d - k_{z1}^d)(k_{z11}^d - k_{z1}^u)(k_{z11}^d - k_{z11}^u)} e^{i\vec{k}_{11}^d \cdot (\vec{r} - \vec{r}')} \end{array} \right) dk_x dk_y \quad (3.4-1)$$

For $z > z'$

$$\overline{\overline{G}}(\vec{r}, \vec{r}') = -\frac{i}{(2\pi)^2} \int_{-\infty}^{\infty} \int_{-\infty}^{\infty} \left(\begin{array}{l} \frac{\lambda(k_{z1}^u) \hat{e}(k_{z1}^u) \hat{v}(k_{z1}^u)}{a_4(k_{z1}^u - k_{z1}^d)(k_{z1}^u - k_{z11}^u)(k_{z1}^u - k_{z11}^d)} e^{i\vec{k}_1^u \cdot (\vec{r} - \vec{r}')} \\ + \frac{\lambda(k_{z11}^u) \hat{e}(k_{z11}^u) \hat{v}(k_{z11}^u)}{a_4(k_{z11}^u - k_{z1}^d)(k_{z11}^u - k_{z1}^u)(k_{z11}^u - k_{z11}^d)} e^{i\vec{k}_{11}^u \cdot (\vec{r} - \vec{r}')} \end{array} \right) dk_x dk_y \quad (3.4-2)$$

In Eq. (3.4-1) and Eq. (3.4-2), a_4 indicates the coefficient for the fourth order term of k_z in the expansion of the polynomial in terms of k_z for the electric wave matrix $|\mathcal{W}_E|$. For example, if the anisotropic medium is a gyroelectric medium with the biasing magnetic field along an arbitrary direction of θ_B and φ_B , then $a_4 = k_o^2 (\varepsilon_1 \sin^2 \theta_B + \varepsilon_3 \cos^2 \theta_B)$. The eigenvalue $\lambda(k_{z1}^u)$ and eigenvectors $\hat{e}(k_{z1}^u)$ and $\hat{v}(k_{z1}^u)$ are defined in Section 2.3.1.

For the comparison of dyadic Green's function obtained using the direct construction method and the dyadic Green's function obtained using the modified symmetrical property as presented in the previous section, the common term $\frac{i}{8\pi^2 k_{0z}}$ is extracted purposely from the dyadic Green's function, and Eq. (3.4-1) and Eq. (3.4-2) are rewritten as follows.

For $z > z'$

$$\overline{\overline{G}}(\vec{r}, \vec{r}') = \frac{i}{8\pi^2} \int_{-\infty}^{\infty} \int_{-\infty}^{\infty} dk_x dk_y \frac{1}{k_{0z}} \begin{pmatrix} c_I^u(k_{zI}^u) \hat{e}_I^u(\hat{v}_I^u) e^{i\vec{k}_I \cdot (\vec{r} - \vec{r}')} \\ + c_{II}^u(k_{zII}^u) \hat{e}_{II}^u(\hat{v}_{II}^u) e^{i\vec{k}_{II} \cdot (\vec{r} - \vec{r}')} \end{pmatrix} \quad (3.4-3)$$

For $z < z'$

$$\overline{\overline{G}}(\vec{r}, \vec{r}') = \frac{i}{8\pi^2} \int_{-\infty}^{\infty} \int_{-\infty}^{\infty} \frac{1}{k_{0z}} dk_x dk_y \begin{pmatrix} c_I^d(k_{zI}^d) \hat{e}_I^d(\hat{v}_I^d) e^{i\vec{k}_I \cdot (\vec{r} - \vec{r}')} \\ + c_{II}^d(k_{zII}^d) \hat{e}_{II}^d(\hat{v}_{II}^d) e^{i\vec{k}_{II} \cdot (\vec{r} - \vec{r}')} \end{pmatrix} \quad (3.4-4)$$

where

$$c_I^u(k_{zI}^u) = -\frac{2k_{0z} \lambda_I^u}{a_4(k_{zI}^u - k_{zII}^u)(k_{zI}^u - k_{zI}^d)(k_{zI}^u - k_{zII}^d)}, \quad c_{II}^u(k_{zII}^u) = -\frac{2k_{0z} \lambda_{II}^u}{a_4(k_{zII}^u - k_{zI}^u)(k_{zII}^u - k_{zI}^d)(k_{zII}^u - k_{zII}^d)}$$

$$c_I^d(k_{zI}^d) = \frac{2k_{0z} \lambda_I^d}{a_4(k_{zI}^d - k_{zII}^d)(k_{zI}^d - k_{zI}^u)(k_{zI}^d - k_{zII}^u)}, \quad c_{II}^d(k_{zII}^d) = \frac{2k_{0z} \lambda_{II}^d}{a_4(k_{zII}^d - k_{zI}^d)(k_{zII}^d - k_{zI}^u)(k_{zII}^d - k_{zII}^u)}$$

The second step of the direct construction method is to apply the matrix method to the unbounded DGFs obtained from the eigen-decomposition method. The matrix method has already been used in Section 3.1 to obtain the DGFs of a two-layer problem with a source in the isotropic medium. In that case, the direct wave was the downward incident wave in the isotropic medium. However, in this section, the direct upward and downward waves from the source in Region 1 as shown in Fig. 3-5 are used to construct the DGF.

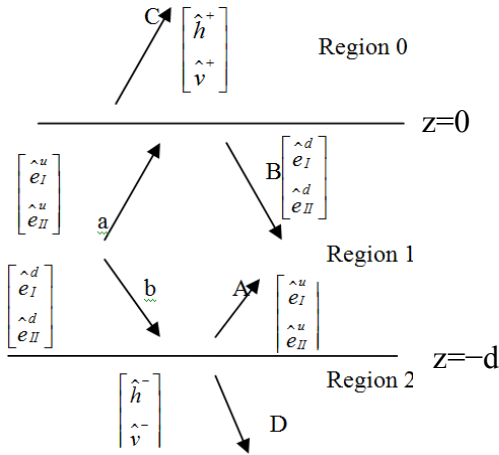


Fig. 3-5: Geometry of the two-layer problem with source inside the anisotropic region.

In Fig. 3-5, the ‘a’ and ‘b’ stand for the amplitude coefficient matrices of the unit vectors corresponding to the upward and downward waves generated by the source located inside the anisotropic region (Region 1) bounded by $z=0$ and $z=-d$. ‘A’ and ‘B’ represent the amplitude coefficient matrices for the unit vectors of the total upward and downward waves existing in Region 1 due to the multiple reflections of the ‘a’ and the ‘b’ waves at both the boundaries of $z=0$ and $z=-d$. ‘C’ and ‘D’ represent the amplitude coefficient matrix for the unit vectors of the transmitted waves in Region 0 and Region 2, respectively. As indicated in Fig. 3-5, all the waves in each region include two different polarizations. Inside the anisotropic region, the waves ‘A’ and ‘B’ include Type I and Type II polarizations, while the transmitted waves ‘C’ and ‘D’ inside the isotropic regions include the h and v -polarizations as described in Section 2.3.

The two-layer geometry under consideration can be decomposed into two half-space problems with one corresponding to the reflection and transmission at the boundary $z = 0$ (separating Region 0 and Region 1) and the other one corresponding to the reflection and transmission at the boundary $z=-d$ (separating Region 1 and Region 2). The waves in each

region can then be related through the half-space reflection and transmission coefficient matrices below.

$$A = \overset{=12}{R} (b + B), \quad B = \overset{=10}{R} (a + A), \quad C = \overset{=10}{X} (a + A), \quad D = \overset{=12}{X} (b + B) \quad (3.4-5)$$

where $\overset{=pq}{R}$ and $\overset{=pq}{X}$ are the half-space reflection and transmission coefficient matrices with wave incident from Region p to Region q defined in Eq. (3.1-16) - Eq. (3.1-18). Rewriting Eq. (3.4-5) such that A, B, C, and D are expressed in terms of the direct waves generated by the source in Region 1, we obtain

$$\begin{aligned} A &= \overset{=a}{A} a + \overset{=b}{A} b & B &= \overset{=a}{B} a + \overset{=b}{B} b & C &= \overset{=a}{X} a + \overset{=b}{X} b & D &= \overset{=a}{T} a + \overset{=b}{T} b \\ \overset{=a}{A} &= \begin{bmatrix} R_{e_i^u e_i^u} & R_{e_{ii}^u e_i^u} \\ R_{e_i^u e_{ii}^u} & R_{e_{ii}^u e_{ii}^u} \end{bmatrix} = (I - \overset{=12}{R} \overset{=10}{R})^{-1} \overset{=12}{R} \overset{=10}{R}, & \overset{=b}{A} &= \begin{bmatrix} R_{e_i^d e_i^u} & R_{e_{ii}^d e_i^u} \\ R_{e_i^d e_{ii}^u} & R_{e_{ii}^d e_{ii}^u} \end{bmatrix} = (I - \overset{=12}{R} \overset{=10}{R})^{-1} \overset{=12}{R} \\ \overset{=a}{B} &= \begin{bmatrix} R_{e_i^u e_i^d} & R_{e_{ii}^u e_i^d} \\ R_{e_i^u e_{ii}^d} & R_{e_{ii}^u e_{ii}^d} \end{bmatrix} = (I - \overset{=10}{R} \overset{=12}{R})^{-1} \overset{=10}{R}, & \overset{=b}{B} &= \begin{bmatrix} R_{e_i^d e_i^d} & R_{e_{ii}^d e_i^d} \\ R_{e_i^d e_{ii}^d} & R_{e_{ii}^d e_{ii}^d} \end{bmatrix} = (I - \overset{=10}{R} \overset{=12}{R})^{-1} \overset{=10}{R} \\ \overset{=a}{X} &= \begin{bmatrix} X_{e_i^h} & X_{e_{ii}^h} \\ X_{e_i^v} & X_{e_{ii}^v} \end{bmatrix} = \overset{=10}{X} (I - \overset{=12}{R} \overset{=10}{R})^{-1}, & \overset{=b}{X} &= \begin{bmatrix} X_{e_i^h} & X_{e_{ii}^h} \\ X_{e_i^v} & X_{e_{ii}^v} \end{bmatrix} = \overset{=10}{X} (I - \overset{=12}{R} \overset{=10}{R})^{-1} \\ \overset{=a}{T} &= \begin{bmatrix} T_{e_i^h} & T_{e_{ii}^h} \\ T_{e_i^v} & T_{e_{ii}^v} \end{bmatrix} = \overset{=12}{X} (I - \overset{=10}{R} \overset{=12}{R})^{-1} \overset{=10}{R}, & \overset{=b}{T} &= \begin{bmatrix} T_{e_i^h} & T_{e_{ii}^h} \\ T_{e_i^v} & T_{e_{ii}^v} \end{bmatrix} = \overset{=12}{X} (I - \overset{=10}{R} \overset{=12}{R})^{-1} \end{aligned} \quad (3.4-6)$$

Using the coefficients above, the dyadic Green's functions in each region when a source is located in the anisotropic region can be constructed. The construction of the DGF in Region 1 is first considered and it needs special attention. The anisotropic medium is separated into two regions with one corresponding to the space above the source point (z') and the other corresponding to the space below the source point. For region above the source point, the direct wave includes the upward wave only, and for the region below source point, the direct wave

includes downward wave only. With the DGFs for the unbounded anisotropic region (Eq. (3.4-3) and Eq. (3.4-4)) and coefficients obtained from Eq. (3.4-6), we have for $z' < z < 0$,

For $z' < z < 0$

$$\begin{aligned} & \stackrel{=(1,1)}{G}(\bar{r}, \bar{r}') = \\ & \frac{i}{8\pi^2 k_{0z}} \int_{-\infty}^{\infty} \int_{-\infty}^{\infty} dk_x dk_y \left(\begin{array}{l} c_I^u(k_{zI}^u) \hat{e}_I^u(\hat{v}_I^u) e^{i\bar{k}_I \cdot (\bar{r} - \bar{r}')} + c_{II}^u(k_{zII}^u) \hat{e}_{II}^u(\hat{v}_{II}^u) e^{i\bar{k}_{II} \cdot (\bar{r} - \bar{r}')} \\ + \hat{e}_I^d e^{i\bar{k}_I \cdot \bar{r}'} \left[\begin{array}{l} R_{e_I^d e_I^u} c_I^u(\hat{v}_I^u) e^{-i\bar{k}_I \cdot \bar{r}} + R_{e_{II}^d e_I^u} c_{II}^u(\hat{v}_{II}^u) e^{-i\bar{k}_{II} \cdot \bar{r}} \\ + R_{e_I^d e_I^d} c_I^d(\hat{v}_I^d) e^{-i\bar{k}_I \cdot \bar{r}} + R_{e_{II}^d e_I^d} c_{II}^d(\hat{v}_{II}^d) e^{-i\bar{k}_{II} \cdot \bar{r}} \end{array} \right] \\ + \hat{e}_{II}^d e^{i\bar{k}_{II} \cdot \bar{r}'} \left[\begin{array}{l} R_{e_I^d e_{II}^u} c_I^u(\hat{v}_I^u) e^{-i\bar{k}_I \cdot \bar{r}} + R_{e_{II}^d e_{II}^u} c_{II}^u(\hat{v}_{II}^u) e^{-i\bar{k}_{II} \cdot \bar{r}} \\ + R_{e_I^d e_{II}^d} c_I^d(\hat{v}_I^d) e^{-i\bar{k}_I \cdot \bar{r}} + R_{e_{II}^d e_{II}^d} c_{II}^d(\hat{v}_{II}^d) e^{-i\bar{k}_{II} \cdot \bar{r}} \end{array} \right] \\ + \hat{e}_I^u e^{i\bar{k}_I \cdot \bar{r}'} \left[\begin{array}{l} R_{e_I^d e_I^u} c_I^u(\hat{v}_I^u) e^{-i\bar{k}_I \cdot \bar{r}} + R_{e_{II}^d e_I^u} c_{II}^u(\hat{v}_{II}^u) e^{-i\bar{k}_{II} \cdot \bar{r}} \\ + R_{e_I^d e_I^d} c_I^d(\hat{v}_I^d) e^{-i\bar{k}_I \cdot \bar{r}} + R_{e_{II}^d e_I^d} c_{II}^d(\hat{v}_{II}^d) e^{-i\bar{k}_{II} \cdot \bar{r}} \end{array} \right] \\ + \hat{e}_{II}^u e^{i\bar{k}_{II} \cdot \bar{r}'} \left[\begin{array}{l} R_{e_I^d e_{II}^u} c_I^u(\hat{v}_I^u) e^{-i\bar{k}_I \cdot \bar{r}} + R_{e_{II}^d e_{II}^u} c_{II}^u(\hat{v}_{II}^u) e^{-i\bar{k}_{II} \cdot \bar{r}} \\ + R_{e_I^d e_{II}^d} c_I^d(\hat{v}_I^d) e^{-i\bar{k}_I \cdot \bar{r}} + R_{e_{II}^d e_{II}^d} c_{II}^d(\hat{v}_{II}^d) e^{-i\bar{k}_{II} \cdot \bar{r}} \end{array} \right] \end{array} \right) \end{aligned} \quad (3.4-7)$$

Similarly, for the region below the source point, we have for $-d < z < z'$,

For $-d < z < z'$

$$\begin{aligned} \overline{\overline{G}}^{(1,1)}(\vec{r}, \vec{r}') = & \\ & \left(\begin{aligned} & c_I^d(k_{z'}^d) \hat{e}_I^d(\hat{v}_I^d) e^{i\vec{k}_I \cdot (\vec{r} - \vec{r}')} + c_{II}^d(k_{z'}^d) \hat{e}_{II}^d(\hat{v}_{II}^d) e^{i\vec{k}_{II} \cdot (\vec{r} - \vec{r}')} \\ & + e_I^{\hat{d}} e^{i\vec{k}_I \cdot \vec{r}} \left[\begin{aligned} & R_{e_I^u e_I^d} c_I^u(\hat{v}_I^u) e^{-i\vec{k}_I \cdot \vec{r}'} + R_{e_{II}^u e_I^d} c_{II}^u(\hat{v}_{II}^u) e^{-i\vec{k}_{II} \cdot \vec{r}'} \\ & + R_{e_I^d e_I^d} c_I^d(\hat{v}_I^d) e^{-i\vec{k}_I \cdot \vec{r}'} + R_{e_{II}^d e_I^d} c_{II}^d(\hat{v}_{II}^d) e^{-i\vec{k}_{II} \cdot \vec{r}'} \end{aligned} \right] \\ & + e_{II}^{\hat{d}} e^{i\vec{k}_{II} \cdot \vec{r}} \left[\begin{aligned} & R_{e_I^u e_{II}^d} c_I^u(\hat{v}_I^u) e^{-i\vec{k}_I \cdot \vec{r}'} + R_{e_{II}^u e_{II}^d} c_{II}^u(\hat{v}_{II}^u) e^{-i\vec{k}_{II} \cdot \vec{r}'} \\ & + R_{e_I^d e_{II}^d} c_I^d(\hat{v}_I^d) e^{-i\vec{k}_I \cdot \vec{r}'} + R_{e_{II}^d e_{II}^d} c_{II}^d(\hat{v}_{II}^d) e^{-i\vec{k}_{II} \cdot \vec{r}'} \end{aligned} \right] \\ & + e_I^{\hat{u}} e^{i\vec{k}_I \cdot \vec{r}} \left[\begin{aligned} & R_{e_I^d e_I^u} c_I^u(\hat{v}_I^u) e^{-i\vec{k}_I \cdot \vec{r}'} + R_{e_{II}^d e_I^u} c_{II}^u(\hat{v}_{II}^u) e^{-i\vec{k}_{II} \cdot \vec{r}'} \\ & + R_{e_I^d e_I^d} c_I^d(\hat{v}_I^d) e^{-i\vec{k}_I \cdot \vec{r}'} + R_{e_{II}^d e_I^d} c_{II}^d(\hat{v}_{II}^d) e^{-i\vec{k}_{II} \cdot \vec{r}'} \end{aligned} \right] \\ & + e_{II}^{\hat{u}} e^{i\vec{k}_{II} \cdot \vec{r}} \left[\begin{aligned} & R_{e_I^u e_{II}^u} c_I^u(\hat{v}_I^u) e^{-i\vec{k}_I \cdot \vec{r}'} + R_{e_{II}^u e_{II}^u} c_{II}^u(\hat{v}_{II}^u) e^{-i\vec{k}_{II} \cdot \vec{r}'} \\ & + R_{e_I^d e_{II}^u} c_I^d(\hat{v}_I^d) e^{-i\vec{k}_I \cdot \vec{r}'} + R_{e_{II}^d e_{II}^u} c_{II}^d(\hat{v}_{II}^d) e^{-i\vec{k}_{II} \cdot \vec{r}'} \end{aligned} \right] \end{aligned} \right) \quad (3.4-8) \end{aligned}$$

Observation of Eq. (3.4-7) and Eq. (3.4-8) indicates that the first two terms inside the integral represent the direct waves due to the sources, which are obtained from the DGFs of the unbounded anisotropic region as shown in Section 2.2. All the other terms represent the upward ('A') and downward ('B') propagating waves reflected at the two boundaries. The tangential electric field and magnetic field must satisfy boundary condition at $z=0$. The Green's function for Region 0 ($z > 0$) when a source is located in the anisotropic region can be expressed in terms of coefficients from Eq. (3.4-6), which are obtained for the transmitted wave 'C' as

For $z > 0$

$$\begin{aligned} & \overline{\overline{G}}^{(0,1)}(\bar{r}, \bar{r}') \\ &= \int_{-\infty}^{\infty} \int_{-\infty}^{\infty} dk_x dk_y \frac{i}{8\pi^2 k_{0z}} \left(\begin{aligned} & \left[X_{e_{Ih}^u} \hat{h}_0^+ e^{i\bar{k}_0 \cdot \bar{r}} + X_{e_{Iv}^u} \hat{v}_0^+ e^{i\bar{k}_0 \cdot \bar{r}} \right] c_I^u(k_{zI}^u) \left(\hat{v}_I^u \right) e^{-i\bar{k}_I \cdot \bar{r}'} \\ & + \left[X_{e_{IIh}^u} \hat{h}_0^+ e^{i\bar{k}_0 \cdot \bar{r}} + X_{e_{IIv}^u} \hat{v}_0^+ e^{i\bar{k}_0 \cdot \bar{r}} \right] c_{II}^u(k_{zII}^u) \left(\hat{v}_{II}^u \right) e^{-i\bar{k}_{II} \cdot \bar{r}'} \\ & + \left[X_{e_{Ih}^d} \hat{h}_0^+ e^{i\bar{k}_0 \cdot \bar{r}} + X_{e_{Iv}^d} \hat{v}_0^+ e^{i\bar{k}_0 \cdot \bar{r}} \right] c_I^d(k_{zI}^d) \left(\hat{v}_I^d \right) e^{-i\bar{k}_I \cdot \bar{r}'} \\ & + \left[X_{e_{IIh}^d} \hat{h}_0^+ e^{i\bar{k}_0 \cdot \bar{r}} + X_{e_{IIv}^d} \hat{v}_0^+ e^{i\bar{k}_0 \cdot \bar{r}} \right] c_{II}^d(k_{zII}^d) \left(\hat{v}_{II}^d \right) e^{-i\bar{k}_{II} \cdot \bar{r}'} \end{aligned} \right) \end{aligned} \quad (3.4-9)$$

Similarly, the DGF for Region 2 (isotropic region) below the anisotropic slab can be derived from the coefficients corresponding to the transmitted wave 'D'. Thus we have

For $z < -d$

$$\begin{aligned} & \overline{\overline{G}}^{(2,1)}(\bar{r}, \bar{r}') \\ &= \int_{-\infty}^{\infty} \int_{-\infty}^{\infty} dk_x dk_y \frac{i}{8\pi^2 k_{0z}} \left(\begin{aligned} & \left[T_{e_{Ih}^u} \hat{h}_0^- e^{i\bar{k}_0 \cdot \bar{r}} + T_{e_{Iv}^u} \hat{v}_0^- e^{i\bar{k}_0 \cdot \bar{r}} \right] c_I^u(k_{zI}^u) \left(\hat{v}_I^u \right) e^{-i\bar{k}_I \cdot \bar{r}'} \\ & + \left[T_{e_{IIh}^u} \hat{h}_0^- e^{i\bar{k}_0 \cdot \bar{r}} + T_{e_{IIv}^u} \hat{v}_0^- e^{i\bar{k}_0 \cdot \bar{r}} \right] c_{II}^u(k_{zII}^u) \left(\hat{v}_{II}^u \right) e^{-i\bar{k}_{II} \cdot \bar{r}'} \\ & + \left[T_{e_{Ih}^d} \hat{h}_0^- e^{i\bar{k}_0 \cdot \bar{r}} + T_{e_{Iv}^d} \hat{v}_0^- e^{i\bar{k}_0 \cdot \bar{r}} \right] c_I^d(k_{zI}^d) \left(\hat{v}_I^d \right) e^{-i\bar{k}_I \cdot \bar{r}'} \\ & + \left[T_{e_{IIh}^d} \hat{h}_0^- e^{i\bar{k}_0 \cdot \bar{r}} + T_{e_{IIv}^d} \hat{v}_0^- e^{i\bar{k}_0 \cdot \bar{r}} \right] c_{II}^d(k_{zII}^d) \left(\hat{v}_{II}^d \right) e^{-i\bar{k}_{II} \cdot \bar{r}'} \end{aligned} \right) \end{aligned} \quad (3.4-10)$$

It is noted here that, the vectors of \hat{v}_I and \hat{v}_{II} as the latter parts of the dyads in Eq. (3.4-7) - Eq. (3.4-10) are taken from the results of Eq. (3.4-3) - Eq. (3.4-4) for the DGFs of the unbounded anisotropic medium.

3.4.2 Discussion of DGF $\overline{\overline{G}}^{(0,1)}(\overline{r}, \overline{r}')$ Obtained Using Two Approaches

In this section, the dyadic Green's functions of Region 0 with source located in Region 1 $\overline{\overline{G}}^{(0,1)}(\overline{r}, \overline{r}')$ derived using the symmetrical property and the direct construction method are compared. It shows numerically that both of the two formulations give the consistent results of DGF for $\overline{\overline{G}}^{(0,1)}(\overline{r}, \overline{r}')$ with anisotropic region filled with either reciprocal or non-reciprocal medium.

For a reciprocal medium, Eq. (3.3-38) gives the coefficients of the dyad in the DGF of $\overline{\overline{G}}^{(0,1)}(\overline{r}, \overline{r}')$ computed via the modified symmetrical property. The coefficients in Eq. (3.3-38) are obtained from Eq. (3.1-20) with the tangential wave vector $(-k_x, -k_y)$ substituted. The coefficients of the DGFs using the direct construction method are given in Eq. (3.4-9) and obtained directly from Eq. (3.4-6) with the tangential wave vector of (k_x, k_y) . The coefficients of the DGF obtained using the two different approaches are repeated here in Eq. (3.4-11) and Eq. (3.4-12) for convenience.

$$\overline{\overline{D}} = \begin{bmatrix} A_{hel} & A_{vel} \\ A_{hell} & A_{vell} \end{bmatrix} = (\overline{\overline{I}} - \overline{\overline{R}} \overline{\overline{R}})^{-1} \overline{\overline{X}}^{01} \quad (3.4-11)$$

$$\overline{\overline{U}} = \begin{bmatrix} B_{hel} & B_{vel} \\ B_{hell} & B_{vell} \end{bmatrix} = \overline{\overline{R}} (\overline{\overline{I}} - \overline{\overline{R}} \overline{\overline{R}})^{-1} \overline{\overline{X}}^{01}$$

$$\overline{\overline{X}}^a = \begin{bmatrix} X_{e_i^u h} & X_{e_{ii}^u h} \\ X_{e_i^u v} & X_{e_{ii}^u v} \end{bmatrix} = \overline{\overline{X}}^{10} (\overline{\overline{I}} - \overline{\overline{R}} \overline{\overline{R}})^{-1} \quad (3.4-12)$$

$$\overline{\overline{X}}^b = \begin{bmatrix} X_{e_i^d h} & X_{e_{ii}^d h} \\ X_{e_i^d v} & X_{e_{ii}^d v} \end{bmatrix} = \overline{\overline{X}}^{10} (\overline{\overline{I}} - \overline{\overline{R}} \overline{\overline{R}})^{-1} \overline{\overline{R}}^{12}$$

The coefficients of the DGF obtained using the modified symmetrical property as in Eq. (3.4-11) are composed of the half-space transmission matrix $\overline{\overline{X}}^{=01}$ for the waves incident from Region 0 to Region 1. However, it does not represent the actual physical scenario of the problem of interest since the source is located inside Region 1. On the other hand, the complete coefficients of the dyad obtained via the direct construction method, given by the RHS of Eq. (3.4-12), provide more physical insight to the problem.

It is verified numerically that the following relationship holds for Eq. (3.4-11),

$$\begin{aligned} & \begin{bmatrix} A_{hel}(-k_x, -k_y) & A_{hell}(-k_x, -k_y) \\ A_{vel}(-k_x, -k_y) & A_{vell}(-k_x, -k_y) \end{bmatrix} \\ = & \begin{bmatrix} c_I^u(k_x, k_y)X_{e_{Ih}^u}(k_x, k_y) & -c_{II}^u(k_x, k_y)X_{e_{IIh}^u}(k_x, k_y) \\ -c_I^u(k_x, k_y)X_{e_{Iv}^u}(k_x, k_y) & c_{II}^u(k_x, k_y)X_{e_{IIv}^u}(k_x, k_y) \end{bmatrix} \end{aligned} \quad (3.4-13)$$

$$\begin{aligned} & \begin{bmatrix} B_{hel}(-k_x, -k_y) & B_{hell}(-k_x, -k_y) \\ B_{vel}(-k_x, -k_y) & B_{vell}(-k_x, -k_y) \end{bmatrix} \\ = & \begin{bmatrix} c_I^d(k_x, k_y)X_{e_{Ih}^d}(k_x, k_y) & -c_{II}^d(k_x, k_y)X_{e_{IIh}^d}(k_x, k_y) \\ -c_I^d(k_x, k_y)X_{e_{Iv}^d}(k_x, k_y) & c_{II}^d(k_x, k_y)X_{e_{IIv}^d}(k_x, k_y) \end{bmatrix} \end{aligned} \quad (3.4-14)$$

For a half-space problem, only the upward direct wave will be transmitted through the boundary of Region 0 and Region 1, thus, the $\overline{\overline{G}}^{(0,1)}(r, r')$ of a half-space problem are only associated with the terms of upward direct waves with the coefficients satisfying Eq. (3.4-13). Comparing Eq. (3.4-13) with Eq. (3.3-37) leads directly to the following relation.

$$\gamma = c_I^u(k_{zI}^u) \quad \eta = c_{II}^u(k_{zII}^u) \quad (3.4-15)$$

The relation given by equation (3.4-15) reveals that unknown constants of γ and η (as indicated in [37]) actually has their own physical meanings. These constants represent the

amplitude of the upward direct waves generated by the source in Region 1. This is a new and interesting discovery.

In the case of a layered geometry, both the upward and downward direct waves generated by the source will contribute to the DGF of $\overline{\overline{G}}^{(0,1)}(\underline{r}, \underline{r}')$. As seen in Eq. (3.4-13) and Eq. (3.4-14), each term in the LHS matrix is a product of the coefficients 'c' and 'X'. The coefficients of 'c' represent the amplitudes for the direct waves generated by the source in the unbounded anisotropic medium. The vectors of $c_I^u, c_{II}^u, c_I^d, c_{II}^d$ correspond to the Type I upward wave, Type II upward wave, Type I downward wave and Type II downward wave. The coefficients 'X' of Eq. (3.4-12) correspond to the two-layer transmission coefficients in Eq. (3.4-6) for waves incident from Region 1 (where the source is) to Region 0. Each term of Eq. (3.4-6) has its own physical interpretation. Since the source is located inside the bounded anisotropic slab, the direct wave generated by the source will experience multiple reflections at both boundaries. The total upward wave from the accumulation of all the reflections is indicated by $(\overline{I} - \overline{R} \overline{R})^{-1}$. The transmission of the total upward wave from Region 1 to Region 0 is characterized by the half-space transmission matrix $\overline{X}^{=10}$.

Applying the concept of the eigen-decomposition and the matrix method to obtain the coefficients for the layered geometry, the DGF for the layered problem with a general anisotropic medium when the source is located inside the isotropic region can be obtained. If the source is located inside the anisotropic region and the anisotropic region is a reciprocal medium, the DGF of Region 0 above the source point can be obtained by applying the symmetrical property. If Region 1 is a non-reciprocal medium, then the conventional symmetrical property needs to be modified. It is stated that for a non-reciprocal medium such as a gyrotropic medium,

an interchange of the source and the observation points in the two regions necessitates a reversal of the dc biasing magnetic field to calculate the corresponding DGF.

The modified symmetrical property of DGF simplifies the construction of the DGF. However, applying the modified symmetrical property cannot provide the complete set of DGFs for all the regions when the source is located inside the anisotropic slab. Also, the available symmetrical property doesn't apply to the medium with magnetic anisotropy. A new method to construct the DGFs of layered medium with arbitrary anisotropy directly from the characteristic waves in each region using the eigen-decomposition and matrix method proposed here. This method can easily be extended to calculate the DGFs for a multilayered geometry filled with general anisotropic (electric or magnetic) medium with a source located in any region.

Further, the DGF obtained via direct construction method is compared with the DGF obtained using the symmetrical property for the reciprocal medium case. An interesting relationship for the coefficients of the dyad in the DGFs obtained through two different methods is observed and discussed. Thus, a straightforward physical insight to the DGFs is revealed from the direct construction method when the source is located inside the anisotropic region as compared to the results obtained using the symmetrical property. The DGFs obtained here have wide applications in the scattering and radiation problems with arbitrarily shaped 3D objects located inside the anisotropic region.

4 RADIATION OF A HERTZIAN DIPOLE IN THE PRESENCE OF A LAYERED ANISOTROPIC MEDIUM

In the last few decades, the radiation of a Hertzian dipole in the presence of a layered anisotropic substrate has been extensively studied by the researchers. According to the literature survey in Chapter 1, no numerical results have been given for the radiated field of a Hertzian dipole in the presence of a half-space gyroelectric medium. Also, the radiated field of a Hertzian dipole above or inside the gyroelectric slab with an arbitrary biasing magnetic field is not found from the current literature. To fill this gap, the radiated fields of a Hertzian dipole for the above cases are solved and discussed in this chapter.

This chapter is organized as follows. In Section 4.1, the formulation for the radiated field of a Hertzian dipole is presented for half-space geometry with a source located in both the isotropic and anisotropic regions using the method of stationary phase. In Section 4.2, the analysis of the radiated field of a Hertzian dipole embedded inside either the isotropic or the anisotropic region of two-layer geometry is presented. In Section 4.3, the explicit formulations from previous sections are numerically validated with the available results from current literature. In Section 4.4, detailed discussions are presented on the radiated field of a dipole on top of the half-space gyroelectric medium and inside the layered gyroelectric slab.

4.1 Radiation of a Hertzian Dipole for a Half-Space Problem

As shown in Fig. 4-1, Region 0 of the half-space geometry is denoted as the isotropic region and Region 1 is denoted as the anisotropic region. $\epsilon_{0r}, \epsilon_0$ and μ_{0r}, μ_0 are the permittivity

and permeability for the isotropic region. $\overline{\varepsilon}_0$ and $\overline{\mu}_0$ are the permittivity and permeability tensors for the anisotropic region. ε_0 and μ_0 are the free space permittivity and permeability. It's noted here that in the following discussion, $\varepsilon_{0r} = 1$ and $\mu_{0r} = 1$, while $\overline{\varepsilon}_{1r}$ and $\overline{\mu}_{1r}$ for Region 1 take the following form for a general anisotropic medium.

$$\overline{\varepsilon}_{1r} = \begin{bmatrix} \varepsilon_{xx} & \varepsilon_{xy} & \varepsilon_{xz} \\ \varepsilon_{yx} & \varepsilon_{yy} & \varepsilon_{yz} \\ \varepsilon_{zx} & \varepsilon_{zy} & \varepsilon_{zz} \end{bmatrix} \quad \overline{\mu}_{1r} = \begin{bmatrix} \mu_{xx} & \mu_{xy} & \mu_{xz} \\ \mu_{yx} & \mu_{yy} & \mu_{yz} \\ \mu_{zx} & \mu_{zy} & \mu_{zz} \end{bmatrix} \quad (4.1-1)$$

An arbitrarily oriented Hertzian dipole is located at a distance h_d away from the interface separating the isotropic and anisotropic regions. The dipole can be located either in Region 0 as shown in Fig. 4-1(a) or Region 1 as shown in Fig. 4-1(b).

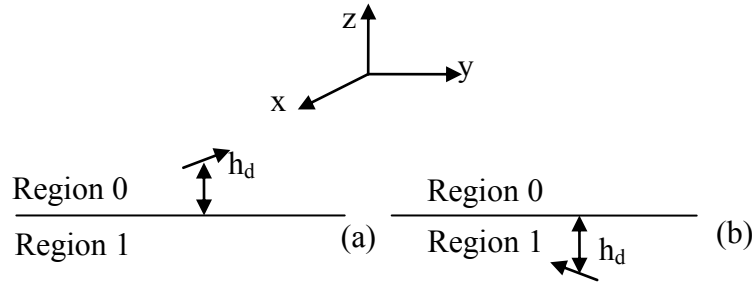


Fig. 4-1: Geometry for the half-space problem with a Hertzian dipole placed at a certain distance away from the boundary separating the isotropic and anisotropic regions. (a) Dipole in Region 0 (isotropic region) and (b) dipole in Region 1 (anisotropic region).

The Hertzian dipole source is given by

$$\overline{J}(\vec{r}) = (I\delta(x)\delta(y)\delta(z \mp h_d))\hat{u} \quad (4.1-2)$$

The negative sign shows that the dipole is located in Region 0 above the interface, while the positive sign indicates that the dipole is located in Region 1 below the interface. The direction of the Hertzian dipole is indicated by the normalized unit vector \hat{u} .

4.1.1 The Source Embedded in the Isotropic Region

To obtain the radiated field in Region 0 for the geometry shown in Fig. 4-1(a), the dyadic Green's function for the region of $z > z'$ when the source is located in Region 0 is required. The DGF of $\overline{\overline{G}}^{(0,0)}(\vec{r}, \vec{r}')$ has been derived in Chapter 3, which is repeated here for convenience.

For $z > z'$

$$\overline{\overline{G}}^{(0,0)}(\vec{r}, \vec{r}') = \frac{i}{8\pi^2} \int_{-\infty}^{\infty} dk_x dk_y \frac{1}{k_{0z}} \left\{ \begin{array}{l} \hat{h}_0(+k_{0z}) e^{i\vec{k}_0 \cdot \vec{r}} \left[\begin{array}{l} \hat{h}_0(+k_{0z}) e^{-i\vec{k}_0 \cdot \vec{r}'} + \\ R_{hh}^{01}(-k_x, -k_y) \hat{h}_0(-k_{0z}) e^{-i\vec{k}_0 \cdot \vec{r}'} \\ -R_{hv}^{01}(-k_x, -k_y) \hat{v}_0(-k_{0z}) e^{-i\vec{k}_0 \cdot \vec{r}'} \end{array} \right] \\ + \hat{v}_0(+k_{0z}) e^{+i\vec{k}_0 \cdot \vec{r}} \left[\begin{array}{l} \hat{v}_0(+k_{0z}) e^{-i\vec{k}_0 \cdot \vec{r}'} \\ -R_{vh}^{01}(-k_x, -k_y) \hat{h}_0(-k_{0z}) e^{-i\vec{k}_0 \cdot \vec{r}'} \\ +R_{vv}^{01}(-k_x, -k_y) \hat{v}_0(-k_{0z}) e^{-i\vec{k}_0 \cdot \vec{r}'} \end{array} \right] \end{array} \right\} \quad (4.1-3)$$

The terms of R_{pq}^{ij} ($i, j = 0, 1$, and $p, q = h, v$) in Eq. (4.1-3) indicate the half-space reflection coefficients. The first index of the superscript i indicates the region of incident wave, and the first index of the subscript indicates the polarization of the incidence wave. The second index of the superscript indicates the region of transmission, and the second index of the subscript indicates the polarization of the reflected wave. For example, R_{hh}^{01} indicates the half-space reflection coefficient of the wave incident from Region 0 to Region 1 with both the incident and reflected waves being h -polarized waves.

It may be shown numerically that the half-space reflection coefficients at the interface of the isotropic and anisotropic regions satisfy the relation in Eq. (4.1-4), when the anisotropic region (Region 1) is filled with a uniaxial or biaxial medium.

$$\begin{aligned} R_{hh}^{01}(-k_x, -k_y) &= R_{hh}^{01}(k_x, k_y), & R_{hv}^{01}(-k_x, -k_y) &= -R_{vh}^{01}(k_x, k_y) \\ R_{vh}^{01}(-k_x, -k_y) &= -R_{hv}^{01}(k_x, k_y), & R_{vv}^{01}(-k_x, -k_y) &= R_{vv}^{01}(k_x, k_y) \end{aligned} \quad (4.1-4)$$

If Region 1 is filled with a non-reciprocal medium, the above relation is not valid between the reflection coefficients for incident wave with $(-k_x, -k_y)$ and the reflection coefficients for incident wave with (k_x, k_y) . However, the above relationship is still valid if the LHS and RHS of the above formulas are calculated for the half-space problem with the anisotropic region of $\bar{\varepsilon}$ and $\bar{\varepsilon}^T$, respectively.

If Region 1 is filled with a uniaxial or biaxial medium, using Eq. (4.1-4), the DGF of region $z > z'$ in Eq. (4.1-3) reduces to the following form.

For $z > z'$

$$\begin{aligned} \bar{G}^{(0,0)}(\bar{r}, \bar{r}') &= \\ \frac{i}{8\pi^2} \int_{-\infty}^{\infty} dk_x dk_y \frac{1}{k_{0z}} &\left\{ \begin{array}{l} \hat{h}_0(+k_{0z}) e^{i\bar{k}_0 \cdot \bar{r}'} \left[\begin{array}{l} \hat{h}_0(+k_{0z}) e^{i\bar{k}_0 \cdot \bar{r}} \\ + R_{hh}^{01}(k_x, k_y) \hat{h}_0(-k_{0z}) e^{-i\bar{k}_0 \cdot \bar{r}} \\ + R_{hv}^{01}(k_x, k_y) \hat{v}_0(-k_{0z}) e^{-i\bar{k}_0 \cdot \bar{r}} \end{array} \right] \\ + \hat{v}_0(+k_{0z}) e^{+i\bar{k}_0 \cdot \bar{r}'} \left[\begin{array}{l} \hat{v}_0(+k_{0z}) e^{-i\bar{k}_0 \cdot \bar{r}} \\ + R_{vh}^{01}(k_x, k_y) \hat{h}_0(-k_{0z}) e^{-i\bar{k}_0 \cdot \bar{r}} \\ + R_{vv}^{01}(k_x, k_y) \hat{v}_0(-k_{0z}) e^{-i\bar{k}_0 \cdot \bar{r}} \end{array} \right] \end{array} \right\} \quad (4.1-5) \end{aligned}$$

It is known that the radiated field is related with the current source and the dyadic Green's function in the following form.

$$\bar{E}_0(\bar{r}) = i\omega\mu_0 \iiint_{V'} dv G^{\equiv(0,0)}(\bar{r}, \bar{r}') \cdot \bar{J}(\bar{r}') \quad (4.1-6)$$

Thus, substituting Eq. (4.1-2) and Eq. (4.1-5) into Eq. (4.1-6) gives the electric field in terms of half-space reflection coefficients and eigenvectors in free space in Eq. (4.1-7).

$$\begin{aligned} \bar{E}_0(\bar{r}) &= i\omega\mu_0 \iiint_{V'} dV' \frac{i}{8\pi^2} \int_{-\infty}^{\infty} dk_x dk_y \frac{1}{k_{0z}} \left\{ \begin{array}{l} \hat{h}_0^+ e^{i\bar{k}_0 \cdot \bar{r}} \left[\hat{h}_0^+ e^{i\bar{k}_0 \cdot \bar{r}'} + R_{hh}^{01} \hat{h}_0^- e^{-i\bar{k}_0 \cdot \bar{r}'} \right] \\ + R_{hv}^{01} \hat{v}_0^- e^{-i\bar{k}_0 \cdot \bar{r}'} \end{array} \right\} \cdot \bar{J}(\bar{r}') \\ &= -\frac{\omega\mu_0 l l}{8\pi^2} \int_{-\infty}^{\infty} \int_{-\infty}^{\infty} dk_x dk_y \frac{1}{k_{0z}} \left\{ \begin{array}{l} \hat{h}_0^+ e^{i\bar{k}_0 \cdot \bar{r}} \left[\hat{h}_0^+ e^{-ik_{0z} h_d} + R_{hh}^{01} \hat{h}_0^- e^{ik_{0z} h_d} \right] \\ + R_{hv}^{01} \hat{v}_0^- e^{ik_{0z} h_d} \end{array} \right\} \cdot \hat{u} \end{aligned} \quad (4.1-7)$$

In general, the integral in Eq. (4.1-7) cannot be obtained analytically. However, the far field radiation pattern can be approximately obtained using the method of stationary phase [71]. This technique assumes that the phase term $e^{i\bar{k}_0 \cdot \bar{r}}$ is oscillating so rapidly that on average the contributions to the integral are mostly from the point which corresponds to the minima of the phase function $\bar{k}_0 \cdot \bar{r}$, and it is assumed that the dyad and k_{0z} is almost constant around this stationary point. Extracting all the dyadic elements and the slowly varying scalar function from the integrand gives

$$\bar{E}_0(\bar{r}) = -\frac{\omega\mu_0 l l}{8\pi^2} \frac{1}{k_{0z}} \left\{ \begin{array}{l} \hat{h}_0^+ \left[\hat{h}_0^+ e^{-ik_{0z} h_d} + R_{hh}^{01} \hat{h}_0^- e^{ik_{0z} h_d} + R_{hv}^{01} \hat{v}_0^- e^{ik_{0z} h_d} \right] \\ + \hat{v}_0^+ \left[\hat{v}_0^+ e^{-ik_{0z} h_d} + R_{vh}^{01} \hat{h}_0^- e^{ik_{0z} h_d} + R_{vv}^{01} \hat{v}_0^- e^{ik_{0z} h_d} \right] \end{array} \right\} \int_{-\infty}^{\infty} \int_{-\infty}^{\infty} dk_x dk_y e^{i\bar{k}_0 \cdot \bar{r}} \cdot \hat{u} \quad (4.1-8)$$

The stationary phase point can be obtained by taking the partial derivatives of the phase term $\bar{k}_0 \cdot \bar{r}$ with respect to k_x, k_y and setting the derivatives equal to zero. The stationary phase point occurs when the propagation vector is aligned with the field point vector [71, p.143]. The final expressions of the radiated field for a Hertzian dipole over the half-space geometry filled with reciprocal and non-reciprocal media are given in Eq. (4.1-9) and Eq. (4.1-10), respectively.

For a half-space reciprocal medium, the radiated field in the region of $z > z'$ is

$$\bar{E}_0(\bar{r}) = -\frac{\omega\mu_0 I l}{4\pi r} e^{ik_0 r} \left\{ \begin{array}{l} \hat{h}_0^+ \left[\hat{h}_0^+ e^{-ik_0 z h_d} + R_{hh}^{01} \hat{h}_0^- e^{ik_0 z h_d} + R_{vh}^{01} \hat{v}_0^- e^{ik_0 z h_d} \right] \\ + \hat{v}_0^+ \left[\hat{v}_0^+ e^{-ik_0 z h_d} + R_{hv}^{01} \hat{h}_0^- e^{ik_0 z h_d} + R_{vv}^{01} \hat{v}_0^- e^{ik_0 z h_d} \right] \end{array} \right\} \bullet \hat{u} \quad (4.1-9)$$

For a half-space non-reciprocal medium, the radiated field in the region of $z > z'$ is

$$\bar{E}_0(\bar{r}) = -\frac{\omega\mu_0 I l}{4\pi r} e^{ik_0 r} \left\{ \begin{array}{l} \hat{h}_0^+ \left[\hat{h}_0^+ e^{-ik_0 z h_d} + R_{hh}^{01}(-k_x, -k_y) \hat{h}_0^- e^{ik_0 z h_d} \right] \\ - R_{hv}^{01}(-k_x, -k_y) \hat{v}_0^- e^{ik_0 z h_d} \\ + \hat{v}_0^+ \left[\hat{v}_0^+ e^{-ik_0 z h_d} - R_{vh}^{01}(-k_x, -k_y) \hat{h}_0^- e^{ik_0 z h_d} \right] \\ + R_{vv}^{01}(-k_x, -k_y) \hat{v}_0^- e^{ik_0 z h_d} \end{array} \right\} \bullet \hat{u} \quad (4.1-10)$$

4.1.2 The Source Embedded in the Anisotropic Region

For the region above the source point ($z > z'$), the radiated field of a Hertzian dipole correlates with the current source through the dyadic Green's function of $\bar{G}^{(0,1)}(\bar{r}, \bar{r}')$ in the following form.

$$\bar{E}_0(\bar{r}) = i\omega\mu_0 \iiint_{V'} dv \bar{G}^{(0,1)}(\bar{r}, \bar{r}') \bullet \bar{J}(\bar{r}') \quad (4.1-11)$$

$\overline{\overline{G}}^{(0,1)}(\vec{r}, \vec{r}')$ is the dyadic Green's function of Region 0 when the source is located in Region 1. As derived in Chapter 3, the dyadic Green's function of $\overline{\overline{G}}^{(0,1)}(\vec{r}, \vec{r}')$ can be obtained through the direct construction method as well as through applying the symmetrical property to the DGF of $\overline{\overline{G}}^{(1,0)}(\vec{r}, \vec{r}')$. These two approaches give the consistent dyadic Green's functions.

Since the radiated fields of a Hertzian dipole in the presence of both layered reciprocal and non-reciprocal media are of interest, it's more straightforward to utilize the DGF formulated with the direct construction method. For convenience, the DGF of $\overline{\overline{G}}^{(0,1)}(\vec{r}, \vec{r}')$ obtained through the direct construction method is repeated below.

$$\overline{\overline{G}}^{(0,1)}(\vec{r}, \vec{r}') = \frac{i}{8\pi^2} \int_{-\infty}^{\infty} \int_{-\infty}^{\infty} dk_x dk_y \frac{1}{k_{0z}} \left(\begin{aligned} & \left[X_{e_h^u}^{10} \hat{h}_0^+ e^{i\vec{k}_0 \cdot \vec{r}} + X_{e_v^u}^{10} \hat{v}_0^+ e^{i\vec{k}_0 \cdot \vec{r}} \right] c_I^u(k_{zI}^u) \left(\hat{v}_I^u \right) e^{-i\vec{k}_I \cdot \vec{r}'} \\ & + \left[X_{e_h^d}^{10} \hat{h}_0^+ e^{i\vec{k}_0 \cdot \vec{r}} + X_{e_v^d}^{10} \hat{v}_0^+ e^{i\vec{k}_0 \cdot \vec{r}} \right] c_{II}^u(k_{zII}^u) \left(\hat{v}_{II}^u \right) e^{-i\vec{k}_{II} \cdot \vec{r}'} \end{aligned} \right) \quad (4.1-12)$$

where the coefficients are defined as

$$\overline{\overline{X}}^{10} = \begin{bmatrix} X_{e_h^u}^{10} & X_{e_h^d}^{10} \\ X_{e_v^u}^{10} & X_{e_v^d}^{10} \end{bmatrix} \quad \begin{aligned} c_I^u(k_{zI}^u) &= -\frac{2k_{0z} \lambda_I^u}{a_4(k_{zI}^u - k_{zII}^u)(k_{zI}^u - k_{zI}^d)(k_{zI}^u - k_{zII}^d)} \\ c_{II}^u(k_{zII}^u) &= -\frac{2k_{0z} \lambda_{II}^u}{a_4(k_{zII}^u - k_{zI}^u)(k_{zII}^u - k_{zI}^d)(k_{zII}^u - k_{zII}^d)} \end{aligned} \quad (4.1-13)$$

In Eq. (4.1-13), a_4 is the coefficient of the fourth order term of k_z in Booker quartic equation, which is the fourth order polynomial of the determinant of the electric wave matrix expanded in terms of k_z . k_{zp}^q ($p = I, II$; $q = u, d$) are the four roots of the Booker quartic equation. The terms of

X_{pq}^{ij} ($i, j = 0, 1$; $p = e_I^u, e_{II}^u$; $q = h, v$) indicate the half-space transmission coefficients. The first index of the superscript i indicates the region where the wave is incident from, and the first

index of the subscript p indicates the polarization of the incidence wave. The second index of the superscript j indicates the region where the transmitted wave exists, and the second index of the subscript q indicates the polarization of the transmitted wave. For example, $X_{e_h'}^{10}$ indicates the half-space transmission coefficient for a wave incident from Region 1 to Region 0, while the incident and transmitted waves are Type I and h -polarized, respectively.

Applying the method of stationary phase as in Section 4.1.1, it yields the radiated field for the isotropic region of Region 1 as follows.

$$\bar{E}_0(\bar{r}) = i \frac{\omega \mu_0 I l}{4\pi r} e^{i \bar{k}_0 \cdot \bar{r}} \left(\begin{aligned} & \left[X_{e_h'}^{10} \hat{h}_0^+ + X_{e_v'}^{10} \hat{v}_0^+ \right] c_I^u(k_{zI}^u) \left(\hat{v}_I^u \right) e^{i k_{zI}^u h_d} \\ & + \left[X_{e_h'}^{10} \hat{h}_0^+ + X_{e_v'}^{10} \hat{v}_0^+ \right] c_{II}^u(k_{zII}^u) \left(\hat{v}_{II}^u \right) e^{i k_{zII}^u h_d} \end{aligned} \right) \cdot \hat{u} \quad (4.1-14)$$

4.2 Radiation of a Hertzian Dipole for a Two-Layer Problem

In this section, the radiated fields of a Hertzian dipole located above and inside an anisotropic slab are formulated. The two-layer geometries with a Hertzian dipole source placed in Region 0 and in Region 1 (anisotropic) are shown in Fig. 4-2(a) and (b), respectively.

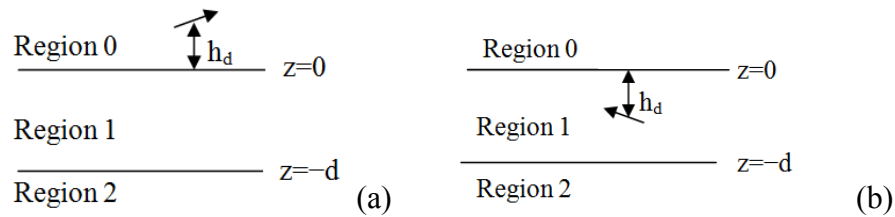


Fig. 4-2: Two-layer geometry: (a) The dipole is located in Region 0 (isotropic medium) and (b) The dipole is located in Region 1 (anisotropic medium).

In both cases, it is assumed that the Hertzian dipole is positioned at a distance of h_d away from the interface separating Region 1 (anisotropic) and Region 0 (isotropic). For a two-layer

problem here, Region 0 is isotropic region with relative permittivity and permeability of $\varepsilon_{0r}, \mu_{0r}$, Region 1 is denoted as the anisotropic region with relative permittivity and permeability tensors of $\overline{\varepsilon}_{1r}, \overline{\mu}_{1r}$, and Region 2 is isotropic region with relative permittivity and permeability of $\varepsilon_{2r}, \mu_{2r}$. The thickness of anisotropic region (Region 1) is d .

4.2.1 The Source Embedded in the Isotropic Region

The first case considered here is the radiation of a Hertzian dipole when it is located in the isotropic region as shown in Fig. 4-2(a). The half-space problem with source inside the isotropic region as presented in Section 4.1.1 can be treated as one special case of a two-layer problem. In order to calculate the radiated field for the region of $z > z'$, the DGF of the corresponding region for the two-layer geometry is required. The detailed derivation of the DGF of the two-layer geometry has been discussed in Section 3.4. For convenience, the DGF of the two-layer geometry for region of $z > z'$ is repeated below.

For $z > z'$

$$\overline{\overline{G}}^{(0,0)}(\vec{r}, \vec{r}') = \frac{i}{8\pi^2} \int_{-\infty}^{\infty} dk_x dk_y \frac{1}{k_{0z}} \left\{ \begin{array}{l} \hat{h}_0(+k_{0z}) e^{i\vec{k}_0 \cdot \vec{r}'} \left[\begin{array}{l} \hat{h}_0(+k_{0z}) e^{i\vec{k}_0 \cdot \vec{r}} \\ + R_{hh}(-k_x, -k_y) \hat{h}_0(-k_{0z}) e^{-i\vec{k}_0 \cdot \vec{r}} \\ - R_{hv}(-k_x, -k_y) \hat{v}_0(-k_{0z}) e^{-i\vec{k}_0 \cdot \vec{r}} \end{array} \right] \\ + \hat{v}_0(+k_{0z}) e^{+i\vec{k}_0 \cdot \vec{r}'} \left[\begin{array}{l} \hat{v}_0(+k_{0z}) e^{-i\vec{k}_0 \cdot \vec{r}} \\ - R_{vh}(-k_x, -k_y) \hat{h}_0(-k_{0z}) e^{-i\vec{k}_0 \cdot \vec{r}} \\ + R_{vv}(-k_x, -k_y) \hat{v}_0(-k_{0z}) e^{-i\vec{k}_0 \cdot \vec{r}} \end{array} \right] \end{array} \right\} \quad (4.2-1)$$

In Eq. (4.2-1), the two-layer reflection coefficients can be expressed in terms of half-space reflection coefficient matrices as follows.

$$\begin{bmatrix} R_{hh} & R_{hv} \\ R_{vh} & R_{vv} \end{bmatrix} = \overset{=01}{R} + \overset{=10=12}{X} \overset{=10=12}{R} (I - \overset{=10=12}{R} \overset{=10=12}{R})^{-1} \overset{=01}{X} \quad (4.2-2)$$

If Region 1 is filled with a biaxial medium, the relation in Eq. (4.2-3) holds for two-layer reflection coefficients as Eq. (4.1-4) for half-space reflection coefficients. It is noted here that no rigorous proof is given for Eq. (4.2-3). This relation is verified numerically only.

$$\begin{aligned} R_{hh}(-k_x, -k_y) &= R_{hh}(k_x, k_y) \\ R_{hv}(-k_x, -k_y) &= -R_{vh}(k_x, k_y) \\ R_{vh}(-k_x, -k_y) &= -R_{hv}(k_x, k_y) \\ R_{vv}(-k_x, -k_y) &= R_{vv}(k_x, k_y) \end{aligned} \quad (4.2-3)$$

Using Eq. (4.2-3), the DGF of Region 0 as in Eq. (4.2-1) for a two-layer problem with Region 1 filled with a biaxial medium can be simplified to Eq. (4.2-4).

$$\overset{=(0,0)}{G}(\bar{r}, \bar{r}') = \frac{i}{8\pi^2} \int_{-\infty}^{\infty} dk_x dk_y \frac{1}{k_{0z}} \left\{ \begin{array}{l} \hat{h}_0(+k_{0z}) e^{i\bar{k}_0 \cdot \bar{r}} \left[\begin{array}{l} \hat{h}_0(+k_{0z}) e^{i\bar{k}_0 \cdot \bar{r}'} \\ + R_{hh}(k_x, k_y) \hat{h}_0(-k_{0z}) e^{-i\bar{k}_0 \cdot \bar{r}'} \\ + R_{hv}(k_x, k_y) \hat{v}_0(-k_{0z}) e^{-i\bar{k}_0 \cdot \bar{r}'} \end{array} \right] \\ + \hat{v}_0(+k_{0z}) e^{i\bar{k}_0 \cdot \bar{r}} \left[\begin{array}{l} \hat{v}_0(+k_{0z}) e^{-i\bar{k}_0 \cdot \bar{r}'} \\ + R_{vh}(k_x, k_y) \hat{h}_0(-k_{0z}) e^{-i\bar{k}_0 \cdot \bar{r}'} \\ + R_{vv}(k_x, k_y) \hat{v}_0(-k_{0z}) e^{-i\bar{k}_0 \cdot \bar{r}'} \end{array} \right] \end{array} \right\} \quad (4.2-4)$$

If Region 1 is filled with a non-reciprocal medium, such as a gyrotropic medium, then the relation Eq. (4.2-4) no longer holds. DGF of Eq. (4.2-1) must be used for the calculation of the electric field in Region 0. The electric field in Region 0 is expressed in terms of the dyadic Green's function of Region 0 as follows.

$$\bar{E}_0(\bar{r}) = i\omega\mu_0 \iiint_{V'} dV' \overset{=(0,0)}{G}(\bar{r}, \bar{r}') \cdot \bar{J}(\bar{r}') \quad (4.2-5)$$

To obtain the radiated field for the region of $z < -h_1$, Eq. (4.2-5) still applies with the DGF of $\overline{\overline{G}}^{(0,0)}(\bar{r}, \bar{r}')$ in Region 0 replaced with the DGF of $\overline{\overline{G}}^{(2,0)}(\bar{r}, \bar{r}')$ for Region 2 ($z < -h_1$). The detailed derivation about how to obtain the DGF of $\overline{\overline{G}}^{(2,0)}(\bar{r}, \bar{r}')$ is presented in Section 3.4, and it is repeated here for convenience.

$$\overline{\overline{G}}^{(2,0)}(\bar{r}, \bar{r}') = \frac{i}{8\pi^2} \int_{-\infty}^{\infty} dk_x dk_y \frac{1}{k_{0z}} \left\{ \begin{aligned} & \left[X_{hh} \hat{h}_2(-k_{2z}) e^{i\bar{k}_2 \cdot \bar{r}} + X_{hv} \hat{v}_2(-k_{2z}) e^{i\bar{k}_2 \cdot \bar{r}} \right] \hat{h}_0(-k_{0z}) \\ & + \left[X_{vh} \hat{h}_2(-k_{2z}) e^{i\bar{k}_2 \cdot \bar{r}} + X_{vv} \hat{v}_2(-k_{2z}) e^{i\bar{k}_2 \cdot \bar{r}} \right] \hat{v}_0(-k_{0z}) \end{aligned} \right\} e^{-i\bar{k}_0 \cdot \bar{r}'} \quad (4.2-6)$$

The two-layer transmission coefficients are given in the following form.

$$\overline{\overline{X}} = \begin{bmatrix} X_{hh} & X_{hv} \\ X_{vh} & X_{vv} \end{bmatrix} = \overline{\overline{X}}^{12} (I - \overline{\overline{R}} \overline{\overline{R}})^{-1} \overline{\overline{X}}^{01} \quad (4.2-7)$$

Substituting Eq. (4.2-1) and Eq. (4.2-7) into Eq. (4.2-3) gives the radiated electric field

$$\overline{\overline{E}}_0(\bar{r}) = i\omega\mu_0 \iiint_{V'} dv \frac{i}{8\pi^2} \int_{-\infty}^{\infty} dk_x dk_y \frac{1}{k_{0z}} \left\{ \begin{aligned} & \hat{h}_0^+ e^{i\bar{k}_0 \cdot \bar{r}} \left[\hat{h}_0^+ e^{i\bar{k}_0 \cdot \bar{r}'} + R_{hh}(-k_x, -k_y) \hat{h}_0^- e^{-i\bar{k}_0 \cdot \bar{r}'} \right] \\ & - R_{hv}(-k_x, -k_y) \hat{v}_0^- e^{-i\bar{k}_0 \cdot \bar{r}'} \\ & + \hat{v}_0^+ e^{+i\bar{k}_0 \cdot \bar{r}} \left[\hat{v}_0^+ e^{-i\bar{k}_0 \cdot \bar{r}'} - R_{vh}(-k_x, -k_y) \hat{h}_0^- e^{-i\bar{k}_0 \cdot \bar{r}'} \right] \\ & + R_{vv}(-k_x, -k_y) \hat{v}_0^- e^{-i\bar{k}_0 \cdot \bar{r}'} \end{aligned} \right\} \cdot \overline{\overline{J}}(\bar{r}') \quad (4.2-8)$$

When the dipole source is located at $z' = h_d$, the above equation reduces to Eq. (4.2-9)

$$\bar{E}_0(\bar{r}) = -\frac{\omega\mu_0 I l}{8\pi^2} \iiint_{V'} dv \int_{-\infty}^{\infty} \int_{-\infty}^{\infty} dk_x dk_y \frac{1}{k_{0z}} \left\{ \begin{array}{l} \hat{h}_0^+ e^{i\bar{k}_0 \cdot \bar{r}} \left[\hat{h}_0^+ e^{-ik_{0z}h_d} + R_{hh}(-k_x, -k_y) \hat{h}_0^- e^{ik_{0z}h_d} \right] \\ -R_{hv}(-k_x, -k_y) \hat{v}_0^- e^{ik_{0z}h_d} \\ +\hat{v}_0^+ e^{+i\bar{k}_0 \cdot \bar{r}} \left[\hat{v}_0^+ e^{-ik_{0z}h_d} - R_{vh}(-k_x, -k_y) \hat{h}_0^- e^{ik_{0z}h_d} \right] \\ +R_{vv}(-k_x, -k_y) \hat{v}_0^- e^{ik_{0z}h_d} \end{array} \right\} \bullet \hat{u} \quad (4.2-9)$$

Applying the method of stationary phase as discussed in Section 4.1.1, the radiated fields of a Hertzian dipole in the isotropic region of Region 0 are expressed in Eq. (4.2-10) and Eq (4.2-11).

dipole placed over a layered reciprocal medium

$$\bar{E}_0(\bar{r}) = i \frac{\omega\mu_0 I l}{4\pi r} e^{ik_0 r} \left\{ \begin{array}{l} \hat{h}_0^+ \left[\hat{h}_0^+ e^{-ik_{0z}h_d} + R_{hh} \hat{h}_0^- e^{ik_{0z}h_d} + R_{vh} \hat{v}_0^- e^{ik_{0z}h_d} \right] \\ +\hat{v}_0^+ \left[\hat{v}_0^+ e^{-ik_{0z}h_d} + R_{hv} \hat{h}_0^- e^{ik_{0z}h_d} + R_{vv} \hat{v}_0^- e^{ik_{0z}h_d} \right] \end{array} \right\} \bullet \hat{u}, \quad (4.2-10)$$

dipole placed over a layered non-reciprocal medium

$$\bar{E}_0(\bar{r}) = i \frac{\omega\mu_0 I l}{4\pi r} e^{ik_0 r} \left\{ \begin{array}{l} \hat{h}_0^+ \left[\hat{h}_0^+ e^{-ik_{0z}h_d} + R_{hh}(-k_x, -k_y) \hat{h}_0^- e^{ik_{0z}h_d} \right] \\ -R_{hv}(-k_x, -k_y) \hat{v}_0^- e^{ik_{0z}h_d} \\ +\hat{v}_0^+ \left[\hat{v}_0^+ e^{-ik_{0z}h_d} - R_{vh}(-k_x, -k_y) \hat{h}_0^- e^{ik_{0z}h_d} \right] \\ +R_{vv}(-k_x, -k_y) \hat{v}_0^- e^{ik_{0z}h_d} \end{array} \right\} \bullet \hat{u} \quad (4.2-11)$$

The radiated field for Region 2 ($z < -d$) below the source point takes the same form for both the layered reciprocal and non-reciprocal media as follows.

$$\bar{E}_2(\bar{r}) = i \frac{\omega\mu_0 I l}{4\pi r} e^{ik_2 r} \left\{ \left[X_{hh} \hat{h}_2^- + X_{hv} \hat{v}_2^- \right] \hat{h}_0^- e^{ik_{0z}h_d} + \left[X_{vh} \hat{h}_2^- + X_{vv} \hat{v}_2^- \right] \hat{v}_0^- e^{ik_{0z}h_d} \right\} \bullet \hat{u} \quad (4.2-12)$$

In Eq. (4.2-10) - Eq. (4.2-12) above, the wave vectors, the h - and v -polarized waves in Region 0 and 2 are defined as follows.

$$\begin{aligned}
\bar{k}_n &= \hat{x}k_x + \hat{y}k_y + \hat{z}k_{nz}, \quad \bar{\kappa}_n = \hat{x}k_x + \hat{y}k_y - \hat{z}k_{nz} \\
\hat{h}_n(+k_{nz}) &= \hat{h}_n(-k_{nz}) = \frac{\hat{z} \times \bar{k}_n}{k_\rho}, \\
\hat{v}_n(+k_{nz}) &= \frac{\hat{h}_n(+k_{nz}) \times \bar{k}_n}{k_n}, \quad \hat{v}_n(-k_{nz}) = \frac{\hat{h}_n(-k_{nz}) \times \bar{\kappa}_n}{k_n}, \quad n = 0 \text{ or } 2,
\end{aligned} \tag{4.2-13}$$

The h - and v -polarized waves can be expanded as follows.

$$\hat{h}_n^+ = \hat{h}_n^- = \begin{bmatrix} \frac{-k_y}{k_\rho} \\ \frac{k_x}{k_\rho} \\ 0 \end{bmatrix}, \quad \hat{v}_n^+ = \begin{bmatrix} \frac{k_x k_{nz}}{k_0 k_\rho} \\ \frac{k_y k_{nz}}{k_n k_\rho} \\ -\frac{k_\rho}{k_n} \end{bmatrix}, \quad \hat{v}_n^- = \begin{bmatrix} -\frac{k_x k_{nz}}{k_n k_\rho} \\ \frac{k_y k_{nz}}{k_n k_\rho} \\ -\frac{k_\rho}{k_n} \end{bmatrix}, \quad \begin{aligned} k_\rho &= \sqrt{k_x^2 + k_y^2}, \\ k_{nz} &= \sqrt{k_n^2 - k_x^2 - k_y^2} \\ k_n &= \omega \sqrt{\mu_0 \epsilon_0 \mu_{nr} \epsilon_{nr}} \\ n &= 0 \text{ or } 2 \end{aligned} \tag{4.2-14}$$

where k_x, k_y are the tangential components of the wave vector for a specific direction.

Observing Eq. (4.2-11) shows that the total electric field in the far field region includes two parts.

$$\left\{ \hat{h}_0^+ \hat{h}_0^+ e^{-ik_{0z} h_d} + \hat{v}_0^+ \hat{v}_0^+ e^{-ik_{0z} h_d} \right\} \cdot \hat{u} \tag{4.2-15}$$

$$\left\{ \hat{h}_0^+ \begin{bmatrix} R_{hh}(-k_x, -k_y) \hat{h}_0^- e^{ik_{0z} h_d} \\ -R_{hv}(-k_x, -k_y) \hat{v}_0^- e^{ik_{0z} h_d} \end{bmatrix} + \hat{v}_0^+ \begin{bmatrix} -R_{vh}(-k_x, -k_y) \hat{h}_0^- e^{ik_{0z} h_d} \\ +R_{vv}(-k_x, -k_y) \hat{v}_0^- e^{ik_{0z} h_d} \end{bmatrix} \right\} \cdot \hat{u} \tag{4.2-16}$$

The first part shown in Eq. (4.2-15) indicates the waves generated by the source in the isotropic region of Region 0 in the absence of the anisotropic medium. The second part shown in Eq. (4.2-16) has four terms that indicate the reflected field from the boundary of isotropic and anisotropic regions. Comparing Eq. (4.2-11) with Eq. (4.1-9) reveals that the radiated fields of two-layer and half-space problems take the same form with different coefficients of the dyad.

It can also be observed from Eq. (4.2-16) that in a given direction only one elementary wave, having the same incidence angle as the observation angle, contributes significantly to the reflected field. The terms associated with reflection coefficients of $R_{hv}^{01}(-k_x, -k_y)$ and $R_{vh}^{01}(-k_x, -k_y)$ indicate that the reflected waves at the interface of the Region 0 and Region 1 have excited both the polarizations of \bar{E}_v and \bar{E}_h . This is due to the cross-coupling of the two characteristic waves inside the anisotropic region. The cross-coupling generally results in an elliptically polarized wave instead of a linearly polarized wave that occurs in free space.

When the dipole is oriented in the \hat{x} -direction, indicating $\hat{u} = \hat{x}$, and then Eq. (4.2-11) can be written in Eq. (4.2-17) decomposed into the horizontal and vertical components as follows.

$$\bar{E}_0(\bar{r}) = \bar{E}_h(\bar{r}) + \bar{E}_v(\bar{r}) \quad (4.2-17)$$

$$\begin{aligned} \bar{E}_h(\bar{r}) &= i \frac{\omega \mu_0 I l}{4\pi r} e^{ik_0 r} \left[\frac{-k_y}{k_\rho} \left(e^{-ik_0 z h_d} + R_{hh}^{01}(-k_x, -k_y) e^{ik_0 z h_d} \right) + \frac{k_x k_{0z}}{k_0 k_\rho} R_{hv}^{01}(-k_x, -k_y) e^{ik_0 z h_d} \right] \hat{h}_0^+ \\ \bar{E}_v(\bar{r}) &= i \frac{\omega \mu_0 I l}{4\pi r} e^{ik_0 r} \left[\frac{k_x k_{0z}}{k_0 k_\rho} \left(e^{-ik_0 z h_d} - R_{vv}^{01}(-k_x, -k_y) e^{ik_0 z h_d} \right) + \frac{k_y}{k_\rho} R_{vh}^{01}(-k_x, -k_y) e^{ik_0 z h_d} \right] \hat{v}_0^+ \end{aligned} \quad (4.2-18)$$

When the dipole is oriented in the \hat{y} direction, as equivalent to $\hat{u} = \hat{y}$, then the radiated field can be simplified to Eq. (4.2-17) with the horizontal and vertical components shown below.

$$\begin{aligned} \bar{E}_h(\bar{r}) &= i \frac{\omega \mu_0 I l}{4\pi r} e^{ik_0 r} \left[\frac{k_x}{k_\rho} \left(e^{-ik_0 z h_d} + R_{hh}^{01}(-k_x, -k_y) e^{ik_0 z h_d} \right) + \frac{k_y k_{0z}}{k_0 k_\rho} R_{hv}^{01}(-k_x, -k_y) e^{ik_0 z h_d} \right] \hat{h}_0^+ \\ \bar{E}_v(\bar{r}) &= i \frac{\omega \mu_0 I l}{4\pi r} e^{ik_0 r} \left[\frac{k_y k_{0z}}{k_0 k_\rho} \left(e^{-ik_0 z h_d} - R_{vv}^{01}(-k_x, -k_y) e^{ik_0 z h_d} \right) - \frac{k_x}{k_\rho} R_{vh}^{01}(-k_x, -k_y) e^{ik_0 z h_d} \right] \hat{v}_0^+ \end{aligned} \quad (4.2-19)$$

When the dipole is oriented in \hat{z} direction, implying $\hat{u} = \hat{z}$, then Eq. (4.2-11) can be written in the form of Eq. (4.2-17) with the horizontal and vertical polarized components shown below.

$$\begin{aligned}\bar{E}_h(\bar{r}) &= i \frac{\omega\mu_0 I l}{4\pi r} e^{ik_0 r} \hat{h}_0^+ \left[\frac{k_\rho}{k_0} R_{hv}^{01}(-k_x, -k_y) e^{ik_0 z h_d} \right] \\ \bar{E}_v(\bar{r}) &= i \frac{\omega\mu_0 I l}{4\pi r} e^{ik_0 r} \hat{v}_0^+ \left[-\frac{k_\rho}{k_0} \left(e^{-ik_0 z h_d} + R_{vv}^{01}(-k_x, -k_y) e^{ik_0 z h_d} \right) \right]\end{aligned}\quad (4.2-20)$$

It is observed from Eq. (4.2-18) and Eq. (4.2-19) that for a horizontally oriented dipole, both \hat{h} and \hat{v} polarized waves are excited from the reflection of the direct waves at the interface, indicating both the co-polarized and cross-polarized reflections contribute to the reflected waves.

However, for a vertically oriented dipole, as shown in Eq. (4.2-20) only the \hat{v} polarized direct wave can be excited while the \hat{h} polarized direct wave cannot be excited. Thus, the \hat{h} polarized component of the total radiated field comes only from the cross-polarized reflection due to the \hat{v} polarized direct wave. The \hat{v} component of the total radiated field is from the direct wave of the \hat{v} polarization and the co-polarized reflection with the \hat{v} polarized incidence wave only. No cross-polarized reflected wave exists, since no direct \hat{h} polarized wave can be excited for \hat{z} -directed dipole. It is noted here that in the spherical coordinate system, the \hat{h} component of the far field corresponds to the $\hat{\phi}$ component and the \hat{v} component of the far field corresponds to the $\hat{\theta}$ component.

4.2.2 The Source Embedded in the Anisotropic Region

If the source is embedded inside the anisotropic region instead of the isotropic region, the following dyadic Green's functions obtained in Section 3.4 are required to calculate the radiated field.

For $z > 0$

$$\begin{aligned} \overline{\overline{G}}^{(0,1)}(\vec{r}, \vec{r}') = \frac{i}{8\pi^2} \int_{-\infty}^{\infty} \int_{-\infty}^{\infty} dk_x dk_y \frac{1}{k_{0z}} & \left(\begin{aligned} & \left[X_{e_{\eta}^u h}^+ \hat{h}_0 e^{i\vec{k}_0 \cdot \vec{r}} + X_{e_{\eta}^u v}^+ \hat{v}_0 e^{i\vec{k}_0 \cdot \vec{r}} \right] c_I^u(k_{zI}^u) \left(\hat{v}_I^u \right) e^{-i\vec{k}_I \cdot \vec{r}'} \\ & + \left[X_{e_{\eta}^u h}^+ \hat{h}_0 e^{i\vec{k}_0 \cdot \vec{r}} + X_{e_{\eta}^u v}^+ \hat{v}_0 e^{i\vec{k}_0 \cdot \vec{r}} \right] c_{II}^u(k_{zII}^u) \left(\hat{v}_{II}^u \right) e^{-i\vec{k}_{II} \cdot \vec{r}'} \\ & + \left[X_{e_{\eta}^d h}^+ \hat{h}_0 e^{i\vec{k}_0 \cdot \vec{r}} + X_{e_{\eta}^d v}^+ \hat{v}_0 e^{i\vec{k}_0 \cdot \vec{r}} \right] c_I^d(k_{zI}^d) \left(\hat{v}_I^d \right) e^{-i\vec{k}_I \cdot \vec{r}'} \\ & + \left[X_{e_{\eta}^d h}^+ \hat{h}_0 e^{i\vec{k}_0 \cdot \vec{r}} + X_{e_{\eta}^d v}^+ \hat{v}_0 e^{i\vec{k}_0 \cdot \vec{r}} \right] c_{II}^d(k_{zII}^d) \left(\hat{v}_{II}^d \right) e^{-i\vec{k}_{II} \cdot \vec{r}'} \end{aligned} \right) \end{aligned} \quad (4.2-21)$$

For $z < -d$

$$\begin{aligned} \overline{\overline{G}}^{(2,1)}(\vec{r}, \vec{r}') = \frac{i}{8\pi^2} \int_{-\infty}^{\infty} \int_{-\infty}^{\infty} dk_x dk_y \frac{1}{k_{0z}} & \left(\begin{aligned} & \left[T_{e_{\eta}^u h}^- \hat{h}_0 e^{i\vec{k}_0 \cdot \vec{r}} + T_{e_{\eta}^u v}^- \hat{v}_0 e^{i\vec{k}_0 \cdot \vec{r}} \right] c_I^u(k_{zI}^u) \left(\hat{v}_I^u \right) e^{-i\vec{k}_I \cdot \vec{r}'} \\ & + \left[T_{e_{\eta}^u h}^- \hat{h}_0 e^{i\vec{k}_0 \cdot \vec{r}} + T_{e_{\eta}^u v}^- \hat{v}_0 e^{i\vec{k}_0 \cdot \vec{r}} \right] c_{II}^u(k_{zII}^u) \left(\hat{v}_{II}^u \right) e^{-i\vec{k}_{II} \cdot \vec{r}'} \\ & + \left[T_{e_{\eta}^d h}^- \hat{h}_0 e^{i\vec{k}_0 \cdot \vec{r}} + T_{e_{\eta}^d v}^- \hat{v}_0 e^{i\vec{k}_0 \cdot \vec{r}} \right] c_I^d(k_{zI}^d) \left(\hat{v}_I^d \right) e^{-i\vec{k}_I \cdot \vec{r}'} \\ & + \left[T_{e_{\eta}^d h}^- \hat{h}_0 e^{i\vec{k}_0 \cdot \vec{r}} + T_{e_{\eta}^d v}^- \hat{v}_0 e^{i\vec{k}_0 \cdot \vec{r}} \right] c_{II}^d(k_{zII}^d) \left(\hat{v}_{II}^d \right) e^{-i\vec{k}_{II} \cdot \vec{r}'} \end{aligned} \right) \end{aligned} \quad (4.2-22)$$

where the coefficients are defined as

$$\begin{aligned} c_I^u(k_{zI}^u) &= -\frac{2k_{0z}\lambda_I^u}{a_4(k_{zI}^u - k_{zII}^u)(k_{zI}^u - k_{zI}^d)(k_{zI}^u - k_{zII}^d)}, & c_{II}^u(k_{zII}^u) &= -\frac{2k_{0z}\lambda_{II}^u}{a_4(k_{zII}^u - k_{zI}^u)(k_{zII}^u - k_{zI}^d)(k_{zII}^u - k_{zII}^d)} \\ c_I^d(k_{zI}^d) &= \frac{2k_{0z}\lambda_I^d}{a_4(k_{zI}^d - k_{zII}^d)(k_{zI}^d - k_{zI}^u)(k_{zI}^d - k_{zII}^u)}, & c_{II}^d(k_{zII}^d) &= \frac{2k_{0z}\lambda_{II}^d}{a_4(k_{zII}^d - k_{zI}^d)(k_{zII}^d - k_{zI}^u)(k_{zII}^d - k_{zII}^u)} \\ \overline{\overline{X}}_a &= \begin{bmatrix} X_{e_{\eta}^u h} & X_{e_{\eta}^u h} \\ X_{e_{\eta}^u v} & X_{e_{\eta}^u v} \end{bmatrix} = \overline{\overline{X}}^{\equiv 10} \overline{\overline{(I-R \ R)}}^{\equiv 12} \overline{\overline{(I-R \ R)}}^{\equiv 10}{}^{-1}, & \overline{\overline{X}}_b &= \begin{bmatrix} X_{e_{\eta}^d h} & X_{e_{\eta}^d h} \\ X_{e_{\eta}^d v} & X_{e_{\eta}^d v} \end{bmatrix} = \overline{\overline{X}}^{\equiv 10} \overline{\overline{(I-R \ R)}}^{\equiv 12} \overline{\overline{(I-R \ R)}}^{\equiv 10}{}^{-1} R^{\equiv 12} \\ \overline{\overline{T}}_a &= \begin{bmatrix} T_{e_{\eta}^u h} & T_{e_{\eta}^u h} \\ T_{e_{\eta}^u v} & T_{e_{\eta}^u v} \end{bmatrix} = \overline{\overline{T}}^{\equiv 12} \overline{\overline{(I-R \ R)}}^{\equiv 10} \overline{\overline{(I-R \ R)}}^{\equiv 12}{}^{-1} R^{\equiv 10}, & \overline{\overline{T}}_b &= \begin{bmatrix} T_{e_{\eta}^d h} & T_{e_{\eta}^d h} \\ T_{e_{\eta}^d v} & T_{e_{\eta}^d v} \end{bmatrix} = \overline{\overline{T}}^{\equiv 12} \overline{\overline{(I-R \ R)}}^{\equiv 10} \overline{\overline{(I-R \ R)}}^{\equiv 12}{}^{-1} \end{aligned}$$

Applying the method of stationary phase yields

For $z > 0$

$$\bar{E}_0(\bar{r}) = \frac{i\omega\mu_0 I l e^{ik_0 r}}{4\pi r} \begin{pmatrix} \left[X_{e_{Ih}^u} \hat{h}_0^+ + X_{e_{Iv}^u} \hat{v}_0^+ \right] c_I^u(k_{zI}^u) \left(\hat{v}_I^u \right) e^{ik_{zI}^u h_d} \\ + \left[X_{e_{IIh}^u} \hat{h}_0^+ + X_{e_{IIv}^u} \hat{v}_0^+ \right] c_{II}^u(k_{zII}^u) \left(\hat{v}_{II}^u \right) e^{ik_{zII}^u h_d} \\ + \left[X_{e_{Ih}^d} \hat{h}_0^+ + X_{e_{Iv}^d} \hat{v}_0^+ \right] c_I^d(k_{zI}^d) \left(\hat{v}_I^d \right) e^{ik_{zI}^d h_d} \\ + \left[X_{e_{IIh}^d} \hat{h}_0^+ + X_{e_{IIv}^d} \hat{v}_0^+ \right] c_{II}^d(k_{zII}^d) \left(\hat{v}_{II}^d \right) e^{ik_{zII}^d h_d} \end{pmatrix} \cdot \hat{u} \quad (4.2-23)$$

For $z < -d$

$$\bar{E}_0(\bar{r}) = \frac{i\omega\mu_0 I l e^{ik_0 r}}{4\pi r} \begin{pmatrix} \left[T_{e_{Ih}^u} \hat{h}_0^+ + T_{e_{Iv}^u} \hat{v}_0^+ \right] c_I^u(k_{zI}^u) \left(\hat{v}_I^u \right) e^{ik_{zI}^u h_d} \\ + \left[T_{e_{IIh}^u} \hat{h}_0^+ + T_{e_{IIv}^u} \hat{v}_0^+ \right] c_{II}^u(k_{zII}^u) \left(\hat{v}_{II}^u \right) e^{ik_{zII}^u h_d} \\ + \left[T_{e_{Ih}^d} \hat{h}_0^+ + T_{e_{Iv}^d} \hat{v}_0^+ \right] c_I^d(k_{zI}^d) \left(\hat{v}_I^d \right) e^{ik_{zI}^d h_d} \\ + \left[T_{e_{IIh}^d} \hat{h}_0^+ + T_{e_{IIv}^d} \hat{v}_0^+ \right] c_{II}^d(k_{zII}^d) \left(\hat{v}_{II}^d \right) e^{ik_{zII}^d h_d} \end{pmatrix} \cdot \hat{u} \quad (4.2-24)$$

Observing the formulas above shows that when the source is located inside the anisotropic region, the radiated field in Region 0 consists both \hat{h} -polarized and \hat{v} -polarized transmitted waves. Each of these waves is due to the transmission of both upward waves characterized by $\hat{e}_I^u, \hat{e}_{II}^u$ and downward waves characterized by $\hat{e}_I^d, \hat{e}_{II}^d$.

Comparing the transmission matrix $\overline{\overline{X}}_b$ (as it corresponds to the transmission of the downward waves $\hat{e}_I^d, \hat{e}_{II}^d$) with transmission matrix $\overline{\overline{X}}_a$ (as it corresponds to the transmission of the upward waves $\hat{e}_I^u, \hat{e}_{II}^u$) reveals that $\overline{\overline{X}}_b = \overline{\overline{X}}_a \overline{\overline{R}}^{=12}$, which implies that the downward wave is first reflected at the boundary of Region 1 and Region 2 and then transmitted into Region 0.

The radiated field in Region 2 consists of the \hat{h} and \hat{v} waves transmitted from both the upward and downward waves. Observing the transmission matrix $\overline{\overline{T}}_a$ shows that the downward waves a are transmitted directly. On the other hand, the upward waves are first reflected at the boundary of Region 0 and Region 1 and then transmitted through the boundary of Region 1 and Region 2 as indicated by $\overline{\overline{T}}_b$.

4.3 Analytic and Numerical Validation

In order to validate the radiation fields obtained in the previous sections, three cases are considered in this section. Case I corresponds to the self-check of the analytical results obtained in the previous two sections. Case II presents the radiation of a Hertzian dipole in the presence of a biaxial slab as shown in [37]. Case III corresponds to the two-layer slab filled with gyroelectric and gyromagnetic media with the source located in the free space.

4.3.1 Case I: Self-check of $\overline{\overline{G}}^{(0,0)}$ and $\overline{\overline{G}}^{(0,1)}$

The geometry considered here is shown in Fig. 4-3.

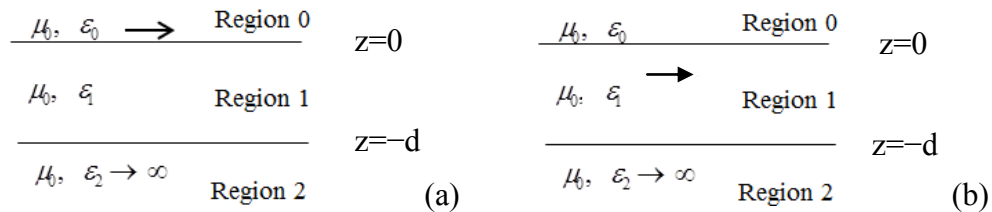


Fig. 4-3: Geometry of Case I with (a) DGF $\overline{\overline{G}}^{(0,0)}$ (b) DGF $\overline{\overline{G}}^{(0,1)}$.

The dipole is placed right at the interface between Region 0 and Region 1. Region 1 is assumed to be isotropic having the same permittivity as Region 0 with $\varepsilon_1 = \varepsilon_0$. Region 2 is assumed to be a ground plane with $\varepsilon_2 \rightarrow \infty$. The thickness of the slab is assumed to be d .

The radiated fields of a vertical dipole placed at the interface of $h_d = 0$ are solved using $\overset{=}{G}^{(0,0)}$ and $\overset{=}{G}^{(0,1)}$, respectively. Since Region 0 and Region 1 are assumed to be the same, it is expected to obtain the exact same expressions for radiated fields derived from either $\overset{=}{G}^{(0,0)}$ or $\overset{=}{G}^{(0,1)}$. First, the general expressions for the radiated fields of a z-directed dipole obtained using $\overset{=}{G}^{(0,0)}$ as in Eq. (4.2-20) are repeated here in Eq. (4.3-1) for convenience.

$$\begin{aligned}\bar{E}_h(\bar{r}) &= i \frac{\omega \mu_0 I l}{4\pi r} e^{ik_0 r} \hat{h}_0^+ \left[\frac{k_\rho}{k_0} R_{hv}^{01}(-k_x, -k_y) e^{ik_0 z h_d} \right] \\ \bar{E}_v(\bar{r}) &= i \frac{\omega \mu_0 I l}{4\pi r} e^{ik_0 r} \hat{v}_0^+ \left[-\frac{k_\rho}{k_0} \left(e^{-ik_0 z h_d} + R_{vv}^{01}(-k_x, -k_y) e^{ik_0 z h_d} \right) \right]\end{aligned}\quad (4.3-1)$$

When Regions 0 and Region 1 are the same media, the half-space reflection and transmission matrices at the interface of Region 0 and Region 1 take the following forms.

$$\overset{=}{R}^{01} = \overset{=}{R}^{10} = \begin{bmatrix} 0 & 0 \\ 0 & 0 \end{bmatrix}, \quad \overset{=}{X}^{01} = \overset{=}{X}^{10} = \begin{bmatrix} 1 & 0 \\ 0 & 1 \end{bmatrix}\quad (4.3-2)$$

Then, the two-layer reflection coefficient matrix of the geometry reduces to Eq. (4.3-3).

$$\begin{bmatrix} R_{hh} & R_{hv} \\ R_{vh} & R_{vv} \end{bmatrix} = \overset{=}{R}^{01} + \overset{=}{X}^{10} \overset{=}{R}^{10=12} = \overset{=}{R}^{10=12} (\overset{=}{I} - \overset{=}{R}^{10=12} \overset{=}{X}^{01})^{-1} \overset{=}{X}^{01} = \overset{=}{R}^{12}\quad (4.3-3)$$

$\overset{=}{R}^{12}$ can be calculated as follows with $d_1 = -d$.

$$\stackrel{=12}{R} = \begin{bmatrix} e^{-ik_{zI}^u d_1} & 0 \\ 0 & e^{-ik_{zII}^u d_1} \end{bmatrix} \begin{bmatrix} -1 & 0 \\ 0 & 1 \end{bmatrix} \begin{bmatrix} e^{ik_{zI}^d d_1} & 0 \\ 0 & e^{ik_{zII}^d d_1} \end{bmatrix} = \begin{bmatrix} -e^{i2k_{0z}d} & 0 \\ 0 & e^{i2k_{0z}d} \end{bmatrix} \quad (4.3-4)$$

The above expression of Eq. (4.3-1) for the z-directed dipole reduces to the following form.

$$\bar{E}_h(\bar{r}) \rightarrow 0, \quad \bar{E}_v = i \frac{\omega \mu_0 I l}{4\pi r} e^{ik_0 r} \left(-\frac{(1 + e^{i2k_{0z}d})k_\rho}{k_0} \right) \hat{v}_0^+ \quad (4.3-5)$$

When the same problem is solved using $\stackrel{=(0,1)}{G}$, the radiated field for the region above the source point can be obtained using Eq. (4.2-23), which is repeated here for convenience.

$$\bar{E}_0(\bar{r}) = \frac{i\omega\mu_0 I l e^{ik_0 r}}{4\pi r} \begin{pmatrix} \begin{bmatrix} X_{e_I^u h} \hat{h}_0^+ + X_{e_I^u v} \hat{v}_0^+ \\ X_{e_{II}^u h} \hat{h}_0^+ + X_{e_{II}^u v} \hat{v}_0^+ \\ X_{e_I^d h} \hat{h}_0^+ + X_{e_I^d v} \hat{v}_0^+ \\ X_{e_{II}^d h} \hat{h}_0^+ + X_{e_{II}^d v} \hat{v}_0^+ \end{bmatrix} \begin{matrix} c_I^u(k^u) (\hat{v}_I^u) e^{ik_{zI}^u h_d} \\ c_{II}^u(k^u) (\hat{v}_{II}^u) e^{ik_{zII}^u h_d} \\ c_I^d(k^d) (\hat{v}_I^d) e^{ik_{zI}^d h_d} \\ c_{II}^d(k^d) (\hat{v}_{II}^d) e^{ik_{zII}^d h_d} \end{matrix} \end{pmatrix} \cdot \hat{u} \quad (4.3-6)$$

Since Region 0 and Region 1 are the same, the transmission coefficients reduce to the following form.

$$\stackrel{=}{X}_a = \begin{bmatrix} X_{e_I^u h} & X_{e_{II}^u h} \\ X_{e_I^u v} & X_{e_{II}^u v} \end{bmatrix} = \stackrel{=10}{X} = \begin{bmatrix} 1 & 0 \\ 0 & 1 \end{bmatrix} \quad (4.3-7)$$

$$\stackrel{=}{X}_b = \begin{bmatrix} X_{e_I^d h} & X_{e_{II}^d h} \\ X_{e_I^d v} & X_{e_{II}^d v} \end{bmatrix} = \stackrel{=10=12}{X} \stackrel{=12}{R} = \stackrel{=12}{R} = \begin{bmatrix} -e^{i2k_{0z}d} & 0 \\ 0 & e^{i2k_{0z}d} \end{bmatrix} \quad (4.3-8)$$

The characteristic wave vectors of \hat{v}_I^u , \hat{v}_I^d , \hat{v}_{II}^u , \hat{v}_{II}^d in Region 1 reduce to

\hat{h}_0^+ , \hat{h}_0^- , \hat{v}_0^+ , \hat{v}_0^- and the amplitude coefficients of c_I^u , c_I^d , c_{II}^u , c_{II}^d reduce to 1 since the

Region 1 and in Region 0 are the same isotropic media. Thus, Eq. (4.3-7) reduces to Eq. (4.3-9).

$$\begin{aligned}\bar{E}_0(\bar{r}) &= \frac{i\omega\mu_0 I l e^{ik_0 r}}{4\pi r} \left(\begin{aligned} &\left[X_{e_{\eta}^u h} \hat{h}_0^+ + X_{e_{\eta}^u v} \hat{v}_0^+ \right] \left(\hat{h}^+ \right) + \left[X_{e_{\eta}^u h} \hat{h}_0^+ + X_{e_{\eta}^u v} \hat{v}_0^+ \right] \left(\hat{v}^+ \right) \\ &+ \left[X_{e_{\eta}^d h} \hat{h}_0^+ + X_{e_{\eta}^d v} \hat{v}_0^+ \right] \left(\hat{h}^- \right) + \left[X_{e_{\eta}^d h} \hat{h}_0^+ + X_{e_{\eta}^d v} \hat{v}_0^+ \right] \left(\hat{v}^- \right) \end{aligned} \right) \cdot \hat{z} \\ &= \frac{i\omega\mu_0 I l e^{ik_0 r}}{4\pi r} \left(X_{e_{\eta}^u h} \hat{h}_0^+ + X_{e_{\eta}^u v} \hat{v}_0^+ + X_{e_{\eta}^d h} \hat{h}_0^+ + X_{e_{\eta}^d v} \hat{v}_0^+ \right) \left(-\frac{k_\rho}{k_0} \right)\end{aligned}\quad (4.3-9)$$

Substituting the transmission coefficients of Eq. (4.3-7) and Eq. (4.3-8) back into Eq. (4.3-9) gives the following expression of the far field in Region 0.

$$\bar{E}_h(\bar{r}) = 0, \quad \bar{E}_v(\bar{r}) = \frac{i\omega\mu_0 I l e^{ik_0 r}}{4\pi r} \left(-\frac{(1 + e^{i2k_0 z^d})k_\rho}{k_0} \right) \hat{v}_0^+ \quad (4.3-10)$$

Inspecting Eq. (4.3-10) and Eq. (4.3-5) shows that the radiated field of the \hat{z} -directed dipole calculated using either $\bar{G}^{(0,0)}$ or $\bar{G}^{(0,1)}$ of the two-layer geometry gives the exactly same results. Assuming Region 0 and Region 1 are both free space with the thickness for Region 1 being $h_1 = 0.05\lambda_0$, and Region 2 being PEC or same as Region 0 (equivalent to an unbounded problem), the radiation patterns of a z-directed Hertzian dipole placed at the interface of Region 0 and Region 1 are plotted in Fig. 4-4. Fig. 4-4(a) plots the radiated field of a vertical dipole calculated using DGF of $\bar{G}^{(0,0)}$, while Fig. 4-4(b) plots the radiated field of a vertical dipole calculated using DGF of $\bar{G}^{(0,1)}$.

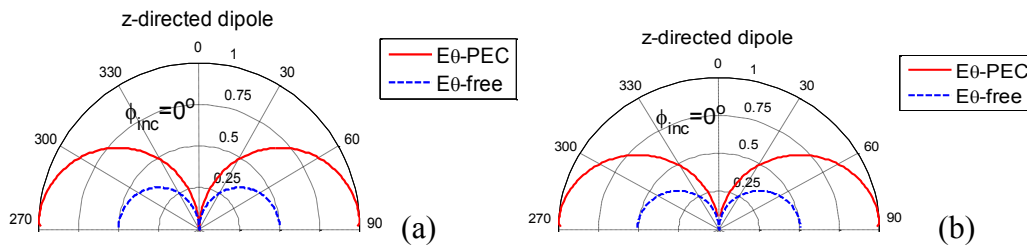


Fig. 4-4: Radiated fields calculated using (a) DGF of $\bar{G}^{(0,0)}$ and (b) DGF of $\bar{G}^{(0,1)}$.

Inspecting Fig. 4-4(a) and Fig. 4-4(b) shows that radiation patterns calculated using both the DGFs give the exactly same results. Applying the same procedure, the radiated fields of a horizontal \hat{x} -directed dipole at the interface of a layered geometry with Region 0 and Region 1 being different media are derived. It is shown in Eq. (4.3-11) that a horizontal dipole's radiated fields derived from both the DGFs of $\overline{\overline{G}}^{(0,0)}$ and $\overline{\overline{G}}^{(0,1)}$ give the same results.

$$\begin{aligned}\overline{E}_h(\bar{r}) &= \frac{i\omega\mu_0 I l e^{ik_0 r}}{4\pi r} \begin{pmatrix} -k_y \\ k_\rho \end{pmatrix} (1 + R_{hh}(-k_x, -k_y)) \\ \overline{E}_v(\bar{r}) &= \frac{i\omega\mu_0 I l e^{ik_0 r}}{4\pi r} \begin{pmatrix} k_x k_{0z} \\ k_\rho k_0 \end{pmatrix} (1 - R_{vv}(-k_x, -k_y))\end{aligned}\quad (4.3-11)$$

It is noted here that if both regions of the layered geometry are filled with different media, the radiated field for a vertical dipole placed at the interface of Region 0 and Region 1, obtained using $\overline{\overline{G}}^{(0,0)}$ and $\overline{\overline{G}}^{(0,1)}$, are usually not the same because the normal component of the electric field is not continuous across the boundary. For this reason, Region 0 and Region 1 are assumed to be the same in the derivation of the radiated field for a vertical dipole.

4.3.2 Case II: Unbounded Isotropic Medium and Layered Biaxial Medium

In this section, we show that the formulas of radiated fields obtained in Section 4.2 when the source is located in Region 0 and Region 1 are consistent with a number of known cases.

A. Unbounded Isotropic Medium

The first problem analyzed is shown in Fig. 4-5, where both Region 0 and Region 1 are isotropic with permittivity ϵ_0 , i.e., it is an unbounded problem. The far field radiation pattern was calculated in the $\varphi = 0$ plane with a Hertzian dipole oriented along x, y and z directions.

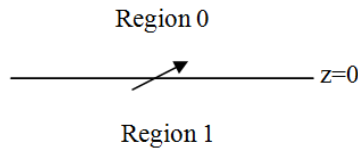


Fig. 4-5: Geometry of unbounded isotropic medium.

It is known that the theoretical normalized radiated field pattern for a z-directed dipole in unbounded isotropic medium is as follows.

$$f_z(\theta) = \sin \theta \quad (4.3-12)$$

For an x-directed dipole, the normalized radiated field pattern is given by

$$f_x(\theta, \phi) = \sqrt{1 - \sin^2 \theta \cos^2 \phi} \quad (4.3-13)$$

while for a y-directed dipole, the normalized radiated field pattern is

$$f_y(\theta, \phi) = \sqrt{1 - \sin^2 \theta \sin^2 \phi} \quad (4.3-14)$$

The calculated and exact results for the x, y and z-directed Hertzian dipoles are shown in Fig. 4-6(a), (b) and (c). Excellent agreement between the numerical solution and the exact solution is observed for all three cases.

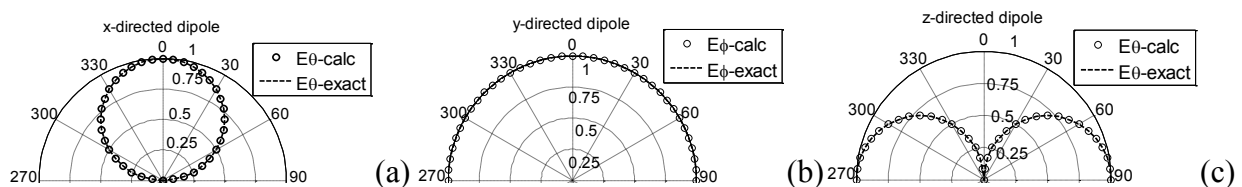


Fig. 4-6: Radiation pattern of the x, y and z-directed Hertzian dipole in unbounded medium in the XZ plane.

It is noted here that to calculate the radiation field of a Hertzian dipole with Region 1 being isotropic medium such as the case of the free space, the three diagonal elements of the

permittivity tensor for Region 1 are chosen as $\bar{\varepsilon} = (1, 1, 1.00001)$, so the anisotropic medium reduces to the isotropic case. Choosing $\bar{\varepsilon} = (1, 1, 1.00001)$ instead of $\bar{\varepsilon} = (1, 1, 1)$ is because the adjoint wave electric matrix is always zero for an isotropic medium, and the eigen-decomposition method is no longer applied. The detail has been explained in Chapter 2.

B. Biaxial Medium

Now we consider the radiation of a Hertzian dipole in the presence of a biaxial slab. The radiations of a Hertzian dipole, located in an isotropic or biaxially anisotropic region for the half-space and two-layer problems, have been thoroughly analyzed by Pettis [37]. To verify with the results in [37], radiation patterns for the following four different cases are given.

First, let Region 1 and Region 2 as shown in Fig. 4-2 are the same medium; then, the two-layer problem reduces to a half-space problem. The radiation patterns of the Hertzian dipole when it is located in the isotropic region and biaxial region are shown in Fig. 4-7 and Fig. 4-8, respectively.

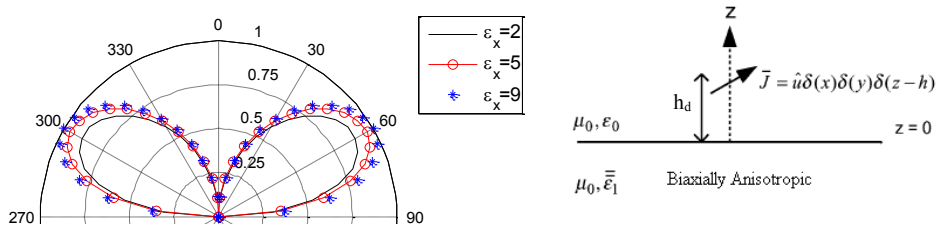


Fig. 4-7: $|E_\theta|$ vs. θ in the $\varphi = 45^\circ$ plane for a z-directed Hertzian dipole in Region 0 (free space) with $h_d = 0.1\lambda_0$ and $\bar{\varepsilon} = (\varepsilon_x, 2, 3)$, $\varepsilon_x = 2, 5, 9$.

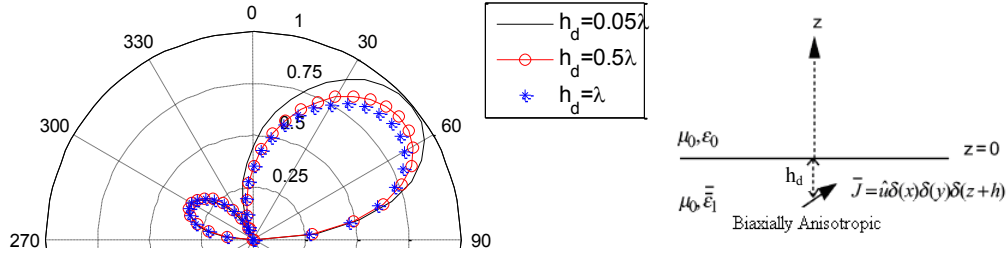


Fig. 4-8: $|E_\theta|$ vs. h_d in the $\varphi = 45^\circ$ plane for a z-directed Hertzian dipole in Region 1 with $(\epsilon_x, \epsilon_y, \epsilon_z) = (2, 8, 4)$, $(\alpha, \beta, \gamma) = (30^\circ, 20^\circ, 0^\circ)$.

Now let Region 2 be an isotropic medium, then the radiated field can be calculated using the formula derived in Section 4.2, and the results are displayed in Fig. 4-9 and Fig. 4-10, respectively.

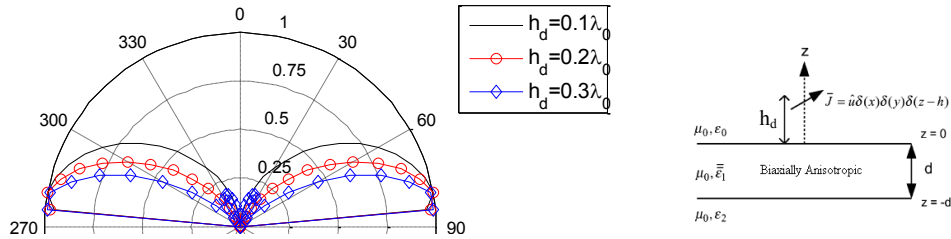


Fig. 4-9: $|E_\theta|$ vs. θ in the $\varphi = 90^\circ$ plane for various values of h_d for a z-directed Hertzian dipole positioned in region 0 of a two-layer problem. Region 1 is biaxial with $(\epsilon_x, \epsilon_y, \epsilon_z) = (2, 8, 4)$, $(\alpha, \beta, \gamma) = (0, 0, 0)$ and slab thickness is $0.4\lambda_0$.

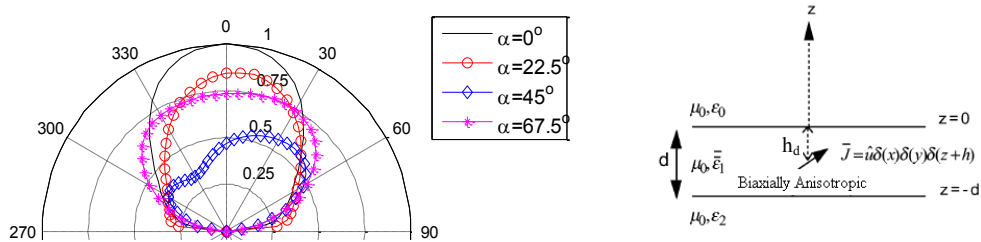


Fig. 4-10: $|E_\phi|$ vs. θ in the $\varphi = 0^\circ$ plane for various values of α (rotation angle) and an x-directed Hertzian dipole positioned in Region 1 of a two-layer problem. Region 1 is biaxial with $(\epsilon_x, \epsilon_y, \epsilon_z) = (2, 8, 4)$, $(\alpha, \beta, \gamma) = (0^\circ, 70^\circ, 0^\circ)$ and with $h_d = 0.3\lambda_0$, $d = 0.4\lambda_0$.

Fig. 4-9 is consistent with the result of Fig. 5.45 shown in [37]. Fig. 4-10 is consistent with result of Fig. 5.53 shown in [37]. As shown in Fig. 4-9, the radiation pattern of a Hertzian dipole is symmetric when the dipole is placed in the isotropic region, while it is not when the dipole is inside the biaxial slab. The numerical results validate the use of the Green's function obtained in Chapter 3. Since the purpose here is for validation only, detailed discussion about the biaxial anisotropic effect on the radiation of a Hertzian dipole is omitted here.

4.3.3 The Anisotropic Region Filled with Gyroelectric and Gyromagnetic Media

Now let us consider the radiation of a Hertzian dipole in the presence of a non-reciprocal slab filled with gyrotropic media.

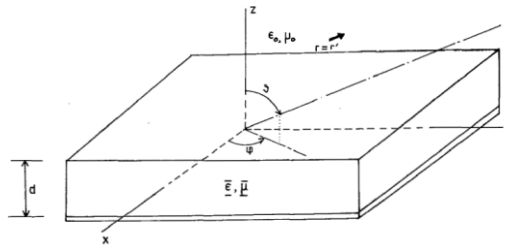


Fig. 4-11: Geometry of the grounded gyroelectric slab in [46].

A. Gyroelectric Medium

The first case shown here is for a numerical verification with the work of Wu [46]. The dipole is placed in the isotropic region over a grounded gyroelectric slab as shown in Fig. 4-11. The numerically obtained radiation patterns of the dipole over a grounded slab of different thickness are plotted in Fig. 4-12. The distance of the dipole away from the interface between Region 0 and Region 1 is $h_d = 0.55\lambda_0$ and the thickness of the slab is chosen as $0.05\lambda_0$, $0.3\lambda_0$ and $0.55\lambda_0$. The relative frequency for the gyroelectric medium is chosen as $\frac{\omega_b}{\omega} = 2.2$, $\frac{\omega_p}{\omega} = 0.6$.

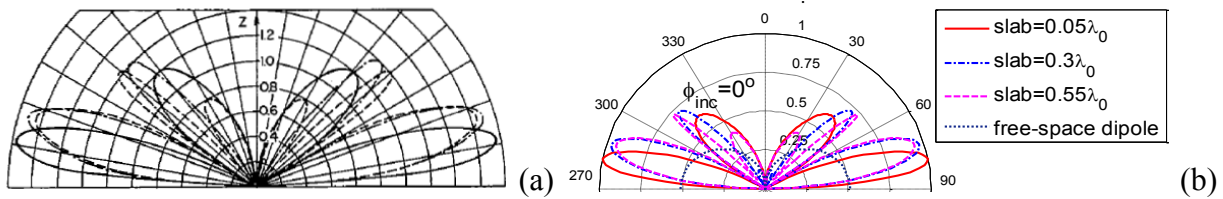


Fig. 4-12: $|E_\theta|$ vs. θ in the plane of $\varphi = 0^\circ$ for a z -directed Hertzian dipole located in Region 0, with $h_d = 0.55\lambda_0$ away from the interface of free space and gyroelectric slab. (a) Result from Wu [46] and (b) Radiated field using the formula in this chapter.

Fig. 4-12(a) displays the numerical results obtained from [46], while Fig. 4-12(b) displays the radiation pattern calculated using the formulas derived in this chapter. As observed in Fig. 4-12, very good agreement is obtained between our results and the results from [46].

B. Gyromagnetic Medium

The second case will establish consistency between the numerical results obtained here and these of Tsalamengas and Uzunoglu [54]. The geometry of the problem is shown in Fig. 4-13.

The dipole is located in Region 0 along the vector $\hat{x} + \hat{y} + \hat{z}$ at a distance of 6cm from the ferrite slab whose thickness is 5mm and the radiated field in Region 2 is of interest. Region 1 is filled with a ferrite medium, which is electrically isotropic with $\epsilon_{1r} = 14.8$ and magnetically gyrotropic with $\omega_0 = 2\pi \times 2.8 \times 10^9 \text{ rad/s}$, $\omega_m = 21.111 \times 10^9 \text{ rad/s}$. The incident frequency is 10 GHz.

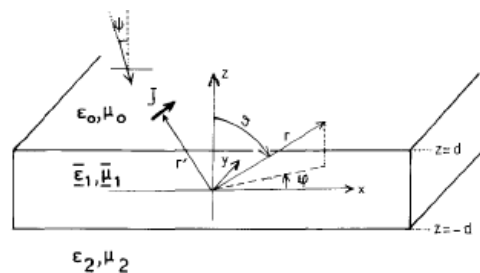


Fig. 4-13: Geometry of a two-layer problem filled with gyromagnetic medium.

Normalized radiation patterns of $|E_\theta|$ and $|E_\phi|$ for the XZ-plane are shown in Fig. 4-14 (a1), (b1), while normalized radiation patterns of $|E_\theta|$ and $|E_\phi|$ for the YZ-plane are shown in Fig. 4-14(c1), (d1). The radiation patterns obtained from [54] are displayed in Fig. 4-14(a2)-(d2).

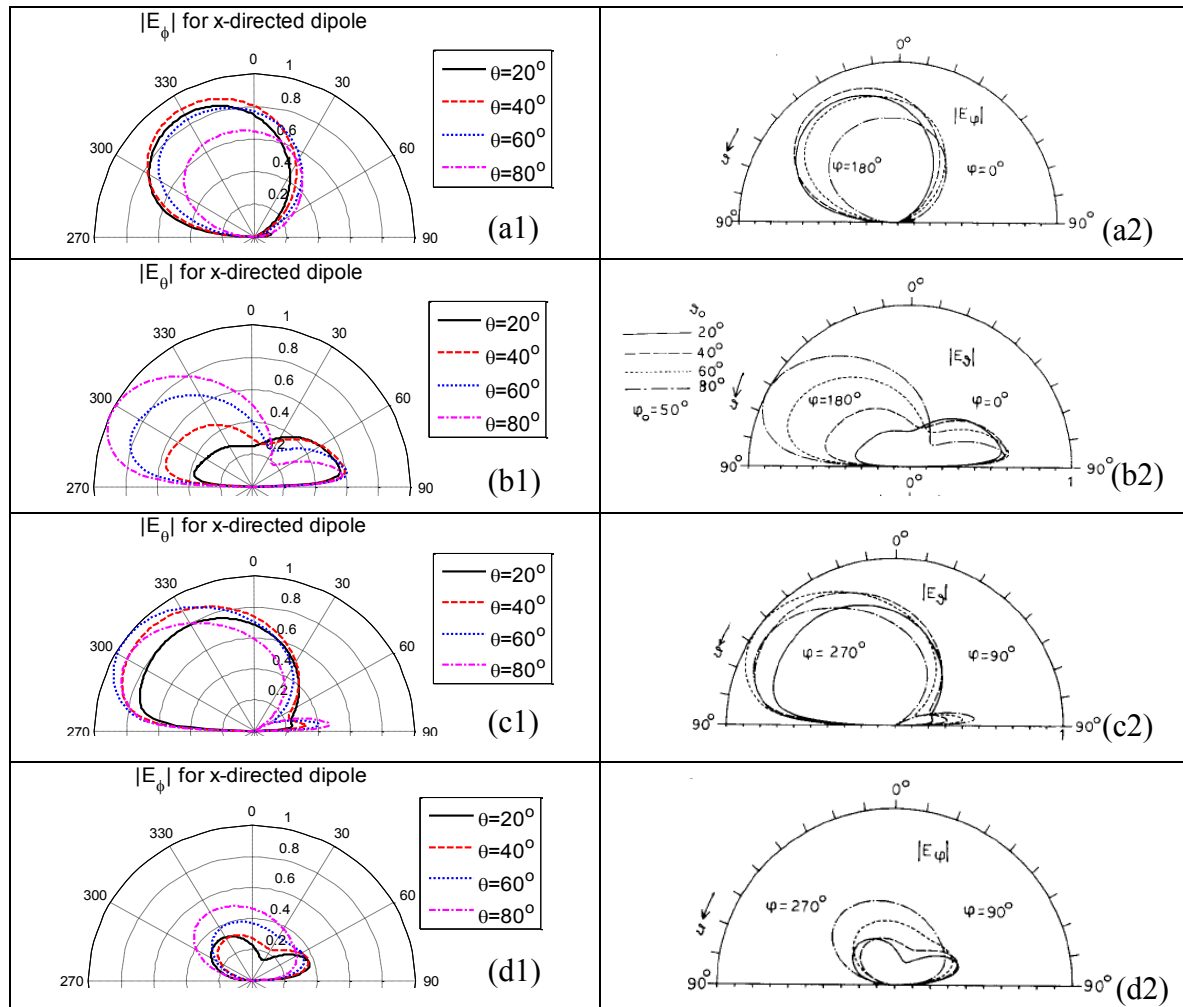


Fig. 4-14: $|E_\theta|$ and $|E_\phi|$ vs. θ in the plane of $\varphi = 0^\circ, 90^\circ$ with the source in Region 0 and the field in Region 2.

Each subplot shows four curves, corresponding to the radiated fields of an x-directed dipole on the layered ferrite slab with four distinct orientations of the biasing magnetic field: $(\theta, \varphi) = (20^\circ, 50^\circ), (40^\circ, 50^\circ), (60^\circ, 50^\circ), (80^\circ, 50^\circ)$. It is seen that the radiation patterns of

the transmitted field for Region 2 obtained using the E-DGF developed here (Eq. (4.2-12)) give very good agreement with what is obtained in [54].

4.4 Radiation of a Hertzian Dipole in the Presence of Gyroelectric Medium

In this section, we will investigate the radiation of a Hertzian dipole in the presence of a gyroelectric medium. First, the radiation of a Hertzian dipole above a half-space gyroelectric medium is presented in Section 4.4.1. Then the radiations of a Hertzian dipole when it is above and inside a two-layer gyroelectric slab are presented in Sections 4.4.2 and 4.4.3, respectively.

4.4.1 Radiation of a Vertical Dipole on Top of a Half-space Gyroelectric Medium

Since the gyroelectric medium is dispersive, the medium property is dependent on the frequency of the incident wave. According to the specific wave type that can propagate inside the gyroelectric medium, the whole frequency is divided into eight different frequency bands [72]. For convenience, the eighth frequency bands are repeated in Table 4-1. It is seen from Table 4-1 that Regions 1, 2, 3 and Region 8 always exist. If $\omega_b > \omega_p$, Region 4 and Region 5 cannot exist. If $\omega_b < \omega_p / \sqrt{2}$, Region 6 and Region 7 cannot exist.

Both characteristic waves propagate in Region 1 and Region 6 and do not depend on the direction of propagation. In Region 3 and Region 7, the Type I wave always exists, while the Type II wave exists only for certain propagation directions with respect to the biasing magnetic field. In Region 2, the Type I wave exists for all the propagation directions. In Region 4, type II wave exists for all the propagation directions, while in Region 8, the Type II wave exists only for

certain propagation directions with respect to the biasing magnetic field. There is no propagation in Region 5.

	Frequency Band	Wave Propagating	
Region 1	$\omega > \omega_1$	Type I, Type II	Always exist
Region 2	$\omega_2 < \omega < \omega_1$	Type I	Always exist
Region 3	$\max(\omega_b, \omega_p) < \omega < \omega_2$	Type I, Type II	Always exist
Region 4	$\max(\omega_b, \omega_3) < \omega < \omega_p$	Type II	Exist only if $\omega_b < \omega_p$
Region 5	$\omega_b < \omega < \omega_3$	No propagation	Exist only if $\omega_b < \frac{\omega_p}{\sqrt{2}}$
Region 6	$\omega_p < \omega < \omega_b$	Type I, Type II	Exist only if $\omega_b > \omega_p$
Region 7	$\omega_3 < \omega < \min(\omega_b, \omega_p)$	Type I, Type II	Exist only if $\omega_b > \frac{\omega_p}{\sqrt{2}}$
Region 8	$0 < \omega < \min(\omega_b, \omega_3)$	Type II	Always exist
$\omega_1 = \frac{\omega_b}{2} + \sqrt{\frac{\omega_b^2}{4} + \omega_p^2}, \quad \omega_2 = \sqrt{\omega_b^2 + \omega_p^2}, \quad \omega_3 = -\frac{\omega_b}{2} + \sqrt{\frac{\omega_b^2}{4} + \omega_p^2}, \quad \omega_3 < \omega_p < \omega_2 < \omega_1,$			

Table 4-1: Frequency bands with different propagating waves for a gyroelectric medium.

The far field of a Hertzian dipole placed on top of a half-space gyroelectric medium for different incident frequencies is analyzed in this section using the formula proposed in the previous sections. The Hertzian dipole is z-oriented ($\hat{u} = \hat{z}$); and the distance from the dipole to the interface is 0. In this case, the field expression reduces to

$$\bar{E}_0(\bar{r}) = i \frac{\omega \mu_0 I l}{4\pi r} e^{ik_0 r} \left\{ \begin{array}{l} \hat{h}_0^+ \left[-R_{hv}(-k_x, -k_y) v_{0z}^- \right] \\ + \hat{v}_0^+ \left[v_{0z}^+ + R_{vv}(-k_x, -k_y) v_{0z}^- \right] \end{array} \right\} \quad (4.4-1)$$

where

$$k_x = k_0 \sin \theta_{obs} \cos \varphi_{obs}, \quad k_y = k_0 \sin \theta_{obs} \sin \varphi_{obs}$$

Spherical components of the far field are obtained as follows.

$$E_\varphi(\bar{r}) = i \frac{\omega \mu_0 I l}{4\pi r} e^{ik_0 r} R_{hv}(-\theta_{obs}, \varphi_{obs}) \sin \theta_{obs} \quad (4.4-2)$$

$$E_\theta = -i \frac{\omega \mu_0 I l}{4\pi r} e^{ik_0 r} (1 + R_{vv}(-\theta_{obs}, \varphi_{obs})) \sin \theta_{obs} \quad (4.4-3)$$

Then, the normalized field pattern for the z-directed dipole is obtained as follows.

$$f_\theta(\theta_{obs}, \varphi_{obs}) = \frac{|1 + R_{vv}(-\theta_{obs}, \varphi_{obs})|}{\max |1 + R_{vv}(-\theta_{obs}, \varphi_{obs})|} \sin \theta_{obs} \quad (4.4-4)$$

$$f_\varphi(\theta_{obs}, \varphi_{obs}) = \frac{|R_{hv}(-\theta_{obs}, \varphi_{obs})|}{\max |R_{hv}(-\theta_{obs}, \varphi_{obs})|} \sin \theta_{obs}$$

It is seen from Eq. (4.4-4) that when the \hat{z} -oriented Hertzian dipole is placed at the interface of free space and a gyroelectric medium, both co-polarized and cross-polarized field components exist if the cross-polarized reflection coefficient $R_{hv}(-\theta_{obs}, \varphi_{obs})$ is non-zero. It is also seen that the co-polarized field pattern f_θ is the free space pattern $\sin \theta$ multiplied by the co-polarized reflection factor $(1 + R_{vv}(-\theta_{obs}, \varphi_{obs}))$, and the cross-polarized field pattern f_φ is the free space pattern $\sin \theta$ multiplied by the cross-polarized reflection factor $R_{hv}(-\theta_{obs}, \varphi_{obs})$. It needs to be noted here that such simple relations only hold for a z-directed dipole when it is located at the interface with $h_d = 0$. The radiation pattern of a \hat{z} -directed dipole is first studied for a half-space

gyroelectric medium with different frequencies and a biasing magnetic field along different orientations.

4.4.1.1 Parametric Effect of Frequency and Biasing Magnetic Field

A. Effect of Frequency

Since the gyroelectric medium is dispersive, the first parameter of interest is the frequency of the incident wave. The following numerical results and discussions investigate the effect of the frequency of the incident wave to the radiation with $\omega_p = 2\pi 10^9$ and $\omega_b = 1.9\omega_p$.

Considering a z -directed Hertzian dipole in Region 0 at the interface of the half-space gyroelectric medium, the radiation patterns $|E_\theta|$ in the plane of $\varphi = 0^\circ$ are displayed in Fig.

4-15. Fig. 4-15(a) and (b) correspond to the cases with the biasing magnetic field of a gyroelectric medium along z -direction and y -direction, respectively. It is seen in Fig. 4-15 that the main beam direction varies with frequency of incidence wave. For the case of a biasing magnetic field along the y -direction, the main beam will become narrower with a side lobe also appearing as the frequency is increased.

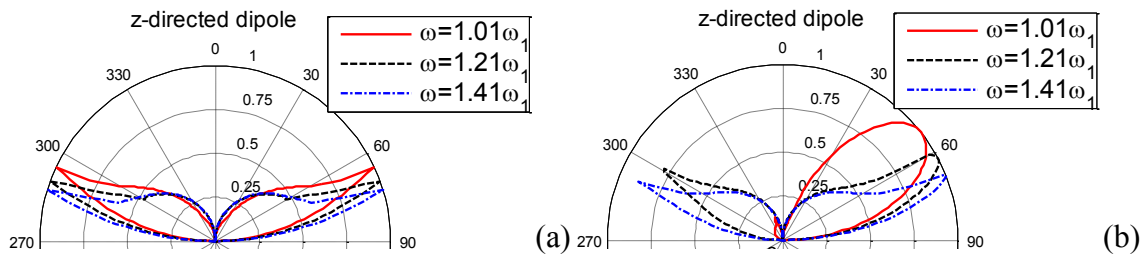


Fig. 4-15: $|E_\theta|$ vs. θ in the plane of $\varphi = 0^\circ$ for a z -directed Hertzian dipole located in Region 0 with $h_d = 0$ away from the interface of free space and gyroelectric medium. The biasing magnetic field is along the (a) z and (b) y directions.

B. Effect of the Biasing Magnetic Field Direction

Then, the effect of the biasing magnetic field direction to the radiation pattern is studied.

Fig. 4-16(a) and (b) show the co-polarized field pattern $|E_\theta|$ and cross-polarized field pattern $|E_\phi|$ in the XZ plane, while Fig. 4-16(c) and (d) show the co-polarized and cross-polarized field patterns $|E_\theta|$ and $|E_\phi|$ in the YZ plane. In each subplot of Fig. 4-16, there exist four curves which correspond to the radiation patterns of a Hertzian dipole on the gyroelectric substrates with four different biasing magnetic fields.

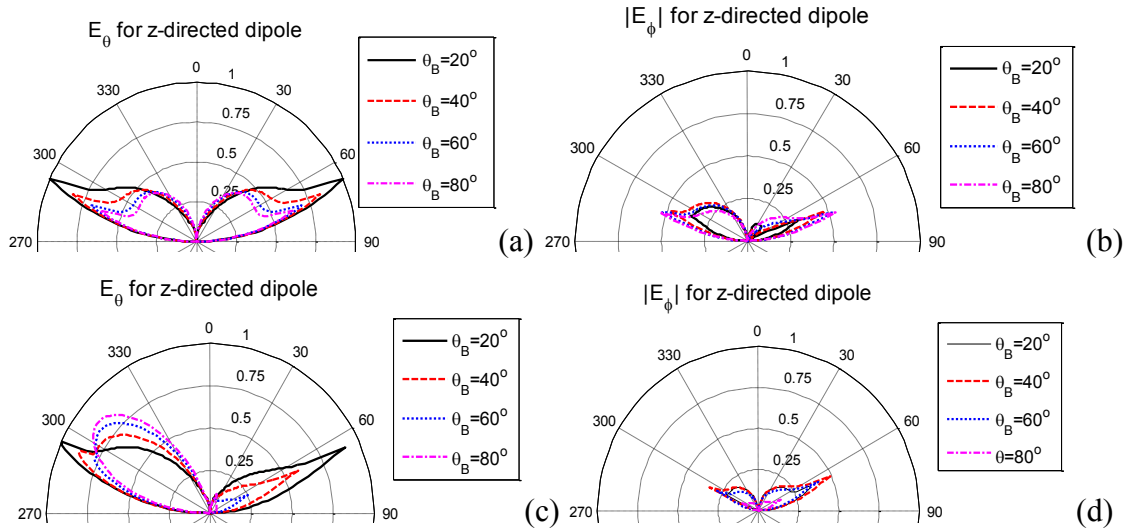


Fig. 4-16: Field pattern for a z -directed Hertzian dipole located in Region 0 with $h_d = 0$ away from the interface of free space and gyroelectric medium. The biasing magnetic field is along $\theta_B = 20^\circ, 40^\circ, 60^\circ, 80^\circ, \varphi_B = 0^\circ$ and the frequency of the incidence wave is $1.01 \omega_1$. (a) $|E_\theta|$ and (b) $|E_\phi|$ vs. θ in the plane of $\varphi = 0^\circ$; (c) $|E_\theta|$ and (d) $|E_\phi|$ vs. θ in the plane of $\varphi = 90^\circ$.

When the biasing magnetic field is in the XZ plane ($\varphi_B = 0^\circ$), it is seen in Fig. 4-16(a) that the co-polarized field patterns in the XZ plane ($\varphi = 0^\circ$) are always symmetric for different directions of $\theta_B = 20^\circ, 40^\circ, 60^\circ, 80^\circ$; further, the main beam of the co-polarized field for the

XZ plane is constant and around 70 degrees. However, the co-polarized field pattern in the YZ plane ($\varphi = 90^\circ$) is not symmetric, as shown in Fig. 4-16(c), and the direction of the main beam varies with θ_B . As θ_B increases, the cross-polarized field pattern in the XZ plane increases, as shown in Fig. 4-16(b), and the cross-polarized field pattern of YZ plane decreases, as shown in Fig. 4-16(d).

4.4.1.2 Relation of Directive Radiation with Total Internal Reflection

As shown in the previous section that the directive radiation exists. In this section, the relation of the directive radiation with the total internal reflection associated with the characteristic waves of the gyroelectric medium is revealed. To be consistent with the discussion of previous section, the plasma frequency and gyrofrequency for the gyroelectric medium are chosen as $\omega_p = 2\pi 10^9$ and $\omega_b = 1.9\omega_p$, such that both Type I and Type II waves exist [72].

When the frequency of the incident wave is in Region 1 as $\omega = 1.01\omega_1$, $\omega_1 = \frac{\omega_b}{2} + \sqrt{\frac{\omega_b^2}{4} + \omega_p^2}$ and the biasing magnetic field is along the z-direction, the relative permittivity and permeability of the gyroelectric medium are given by

$$\bar{\epsilon}_{1r} = \begin{bmatrix} 0.4805 & 0.4196i & 0 \\ -0.4196i & 0.4805 & 0 \\ 0 & 0 & 0.8193 \end{bmatrix}, \quad \mu_{1r} = 1 \quad (4.4-5)$$

The study of the radiation pattern starts with the analysis of the reflection coefficients as it is seen from Eq. (4.4-4) that the co-polarized and cross-polarized reflection factors of $(1 + R_{vv}(-\theta_{obs}, \varphi_{obs}))$ and $R_{lv}(-\theta_{obs}, \varphi_{obs})$ are essential to the corresponding field patterns of f_θ and f_φ . Total internal reflection is one of the most interesting phenomena analyzed here.

It is known that when the wave is incident from dense medium upon less dense medium (assuming both media are isotropic), there exists one critical angle beyond which total internal reflection occurs with the magnitude of the reflection coefficient to be 1. If the wave is incident from an isotropic medium upon an anisotropic medium, there usually exist two critical angles since there are two types of waves in an anisotropic medium.

To demonstrate the concept of the total internal reflection, the magnitude of the wave vector surface for waves propagating in the isotropic medium and the gyroelectric medium characterized by Eq. (4.4-5) is plotted in Fig. 4-17.

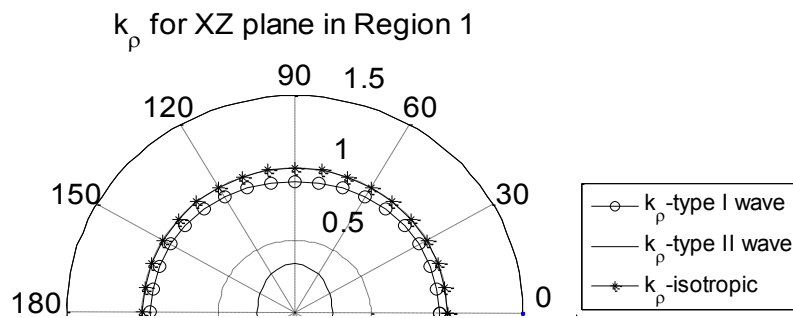


Fig. 4-17: Normalized wave vector surface of an isotropic medium and these for Type I and Type II waves of a gyroelectric medium vs. θ in the plane of $\varphi = 0^\circ$.

It is noted here that the magnitudes of the wave vector for each case have been renormalized to the wave number of the isotropic medium. It is observed from Fig. 4-17 that since the wave vector surfaces for both Type I and Type II waves are within that of the isotropic medium, the total internal reflection will exist. It is easy to determine the critical angle at the interface of two isotropic media using $\theta_c = \sin^{-1}\left(\frac{k_t}{k_i}\right)$, where k_i and k_t are the wave numbers of the incident and transmitted regions. However, unlike a wave vector surface of an isotropic medium, the magnitude of the wave vector in an anisotropic medium varies along different propagation

directions. Thus, it is important to get the magnitudes of the wave vectors for both two types of waves along the direction at which the total reflection occurs, denoted as k_I and k_{II} .

Assuming total reflection occurs for a wave incident from an angle of $\theta_{in}, \varphi_{in}$, it leads to the transmitted wave of the specific type propagating along $\theta_t = 90^\circ, \varphi_t = \varphi_{in}$. Then the angle ψ between the propagation direction of the transmitted wave and the direction of the biasing magnetic field (θ_B, φ_B) of the gyroelectric medium can be calculated by

$$\cos^2 \psi = \sin^2 \theta_B \cos^2(\varphi_{in} - \varphi_B) \quad (4.4-6)$$

The wave numbers k_I, k_{II} can be expressed in terms of the permittivity of the medium and angle ψ and have been derived as follows.

$$\frac{k_I^2}{k_0^2} = \frac{(\varepsilon_\perp - \varepsilon_g^2) \sin^2 \psi + \varepsilon_\perp \varepsilon_{//} (1 + \cos^2 \psi)}{2(\varepsilon_\perp \sin^2 \psi + \varepsilon_{//} \cos^2 \psi)} + \frac{\sqrt{(\varepsilon_\perp - \varepsilon_g^2 - \varepsilon_\perp \varepsilon_{//}) \sin^4 \psi + 4\varepsilon_g^2 \varepsilon_{//}^2 \cos^2 \psi}}{2(\varepsilon_\perp \sin^2 \psi + \varepsilon_{//} \cos^2 \psi)} \quad (4.4-7)$$

$$\frac{k_{II}^2}{k_0^2} = \frac{(\varepsilon_\perp - \varepsilon_g^2) \sin^2 \psi + \varepsilon_\perp \varepsilon_{//} (1 + \cos^2 \psi)}{2(\varepsilon_\perp \sin^2 \psi + \varepsilon_{//} \cos^2 \psi)} - \frac{\sqrt{(\varepsilon_\perp - \varepsilon_g^2 - \varepsilon_\perp \varepsilon_{//}) \sin^4 \psi + 4\varepsilon_g^2 \varepsilon_{//}^2 \cos^2 \psi}}{2(\varepsilon_\perp \sin^2 \psi + \varepsilon_{//} \cos^2 \psi)} \quad (4.4-8)$$

The typical equations $\theta_{cI} = \sin^{-1} \left(\frac{k_I}{k_i} \right), \theta_{cII} = \sin^{-1} \left(\frac{k_{II}}{k_i} \right)$ can be used to calculate the critical angles for Type I and Type II waves in a gyroelectric medium. It is noted here that the above critical angles are derived based on the assumption that both Type I and Type II waves can exist in a gyroelectric medium. Actually it is known that since a gyroelectric medium is dispersive, one type of wave or both types of waves may not exist in the gyroelectric medium depending on the frequency of the incident wave. Eq. (4.4-4) indicates that the radiated field is closely related with the reflection coefficients $R_{\nu}(-\theta_{obs}, \varphi_{obs})$ and $R_{\nu'}(-\theta_{obs}, \varphi_{obs})$, which are the

co-polarized and cross-polarized reflection coefficients when the incidence angles are $-\theta_{obs}$ and φ_{obs} . Thus, the magnitude and phase of the reflection coefficients of $R_{vv}(-\theta_{obs}, \varphi_{obs} = 0)$ and $R_{hv}(-\theta_{obs}, \varphi_{obs} = 0)$ are plotted with respect to different incidence angles in Fig. 4-18. The relative permittivity of the gyroelectric medium is given by Eq. (4.4-5), with

$$\omega = 1.01\omega_1, \quad \omega_1 = \frac{\omega_b}{2} + \sqrt{\frac{\omega_b^2}{4} + \omega_p^2}, \quad \text{and the biasing magnetic field along } z\text{-direction } \theta_B = 0^\circ.$$

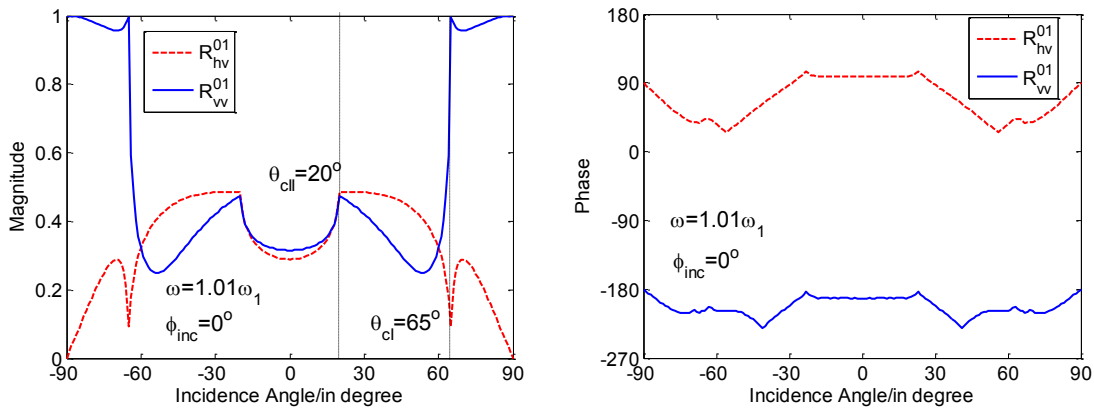


Fig. 4-18: Magnitude and phase of reflection coefficients R_{vv}^{01} , R_{hv}^{01} vs. different incidence angles for an incidence plane of $\varphi = 0^\circ$.

It is observed from Fig. 4-18 that $\theta_{cl} = 65^\circ$ and $\theta_{cl} = 20^\circ$ correspond to the critical angles of Type I and Type II characteristic waves, respectively. It is known that for transverse waves with the propagation direction perpendicular to the biasing magnetic field, the Type I wave corresponds to an ordinary characteristic wave with a linear polarization, while Type II wave is an extraordinary wave with an elliptical polarization. This is consistent with the phenomenon that only co-polarized reflection coefficient exists at 65° with the cross-polarized reflection coefficient to be 0, while at 20° both co-polarized and cross-polarized reflection coefficients exist with the phase difference of 90° . As expected, a linearly polarized radiated field is

observed at 65° and an elliptically polarized wave (circular polarization is possible depending on the property of the medium) is observed at 20° .

In addition, since the biasing magnetic field is along the z-direction, all of the co-polarized and cross-polarized reflection coefficients are independent of φ_{obs} and symmetric with respect to θ_{obs} as shown in Fig. 4-18. Thus, the normalized field pattern for a z-directed dipole located at the interface is also independent of the angle φ and symmetric with respect to the z-axis.

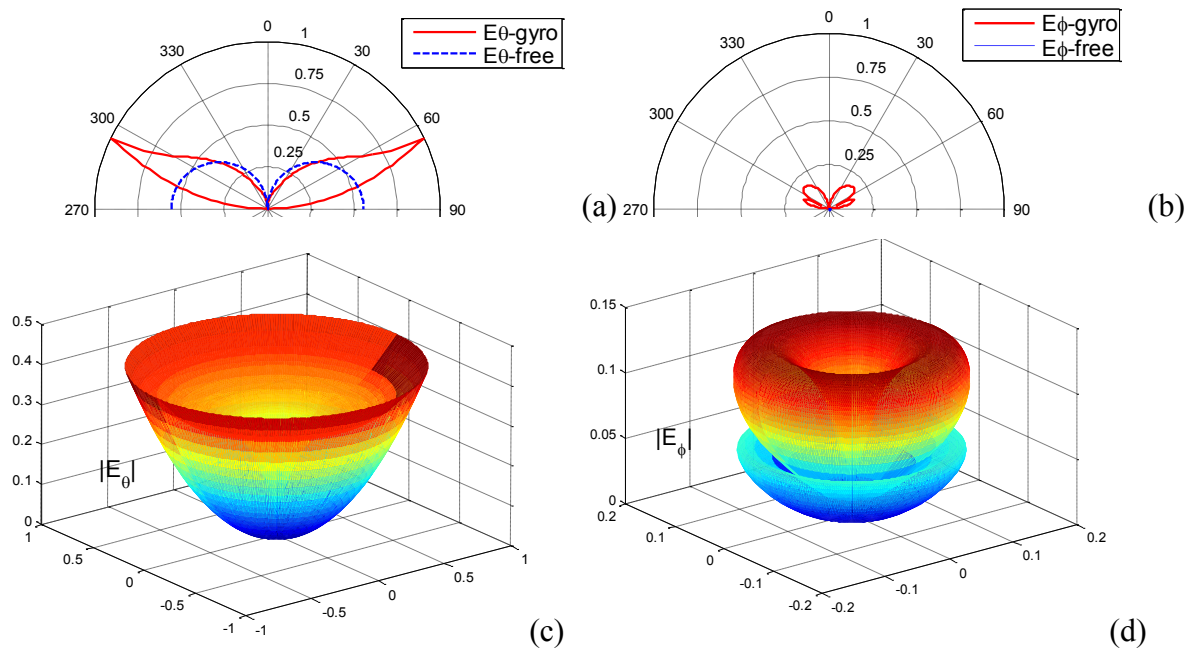


Fig. 4-19: (a) E_θ and (b) $|E_\phi|$ vs. θ in the plane of $\varphi=0^\circ$ for a z-directed Hertzian dipole located in region 0 with $h_t=0$ away from the interface of free space and gyroelectric medium with the direction of biasing magnetic field along $\theta_B=0^\circ$. $\omega_p = 2\pi 10^9$, $\omega_b = 1.9\omega_p$, $\omega = 1.01\omega_1$,

$$\omega_1 = \frac{\omega_b}{2} + \sqrt{\frac{\omega_b^2}{4} + \omega_p^2}.$$

Renormalizing the field components of the radiated field of the Hertzian dipole for both half-space and free-space to the same maximum value of $\max(|E_\theta|)_{half-gyro}$, the 2D patterns of

$|E_\theta|$ and $|E_\phi|$ of $\varphi = 0^\circ$ are shown in Fig. 4-19(a) and (b), while the 3D patterns are shown in Fig. 4-19(c) and (d). It is seen from Fig. 4-19(a) that the co-polarized field pattern is not symmetric and more directive compared to the radiation of the dipole in free space. Also, the cross-polarized pattern occurs as shown in Fig. 4-19(b). The co-polarized field pattern $|E_\theta|$ has a maximum radiation angle around $\theta = 65^\circ$, which corresponds to the total internal reflection angle for the Type I wave. This can be verified with the magnitude of the reflection coefficient $R_{\nu\nu}^{01}$ as shown in Fig. 4-18(a). Meanwhile, the cross-polarized field pattern $|E_\phi|$ has a null around $\theta = 65^\circ$, which corresponds to the minimum of the magnitude of the reflection coefficients of $R_{\nu\nu}^{01}$ as displayed in Fig. 4-18(a).

Consider a z-oriented dipole placed at the interface of the isotropic and gyroelectric media with the biasing magnetic field along the y-direction of $\theta_B = 90^\circ, \varphi_B = 90^\circ$. The radiated field patterns for the XZ plane ($\varphi = 0^\circ$) and YZ plane ($\varphi = 90^\circ$) are plotted in Fig. 4-20 and Fig. 4-21, respectively.

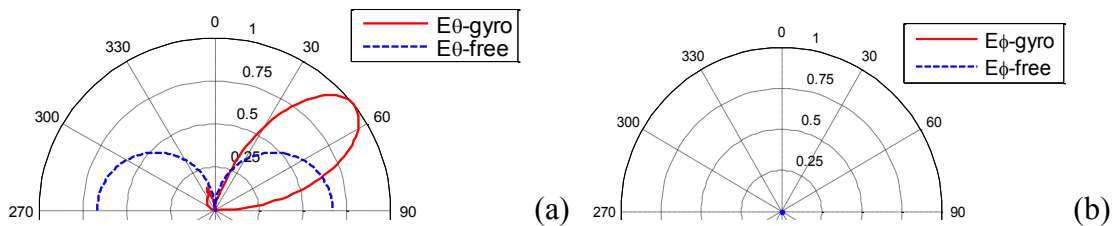


Fig. 4-20: (a) $|E_\theta|$ and (b) $|E_\phi|$ vs. θ in the plane of $\varphi = 0^\circ$ for a z-directed Hertzian dipole located in Region 0 with $h_d = 0$ away from the interface of free space and a gyroelectric medium with $\omega = 1.01\omega_1$ and the biasing magnetic field along $\theta_B = 90^\circ, \varphi_B = 90^\circ$.

Fig. 4-20(a) presents the co-polarized radiation pattern of $|E_\theta|$, and Fig. 4-20(b) displays the cross-polarized radiation pattern of $|E_\phi|$. It is seen in Fig. 4-20(a) that when the biasing

magnetic field is along the y-direction, the maxim radiation occurs at around the angle of $\theta = 52^\circ$, $\varphi = 0^\circ$. Also, it shows that the co-polarized radiation pattern $|E_\theta|$ is no longer symmetric with respect to z-axis in the XZ plane. As expected, for the observation plane of the XZ plane, which is perpendicular to the biasing magnetic field, no-cross polarized field exists, which is obvious in Fig. 4-20(b).

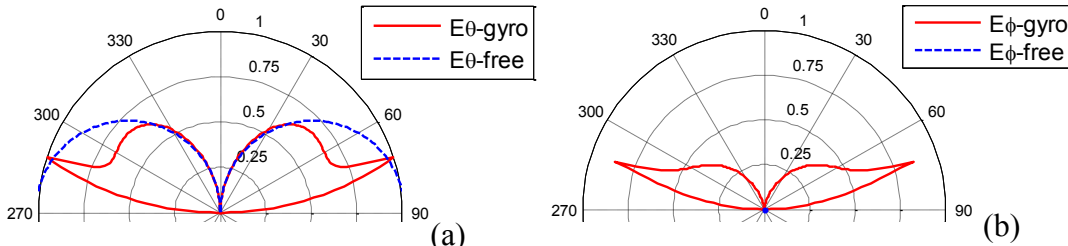


Fig. 4-21: (a) $|E_\theta|$ and (b) $|E_\phi|$ vs. θ in the plane of $\varphi = 90^\circ$ for a z-directed Hertzian dipole in Region 0 with $h_d = 0$ away from the interface of half-space gyroelectric medium with the biasing magnetic field along $\theta_B = 90^\circ$, $\varphi_B = 90^\circ$.

However, as shown in Fig. 4-21(a) and (b), both the co-polarized and cross-polarized patterns are symmetric with respect to the z-axis in the YZ plane. This is because when the observation plane is parallel to the direction of the biasing magnetic field, the reflection coefficients satisfy the symmetric condition, which leads to symmetric radiation patterns. Also, it is observed in Fig. 4-21(b) that the maximum cross-polarized field is in the same order as the co-polarized field. The maximum radiation along the peak directions in both patterns are due to the total internal reflections of the Type I and Type II waves of a gyroelectric medium.

4.4.2 The Two-Layer Problem with a Source above the Anisotropic Region

In reality, radiation of a dipole with a grounded substrate is a more practical problem. Thus, the radiation of a Hertzian dipole located over the grounded gyroelectric slab is discussed in this section. It is known from the image theory that the radiated field of a horizontal dipole

over a ground plane significantly reduces with the decrease of the distance between the dipole and the ground plane. For a horizontal dipole over a ground plane to radiate effectively, a minimum distance of quarter wavelength away from the ground is needed. In this case, the radiated field along the broadside direction will be double the field of dipole in free space.

Here we wish to show that even with an ultra thin grounded gyroelectric slab, enhanced radiation for a horizontal dipole over the slab is still possible. The following assumptions are made for the analysis. The direction of the biasing magnetic field is along the z-direction with $\theta_B = 0^\circ$ and the dipole is located at the interface of $h_d = 0$. The operating frequency range of the gyroelectric medium is changed by varying the plasma frequency while keeping the frequency of the dipole as $\omega = 2\pi \cdot 10^9$ and the ratio of gyrofrequency to the plasma frequency as a constant of $\omega_b = 0.5\omega_p$.

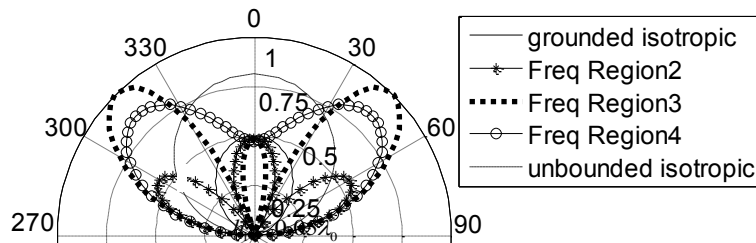


Fig. 4-22: Normalized radiated field E_θ for an x-directed dipole located at the interface of the grounded gyroelectric slab and air in the xz-plane for different frequency regions of the gyroelectric medium.

With the choice of the plasma frequency as the middle frequency point of each existing frequency region as shown in Table 4-1, the normalized co-polarized radiation patterns of a horizontal Hertzian dipole over a grounded gyroelectric slab with thickness of $0.05\lambda_0$ are plotted in Fig. 4-22 for the plane of $\varphi = 0^\circ$. Usually there exist 8 different frequency regions. However,

for a gyroelectric medium with the choice of $\omega = 2\pi 10^9$, $\omega_b = 0.5\omega_p$ here, Region 6 and Region 7 don't exist. Also, no enhanced radiation is observed for the radiation patterns in Region 1, 5 and 8, thus the radiation patterns in these regions are not considered.

It is seen from Fig. 4-22 that when an x-directed dipole is placed $0.05\lambda_0$ away from the ground, the maximum magnitude of the radiated field along the broadside direction (solid line) is less than two thirds of the magnitude of the radiation for a Hertzian dipole in free space (dash line). However, enhanced radiation is still obtained using the gyroelectric slab when it is operated in frequency Region 3 (dotted line). Compared with the radiation of a Hertzian dipole over the ground plane in the absence of the slab (grounded isotropic case), the maximum radiation power is increased by two times (which is around 6dB) and the maximum radiation is around 45° .

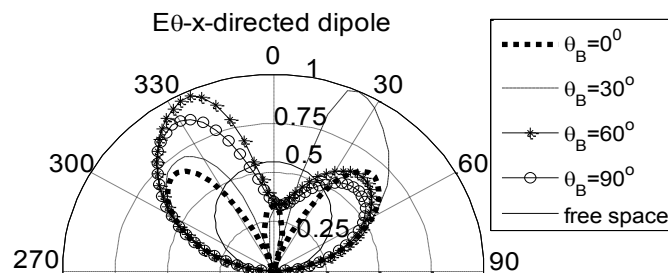


Fig. 4-23: Normalized radiated field patterns E_θ for an x-directed dipole located at an air-gyroelectric medium interface of a grounded slab as a function of different biasing magnetic field directions.

In addition to changing the operating frequency region, additional freedom of tuning the biasing magnetic field for the gyroelectric medium helps to tune the direction of the maximum radiation. Parametric analysis of the effect of the biasing magnetic field for the radiation of an x-directed dipole over the grounded gyroelectric slab operating in frequency Region 3 with

thickness of $h_1 = 0.05\lambda_0$ is shown in Fig. 4-23. It is seen that the direction and the magnitude of the maximum radiation are dependent on the choice of the direction of the biasing magnetic field. About a 2 times (6dB) increase in maximum radiation power relative to the radiation of a dipole in free space is obtained along 20° when $\theta_B = 60^\circ$. It is expected that maximum radiation along the broadside direction is potentially achievable with proper tuning of the direction of the biasing magnetic field. It has been shown in this section that a horizontal dipole placed over an ultrathin gyroelectric slab of $0.05\lambda_0$ can still radiate effectively with the maximum radiation around two times (6dB) higher than the radiation of a dipole in free space. In the next section, focus will be on the radiation of the dipole embedded inside the grounded gyroelectric slab.

4.4.3 The Two-Layer Problem with a Source Embedded in the Anisotropic Region

It has been shown in [73-75] that the enhanced radiated field along the broadside direction can be realized by placing a horizontal dipole inside a grounded isotropic plasma slab with permittivity very close to zero. In the previous work [73-75], the analysis of the directive radiation is considered for a grounded metamaterial slab based on the isotropic dispersive model. Here, the anisotropic effect to the radiation of a Hertzian dipole introduced by applying the biasing magnetic field is considered. It is shown that utilizing the anisotropic effect, the broadside radiation can be obtained for a vertical dipole that is oriented perpendicular to the interface. In addition, it is demonstrated that applying the biasing magnetic field helps to reduce the required thickness of the isotropic plasma slab for the enhanced broadside radiation.

This section is organized as follows. First, the radiation features for a horizontal dipole inside a grounded isotropic slab are studied and compared with the results available in [75]. Then the isotropic slab is extended to an anisotropic slab, and the effect of the anisotropy to the

radiation pattern of the dipole is studied. Finally, the radiation of a vertical dipole inside an anisotropic slab is studied.

4.4.3.1 Radiation of a Horizontal Dipole inside a Grounded Isotropic Plasma Slab

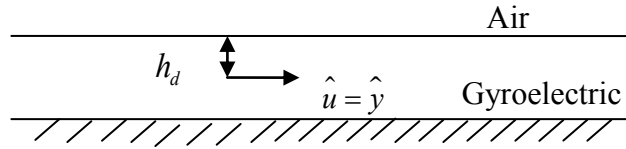


Fig. 4-24: Geometry of a horizontal dipole located inside a grounded gyroelectric slab with a distance h_d away from the air-slab interface.

The geometry of interest is shown in Fig. 4-24. A horizontal dipole is located at the middle of a grounded gyroelectric slab with the orientation of the dipole designated as \hat{u} . The dipole is h_d away from the air-slab interface, and the direction of the biasing magnetic field for the gyroelectric substrate is designated with $\hat{\theta}_B$ and $\hat{\varphi}_B$. The permittivity of the gyroelectric medium with an arbitrarily biasing magnetic field is provided in Eq. (2.3-4). In the absence of the biasing magnetic field, which is equivalent to the choice for the gyrofrequency of $\omega_b = 0$, the gyroelectric medium reduces to an isotropic medium. Setting the plasma frequency being 1 GHz and the operating frequency of the source being 1.1 GHz as shown in Eq. (4.4-9), the dielectric constant of the gyroelectric medium is given in Eq. (4.4-10).

$$\omega_p = 2\pi 10^9 \text{ rad / s}, \quad \omega = 1.1\omega_p = 2.2\pi 10^9 \text{ rad / s} \quad (4.4-9)$$

$$\left(1 - \frac{\omega_p^2}{\omega^2}\right) = \begin{bmatrix} 0.1736 & 0 & 0 \\ 0 & 0.1736 & 0 \\ 0 & 0 & 0.1736 \end{bmatrix} \quad (4.4-10)$$

The first case considered here is where a horizontal dipole oriented along the y-direction ($\hat{u} = \hat{y}$) is embedded at the center of the slab. According to Baccarelliet et al. [73], there exists an optimized frequency to obtain the maximum broadside radiation for a fixed thickness of the slab filled with the isotropic plasma. For the fixed frequency of the dipole, the broadside radiation varies periodically with the thickness of the slab. The observation distance is $r = 40\lambda_0$, where λ_0 is free space wavelength and defined as in Eq. (4.4-11).

$$\lambda_0 = \frac{c}{f}, \quad \lambda_\epsilon = \frac{c}{f} \left(1 - \frac{\omega_p^2}{\omega^2} \right)^{-1/2} = 654 \text{mm} \quad (4.4-11)$$

It is known that the two general characteristic waves inside the isotropic plasma are h -polarized and v -polarized. When the dipole is located inside the slab, the Type I wave is assigned as an h -polarized wave and the Type II wave is assigned as a v -polarized wave in the general expression of the radiated field. If the incidence plane is an XZ-plane ($\varphi = 0^\circ$) and the dipole is oriented along the y-direction, the general expression reduces to the following form.

$$\bar{E}_0(\bar{r}) = \frac{i\omega\mu_0 I e^{ik_0 r}}{4\pi r} \begin{pmatrix} \left[X_{e'_h} \hat{h}_0^+ + X_{e'_v} \hat{v}_0^+ \right] c_I^u(k_{zI}^u) \left(\hat{v}_I^u \right) e^{ik_{zI}^u h_d} \\ + \left[X_{e''_h} \hat{h}_0^+ + X_{e''_v} \hat{v}_0^+ \right] c_{II}^u(k_{zII}^u) \left(\hat{v}_{II}^u \right) e^{ik_{zII}^u h_d} \\ + \left[X_{e'_h} \hat{h}_0^+ + X_{e'_v} \hat{v}_0^+ \right] c_I^d(k_{zI}^d) \left(\hat{v}_I^d \right) e^{ik_{zI}^d h_d} \\ + \left[X_{e''_h} \hat{h}_0^+ + X_{e''_v} \hat{v}_0^+ \right] c_{II}^d(k_{zII}^d) \left(\hat{v}_{II}^d \right) e^{ik_{zII}^d h_d} \end{pmatrix} \cdot \hat{u} \quad (4.4-12)$$

where the coefficients are given in Eq. (4.4-13) and Eq. (4.4-14).

$$\begin{bmatrix} X_{e'_h} & X_{e''_h} \\ X_{e'_v} & X_{e''_v} \end{bmatrix} = \overset{=10}{X} \overset{=12}{(I - R} \overset{=10}{R)}^{-1}, \quad \begin{bmatrix} X_{e'_h} & X_{e''_h} \\ X_{e'_v} & X_{e''_v} \end{bmatrix} = \overset{=10}{X} \overset{=12}{(I - R} \overset{=10}{R)}^{-1} \overset{=12}{R} \quad (4.4-13)$$

For the special case of an isotropic medium, it is straightforward to derive that

$$c_I^u = c_I^d = c_{II}^u = c_{II}^d = \frac{k_{z0}}{k_{z1}}, k_{z1}^u = -k_{z1}^d = k_{z1} = \sqrt{k_0^2 \epsilon_{\parallel} - k_{\rho}^2} \quad (4.4-14)$$

Then, the radiated field in Region 0 can be expressed as

$$\bar{E}_0(\bar{r}) = \frac{i\omega\mu_0 I l e^{ik_0 r}}{4\pi r} \frac{k_{z0}}{k_{z1}} \left(X_{e_I^u h} e^{ik_{z1}^u h_d} + X_{e_I^d h} e^{ik_{z1}^d h_d} \right) \hat{h}_0^+ \quad (4.4-15)$$

For the field along the broadside direction ($k_{\rho} = 0$), $k_{z1}^u = -k_{z1}^d = k_0 \sqrt{\epsilon_{\parallel}}$ and the field can be written as

$$\bar{E}_0(\theta = 0^\circ) = \frac{i\omega\mu_0 I l e^{ik_0 r}}{4\pi r} 2e^{ik_0 \sqrt{\epsilon_{\parallel}} h_d} \left(\frac{1 - e^{-i2k_0 \sqrt{\epsilon_{\parallel}} h_d} e^{i2k_0 \sqrt{\epsilon_{\parallel}} d}}{1 + \sqrt{\epsilon_{\parallel}} + (\sqrt{\epsilon_{\parallel}} - 1)e^{i2k_0 \sqrt{\epsilon_{\parallel}} d}} \right) \hat{h}_0^+ \quad (4.4-16)$$

It is easy to see that if $h_d = d/2$, corresponding to the case of the dipole located in the middle of the slab, the period of $\bar{E}_0(\theta = 0^\circ)$ as function of the slab thickness is λ_{ϵ} , as shown in Eq. (4.4-11). The radiation power density along the broadside direction for different slab thicknesses is shown in Fig. 4-25 with a solid line.

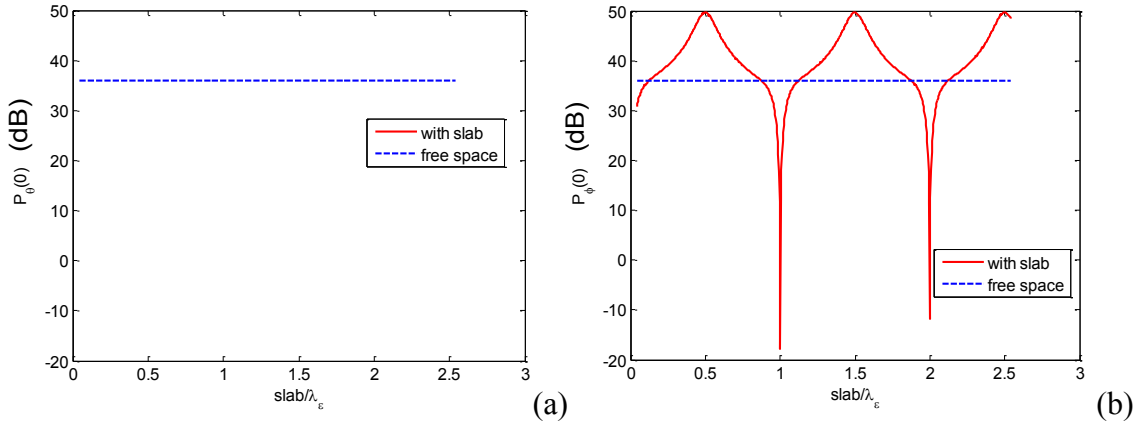


Fig. 4-25: Power density (dB) of (a) θ component and (b) ϕ component as a function of the slab thickness.

It is noted here that to plot Fig. 4-25, the dipole is always placed in the middle of the grounded slab ($h_d = d/2$) for different slab thickness and the permittivity of the slab is characterized by Eq. (4.4-10). It is seen that for an isotropic plasma slab no cross-polarized radiated field E_θ exists. As shown in Fig. 4-25, the power density along the broadside direction for the dipole inside the slab has been increased by 14dB compared with the radiation of a Hertzian dipole in free space (dotted line in Fig. 4-25). It can also be observed that $P_\phi(0)$ is a strictly periodic function of the slab thickness and shows maxima when the thickness of the slab is an odd integer multiple of $\lambda_\epsilon/2$. This result is consistent with the result obtained in [73].

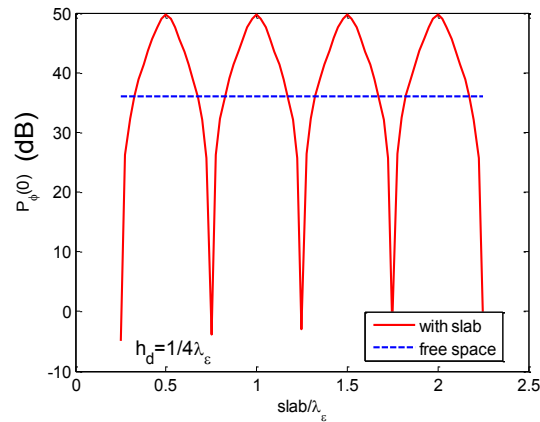


Fig. 4-26: Power density (dB) of ϕ component as a function of the slab thickness. $h_d = 0.25\lambda_\epsilon$ and $f = 1.1f_p$.

If $h_d = \lambda_\epsilon/4$, then it is easy to derive from Eq. (4.4-16) that the period of $\bar{E}_0(\theta = 0^\circ)$ as a function of the slab thickness is $\lambda_\epsilon/2$. This is verified by plotting the radiation power density along the broadside direction versus the thickness of the slab with $h_d = 0.25\lambda_\epsilon$ in Fig. 4-26. It is observed that the maximum broadside radiation occurs when the thickness of the slab is an integer multiple of $\lambda_\epsilon/2$. The maximum radiation has been increased by 14dB compared to the

radiation of a Hertzian dipole in free space, which is the same as the case of the dipole located in the middle of the slab.

Inspection of Fig. 4-25 and Fig. 4-26 shows that the location of the Hertzian dipole will not change the directivity of the dipole when it is embedded inside the slab. However, the period of the slab thickness for the maximum radiation along the broadside direction is affected by the location of the Hertzian dipole. This is due to the different phase advance introduced by the dipole location. This result obtained above is consistent with the conclusion in [73]. It should be noted here that in [73] only the line source is considered.

In the next section, the anisotropic effects introduced by the biasing magnetic field for the radiation of horizontal and vertical dipoles are studied. It will be shown that with the proper choice of the gyrofrequency and the thickness of the grounded gyroelectric slab, directive emission along the broadside direction is achievable.

4.4.3.2 *Radiation of a Horizontal Dipole inside the Grounded Gyroelectric Slab*

In this section, the anisotropic effect introduced due to the biasing magnetic field is studied for the radiation patterns of a horizontal dipole. The analysis starts with the minor anisotropic effect by setting $\omega_b = 0.001\omega_p$. Then, the off-diagonal elements are introduced into the permittivity matrix of the gyroelectric medium as follows.

$$\overset{=}{\varepsilon}_p = \begin{bmatrix} 0.1736 & 0.0008i & 0 \\ -0.0008i & 0.1736 & 0 \\ 0 & 0 & 0.1736 \end{bmatrix} \quad (4.4-17)$$

It is noted here that due to the choice of extremely small $\omega_b = 0.001\omega_p$, all the diagonal elements of the permittivity matrix appear to be same. The power density radiated by the unit current moment Hertzian dipole placed in a grounded slab is plotted in Fig. 4-27.

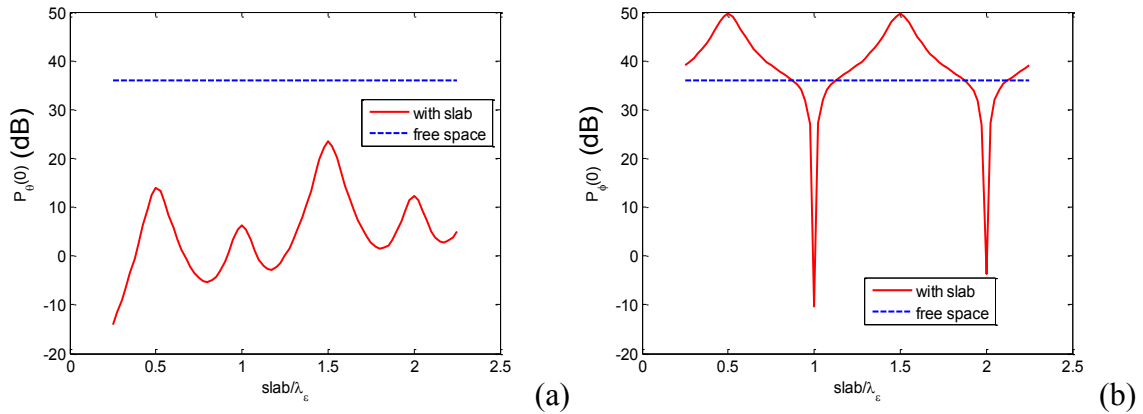


Fig. 4-27: Power density of (a) θ component and (b) ϕ component radiated in broadside direction by a unit current moment y -directed Hertzian dipole placed at the center of a grounded gyroelectric slab as a function of the slab thickness with $\omega_b = 0.001\omega_p$, $f = 1.1f_p$.

It can be observed from Fig. 4-27 that due to the off-diagonal element, the significant cross-polarized radiated component $P_{\phi}(\theta = 0^\circ)$ has been introduced and has maxima every $\lambda_c/2$ in a periodic way versus the thickness of the slab. On the other hand, $P_{\theta}(\theta = 0^\circ)$ is not much affected and still behaves in the same way as the radiation of the horizontal dipole in the grounded isotropic plasma slab.

If the gyrofrequency ω_b is further increased, then the negative elements will be introduced into the diagonal elements of the permittivity matrix. Letting $\omega_b = \omega_p$, $f = 1.1f_p$, the permittivity matrix of the gyroelectric medium is given by

$$\underline{\underline{\varepsilon}}_p = \begin{bmatrix} -3.7619 & 4.3290i & 0 \\ -4.3290i & -3.7619 & 0 \\ 0 & 0 & 0.1736 \end{bmatrix} \quad (4.4-18)$$

The radiation power densities of both θ and φ components along the broadsided direction for the horizontal dipole in the middle of the grounded slab with $\underline{\underline{\varepsilon}}_p$ shown in Eq. (4.4-18) are plotted in Fig. 4-28.

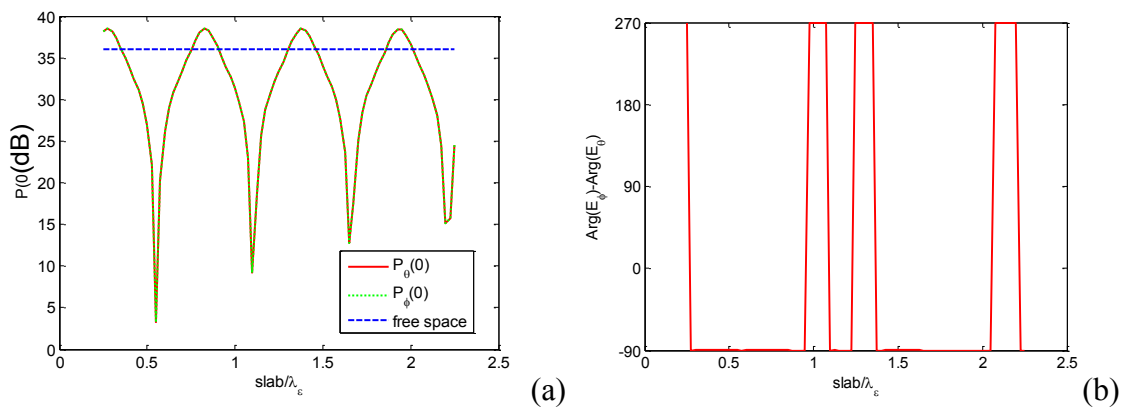


Fig. 4-28: (a) Power density and (b) phase difference of $P_\theta(0)$ and $P_\phi(0)$ for a unit current moment y-directed Hertzian dipole placed in the middle of a grounded gyroelectric slab as a function of the slab thickness with $\omega_b = \omega_p$, $f = 1.1f_p$.

It is observed that the amplitudes of θ and φ components are equal and overlay each other and their phase difference is 270 degrees. Thus, the radiated field along the broadside direction is now a circular polarized wave for the special case of $\omega_b = \omega_p$. Also, it is seen in Fig. 4-28 that the first maximum radiation along the broadside direction occurs when the slab thickness is $0.275\lambda_e$ and maxima repeat when the thickness is increased by every $0.55\lambda_e$. This thickness is only half of the optimum thickness to achieve the maximum radiation when the dipole is placed inside an isotropic plasma slab. Compared to the maximum radiation of power density of the

Hertzian dipole in free space, shown as the straight line in Fig. 4-28(a), the radiation of the Hertzian dipole inside the slab has been increased by 2.5dB for both the θ and φ components.

It has been observed from Fig. 4-25 and Fig. 4-26 that in order to achieve a high directivity along the broadside direction for a horizontal dipole inside the grounded isotropic plasma slab, the thickness of the slab is usually in the order of free space wavelength at the operating frequency. Considering the case of the isotropic plasma slab with $f_p = 10^9 \text{ Hz}$, $f = 1.1f_p$, the optimum thickness for the slab to achieve the maximum radiation along the broadside direction is

$$0.5\lambda_\epsilon = 0.5 \frac{c}{f} \left(1 - \frac{\omega_p^2}{\omega^2} \right)^{-1/2} = 327 \text{ mm} = 1.2\lambda_0 \quad (4.4-19)$$

To reveal the negative impact of the thinner isotropic slab, the radiated fields E_φ versus angles in XZ plane are shown Fig. 4-29 for a y-directed dipole inside such a grounded isotropic plasma slab with different thicknesses of $0.05\lambda_0$, $0.5\lambda_0$ and $1.2\lambda_0$. It is seen that when the thickness of the isotropic plasma slab is reduced from the optimum thickness of $1.2\lambda_0$ to $0.5\lambda_0$, the maximum radiation direction maintains around the broadside direction. However, the amplitude of the maximum radiation is decreased. When the thickness of the isotropic plasma slab is reduced to $0.05\lambda_0$, the radiation power decreases continuously across the whole angular range. Along the broadside direction, the radiation power is 15dB lower than the radiation power of a Hertzian dipole in free space. Only the φ component of the radiated field contributes to the total radiated power since the horizontal dipole is oriented along the y-direction which is perpendicular to the observation plane.

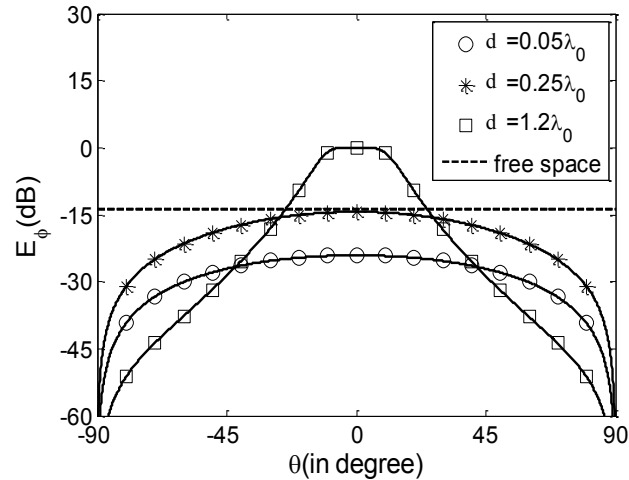


Fig. 4-29: Normalized radiated field for a y-directed dipole located in the middle of the isotropic plasma slab in the XZ-plane as a function of observation angle which is measured from the z-axis.

If the anisotropic gyroelectric slab with $\omega_b = \omega_p$ is used instead of an isotropic slab, a similar kind of behavior can be observed, as shown in Fig. 4-30. The radiation power densities $P_\theta(0)$ and $P_\phi(0)$ for a gyroelectric slab of thicknesses $1.2\lambda_0$, $0.5\lambda_0$, and $0.05\lambda_0$ are shown in Fig. 4-30(a), (b) and (c). The radiation power density of the dipole in the free space is given with a black dotted line in each figure. As shown in Fig. 4-30(a), in addition to the enhanced radiation along the broadside direction, extra three peaks of radiation occur at the angles of 58° , 70° , and 80° . The same phenomenon can be observed for the slab thickness of $0.5\lambda_0$, as shown in Fig. 4-30(b). However, when the thickness of the slab is reduced to $0.05\lambda_0$, no such strong radiation peaks occur any more as shown in Fig. 4-30(c). Actually, when the thickness of the slab reduces to $0.05\lambda_0$, the horizontal dipole can no longer radiates effectively since the image current of the horizontal dipole over PEC cancels out each other. For all the observation angles in the XZ plane, the radiation power of a Hertzian dipole in such a slab has always been lower than the

Hertzian dipole in free space. However, it is a different case if the dipole is vertically oriented (z-oriented). Detailed discussion is given in the next section.

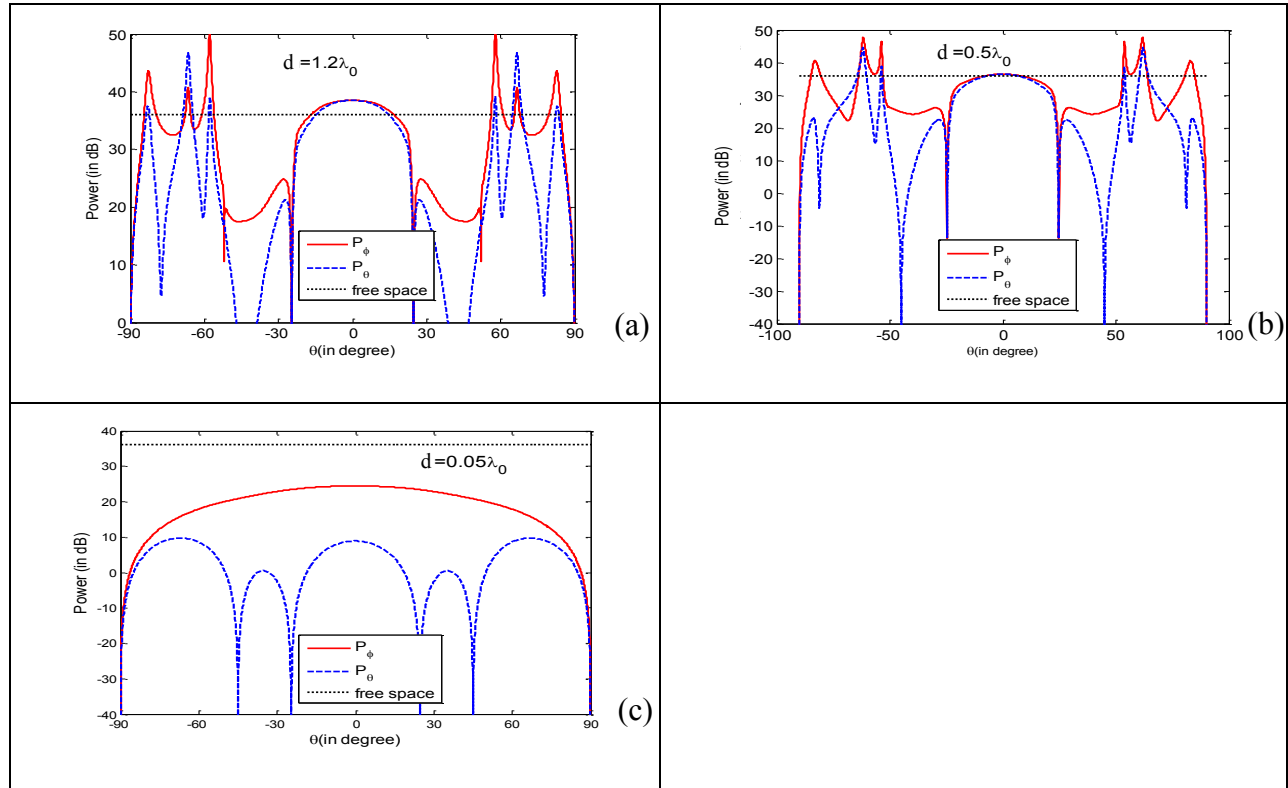


Fig. 4-30: Radiation patterns for a y-oriented dipole located in the middle of the anisotropic gyroelectric slab vs. different slab thicknesses.

4.4.3.3 Radiation of a Vertical Dipole inside the Grounded Gyroelectric Slab

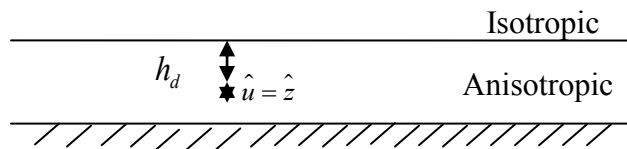


Fig. 4-31: Geometry of a vertical dipole located inside the grounded anisotropic slab with a distance of h_d away from the air-slab interface.

If the dipole inside the slab is oriented to be perpendicular to the interface of the slab as shown in Fig. 4-31, then the thickness of the slab can be chosen very thin and very high directivity can still be achieved along the broadside direction. The parametric study of the effects of frequency, biasing magnetic field direction and the slab thickness is presented in this section to show how the directive radiation along the broadside direction will be achieved with a vertical dipole inside a grounded gyroelectric slab.

A. Effect of Frequency

Assuming the gyro-frequency $\omega_b = 0.8\omega_p$, the effect of the frequency to the radiation features of a vertical dipole inside the gyroelectric slab is first studied. Normalized field patterns $|E_\theta|$ of a vertical dipole inside the grounded gyroelectric slab with different frequencies of $0.9f_p$, $0.95f_p$, $1.05f_p$, and $1.1f_p$ are plotted with a solid line, dashed line, dotted line, and a dash-dot mixed line in Fig. 4-32.

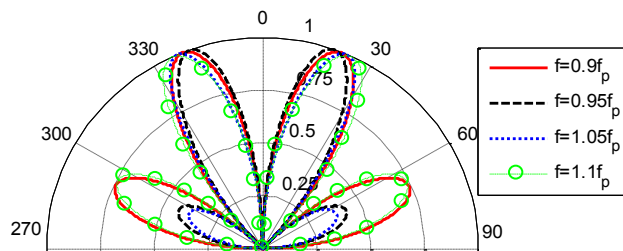


Fig. 4-32: Normalized field pattern of $|E_\theta|$ vs. θ in the plane of $\varphi = 0^\circ$ with vertical dipole located in the middle of the grounded gyroelectric slab of thickness of $0.05\lambda_0$.

It can be seen from the normalized field patterns of $|E_\theta|$ that the beam is symmetric with respect to the z-axis, and the maximum radiation occurs at around 20° for all four cases.

However, the radiations along 70° for the frequencies of $0.95f_p$ and $1.05f_p$ are much smaller than the radiation for the frequencies of $0.9f_p$ and $1.1f_p$.

To gain better understanding of the effect of the frequency of the excitation, the maximum radiation direction and the directivity with respect to the radiation of the dipole in free space vs. the excitation frequency of the source are shown in Fig. 4-33(a) and (b), respectively.

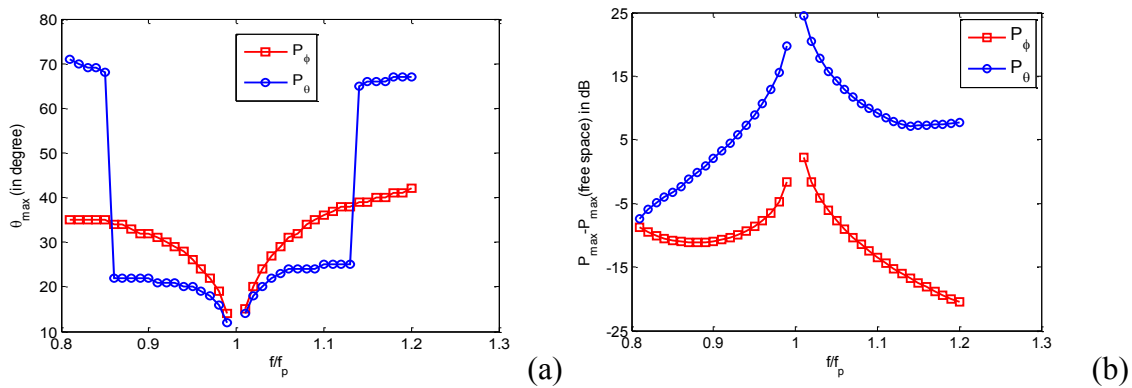


Fig. 4-33: (a) The angle of the maximum radiation of the vertical dipole inside the grounded gyroelectric slab vs. different frequencies. (b) The difference of the radiated power along the maximum radiation direction of the Hertzian dipole inside the slab and in free space vs. different frequencies.

As shown in Fig. 4-33(a), the maximum radiation direction is around 20° when $f = 0.9f_p$ and decreases to around 10° when the frequency increases to the plasma frequency of f_p . It is noted here that the maximum radiation direction of 10° varies with the change of the biasing magnetic field. It is seen in Fig. 4-33(b) that only when the frequency is above $0.9f_p$ the maximum radiation power of the Hertzian dipole inside the slab is stronger than that of the dipole in free space.

Also, the maximum radiation power of both θ and φ components in the XZ observation plane increases when the frequency of the Hertzian dipole approaches the plasma frequency. When the excitation frequency of the vertical Hertzian dipole decreases or increases from the plasma frequency, the difference between the maximum radiation power due to θ and φ components decreases as shown in Fig. 4-33(b). When the frequency reduces to the gyro-frequency $\omega = \omega_b = 0.8\omega_p$, the maximum radiation power for θ and φ components are the same though the maximum radiation of θ component occurs at around 75° and the maximum radiation power of φ component occurs at around 35° as shown in Fig. 4-33(a). For now, only the radiation of a vertical Hertzian dipole inside a grounded gyroelectric slab with a z-oriented biasing magnetic field is considered. The effect of different directions of the biasing magnetic field is presented in the following discussion.

B. Effect of Biasing Magnetic Field Direction

Normalized field patterns for the different biasing magnetic directions are shown in Fig. 4-34. When the biasing magnetic field is along the x-axis (e.g., $\theta_B = 90^\circ$, $\varphi_B = 0^\circ$), which is parallel to the XZ plane, the normalized field pattern $|E_\theta|$ is symmetric with respect to the z-axis. When the biasing magnetic field is perpendicular to the observation plane (e.g., $\theta_B = 90^\circ$, $\varphi_B = 90^\circ$), only the co-polarized field component $|E_\theta|$ exists and the cross-polarized field component $|E_\varphi|$ does not exist, because the two types of characteristic waves of the gyroelectric medium are decoupled, one of the waves corresponding to the h -polarized wave in free space, and the other wave corresponding to the v -polarized wave in free space. It is noted

here that in Fig. 4-34, all the field patterns are normalized to the maximum value of both $|E_\theta|$ and $|E_\phi|$.

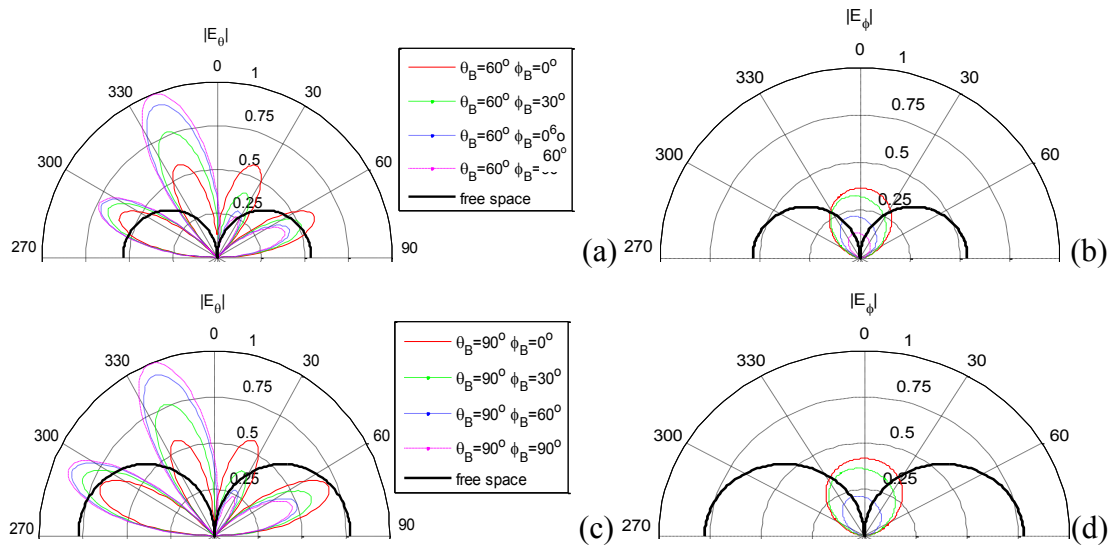


Fig. 4-34: Normalized field pattern of $|E_\theta|$ and $|E_\phi|$ (xz plane) for a vertical dipole located in the middle of a grounded gyroelectric slab of thickness $0.05\lambda_0$ (free space wavelength) with different direction of the biasing magnetic field. $\omega_p = 2\pi 10^9$, $\omega_b = 0.8\omega_p$, $\omega = 1.1\omega_p$.

C. Effect of Slab Thickness

Assuming the biasing magnetic field is along the y-axis (perpendicular to the incidence plane), the radiation patterns of a vertical dipole in the presence of the gyroelectric slab with different thicknesses are shown in Fig. 4-35. It is known that since the biasing magnetic field is perpendicular to the observation plane (XZ plane), the cross-polarized field component does not exist ($|E_\phi| = 0$) for both the grounded gyroelectric slab and the grounded isotropic slab. Thus, only $|E_\theta|$ is displayed here. It is seen from Fig. 4-35(a) and (b) that a z-oriented dipole can radiate along the broadside direction if it is located inside a grounded gyroelectric slab instead of a grounded isotropic slab.

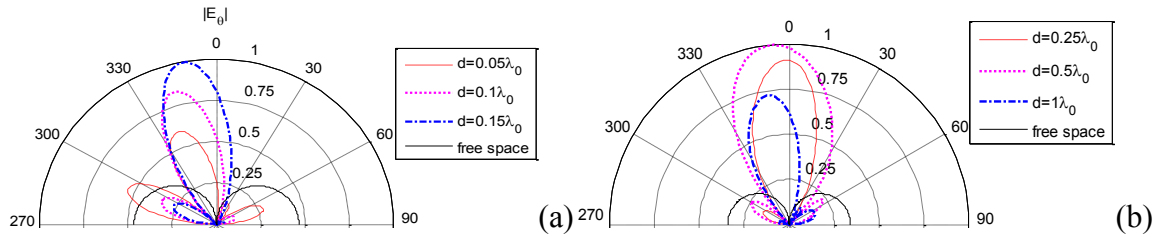


Fig. 4-35: Normalized field pattern of $|E_\theta|$ (XZ plane) for the vertical dipole located in the middle of the grounded gyroelectric slab with the biasing magnetic field perpendicular to the observation plane as a function of different thickness. $\omega_p = 2\pi 10^9$, $\omega_b = 0.8\omega_p$, $\omega = 1.1\omega_p$.

For the purpose of comparison, the normalized field patterns of $|E_\theta|$ (XZ plane) for a vertical dipole located in the middle of a grounded isotropic slab with different thicknesses are shown in Fig. 4-36.

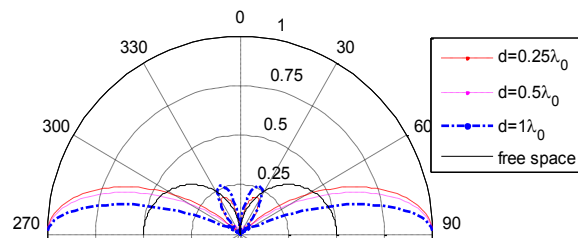


Fig. 4-36: Normalized field pattern of $|E_\theta|$ (XZ plane) for a vertical dipole located in the middle of a grounded isotropic slab of $\epsilon = 1$ vs. different slab thickness.

With the increase of the thickness of the slab, the direction of the maximum radiation shifts from 20° to the broadside direction, and the maximum radiation power also increases. The optimum height to radiate along the broadside direction is around one $0.25\lambda_0$, the radiated field along the broadside direction is now almost 8.5 dB higher than the radiation of the dipole in free space. This height is much less than the optimum height of $1.2\lambda_0$ for the enhanced radiation of a horizontal dipole inside a grounded isotropic slab with the same choice of the plasma frequency. When the thickness of the slab increases beyond one quarter of free space wavelength, the

maximum radiation direction again shifts away from the broadside direction. It is to be noted here that the vertical dipole can radiate effectively along the broadside direction only for the biasing magnetic field perpendicular to the slab. When the biasing magnetic field is along the z -axis, no broadside radiation occurs.

In this chapter, the radiated field of an arbitrarily oriented Hertzian dipole located either above or inside a layered anisotropic medium is obtained by applying the method of stationary phase to the corresponding E-DGFs. Numerical analysis for the radiation of an elementary dipole is presented for three different cases including the dipole located over a half-space gyroelectric medium, above a grounded layered gyroelectric slab, and immersed inside the slab.

The radiation for a vertical dipole on top of a half-space gyroelectric medium is first presented. Through the analysis of reflection coefficients as a function of incidence angle, it is revealed that the maximum radiation direction for a vertical dipole on top of a half-space gyroelectric medium is closely related to the critical angles of the characteristic waves of the gyroelectric medium. The radiation of a Hertzian dipole in the presence of a grounded gyroelectric slab is further analyzed. The analysis indicates that a grounded gyroelectric slab can be used to achieve the directive radiation using two different mechanisms. One is through the reflection by placing the dipole over the slab, and the other is through the transmission by placing the dipole inside the slab.

When a horizontal dipole is placed over a grounded gyroelectric slab, the parametric study of the effect of the frequency range and the biasing magnetic field of the gyroelectric medium indicates that the directive radiation is still achievable even for an ultra-thin slab. A maximum 6 dB (twice the radiated field of a dipole in free space) increase in the radiation is observed for a

dipole placed above the gyroelectric slab of $0.05\lambda_0$, when the direction of the biasing magnetic field is 60° and the frequency is operated in Frequency Region 3. The maximum radiation direction for the dipole over a gyroelectric slab can be further changed through the adjustment of the biasing magnetic field. Even higher radiation is possible by placing a Hertzian dipole inside a gyroelectric slab and changing its orientation from horizontal to vertical. In particular, almost 8.5 dB enhanced radiation along the broadside direction, compared to the radiation of the dipole in free space, is obtained with the proper adjustment of the thickness of the slab and the magnitude and direction of the biasing magnetic field. Without the biasing magnetic field, the gyroelectric medium reduces to isotropic plasma, and the optimum thickness required to achieve the directive emission along the broadside direction with a horizontal dipole inside the slab is significantly larger.

This analysis may lead to a method whereby the volume of the radiator can be reduced simply by changing the orientation of the magnetic field and using a z-directed radiator. This size reduction may make it possible to create a miniaturized antenna, which is the goal of most antenna manufacturers.

5 RADIATION OF A MICROSTRIP DIPOLE PRINTED ON AN ANISOTROPIC SUBSTRATE

Currently, there is an increasing interest in complete monolithic systems which combine antenna elements or antenna arrays on the same substrate as the integrated RF/IF front end network. One type of the most popular antenna elements is the printed antenna due to its characteristics of low-cost, low-profile, conformability, and ease of manufacturing. The literature survey from Chapter 1 shows that existing works mainly study printed antennas on an isotropic substrate [57-59, 63] or on a specific type of anisotropic substrates such as uniaxial medium [4], ferrite medium [8], and biaxial medium [37, 65].

To demonstrate the general feasibility and validity of the eigenvector dyadic Green's functions developed in previous chapters, we apply the developed E-DGFs with the method of moments (MOM) to solve a microstrip dipole printed on a general anisotropic substrate in this chapter. Particularly, previous literature indicates that there exist few results on the application of a gyroelectric medium to the printed antenna. To fill the gap, detailed analysis on the radiation behavior of a printed dipole on a gyroelectric substrate will be presented utilizing the methods developed in this chapter.

This chapter is organized as follows. First the formulation of the method of moment is presented. Since the DGF discussed in the previous chapter is obtained using the eigen-decomposition method, and it applies to the general anisotropic medium with no restrictions imposed on the property of the medium, the formulation of MOM is applicable to a printed dipole on a general anisotropic substrate. In the second section, the numerical results of a printed dipole over different grounded substrates are presented for the purpose of validation. The input

impedance, resonant length, and radiation patterns of a microstrip dipole over a grounded isotropic slab, a grounded biaxial slab, and a grounded ferrite slab are calculated and compared with the previous research. As will be made clear, the comparisons suggest that the current study is in agreement with previous research. In the third section, numerical results and discussions will be presented in detail to illustrate the effect of the magnitude and direction of the biasing magnetic field to the current distribution, input impedance, resonant length, and radiation pattern of a microstrip dipole on a gyroelectric substrate. It will be shown that tunable resonant length and radiation patterns of a printed dipole are achievable to a certain degree by changing the material properties through adjusting the biasing magnetic field of the gyroelectric medium.

5.1 Formulation of Method of Moment (MOM)

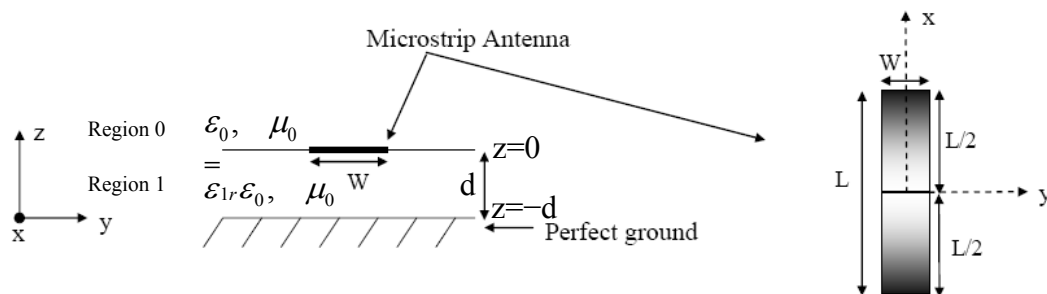


Fig. 5-1: Geometry of the microstrip dipole problem.

Geometry of a microstrip dipole is shown in Fig. 5-1. The dipole is printed at the interface of an isotropic medium and an anisotropic medium. It is assumed that the geometry extends laterally to infinite in both regions. The length of the dipole antenna is denoted as L , and the dipole is assumed to be oriented along the x -axis. The width of the antenna is W , and it is measured along the y -axis. Furthermore, it is also assumed that the width of the antenna is much

less than the wavelength. Hence, transverse currents are neglected, and current is assumed to flow only in the x-direction. Method of moment formulation for the microstrip dipole is presented in this section. The formulation presented in this section is similar to the approach in [59], which analyzed the radiation properties of the microstrip dipoles utilizing the Green's functions in the spectral form by the methods of moment.

5.1.1 Basis Function

If the width of the dipole is a small fraction of wavelength, the current distribution along the x-axis is assumed. It is also assumed that the current is separable in its x and y dependence.

$$J_n(x, y) = J_n(x)J_n(y), \quad n=x \text{ or } y \quad (5.1-1)$$

For a thin dipole, current is floating exclusively in the x-direction and dipole current is

$$J_x(x, y) = J_x(x)J_x(y) \quad (5.1-2)$$

To approximate arbitrary current distributions, subdomain basis functions instead of entire domain basis functions are used here as the current basis functions in the longitudinal direction. Particularly, triangular basis functions instead of sinusoidal expansion function [59] are used.

$$J_x(x) = \begin{cases} \frac{1}{a}(x - (x_p - a)), & (x_p - a) < x < x_p \\ \frac{1}{a}((x_p + a) - x), & x_p < x < (x_p + a) \end{cases} \quad (5.1-3)$$

where $a = L / N$, L is the length of the dipole, N is the number of subdivisions used along x-direction, x_p is the x-coordinate of the center of the basis function.

For the analysis along the length of the dipole, the Fourier transform of the triangular basis function is given as

$$\tilde{J}_x(k_x) = ae^{-ik_x x_p} \sin^2\left(\frac{1}{2}k_x a\right) / \left(\frac{1}{2}k_x a\right)^2 \quad (5.1-4)$$

For the transverse current distribution, the pulse function is used as the basis function.

$$J_x(y) = \begin{cases} \frac{M}{W}, & |y - y_p| < \frac{W}{2M} \\ 0, & \text{else} \end{cases} \quad (5.1-5)$$

where y_p is the y-coordinate of the center of the basis function, and W is the width of the dipole.

M is the number of subdivisions used along y-direction.

The Fourier transform of the transverse current distribution is as follows.

$$\tilde{J}_x(k_y) = \frac{2M}{Wk_y} e^{-ik_y y_p} \sin\left(\frac{Wk_y}{2M}\right), \quad k_y \rightarrow 0, \tilde{J}_x(k_y) \rightarrow 1 \quad (5.1-6)$$

In the following analysis, it is assumed that an arbitrary number of pulses are presented in the transverse direction. However, for exceedingly narrow microstrip dipole, the width of the dipole is usually equal to the width of the basis function. This implies that only a single transverse pulse is used for the analysis.

We order the location of the centers of the basis functions in the following convention. Total number of basis function is $M(N-1)$. $m = 1, 2, \dots, (N-1)M$.

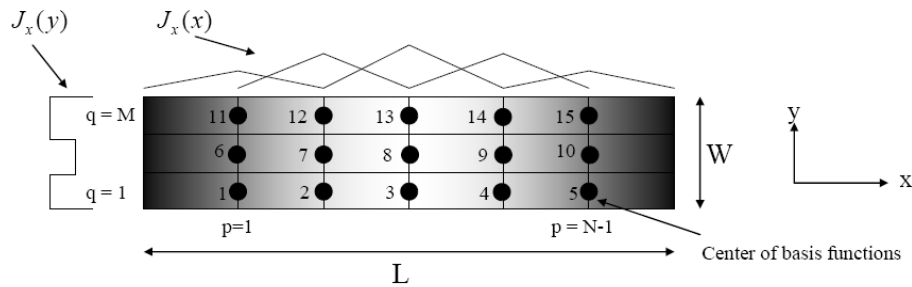


Fig. 5-2: Locations of the subdomain basis functions $J_x(x)$ and $J_x(y)$ along x-direction.

The m^{th} basis function corresponds to the p^{th} element in the row and the q^{th} element in the column with p and q calculated as follows.

$$q = \left\lceil \frac{m}{N-1} \right\rceil \rightarrow \begin{cases} 1 \leq m \leq N-1 & \rightarrow q = 1 \\ N \leq m \leq 2(N-1) & \rightarrow q = 2 \end{cases} \quad (5.1-7)$$

$$p = m - (q-1)(N-1)$$

The center coordinate of the m^{th} basis function is

$$x_o^m = x_c - \frac{L}{2} + p \frac{L}{N} = x_c - \frac{L}{2} + pa, \quad p = 1, \dots, N-1 \quad (5.1-8)$$

$$y_o^m = y_c - \frac{W}{2} \left(1 - \frac{1}{M}\right) + (q-1) \frac{W}{M}, \quad q = 1, \dots, M, \quad m = 1, \dots, (N-1)M$$

The absolute coordinate of the center of the microstrip dipole is represented as (x_c, y_c) .

5.1.2 Excitation

For a microstrip dipole, the excitation is assumed as a simple delta gap source located in the $z = 0$ plane which imposes a known electric field given by

$$\bar{E}_{\text{tan}}^{\text{imp}} = \hat{x} \delta(x - x_f) \left[u\left(y - \left(y_f - \frac{W}{2}\right)\right) - u\left(y - \left(y_f + \frac{W}{2}\right)\right) \right] \quad (5.1-9)$$

where $u(y)$ represents the Heaviside step function, and (x_f, y_f) represents the center location of the feeding point of dipole.

In order to have only one non-zero basis function at the location of delta gap source, the number of basis functions along longitudinal (x) direction (N-1) is taken as odd. Through the analysis, the feeding point is at the coordinate center of dipole $(x_f, y_f) = (x_c, y_c)$. Applying the PEC (perfect electric conductor) boundary condition along the microstrip antenna, we have

$$\overline{E}_{\tan}^{imp} + \overline{E}_{\tan}^s = 0 \rightarrow \overline{E}_{\tan}^{imp} = -\overline{E}_{\tan}^s \quad (5.1-10)$$

$\overline{E}_{\tan}^{imp}$ is the tangential component of the electric field due to the impressed source while \overline{E}_{\tan}^s is the tangential component of the electric field due to the current induced along the microstrip dipole. Since the scattered field \overline{E}_{\tan}^s can be written in terms of the dyadic Green's function and source current, Eq. (5.1-10) can be written as follows.

$$\begin{aligned} & -\iint_s ds' \overline{\overline{G}}^{(0,0)}(\overline{r}, \overline{r}') \cdot \overline{J}_s(\overline{r}') = \\ & \hat{x} \delta(x - x_f) \left[u\left(y - \left(y_f - \frac{W}{2}\right)\right) - u\left(y - \left(y_f + \frac{W}{2}\right)\right) \right] \end{aligned} \quad (5.1-11)$$

where $\overline{J}_s(\overline{r}')$ is the surface current floating on the antenna in the $z' = 0$ plane and $\overline{\overline{G}}^{(0,0)}(\overline{r}, \overline{r}')$ is the appropriate electric type dyadic Green's function for the geometry.

Since we have assumed an x-directed current, the current vector can be written as

$$\overline{J}_s(\overline{r}') = \hat{x} J_x(x', y') = \hat{x} \sum_{m=1}^{M(N-1)} a_m J_x^m(x') J_x^m(y') \quad (5.1-12)$$

Substituting Eq. (5.1-12) and Eq. (5.1-11) into the above boundary condition Eq. (5.1-10)

and it gives

$$\begin{aligned} & -\iint_s ds' \left(G_{xx}^{(0,0)}(\overline{r}, \overline{r}') \hat{x} + G_{yx}^{(0,0)}(\overline{r}, \overline{r}') \hat{y} \right) \sum_{m=1}^{M(N-1)} a_m J_x^m(x') J_x^m(y') \\ & = \hat{x} \delta(x - x_f) \left[u\left(y - \left(y_f - \frac{W}{2}\right)\right) - u\left(y - \left(y_f + \frac{W}{2}\right)\right) \right] \end{aligned} \quad (5.1-13)$$

where

$$\overline{\overline{G}}^{(0,0)}(\overline{r}, \overline{r}') = \frac{1}{4\pi^2} \int_{-\infty}^{\infty} \overline{\overline{G}}^{(0,0)} e^{ik_x(x-x')} e^{ik_y(y-y')} dk_x dk_y \quad (5.1-14)$$

The spectral domain DGF $\overset{\equiv}{G}^{(0,0)}$ takes the following form.

$$\overset{\equiv}{G}^{(0,0)} = \frac{i}{2} \frac{1}{k_{0z}} \left\{ \begin{array}{l} e^{ik_{0z}(z-z')} \left(\hat{h}_0(+k_{0z}) \hat{h}_0(+k_{0z}) + \hat{v}_0(+k_{0z}) \hat{v}_0(+k_{0z}) \right) \\ + e^{ik_{0z}(z+z')} \left(\begin{array}{l} R_{hh}(-k_x, -k_y) \hat{h}_0(+k_{0z}) \hat{h}_0(-k_{0z}) \\ - R_{hv}(-k_x, -k_y) \hat{h}_0(+k_{0z}) \hat{v}_0(-k_{0z}) \end{array} \right) \\ + e^{ik_{0z}(z+z')} \left(\begin{array}{l} R_{vv}(-k_x, -k_y) \hat{v}_0(+k_{0z}) \hat{v}_0(-k_{0z}) \\ - R_{vh}(-k_x, -k_y) \hat{v}_0(+k_{0z}) \hat{h}_0(-k_{0z}) \end{array} \right) \end{array} \right\} \quad (5.1-15)$$

Substituting Eq. (5.1-15) back into (5.1-13) gives

$$\begin{aligned} & - \iint_s ds' \left\{ \left[\frac{1}{4\pi^2} \int_{-\infty}^{\infty} \int_{-\infty}^{\infty} dk_x dk_y \left(\begin{array}{l} \tilde{G}_{xx}^{(0,0)}(k_x, k_y) \hat{x} + \\ \tilde{G}_{yx}^{(0,0)}(k_x, k_y) \hat{y} \end{array} \right) e^{ik_x(x-x')} e^{ik_y(y-y')} \right] \cdot \right. \\ & \left. \sum_{m=1}^{M(N-1)} a_m J_x^m(x') J_x^m(y') \right\} \\ & = \hat{x} \delta(x - x_f) \left[u \left(y - \left(y_f - \frac{W}{2} \right) \right) - u \left(y - \left(y_f + \frac{W}{2} \right) \right) \right] \end{aligned} \quad (5.1-16)$$

Since $\tilde{G}_{xx}^{(0,0)}(k_x, k_y)$, $\tilde{G}_{yx}^{(0,0)}(k_x, k_y)$ do not depend on x' and y' , the order of the integration

above can be interchanged as follows.

$$\begin{aligned} & - \frac{1}{4\pi^2} \sum_{m=1}^{M(N-1)} a_m \int_{-\infty}^{\infty} \int_{-\infty}^{\infty} dk_x dk_y \left[\left(\tilde{G}_{xx}^{(0,0)}(k_x, k_y) \hat{x} + \tilde{G}_{yx}^{(0,0)}(k_x, k_y) \hat{y} \right) e^{ik_x x} e^{ik_y y} \right. \\ & \left. \cdot \iint_s ds' \left(J_x^m(x') J_x^m(y') e^{-ik_x x'} e^{-ik_y y'} \right) \right] \\ & = \hat{x} \delta(x - x_f) \left[u \left(y - \left(y_f - \frac{W}{2} \right) \right) - u \left(y - \left(y_f + \frac{W}{2} \right) \right) \right] \end{aligned} \quad (5.1-17)$$

Converting the current basis to its spectral form results in

$$\begin{aligned}
& -\frac{1}{4\pi^2} \sum_{m=1}^{M(N-1)} a_m \int_{-\infty}^{\infty} \int_{-\infty}^{\infty} dk_x dk_y \left[\left(\tilde{G}_{xx}^{(0,0)}(k_x, k_y) \hat{x} + \tilde{G}_{yx}^{(0,0)}(k_x, k_y) \hat{y} \right) e^{ik_x x} e^{ik_y y} \right. \\
& \left. \cdot \tilde{J}_x^m(k_x) \tilde{J}_x^m(k_y) \right] \\
& = \hat{x} \delta(x - x_f) \left[u\left(y - \left(y_f - \frac{W}{2}\right)\right) - u\left(y - \left(y_f + \frac{W}{2}\right)\right) \right]
\end{aligned} \tag{5.1-18}$$

Galerkin's method is applied to the above equation here, and the testing function used is same as the assumed basis function which is repeated here.

$$\bar{J}_x^i(x, y) = \hat{x} J_x^i(x) J_x^i(y), \quad i = 1, 2, \dots, M(N-1) \tag{5.1-19}$$

So it leads to

$$\begin{aligned}
& -\iint_s ds \hat{x} \cdot \left\{ \left. \begin{aligned} & J_x^i(x) J_x^i(y) \frac{1}{4\pi^2} \\ & \sum_{m=1}^{M(N-1)} a_m \int_{-\infty}^{\infty} \int_{-\infty}^{\infty} dk_x dk_y \left[\left(\tilde{G}_{xx}^{(0,0)}(k_x, k_y) \hat{x} + \tilde{G}_{yx}^{(0,0)}(k_x, k_y) \hat{y} \right) e^{ik_x x} e^{ik_y y} \tilde{J}_x^m(k_x) \tilde{J}_x^m(k_y) \right] \end{aligned} \right\} \\
& = \iint_s ds \left\{ J_x^i(x) J_x^i(y) \hat{x} \cdot \hat{x} \delta(x - x_f) \left[u\left(y - \left(y_f - \frac{W}{2}\right)\right) - u\left(y - \left(y_f + \frac{W}{2}\right)\right) \right] \right\}
\end{aligned} \tag{5.1-20}$$

Eq. (5.1-20) can then simply reduce to the following form.

$$\begin{aligned}
& -\iint_s ds \left\{ J_x^i(x) J_x^i(y) \frac{1}{4\pi^2} \sum_{m=1}^{M(N-1)} a_m \int_{-\infty}^{\infty} \int_{-\infty}^{\infty} dk_x dk_y \left[\tilde{G}_{xx}^{(0,0)}(k_x, k_y) \tilde{J}_x^m(k_x) \tilde{J}_x^m(k_y) e^{ik_x x} e^{ik_y y} \right] \right\} \\
& = \iint_s ds \left\{ J_x^i(x) J_x^i(y) \delta(x - x_f) \left[u\left(y - \left(y_f - \frac{W}{2}\right)\right) - u\left(y - \left(y_f + \frac{W}{2}\right)\right) \right] \right\}
\end{aligned} \tag{5.1-21}$$

Interchange the integration order for the LHS of Eq. (5.1-21) above leads to

$$\begin{aligned}
& -\frac{1}{4\pi^2} \sum_{m=1}^{M(N-1)} a_m \left[\int_{-\infty}^{\infty} \int_{-\infty}^{\infty} dk_x dk_y \tilde{G}_{xx}^{(0,0)}(k_x, k_y) \tilde{J}_x^m(k_x) \tilde{J}_x^m(k_y) \tilde{J}_x^i(-k_x) \tilde{J}_x^i(-k_y) \right] \\
& = \iint_s ds J_x^i(x) J_x^i(y) \delta(x - x_f) \left[u\left(y - \left(y_f - \frac{W}{2}\right)\right) - u\left(y - \left(y_f + \frac{W}{2}\right)\right) \right]
\end{aligned} \tag{5.1-22}$$

Denoting the RHS of Eq. (5.1-22) as V_i , Eq. (5.1-22) becomes

$$-\frac{1}{4\pi^2} \sum_{m=1}^{M(N-1)} a_m \left[\int_{-\infty}^{\infty} \int_{-\infty}^{\infty} dk_x dk_y \tilde{G}_{xx}^{(0,0)}(k_x, k_y) \tilde{J}_x^m(k_x) \tilde{J}_x^m(k_y) \tilde{J}_x^i(-k_x) \tilde{J}_x^i(-k_y) \right] = V_i \quad (5.1-23)$$

Calculating the integration for V_i gives

$$V_i = \int_{-L/2}^{L/2} dx J_x^i(x) \delta(x - x_f) \int_{-W/2}^{W/2} dy J_x^i(y) \left[u\left(y - \left(y_f - \frac{W}{2}\right)\right) - u\left(y - \left(y_f + \frac{W}{2}\right)\right) \right] \quad (5.1-24)$$

$$= \begin{cases} 1 & i = (M-1)(N-1) + N/2 \\ 0 & \text{else} \end{cases}$$

Then Eq. (5.1-23) can be written in the following matrix form.

$$\left[\overline{\overline{Z}} \right] \overline{\overline{x}} = \overline{\overline{V}} \quad (5.1-25)$$

$$\overline{\overline{x}} = \left[a_1 \quad \dots \quad a_{N/2} \quad \dots \quad a_{(M-1)(N-1)+N/2} \quad \dots \quad a_{(N-1)M} \right]^T, \quad \overline{\overline{V}} = \left[0 \quad \dots \quad 1 \quad \dots \quad 1 \quad \dots \quad 0 \right]^T$$

where $\overline{\overline{Z}}$ is a square matrix of size $M(N-1)$ by $M(N-1)$ and each element of the matrix

$Z_{im} [i = 1, 2, \dots, M(N-1); m = 1, 2, \dots, M(N-1)]$ is

$$Z_{im} = -\frac{1}{4\pi^2} \left[\int_{-\infty}^{\infty} \int_{-\infty}^{\infty} dk_x dk_y \tilde{J}_x^i(-k_x) \tilde{J}_x^i(-k_y) \tilde{G}_{xx}^{(0,0)}(k_x, k_y) \tilde{J}_x^m(k_x) \tilde{J}_x^m(k_y) \right] \quad (5.1-26)$$

As shown in Eq. (5.1-26), the 2D infinite numerical integration of the dyadic Green's function in the spectral domain for Z_{im} is critical to obtain the current distribution coefficients $\overline{\overline{x}}$.

5.1.3 Symmetry Analysis for Impedance Matrix

It is known from the previous section that the impedance matrix $\overline{\overline{Z}}$ is a square matrix of size $M(N-1)$ by $M(N-1)$. It is shown in this section that there exist certain symmetry relations for the matrix elements Z_{im} which help to reduce the computation time.

5.1.3.1 Z_{im} and Z_{mi}

For convenience, the matrix elements Z_{im} in Eq. (5.1-26) obtained from the previous sections are repeated here.

$$Z_{im} = -\frac{1}{4\pi^2} \left[\int_{-\infty}^{\infty} \int_{-\infty}^{\infty} dk_x dk_y \tilde{J}_x^i(-k_x) \tilde{J}_x^i(-k_y) \tilde{G}_{xx}^{(0,0)}(k_x, k_y) \tilde{J}_x^m(k_x) \tilde{J}_x^m(k_y) \right]$$

Substituting the spectral domain current basis functions, Eq. (5.1-4) and Eq. (5.1-6), for $\tilde{J}_x(k_x)$ and $\tilde{J}_x(k_y)$ into the above equation gives

$$Z_{im} = -\frac{1}{4\pi^2} \int_{-\infty}^{\infty} \int_{-\infty}^{\infty} dk_x dk_y \left[\tilde{G}_{xx}^{(0,0)}(k_x, k_y) e^{ik_x(x_i-x_m)} e^{ik_y(y_i-y_m)} \cdot \left(a \frac{\sin^2\left(\frac{1}{2}k_x a\right)}{\left(\frac{1}{2}k_x a\right)^2} \frac{2M}{Wk_y} \sin\left(\frac{Wk_y}{2M}\right) \right)^2 \right] \quad (5.1-27)$$

Similarly, the matrix element Z_{mi} can also be obtained from Eq. (5.1-26) by swapping the first and the second subscripts, and it takes the following form.

$$Z_{mi} = -\frac{1}{4\pi^2} \int_{-\infty}^{\infty} \int_{-\infty}^{\infty} dk_x dk_y \left[\tilde{G}_{xx}^{(0,0)}(k_x, k_y) e^{ik_x(x_m-x_i)} e^{ik_y(y_m-y_i)} \cdot \left(a \frac{\sin^2\left(\frac{1}{2}k_x a\right)}{\left(\frac{1}{2}k_x a\right)^2} \frac{2M}{Wk_y} \sin\left(\frac{Wk_y}{2M}\right) \right)^2 \right] \quad (5.1-28)$$

Let $(k_x, k_y) \rightarrow (-k_x, -k_y)$, then it is easy to see that $Z_{mi} = Z_{im}$ if the following condition Eq. (5.1-29) is satisfied.

$$\tilde{G}_{xx}^{(0,0)}(k_x, k_y) = \tilde{G}_{xx}^{(0,0)}(-k_x, -k_y) \quad (5.1-29)$$

This relation Eq. (5.1-29) holds true if the anisotropic medium is reciprocal. In this case, the impedance matrix $\overline{\overline{Z}}$ is a symmetrical matrix, and only the elements in the top half matrix need to be calculated. Furthermore, if the number of basis function along y-direction is $M=1$, then the matrix elements Z_{mi} shown in Eq. (5.1-28) will be independent of the y-coordinate, thus the following relation can be easily derived.

$$Z_{mi} = Z_{m+1,i+1} \quad (5.1-30)$$

The impedance matrix reduces to a Toeplitz matrix under the condition of Eq. (5.1-30), thus only the elements in the first row of the impedance matrix need to be calculated.

However, if the substrate is a non-reciprocal medium, then the symmetry relation Eq. (5.1-29) for the spectral domain Green's function no longer holds and $Z_{mi} \neq Z_{im}$. So for a general non-reciprocal medium, each element of the impedance matrix needs to be calculated and the computation time is significantly longer than the special case of a reciprocal medium. It is worth to note here that if $M=1$, then Eq. (5.1-30) still applies. In this case, it only requires calculating the elements of the first row and first column in the impedance matrix.

5.1.3.2 Symmetry of Integrand for Z_{im}

This previous section mainly discusses the symmetry relation of the elements Z_{im} of the impedance matrix with Z_{im} in the form of 2D infinite integration in the spectral domain. In this section, it is shown that 2D infinite integration of Z_{im} can be further simplified. For convenience, integral Z_{im} is repeated here.

$$Z_{im} = -\frac{1}{4\pi^2} \left[\int_{-\infty}^{\infty} \int_{-\infty}^{\infty} dk_x dk_y \tilde{J}_x^i(-k_x) \tilde{J}_x^i(-k_y) \tilde{G}_{xx}^{(0,0)}(k_x, k_y) \tilde{J}_x^m(k_x) \tilde{J}_x^m(k_y) \right] \quad (5.1-31)$$

Observation of Z_{im} in Eq. (5.1-31) indicates that its evaluation requires a bidimensional doubly infinite integral to be calculated. Theoretically, this implies the integrand must be integrated over all the four quadrants of the $k_x - k_y$ plane as shown in Fig. 5-3(a) and the integral of Z_{im} can be written as follows.

$$Z_{im} = I_{Q1} + I_{Q2} + I_{Q3} + I_{Q4} \quad (5.1-32)$$

$$\begin{aligned} I_{Q1} &= -\frac{1}{4\pi^2} \left[\int_0^{\infty} \int_0^{\infty} dk_x dk_y \tilde{J}_x^i(-k_x) \tilde{J}_x^i(-k_y) \tilde{G}_{xx}^{(0,0)}(k_x, k_y) \tilde{J}_x^m(k_x) \tilde{J}_x^m(k_y) \right] \\ I_{Q2} &= -\frac{1}{4\pi^2} \left[\int_0^{\infty} \int_{-\infty}^0 dk_x dk_y \tilde{J}_x^i(-k_x) \tilde{J}_x^i(-k_y) \tilde{G}_{xx}^{(0,0)}(k_x, k_y) \tilde{J}_x^m(k_x) \tilde{J}_x^m(k_y) \right] \\ I_{Q3} &= -\frac{1}{4\pi^2} \left[\int_{-\infty}^0 \int_{-\infty}^0 dk_x dk_y \tilde{J}_x^i(-k_x) \tilde{J}_x^i(-k_y) \tilde{G}_{xx}^{(0,0)}(k_x, k_y) \tilde{J}_x^m(k_x) \tilde{J}_x^m(k_y) \right] \\ I_{Q4} &= -\frac{1}{4\pi^2} \left[\int_{-\infty}^0 \int_0^{\infty} dk_x dk_y \tilde{J}_x^i(-k_x) \tilde{J}_x^i(-k_y) \tilde{G}_{xx}^{(0,0)}(k_x, k_y) \tilde{J}_x^m(k_x) \tilde{J}_x^m(k_y) \right] \end{aligned} \quad (5.1-33)$$

It is shown here that the integration area of all the four quadrants can be folded to the only first quadrant of the $k_x - k_y$ plane as shown in Fig. 5-3(c).

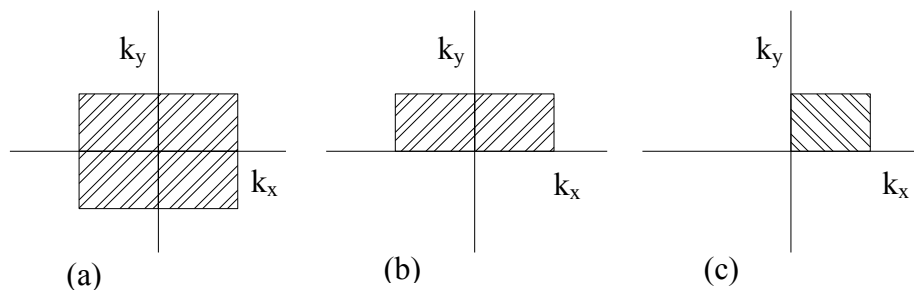


Fig. 5-3: Integration in the $k_x - k_y$ plane. Area over (a) the entire $k_x - k_y$ plane, (b) the upper half-space, and (c) the first quadrant of $k_x - k_y$ plane.

First, replacing (k_x, k_y) with $(-k_x, k_y)$ in I_{Q2} , and it gives,

$$I_{Q2} = -\frac{1}{4\pi^2} \left[\int_0^\infty \int_0^\infty dk_x dk_y \tilde{J}_x^i(k_x) \tilde{J}_x^i(-k_y) \tilde{G}_{xx}^{(0,0)}(-k_x, k_y) \tilde{J}_x^m(-k_x) \tilde{J}_x^m(k_y) \right] \quad (5.1-34)$$

Replacing (k_x, k_y) with $(-k_x, -k_y)$ in I_{Q3} , it gives,

$$I_{Q3} = -\frac{1}{4\pi^2} \left[\int_0^\infty \int_0^\infty dk_x dk_y \tilde{J}_x^i(k_x) \tilde{J}_x^i(k_y) \tilde{G}_{xx}^{(0,0)}(-k_x, -k_y) \tilde{J}_x^m(-k_x) \tilde{J}_x^m(-k_y) \right] \quad (5.1-35)$$

Replacing (k_x, k_y) with $(k_x, -k_y)$ in I_{Q4} , it gives,

$$I_{Q4} = -\frac{1}{4\pi^2} \left[\int_0^\infty \int_0^\infty dk_x dk_y \tilde{J}_x^i(-k_x) \tilde{J}_x^i(k_y) \tilde{G}_{xx}^{(0,0)}(k_x, -k_y) \tilde{J}_x^m(k_x) \tilde{J}_x^m(-k_y) \right] \quad (5.1-36)$$

Combining Eq. (5.1-33) – Eq. (5.1-36) shows that the integral Z_{im} only requires the integration area in the first quadrant. As shown in the last section, the following symmetry relations for the spectral domain DGF exist if the anisotropic medium is reciprocal.

$$\tilde{G}_{xx}^{(0,0)}(k_x, k_y) = \tilde{G}_{xx}^{(0,0)}(-k_x, -k_y), \quad \tilde{G}_{xx}^{(0,0)}(-k_x, k_y) = \tilde{G}_{xx}^{(0,0)}(k_x, -k_y) \quad (5.1-37)$$

The symmetry relations are summarized in Fig. 5-4.

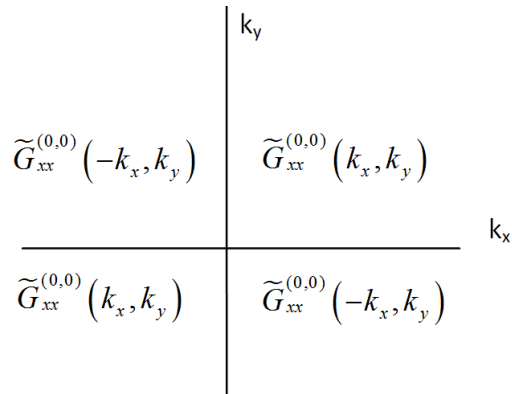


Fig. 5-4: Symmetry relation for the dyadic Green's function elements of $\tilde{G}_{xx}^{(0,0)}(k_x, k_y)$ for a reciprocal medium.

With the aid of the above symmetry relation, Eq. (5.1-37), the expression of Z_{im} reduces to the following form.

$$Z_{im} = -\frac{1}{4\pi^2} \left[\int_0^\infty \int_0^\infty dk_x dk_y \begin{pmatrix} \tilde{J}_x^i(-k_x) \tilde{J}_x^i(-k_y) \tilde{J}_x^m(k_x) \tilde{J}_x^m(k_y) \\ + \tilde{J}_x^i(k_x) \tilde{J}_x^i(k_y) \tilde{J}_x^m(-k_x) \tilde{J}_x^m(-k_y) \end{pmatrix} \tilde{G}_{xx}^{(0,0)}(k_x, k_y) \right. \\ \left. + \int_0^\infty \int_0^\infty dk_x dk_y \begin{pmatrix} \tilde{J}_x^i(k_x) \tilde{J}_x^i(-k_y) \tilde{J}_x^m(-k_x) \tilde{J}_x^m(k_y) \\ + \tilde{J}_x^i(-k_x) \tilde{J}_x^i(k_y) \tilde{J}_x^m(k_x) \tilde{J}_x^m(-k_y) \end{pmatrix} \tilde{G}_{xx}^{(0,0)}(-k_x, k_y) \right] \quad (5.1-38)$$

As shown in Eq. (5.1-38), the bi-dimensional integration over the whole integration area shown in Fig. 5-3(a) can be reduced to integration over the area as shown in Fig. 5-3(c) with the spectral domain DGF evaluated only in the first and second quadrants.

Furthermore, for an isotropic medium, the spectral domain DGFs of the first and second quadrants has the following symmetry relation.

$$\tilde{G}_{xx}^{(0,0)}(-k_x, k_y) = \tilde{G}_{xx}^{(0,0)}(k_x, k_y) \quad (5.1-39)$$

Then the integral Eq. (5.1-31) can be further simplified to Eq. (5.1-40).

$$Z_{im} = -\frac{1}{4\pi^2} \left[\int_0^\infty \int_0^\infty dk_x dk_y \begin{pmatrix} \tilde{J}_x^i(-k_x) \tilde{J}_x^i(-k_y) \tilde{J}_x^m(k_x) \tilde{J}_x^m(k_y) \\ + \tilde{J}_x^i(k_x) \tilde{J}_x^i(k_y) \tilde{J}_x^m(-k_x) \tilde{J}_x^m(-k_y) \\ + \tilde{J}_x^i(k_x) \tilde{J}_x^i(-k_y) \tilde{J}_x^m(-k_x) \tilde{J}_x^m(k_y) \\ + \tilde{J}_x^i(-k_x) \tilde{J}_x^i(k_y) \tilde{J}_x^m(k_x) \tilde{J}_x^m(-k_y) \end{pmatrix} \tilde{G}_{xx}^{(0,0)}(k_x, k_y) \right] \quad (5.1-40)$$

However, the simplifications of Eq. (5.1-37) and Eq. (5.1-39) above do not apply to a general non-reciprocal medium. In this case, Eq. (5.1-32) needs to be used, which requires the evaluation of the spectral domain Green's functions in all four quadrants of the Cartesian coordinate system including $\tilde{G}_{xx}^{(0,0)}(k_x, k_y)$, $\tilde{G}_{xx}^{(0,0)}(-k_x, -k_y)$, $\tilde{G}_{xx}^{(0,0)}(k_x, -k_y)$, and $\tilde{G}_{xx}^{(0,0)}(-k_x, k_y)$.

5.1.3.3 Integration Path

To evaluate impedance matrix elements Z_{im} in Eq. (5.1-31), a 2D infinite integration in the spectral domain is needed. It is desirable to keep the integration path along the real axis of k_x and k_y for simplicity. However, $\tilde{G}_{xx}^{(0,0)}(k_x, k_y)$ (part of the integrand of Z_{im}) is singular for certain real values of k_x and k_y . These values of k_x and k_y where $\tilde{G}_{xx}^{(0,0)}(k_x, k_y)$ is singular actually correspond to the propagating surface wave modes supported by the corresponding layered geometry. Depending on the type of the medium, the loci of the propagation constants for the surface waves vary.

Different methods have been proposed for the treatment of the singularity of the integrand. A pole extraction method was used in [59, 65, 76] for the radiation of the dipole over a grounded isotropic slab which in addition to the numerical integration, requires the calculation of the residues and Cauchy principle values at the singularity points.

However, for a general anisotropic medium, to obtain the location of the singularities usually introduces more complexity into the problems. Thus, instead of extracting each single surface wave pole and calculating the residues due to the poles, the integration path is indented off the real axis. The detailed discussions about the integration path and surface wave pole are presented in Sections 5.2.1 and 5.2.2. Except indenting the integration path off the real axis, another approach to deal with the singularity of the integrand is to move the surface wave pole of the integrand off the real axis by introducing a slight loss to the anisotropic medium. Since the surface wave poles of the integrand $\tilde{G}_{xx}^{(0,0)}(k_x, k_y)$ of the impedance matrix now move off the real axis, the integration path can stay on the real axis.

5.1.3.4 Sampling Rate and Integration Range

As shown in the Section 5.1.3.2, the double infinite integral is reduced to the integral in the first quadrant only. The integration step has been derived in [37]. The sampling rates for k_x and k_y domains are given below, respectively.

$$f_{kx}^{\min} = 10 \frac{L}{N} \left(\frac{N-1}{\pi} \right) \quad (5.1-41)$$

$$f_{ky}^{\min} = 10 \frac{W}{M} \left(\frac{2M+1}{2\pi} \right) \quad (5.1-42)$$

It is worth noting here that if the integration path stays on the real axis without indenting, the sampling rates need to be refined especially in the integration region where the surface wave pole exists by observing the convergence of the integral. The minimum frequency (or maximum step size) for which the integration has converged is then chosen. Also, the limit of the doubly infinite integral can then be chosen by increasing the integration range step by step till the difference of the integral between previous step and current step is converged to a predefined number.

5.2 Properties of the Dyadic Green's Function

As it is stated, the dyadic Green's function for two-layer geometry can be used to calculate the current distribution of a microstrip dipole on an anisotropic substrate. When a current is tangential to the interface, the following dyadic Green's functions $\overline{\overline{G}}^{(0,0)}(\vec{r}, \vec{r}')$, $\overline{\overline{G}}^{(0,1)}(\vec{r}, \vec{r}')$, $\overline{\overline{G}}^{(1,0)}(\vec{r}, \vec{r}')$ and $\overline{\overline{G}}^{(1,1)}(\vec{r}, \vec{r}')$ can be used with the first superscript indicating the field region and

the second superscript indicating the source region. Of all the four types of Green's function,

$\overline{\overline{G}}^{(0,0)}(\bar{r}, \bar{r}')$ is repeated here.

For $0 < z < z'$

$$\overline{\overline{G}}^{(0,0)}(\bar{r}, \bar{r}') = \frac{i}{8\pi^2} \int_{-\infty}^{\infty} dk_x dk_y \frac{1}{k_{0z}} \left\{ \begin{array}{l} e^{-i\bar{k}_0 \cdot \bar{r}} \left[\hat{h}_0(-k_{0z}) e^{i\bar{k}_0 \cdot \bar{r}} + R_{hh}(k_x, k_y) \hat{h}_0(k_{0z}) e^{i\bar{k}_0 \cdot \bar{r}} \right] \hat{h}_0(-k_{0z}) \\ + R_{hv}(k_x, k_y) \hat{v}_0(k_{0z}) e^{i\bar{k}_0 \cdot \bar{r}} \\ + e^{-i\bar{k}_0 \cdot \bar{r}} \left[\hat{v}_0(-k_{0z}) e^{i\bar{k}_0 \cdot \bar{r}} + R_{vh}(k_x, k_y) \hat{h}_0(k_{0z}) e^{i\bar{k}_0 \cdot \bar{r}} \right] \hat{v}_0(-k_{0z}) \\ + R_{vv}(k_x, k_y) \hat{v}_0(k_{0z}) e^{i\bar{k}_0 \cdot \bar{r}} \end{array} \right\} \quad (5.2-1)$$

This can be simplified in the following form,

$$\overline{\overline{G}}^{(0,0)}(\bar{r}, \bar{r}') = \int_{-\infty}^{\infty} \overline{\overline{G}}^{(0,0)} e^{ik_x(x-x')} e^{ik_y(y-y')} dk_x dk_y \quad (5.2-2)$$

$$\overline{\overline{G}}^{(0,0)} = \frac{i}{8\pi^2} \frac{1}{k_{0z}} \left\{ \begin{array}{l} e^{ik_{0z}(z'-z)} \left(\hat{h}_0(-k_{0z}) \hat{h}_0(-k_{0z}) + \hat{v}_0(-k_{0z}) \hat{v}_0(-k_{0z}) \right) \\ + e^{ik_{0z}(z+z')} \left(\begin{array}{l} R_{hh}(k_x, k_y) \hat{h}_0(+k_{0z}) \hat{h}_0(-k_{0z}) \\ R_{hv}(k_x, k_y) \hat{v}_0(+k_{0z}) \hat{h}_0(-k_{0z}) \end{array} \right) \\ + e^{ik_{0z}(z+z')} \left(\begin{array}{l} R_{vv}(k_x, k_y) \hat{v}_0(+k_{0z}) \hat{v}_0(-k_{0z}) \\ R_{vh}(k_x, k_y) \hat{h}_0(k_{0z}) \hat{v}_0(-k_{0z}) \end{array} \right) \end{array} \right\} \quad (5.2-3)$$

It is noted here that to obtain the result for $\overline{\overline{G}}^{(0,0)}$ consistent with what is found in [37], the constant term $i\omega\mu_0 4\pi^2$ needs to be multiplied to the above formula of Eq. (5.2-3). The two-layer reflection coefficients R_{hh} , R_{hv} , R_{vh} and R_{vv} are obtained through half-space reflection and transmission matrices as in Eq. (5.2-4).

$$\begin{aligned}
\overline{\overline{R}}|_{two-layer} &= \begin{bmatrix} R_{hh} & R_{vh} \\ R_{hv} & R_{vv} \end{bmatrix} = \overline{\overline{R}} + \overline{\overline{X}} \overline{\overline{R}} (\overline{\overline{I}} - \overline{\overline{R}} \overline{\overline{R}})^{-1} \overline{\overline{X}} \\
\overline{\overline{R}}^{\overline{\overline{01}}} &= \begin{bmatrix} R_{hh}^{01} & R_{vh}^{01} \\ R_{hv}^{01} & R_{vv}^{01} \end{bmatrix}, \quad \overline{\overline{X}}^{\overline{\overline{01}}} = \begin{bmatrix} X_{hh}^{01} & X_{vh}^{01} \\ X_{hv}^{01} & X_{vv}^{01} \end{bmatrix} \\
\overline{\overline{R}}^{\overline{\overline{10}}} &= \begin{bmatrix} R_{hh}^{10} & R_{vh}^{10} \\ R_{hv}^{10} & R_{vv}^{10} \end{bmatrix}, \quad \overline{\overline{X}}^{\overline{\overline{10}}} = \begin{bmatrix} X_{hh}^{10} & X_{vh}^{10} \\ X_{hv}^{10} & X_{vv}^{10} \end{bmatrix} \\
\overline{\overline{R}}^{\overline{\overline{12}}} &= \begin{bmatrix} R_{el\ell l}^{12} \exp\left[i(-k_{z_l}^d + k_{z_l}^u)d\right] & R_{e\ell\ell l}^{12} \exp\left[i(-k_{z_{ll}}^d + k_{z_l}^u)d\right] \\ R_{\ell\ell\ell l}^{12} \exp\left[i(-k_{z_l}^d + k_{z_{ll}}^u)d\right] & R_{\ell\ell\ell\ell}^{12} \exp\left[i(-k_{z_{ll}}^d + k_{z_{ll}}^u)d\right] \end{bmatrix}
\end{aligned} \tag{5.2-4}$$

where d is the thickness of the slab.

Observing the Green's function Eq. (5.2-3) reveals that the singularity of the dyadic Green's function $\overline{\overline{G}}^{(0,0)}$ occurs in the following two cases.

Case 1) $k_{0z} = 0$, corresponds to the case of $k_\rho = \pm k_0$. This is a branch point of the isotropic medium. Since $k_{0z} = \sqrt{k_0^2 - k_\rho^2}$ is a multi-valued function, $k_\rho = \pm k_0$ is the branch point of the above Green's function $\overline{\overline{G}}^{(0,0)}$. It is noted here that just as the isotropic medium, there also exist branch points for an unbounded biaxial medium. However, these branch points for the unbounded biaxial medium do not pose singularity for $\overline{\overline{G}}^{(0,0)}$; further, the value of $\overline{\overline{G}}^{(0,0)}$ is continuous when these branch points are crossed. How to obtain the branch point loci of the biaxial medium has been discussed in detail in [37] using the so-called Sylvester resultant. As for the branch point of the isotropic medium causing the discontinuity of the function $\overline{\overline{G}}^{(0,0)}$, a vertical branch cut is chosen here.

Case 2) If $\left| \begin{matrix} \bar{I} - \bar{R} & \bar{R} \\ \bar{R} & \bar{R} \end{matrix} \right| = 0$, then the inverse of the matrix $\begin{matrix} \bar{I} - \bar{R} & \bar{R} \\ \bar{R} & \bar{R} \end{matrix}$ does not exist. It will be

shown below that the values of k_ρ making $\left| \begin{matrix} \bar{I} - \bar{R} & \bar{R} \\ \bar{R} & \bar{R} \end{matrix} \right| = 0$ correspond to the surface wave pole loci of the anisotropic slab of thickness d .

5.2.1 Integration Path to Avoid the Singularity of $\bar{G}^{(0,0)}$

The determinant of the matrix $\left| \begin{matrix} \bar{I} - \bar{R} & \bar{R} \\ \bar{R} & \bar{R} \end{matrix} \right| = 0$ results in the singularity of the Green's function. Physically, the values of $\left| \begin{matrix} \bar{I} - \bar{R} & \bar{R} \\ \bar{R} & \bar{R} \end{matrix} \right| = 0$ correspond to the surface wave poles of the geometry. To get the converged result for the integration above, the integration path needs to be carefully chosen to avoid the singularity of the integrand. In this section, the integration path is chosen in the same way as what's used for a printed dipole on a grounded biaxial substrate in [37].

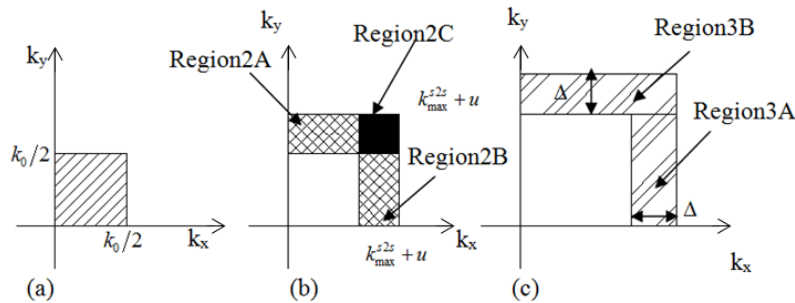


Fig. 5-5: Integration regions in the $k_x - k_y$ plane: (a) Region 1 (b) Region 2 and (c) Region 3.

Since the evaluation of $\bar{G}^{(0,0)}(r, r')$ requires the 2D integration of $\bar{G}^{(0,0)}$, generally, values of

$\bar{G}^{(0,0)}$ in all four quadrants of the spectral domain need to be evaluated for the anisotropic

medium. For the purpose of illustration here, the integration region in the first quadrant of $k_x - k_y$ plane is presented. Usually, the region can be divided into three regions as shown in Fig. 5-5.

In Region 1, there exists no singularity; thus, it is possible to perform the integration along the real axis for both the k_x plane and the k_y plane. The integration paths for the k_x plane and the k_y plane are shown in Fig. 5-6(a) and Fig.5-6(b), respectively.

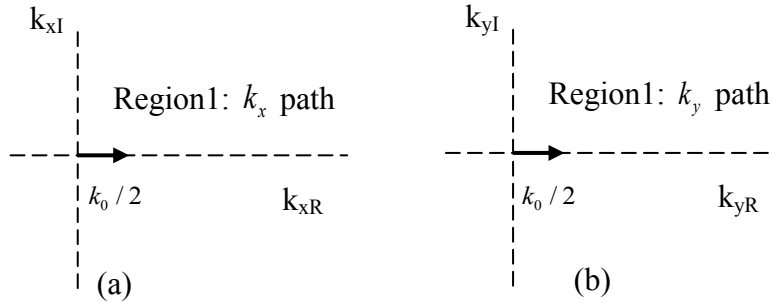


Fig. 5-6: Region 1 integration paths in the k_x and k_y planes: (a) k_x plane, (b) k_y plane.

The path of integration in Region 2 can no longer simply remain on the real axis due to the presence of the surface wave poles. This region is further divided into three regions defined as Region 2A, Region 2B and Region 2C shown in Fig. 5-5(b). Each region is defined below.

$$\text{Region 2A: } 0 < k_x < k_0 / 2; \quad k_0 / 2 < k_y < \left(|k|_{\max}^{s2s} + u \right)$$

$$\text{Region 2B: } 0 < k_y < k_0 / 2; \quad k_0 / 2 < k_x < \left(|k|_{\max}^{s2s} + u \right)$$

$$\text{Region 2C: } k_0 / 2 < k_x < \left(|k|_{\max}^{s2s} + u \right); \quad k_0 / 2 < k_y < \left(|k|_{\max}^{s2s} + u \right)$$

$|k|_{\max}^{s2s}$ is determined by an analysis of the wave-vector surface. This value represents the largest value of k_p where k_z^u or k_z^d turns from real to imaginary. u is an arbitrary positive number used to define the outer boundary of Region 2B.

The integration path for Region 2C is shown in Fig. 5-9 with both k_y and k_x indented off the real axis.

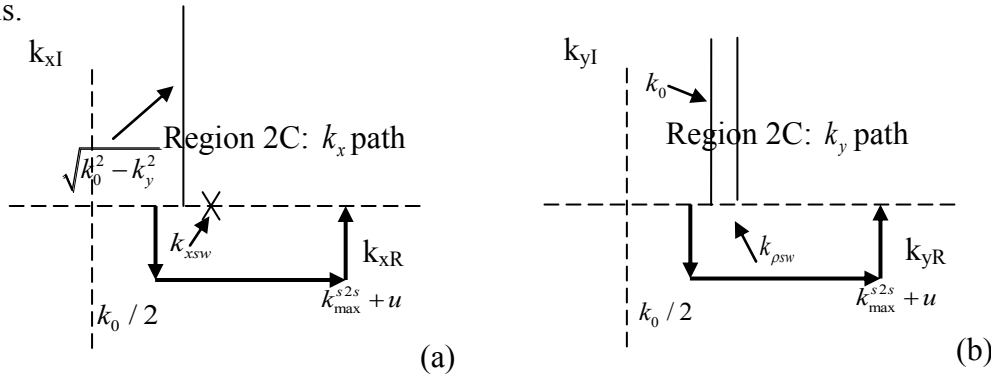


Fig. 5-9: Region 2C integration paths in the k_x and k_y planes: (a) k_x plane, (b) k_y plane.

In Fig. 5-7 – Fig. 5-9, the parameter δ is used to signify how far the path is indented away from the real axis. The offset must be large enough so that the singularities due to the surface wave poles do not cause the Green's function to become exceedingly large on the path of

integration in the k_x plane. To visualize the singularity of $\tilde{G}^{\equiv(0,0)}$, numerical calculation of $\tilde{G}^{\equiv(0,0)}$ for the following special cases are presented.

The grounded biaxial slab has $h = 0.1\lambda_0$ and the permittivity tensor is $(\varepsilon_x, \varepsilon_y, \varepsilon_z) = (5, 3, 4)$.

The biaxial medium is un-rotated; for example, the rotation angle of the medium is

$(\alpha, \beta, \gamma) = (0^\circ, 0^\circ, 0^\circ)$. The magnitude of the integrand $\tilde{G}^{(0,0)}$ for different cases of indent offset

δ is calculated and plotted vs. k_x and k_y in Fig. 5-10. This example shows that when

$\delta = 0.05k_0$ discontinuity occurs for the magnitude of the integrand $\tilde{G}_{xx}^{(0,0)}$ as shown in Fig. 5-10

(a). However, increasing the offset to $\delta = 0.6k_0$ leads the $\tilde{G}_{xx}^{(0,0)}$ to be smooth and continuous, as shown in Fig. 5-10 (b). Thus proper offset for the integration path is critical to avoid the

singularity of the integrand $\tilde{G}_{xx}^{(0,0)}$, which is the key to getting converged and stable results.

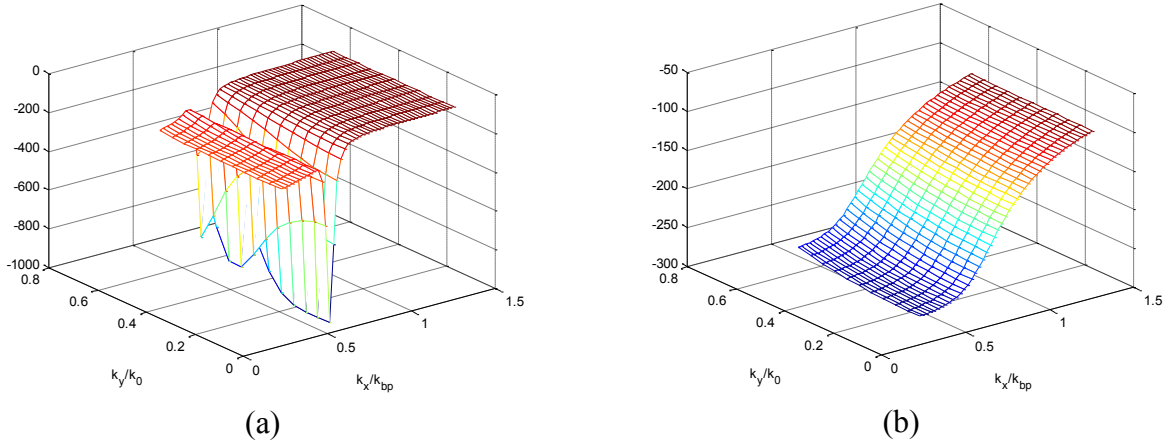


Fig. 5-10: Effect of the magnitude of δ on the calculation of $\text{Re}\left(\tilde{G}_{xx}^{(0,0)}\right)$ in the region 2A. (a)

$\delta = 0.05k_0$, (b) $\delta = 0.6k_0$. $(\varepsilon_x, \varepsilon_y, \varepsilon_z) = (5, 3, 4)$, $(\alpha, \beta, \gamma) = (0^\circ, 0^\circ, 0^\circ)$, and $h = 0.1\lambda_0$.

In summary, a general description about the singularity of $\tilde{G}_{xx}^{(0,0)}$ corresponding to

$\left| \begin{matrix} = & =10 & =12 \\ I - R & R \end{matrix} \right| = 0$ is presented. The integration path to avoid the singularity is discussed. However,

the loci of the values for k_x and k_y making $\left| \begin{matrix} = & =10 & =12 \\ I - R & R \end{matrix} \right| = 0$ and its physical meanings are still

unknown. Thus, in order to demonstrate the physical insight to the values for k_x and k_y giving

$\left| \begin{matrix} = & =10 & =12 \\ I - R & R \end{matrix} \right| = 0$, in the next section, a detailed analysis of the surface waves which are related to

$\left| \begin{matrix} = & =10 & =12 \\ I - R & R \end{matrix} \right| = 0$ will be presented for various media including uniaxial and biaxial media.

5.2.2 Surface Wave Pole

5.2.2.1 A Grounded Isotropic Slab

The first case considered here is shown in Fig. 5-11.

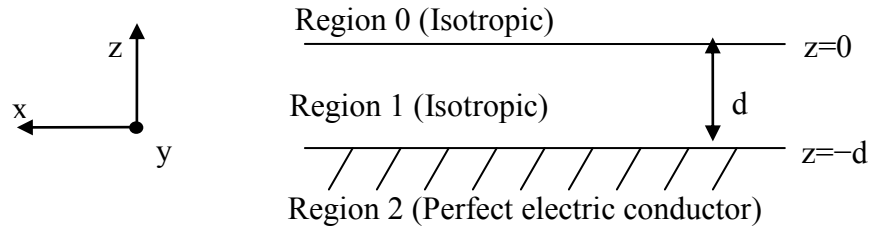


Fig. 5-11: Geometry of the grounded isotropic slab.

Region 0 and Region 1 are isotropic and Region 2 is a perfect electric conductor. Region 0 and Region 1 are assumed to be non-magnetic. The relative permittivities of Region 0 and Region 1 are denoted as ϵ_{0r} and ϵ_{1r} . For convenience, the free space wave number is defined as k_0 where $k_0^2 = \omega^2 \mu_0 \epsilon_0$, ϵ_0 and μ_0 are the permittivity and permeability of free space.

Further, the relation $\begin{vmatrix} I - R & R \\ R & R \end{vmatrix} = 0$ can be reduced to the simple form as follows.

$$\begin{vmatrix} 1 - R_{10}^{hh} R_{12}^{hh} & -R_{10}^{vh} \\ -R_{10}^{hv} & 1 - R_{10}^{vv} R_{12}^{vv} \end{vmatrix} = 0 \quad (5.2-5)$$

Since there is no cross-coupling for an isotropic medium, the corresponding cross-polarized reflection coefficients are zero. Thus, the above formula becomes

$$(1 - R_{10}^{hh} R_{12}^{hh})(1 - R_{10}^{vv} R_{12}^{vv}) = 0 \quad (5.2-6)$$

which is equivalent to

$$(1 - R_{10}^{hh} R_{12}^{hh}) = 0 \quad (5.2-7a)$$

or

$$(1 - R_{10}^{vv} R_{12}^{vv}) = 0 \quad (5.2-7b)$$

Eq. (5.2-7a) is called the guidance condition for the TE wave, which corresponds to the surface wave poles of TE modes, if the structure in Fig. 5-11 is viewed as a waveguide. Eq. (4.2-8b) is called the guidance condition for the TM wave, which corresponds to the surface wave poles of TM modes.

For the surface wave mode, the total internal reflection occurs for the wave incident from Region 1 to Region 0. The normal component k_{0z} of wave vector inside the Region 0 will be purely imaginary. Denoting

$$k_{0z} = i\alpha \quad (5.2-8)$$

Then the half-space reflection coefficients for wave incident from Region 1 to Region 0 can be written as follows

$$R_{10}^{hh} = e^{i2\varphi_{hh}}, \quad R_{10}^{vv} = e^{i2\varphi_{vv}} \quad (5.2-9)$$

where

$$\varphi_{hh} = -\tan^{-1} \frac{\mu_1 \alpha}{\mu_0 k_{1z}}, \quad \varphi_{vv} = -\tan^{-1} \frac{\varepsilon_1 \alpha}{\varepsilon_0 k_{1z}} \quad (5.2-10)$$

If the two-layer geometry is filled with an isotropic medium of thickness “ d ” and backed with PEC, then $R_{12}^{hh} = -1e^{i2k_{1z}d}$ and $R_{12}^{vv} = -1e^{i2k_{1z}d}$. k_{1z} is the normal component of the wave vector for Region 1.

Applying the guidance conditions for both TE and TM modes, we obtain

$$\text{for TE mode } 2\varphi_{hh} + 2k_{1z}d + \pi = 2m\pi, \quad m = 1, 2, \dots \quad (5.2-11)$$

$$\text{for TM mode } 2\varphi_{vv} + 2k_{1z}d + \pi = 2m\pi, \quad m = 0, 1, \dots \quad (5.2-12)$$

Then the guidance conditions for both TE and TM modes can be expanded in the following form.

$$\text{for TE modes} \quad -\cot(k_{1z}d) \frac{\mu_0 k_{1z}}{\mu_1} = \alpha \quad (5.2-13)$$

$$\text{for TM modes} \quad \tan(k_{1z}d) \frac{\varepsilon_0 k_{1z}}{\varepsilon_1} = \alpha \quad (5.2-14)$$

The dispersion relation for the isotropic media of Region 0 and Region 1 (non-magnetic) can be written as

$$k_\rho^2 + k_{0z}^2 = k_0^2 \varepsilon_{0r} \quad (5.2-15)$$

$$k_\rho^2 + k_{1z}^2 = k_0^2 \varepsilon_{1r} \quad (5.2-16)$$

where ε_{0r} and ε_{1r} are relative permittivities of Region 0 and 1, respectively.

Eliminating k_ρ from the above two equations and applying Eq. (5.2-8), the following relation is obtained.

$$k_{1z}^2 + \alpha^2 = k_0^2 (\varepsilon_{1r} - \varepsilon_{0r}) \quad (5.2-17)$$

Combining the guidance conditions in Eq. (5.2-13) and Eq. (5.2-14) for TE mode and TM mode, with the above dispersion relation, Eq. (5.2-17), the tangential components of the wave vector k_ρ for the specific surface wave mode can be determined using the graphical method. One example of two-layer geometry filled with isotropic medium of $\varepsilon_{1r} = 2.55$ and thickness $d = 0.3\lambda_0$ with λ_0 being free space wavelength is shown in Fig. 5-12.

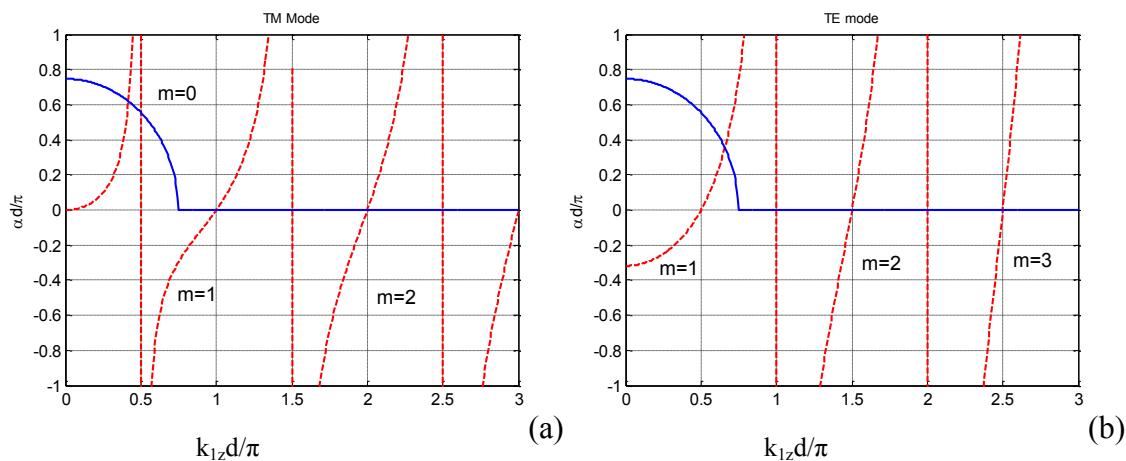


Fig. 5-12: Graphical determination of $k_{1z}d$ for (a) TM and (b) TE modes.

In this example, Region 0 is assumed to be free space with $\epsilon_{0r}=1$. It can be seen from Fig. 5-12 that in this case, TE_1 and TM_0 are the only two propagating modes. It is noted that the dominant TM_0 mode has a zero cutoff frequency.

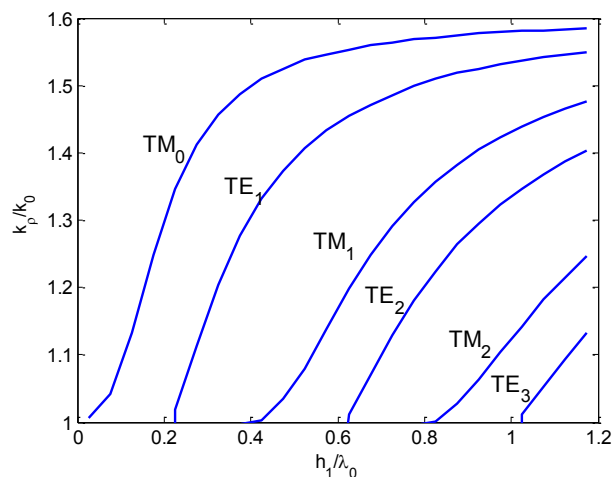


Fig. 5-13: Surface wave propagation constants for a grounded dielectric slab with $\epsilon_{1r}=2.55$, for $d/\lambda_0 = 0$ to 1.2 .

The propagation constants of the first six propagating surface wave modes of a grounded dielectric medium with $\epsilon_{1r}=2.55$ for $d/\lambda_0 = 0$ to 1.2 are calculated by finding the numerical

solution of the guidance conditions and plotted in Fig. 5-13. It is seen from Fig. 5-13 that with the increase of the thickness of the slab, the number of the surface wave modes existing inside the slab also increases.

5.2.2.2 A Grounded Uniaxial Slab

Consider the slab of a uniaxial medium with the optic axis along z-direction as shown in Fig.

5-14. The relative permittivity tensor of uniaxial medium is defined as $\bar{\epsilon}_{1r} = \begin{bmatrix} \epsilon_1 & 0 & 0 \\ 0 & \epsilon_1 & 0 \\ 0 & 0 & \epsilon_{1z} \end{bmatrix}$. For

the purpose of simplicity, the notation of $\bar{\epsilon}_{1r} = (\epsilon_1, \epsilon_1, \epsilon_{1z})$ is used throughout the analysis.

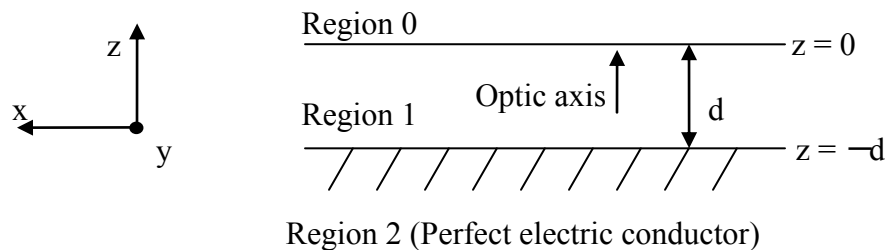


Fig. 5-14: Geometry of the grounded uniaxial slab with the optic axis along z-direction.

It is known that there exist two characteristic waves inside a uniaxial medium – ordinary and extraordinary waves. For an ordinary wave, the electric field is polarized perpendicular to the plane formed by the optic axis and the wave vector, and for an extraordinary wave, the electric field is polarized in the plane formed by the optic axis and the wave vector. When the optic axis is aligned along the z-direction, the ordinary wave will be perpendicular to the incidence plane and the extraordinary wave will be parallel to the incidence plane.

In [65], Type I wave is designated as one of the two characteristics waves with the wave number of plus sign, and Type II wave is designated as the one with the wave number of minus sign. It is noted here that the designations of the Type I and Type II waves won't affect the results presented here. Just to be consistent with the definition used in [65], for a positively uniaxial medium ($\varepsilon_{1z} > \varepsilon_1$), Type I wave is assigned to the extraordinary wave with the larger wave vector surface and Type II wave is assigned to the ordinary wave with the smaller wave vector surface for the example illustrated here.

The unit vectors \hat{e}_I^u , \hat{e}_{II}^u , \hat{e}_I^d , and \hat{e}_{II}^d for the electric field of ordinary and extraordinary waves are shown in Eq. (5.2-18). It is noted here that the subscripts of the unit vectors of \hat{e}_I^u and others indicate the type of wave and the superscripts indicate the direction of a specific propagating wave – upward or downward.

$$\hat{e}_I^u = \begin{bmatrix} \frac{k_x k_{zI}^u}{k_\rho k_s} \\ \frac{k_y k_{zI}^u}{k_\rho k_s} \\ -\frac{\varepsilon_1 k_\rho}{\varepsilon_{1z} k_s} \end{bmatrix}, \quad \hat{e}_I^d = \begin{bmatrix} \frac{k_x k_{zI}^d}{k_\rho k_s} \\ \frac{k_y k_{zI}^d}{k_\rho k_s} \\ -\frac{\varepsilon_1 k_\rho}{\varepsilon_{1z} k_s} \end{bmatrix}, \quad \hat{e}_{II}^u = \hat{e}_{II}^d = \begin{bmatrix} \frac{k_y}{k_\rho} \\ -\frac{k_x}{k_\rho} \\ 0 \end{bmatrix} \quad (5.2-18)$$

$$k_{zI}^u = -k_{zI}^d = \sqrt{k_0^2 \varepsilon_1 - k_\rho^2 \frac{\varepsilon_1}{\varepsilon_{1z}}}, \quad k_s = \sqrt{(k_{zII})^2 + \varepsilon_1^2 k_\rho^2 / \varepsilon_{1z}^2} \quad (5.2-19)$$

$$k_{zII}^u = -k_{zII}^d = \sqrt{k_0^2 \varepsilon_1 - k_\rho^2}, \quad k_\rho = \sqrt{k_x^2 + k_y^2} \quad (5.2-20)$$

where k_x and k_y are the tangential components of the wave vector for any incident wave.

Since Type I and Type II waves are orthogonal to each other (the cross product of the two unit vectors is zero), no cross-polarization exists at the interface of an isotropic medium and a

uniaxial medium, which implies that the reflected field of Type II wave (or Type I wave) from incident Type I wave (or Type II wave) is zero. With the co-polarized reflection coefficients derived for both the Type I and Type II waves incident from Region 1 (uniaxial) to Region 0 (isotropic), the whole reflection matrix $\overset{=10}{R}$ is given as follows.

$$\overset{=10}{R} = \begin{bmatrix} R_{e1e1}^{10} & 0 \\ 0 & R_{e1l1}^{10} \end{bmatrix} \quad (5.2-21)$$

where

$$R_{e1e1}^{10} = \frac{k_{z1}^u - k_{0z} \mathcal{E}_1}{k_{z1}^u + k_{0z} \mathcal{E}_1}, \quad R_{e1l1}^{10} = \frac{k_{z1l}^u - k_{0z}}{k_{z1l}^u + k_{0z}}, \quad R_{e1l1}^{10} = R_{l1e1}^{10} = 0$$

Similarly, the reflection coefficient matrix at the interface of Region 1 (uniaxial medium)

and Region 2 (PEC) denoted as $\overset{=12}{R}$ is given below.

$$\overset{=12}{R} = \begin{bmatrix} R_{e1e1}^{12} \exp[i(-k_{z1}^d + k_{z1}^u)d] & R_{e1l1}^{12} \exp[i(-k_{z1l}^d + k_{z1}^u)d] \\ R_{e1l1}^{12} \exp[i(-k_{z1}^d + k_{z1l}^u)d] & R_{l1e1}^{12} \exp[i(-k_{z1l}^d + k_{z1l}^u)d] \end{bmatrix} \quad (5.2-22)$$

Since

$$\begin{aligned} \hat{e}_1^u &= -\hat{e}_1^d, & \hat{e}_{1l}^u &= \hat{e}_{1l}^d, & \hat{e}_1^u \cdot \hat{e}_{1l}^u &= 0 \\ R_{e1e1}^{12} &= 1, & R_{e1l1}^{12} &= -1, \end{aligned} \quad (5.2-23)$$

We have

$$\overset{=12}{R} = \begin{bmatrix} \exp(i2k_{z1}^u d) & 0 \\ 0 & -\exp(i2k_{z1l}^u d) \end{bmatrix} \quad (5.2-24)$$

As discussed earlier, the Type I wave is polarized with the magnetic field perpendicular to the incidence plane, and the Type II wave is polarized with the electric field perpendicular to the

incidence plane; thus, Type I and Type II waves correspond to TM and TE surface waves, respectively. For convenience, the guidance condition of the surface wave is repeated below.

$$\left| \frac{I - R}{R} \right| = 0 \quad (5.2-25)$$

Substituting Eq. (5.2-22) and Eq. (5.2-24) into Eq. (5.2-25), guidance conditions for TM surface wave (Type I wave) and TE surface wave (Type II wave) inside the uniaxial slab can be obtained through the following derivation.

For TM wave:

$$R_{el}^{10} \exp(i2k_{z1}^u d) = 1 \rightarrow \text{Arg}(R_{el}^{10}) + 2k_{z1}^u d = 2m\pi, \quad m = 0, 1, 2, \dots \quad (5.2-26)$$

$$\text{Arg}(R_{el}^{10}) = \text{Arg}\left(\frac{k_{z1}^u - k_{0z}\epsilon_1}{k_{z1}^u + k_{0z}\epsilon_1}\right) = \text{Arg}\left(\frac{k_{z1}^u - i\alpha\epsilon_1}{k_{z1}^u + i\alpha\epsilon_1}\right) = 2\varphi_{el}, \quad \text{where } \varphi_{el} = -\tan^{-1} \frac{\alpha\epsilon_1}{k_{z1}^u} \quad (5.2-27)$$

$$-\tan^{-1} \frac{\alpha\epsilon_1}{k_{z1}^u} + k_{z1}^u d = m\pi, \quad m = 0, 1, 2, \dots \quad (5.2-28)$$

$$k_{z1}^u \tan(k_{z1}^u d - m\pi) = \alpha\epsilon_1, \quad m = 0, 1, 2, \dots \quad (5.2-29)$$

Using Eq. (5.2-15) (the dispersion relation for isotropic Region 0) together with Eq. (5.2-19) (the dispersion relation for Type I wave of Region 1) and eliminating k_ρ in both equations gives

$$\left(k_{z1}^u\right)^2 \frac{\epsilon_{1z}}{\epsilon_1} + \alpha^2 = k_0^2 (\epsilon_{1z} - \epsilon_{r0}) \quad (5.2-30)$$

Then the propagation constant of the TM surface wave modes can then be obtained using the graphical method by combining both Eq. (5.2-29) and Eq. (5.2-30).

For TE wave:

$$R_{ellell}^{10} \exp(i2k_{zll}^u d) = -1$$

$$\rightarrow \text{Arg}(R_{ellell}^{10}) + 2k_{zll}^u d = (2m-1)\pi, \quad m = 1, 2, \dots \quad (5.2-31)$$

$$\text{Arg}(R_{ellell}^{10}) = \text{Arg}\left(\frac{k_{zll}^u - k_{z0}^u}{k_{zll}^u + k_{z0}^u}\right) = \text{Arg}\left(\frac{k_{zll}^u - i\alpha}{k_{zll}^u + i\alpha}\right) = 2\varphi_{ell}, \quad \varphi_{ell} = -\tan^{-1} \frac{\alpha}{k_{zll}^u} \quad (5.2-32)$$

$$-\tan^{-1} \frac{\alpha}{k_{zll}^u} + k_{zll}^u d = (m - 1/2)\pi, \quad m = 1, 2, \dots \quad (5.2-33)$$

$$k_{zll}^u \tan\left\{k_{zll}^u d - (m - 1/2)\pi\right\} = \alpha, \quad m = 1, 2, \dots \quad (5.2-34)$$

Eliminating k_ρ in both Eq. (5.2-15) and Eq. (5.2-20) (the dispersion relation for isotropic Region 0 and Type II wave of Region 1) gives

$$\left(k_{zll}^u\right)^2 + \alpha^2 = k_0^2(\varepsilon_1 - \varepsilon_{r0}) \quad (5.2-35)$$

Eq. (5.2-34) and Eq. (5.2-35) determine k_ρ for the TE surface wave mode.

Since the optic axis for the uniaxial medium is aligned along the z-axis, the cross-polarized reflection coefficients between Type I and Type II waves are zero. Thus, the guidance conditions of the surface wave modes for the grounded uniaxial slab have a similar form as that of the grounded isotropic slab.

It is also noted here that the dispersion relation for the TE wave of the uniaxial slab of $(\varepsilon_1, \varepsilon_1, \varepsilon_{1z})$ is the same as that of an isotropic slab of ε_1 . However, the dispersion relation for the TM wave is different from that of an isotropic slab with dielectric constant of either ε_1 or ε_{1z} . Thus, it is expected that the TE surface wave of the uniaxial slab is the same as the TE surface wave of the isotropic slab, while the TM surface wave of the uniaxial slab is different from that of the isotropic slab.

One example of using the graphical method to determine the propagation constants for both the TE and TM surface modes is presented here. Assuming the grounded uniaxial slab of $(2.55, 2.55, 4)$, the corresponding surface wave modes (including both TE and TM modes) are shown in Fig. 5-15(a) and in Fig. 5-15(b) for slab thickness of $0.63\lambda_0$ and $1.2\lambda_0$, respectively. To understand the effect of permittivity tensor's variation to the propagating surface wave modes, the propagating constants k_ρ of each mode versus the thickness of the slab corresponding to the four different permittivity tensors are shown in Table 5-1 .

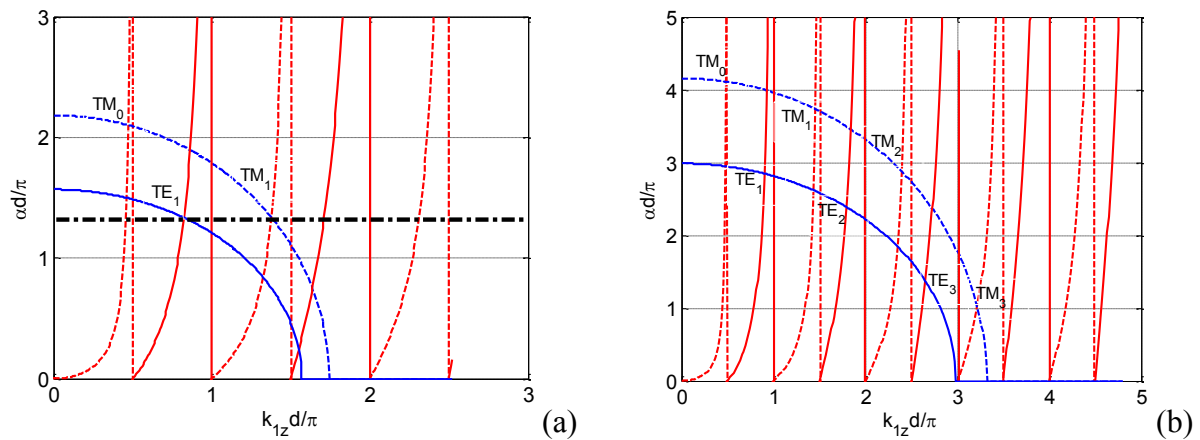


Fig. 5-15: Graphical method to obtain the surface wave modes for a grounded uniaxial slab of $(\varepsilon_1 \ \varepsilon_1 \ \varepsilon_{1z}) = (2.55 \ 2.55 \ 4)$. The slab thickness is (a) $0.63\lambda_0$ and (b) $1.2\lambda_0$.

It is observed in Fig. 5-15(a) that TE_1 and TM_1 modes have the same value of αd , which is around 1.4π as is marked by the black dash line, corresponding to $k_\rho = 1.46k_0$. This is also verified in Table 5-1(d), that is, when the thickness of the slab is $0.63\lambda_0$, TE_1 and TM_1 surface wave modes intersect at $k_\rho = 1.46k_0$. This is an interesting characteristic for a uniaxial slab, which was not observed for a grounded isotropic slab.

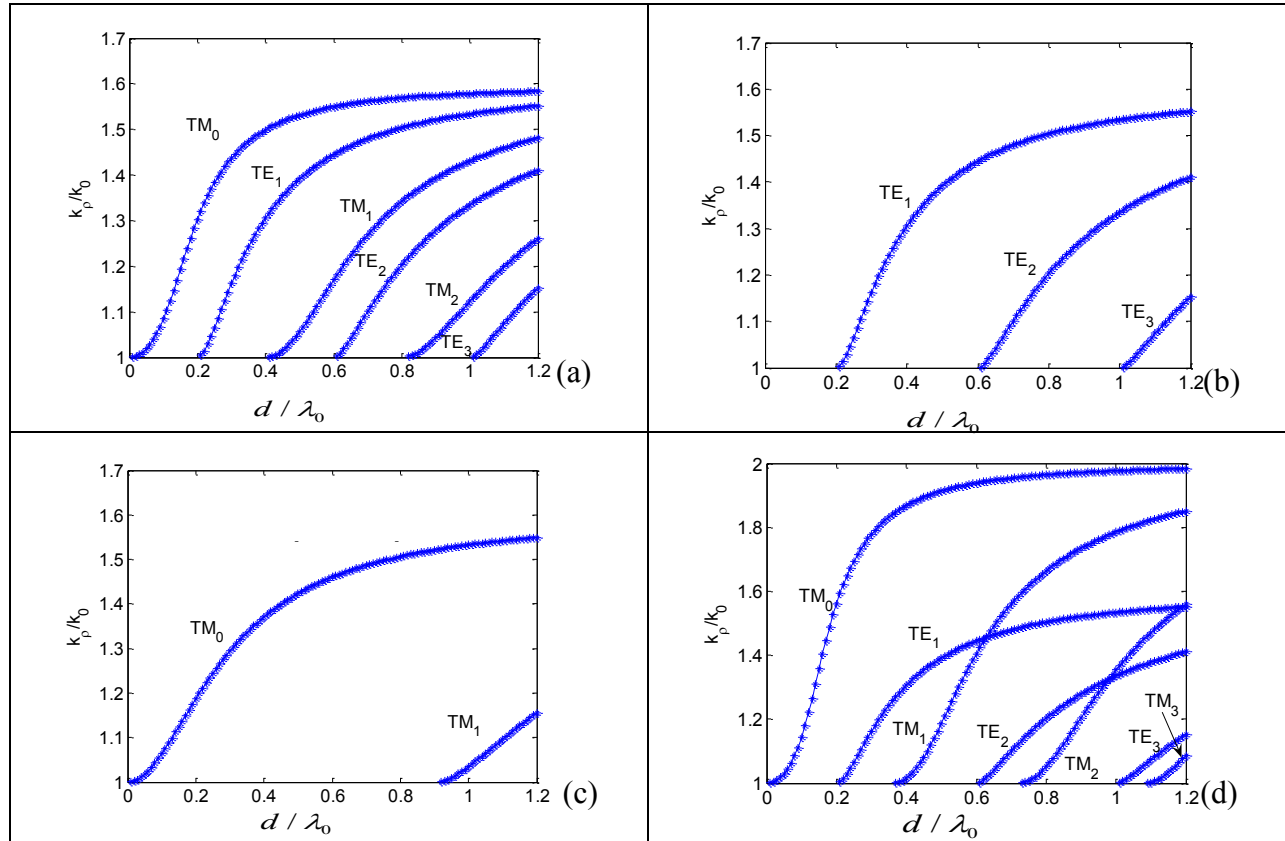


Table 5-1: k_p versus the thickness of the slab for various surface wave modes in a grounded uniaxial slab with (a) $(\epsilon_1, \epsilon_1, \epsilon_{1z}) = (2.55, 2.55, 2.55)$, (b) $(2.55, 2.55, 0.5)$, (c) $(0.5, 0.5, 2.55)$, (d) $(2.55, 2.55, 4)$.

It is also seen in Table 5-1(b) that the TE surface wave modes of a uniaxial slab of $(2.55, 2.55, 0.5)$ are the same as the TE surface wave modes of an isotropic medium of 2.55. It is also apparent that the TM surface wave modes do not exist since $\epsilon_{1z} = 0.5 < 1$. Table 5-1(c) indicates that when $\epsilon_1 < 1$, the TE surface wave modes disappear and only the TM surface wave modes exist. Table 5-1(d) suggests that when $\epsilon_1 > 1, \epsilon_{1z} > 1$, there exist 3 TE surface wave modes and 4 TM surface wave modes. The surface wave mode TM_3 exists in a uniaxial slab, while it doesn't exist for an isotropic slab of 2.55, as seen in Table 5-1(a). For a grounded isotropic slab

of any thickness, either TE or TM surface mode is supported at a specific value of k_ρ . TE and TM surface modes are always separate for different values of k_ρ . However, for a uniaxial slab, both the TE and TM surface wave modes can be supported at the same k_ρ at certain heights as illustrated in Table 5-1(d). The surface wave modes for different combinations of the permittivity of uniaxial medium are summarized in Table 5-2.

Conditions	$\varepsilon_1 > 1$	$\varepsilon_1 < 1$
$\varepsilon_{1z} > 1$	TM and TE	TM
$\varepsilon_{1z} < 1$	TE	None

Table 5-2: Propagating modes for different choices of permittivity

5.2.2.3 *A Grounded Biaxial Slab*

For a grounded isotropic slab and a uniaxial slab with the z-oriented optic axis as shown in the previous sections, TE and TM surface wave modes can be separated from each other, and k_ρ for both modes supported by the slab can be obtained using graphical method by combining the guidance conditions and the dispersion relations.

However, this is not the case for a biaxial slab. Due to the complexity of the permittivity tensor of a biaxial medium, the guidance condition of the surface wave pole ($\left| \begin{matrix} I & -R \\ -R & R \end{matrix} \right| = 0$) for a grounded biaxial slab can no longer be reduced to simple forms with TE and TM surface wave modes differentiated from each other. However, the general rule that the surface wave pole of k_ρ

should be located within the range of $k_0 < k_\rho < k_{\max}^{s2s}$ always applies. k_{\max}^{s2s} is the maximum magnitude of the wave vector on the wave vector surface.

To calculate k_ρ for a specific surface wave mode, the values of $\text{Re}(\tilde{G}_{xx}^{00})$ and $\left| \begin{smallmatrix} \bar{I} & \bar{R} \\ \bar{R} & \bar{I} \end{smallmatrix} \right| = 0$ are plotted versus k_ρ . A grounded biaxial slab of $(\varepsilon_x, \varepsilon_y, \varepsilon_z) = (3, 5, 4)$ with the thickness $d = 0.3\lambda_0$ is considered here. The value of $\text{Re}(\tilde{G}_{xx}^{00})$ versus k_ρ is shown in Fig. 5-16(a), and the determinant $\left| \begin{smallmatrix} \bar{I} & \bar{R} \\ \bar{R} & \bar{I} \end{smallmatrix} \right|$ versus k_ρ is shown in Fig. 5-16(b).

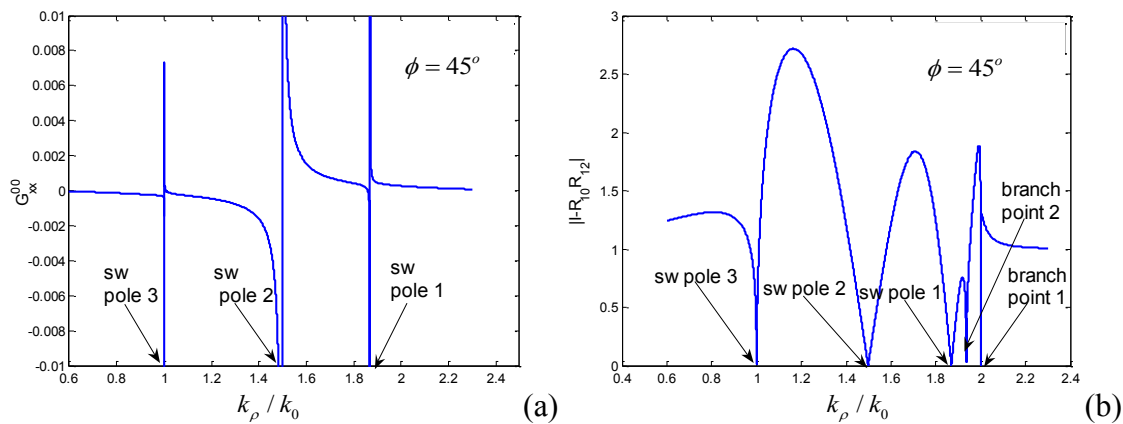


Fig. 5-16: The value of (a) $\text{Re}(\tilde{G}_{xx}^{00})$ and (b) the determinant $\left| \begin{smallmatrix} \bar{I} & \bar{R} \\ \bar{R} & \bar{I} \end{smallmatrix} \right|$ vs. k_ρ for the propagation angle of $\phi = \tan^{-1}(k_y/k_x) = 45^\circ$.

It is seen in Fig. 5-16(b) that there exist certain values of k_ρ where the determinant $\left| \begin{smallmatrix} \bar{I} & \bar{R} \\ \bar{R} & \bar{I} \end{smallmatrix} \right|$ is close to zero. It is numerically verified that these points correspond to the branch points of the biaxial medium and they are marked as branch points in Fig. 5-16(b). However, as shown in Fig. 5-16(a), branch points where $\left| \begin{smallmatrix} \bar{I} & \bar{R} \\ \bar{R} & \bar{I} \end{smallmatrix} \right|$ tends to be zero do not really pose a

singularity for $\text{Re}(\tilde{G}_{xx}^{00})$. The values of $\text{Re}(\tilde{G}_{xx}^{00})$ are still smooth around the branch points. Only those values of k_ρ where the values of $\text{Re}(\tilde{G}_{xx}^{00})$ are discontinuous do truly correspond to the surface wave poles. Thus, it is an interesting discovery here that $\left| \begin{matrix} \bar{I} & \bar{R} \\ \bar{R} & \bar{I} \end{matrix} \right|$ will present the conditions of both the surface wave modes and the branch points. It is assumed the propagation direction is $\varphi = 45^\circ$ in Fig. 5-16. Furthermore, the determinant $\left| \begin{matrix} \bar{I} & \bar{R} \\ \bar{R} & \bar{I} \end{matrix} \right|$ for other propagation directions from 0° to 90° is presented in Fig. 5-17.

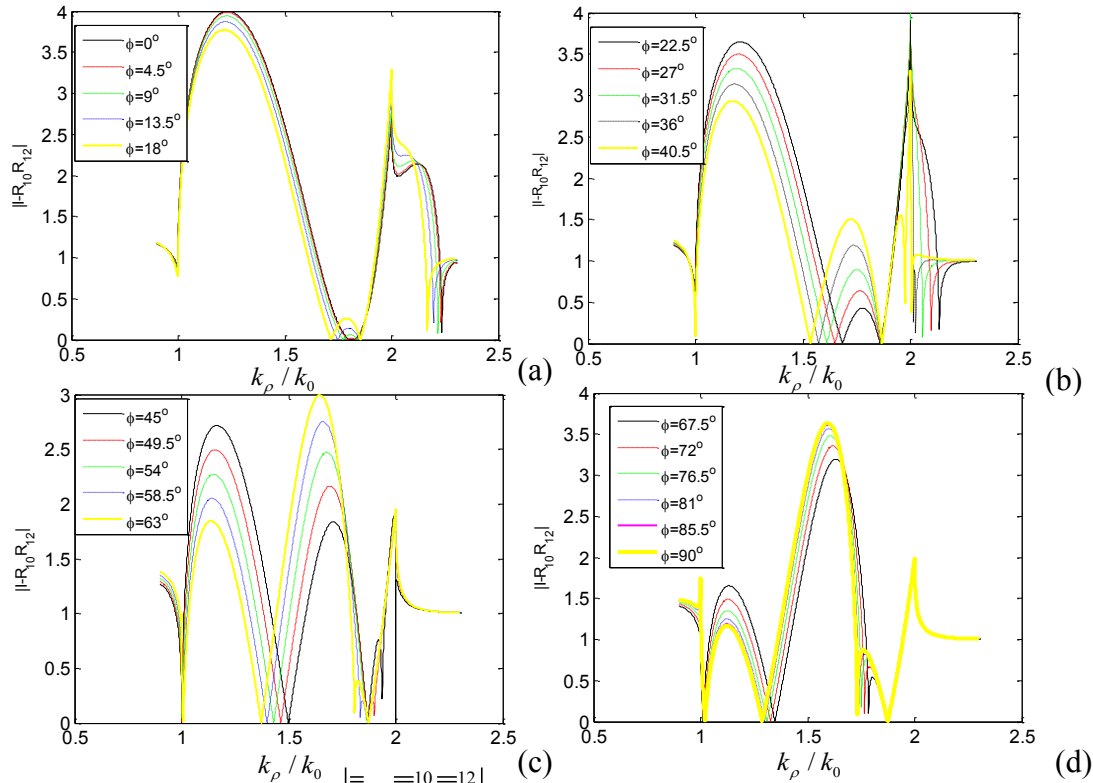


Fig. 5-17: The determinant $\left| \begin{matrix} \bar{I} & \bar{R} \\ \bar{R} & \bar{I} \end{matrix} \right|$ vs. k_ρ for the different propagation angles

$\varphi = \tan^{-1}(k_y/k_x)$ of the surface wave from 0° to 90° .

It is obvious that at 0° of surface wave propagation angle, the tangential propagation constants k_ρ for the first and second surface wave modes are almost the same. With the increase of the propagation angle, the difference between the first and second surface wave modes increases correspondingly. Meanwhile, the third surface wave does not occur until the propagation angle increases up to around 45° . Using the searching criteria discussed above, the full loci for the surface wave and branch points in the $k_x - k_y$ plane are shown in Fig. 5-18.

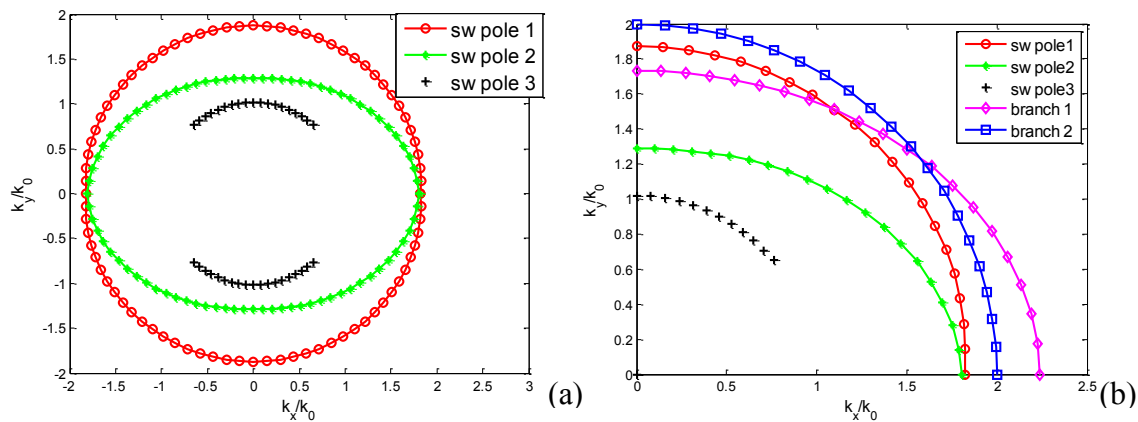


Fig. 5-18: Surface wave poles and branch point loci for a grounded biaxial slab of $(\varepsilon_x, \varepsilon_y, \varepsilon_z) = (3, 5, 4)$ with $d = 0.3\lambda_0$. (a) in all the four quadrants of the $k_x - k_y$ plane, and (b) in the first quadrant of the $k_x - k_y$ plane.

The result is consistent with Fig. 4-42 in [37]. It is noted here that unlike the surface wave locus of a grounded isotropic medium as a circle in the $k_x - k_y$ plane, the surface wave locus for a biaxial medium is usually not a circle and is sometimes even incomplete. Thus for different angles, the dispersion curves for the surface wave modes will also be different. Similar to a grounded isotropic slab, the number of surface wave modes depends on the “electrical thickness” of the medium. The surface wave modes for a conductor backed biaxial slab with a relative permittivity of $(3, 5, 4)$ vs. different thickness for surface wave propagation direction of 0° (

$k_y = 0$) and 90° ($k_x = 0$) are shown in Fig. 5-19(a) and (b), respectively. Same results are obtained using a different method by Pettis in [37].

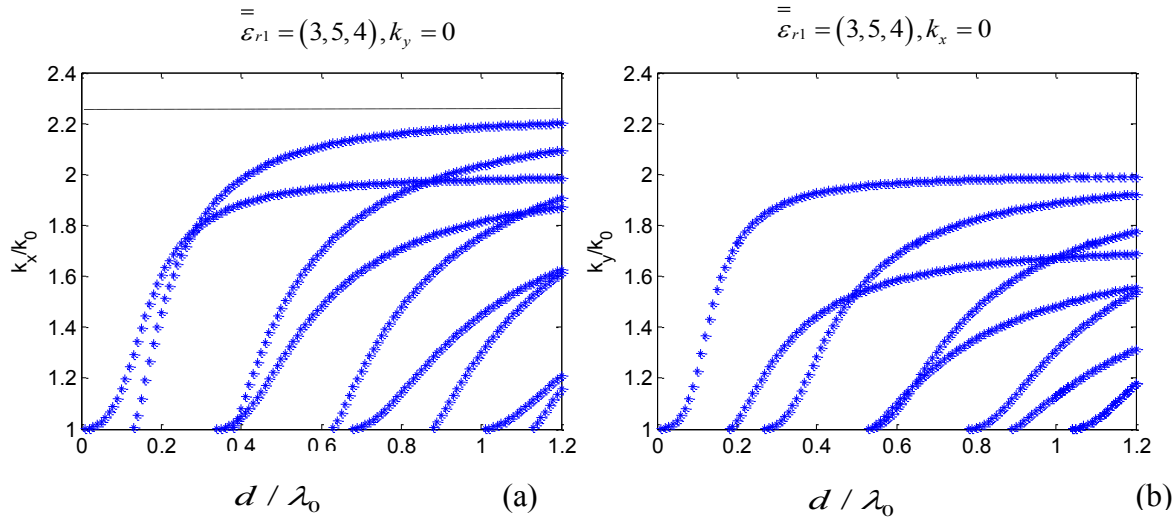


Fig. 5-19: The propagating constant $k_{x,sw}$ (a) (with $k_y = 0$) and (b) $k_{y,sw}$ (with $k_x = 0$) versus the thickness of a biaxial slab for various surface wave modes present in a conductor backed biaxial slab with $(\epsilon_x, \epsilon_y, \epsilon_z) = (3, 5, 4)$.

5.2.2.4 A Grounded Gyroelectric Slab

Since a gyroelectric medium is dispersive, the medium property is dependent on the frequency of the incident wave. According to the specific wave type that can propagate inside a gyroelectric medium, the whole frequency is divided into eight different frequency regions [71]. For convenience, the types of propagating waves for each frequency region are listed in Table 4-1. It is seen in Table 4-1 that Regions 1, 2, 3 and Region 8 always exist. If $\omega_b > \omega_p$, Region 4

and Region 5 cannot exist. If $\omega_b < \frac{\omega_p}{\sqrt{2}}$, Region 6 and Region 7 do not exist. Thus, two different choices of ω_b are considered here.

Case I: $\omega_b = 0.5\omega_p$, Region 6 and Region 7 do not exist.

Case II: $\omega_b = 1.9\omega_p$, Region 4 and Region 5 do not exist.

Provided the direction of the biasing magnetic field (θ_B, φ_B) and the direction of the wave propagation (θ, φ), a second order polynomial about the magnitude of wave vector in this propagating direction can be obtained from the determinant of the electric wave matrix. The coefficients of the polynomial are expressed in terms of $\theta_B, \varphi_B, \theta, \varphi, \omega_b, \omega_p$ and ω . Generally, there exist two solutions to a second order polynomial. Each solution corresponds to the magnitude of the wave vector of a specific type of wave in the predefined propagation direction. The wave vector surfaces of each existing frequency region corresponding to Case I and Case II are plotted in Table 5-3 and Table 5-4, respectively.

It is noted here for Region 1, the frequency is set as $1.01\omega_p$, while for all other existing frequency regions, the operating frequency is always set as the center frequency of the band for the corresponding region. For example, if Region 3 exists, then the wave vector surface is plotted

for the operating frequency as $\omega = \frac{\omega_2 + \max(\omega_b, \omega_p)}{2}$, since Region 3 exists in the band of

$$\max(\omega_b, \omega_p) < \omega < \omega_2.$$

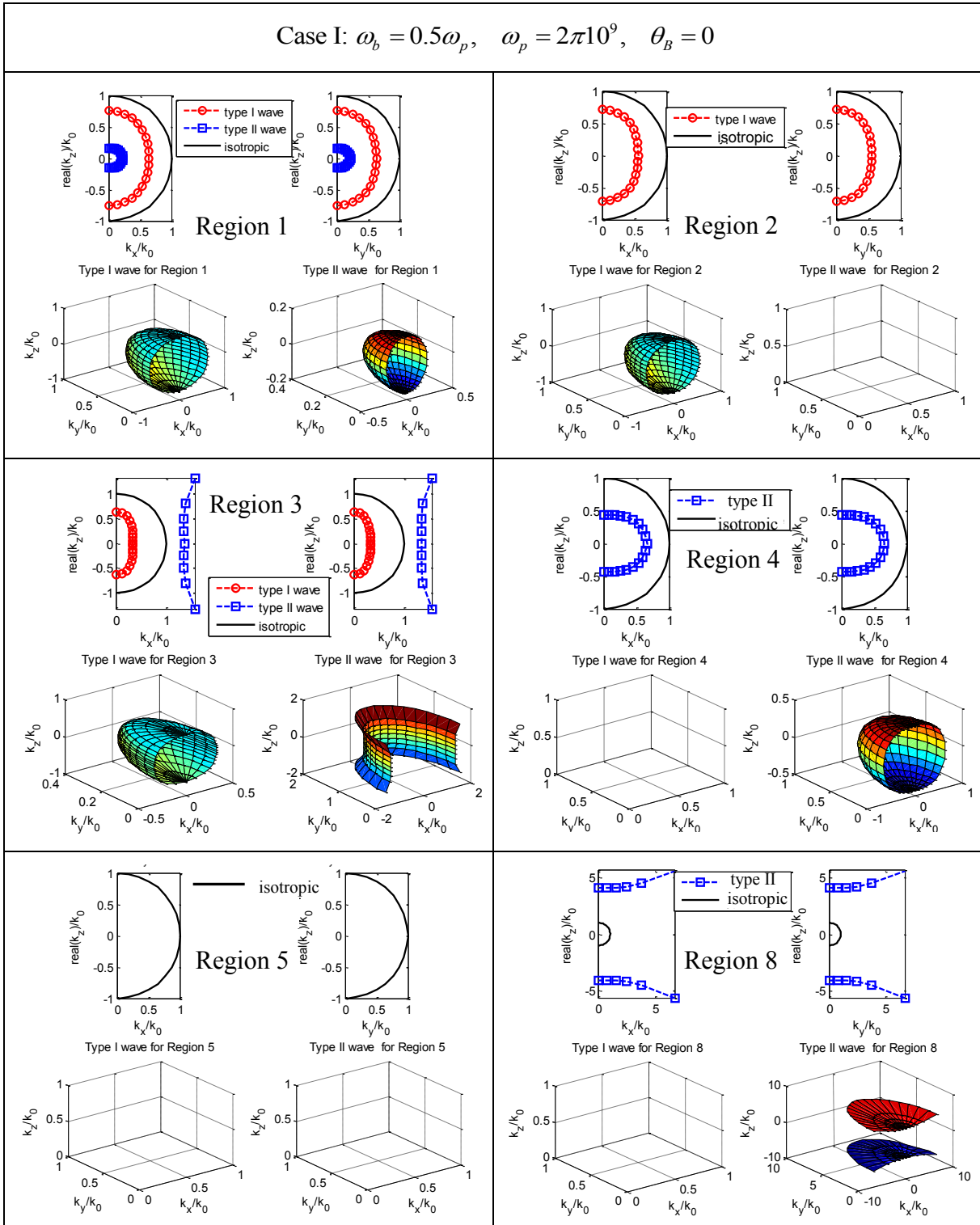


Table 5-3: Wave vector surfaces of all the frequency regions for Case I with the choice of $\omega_b = 0.5\omega_p$.

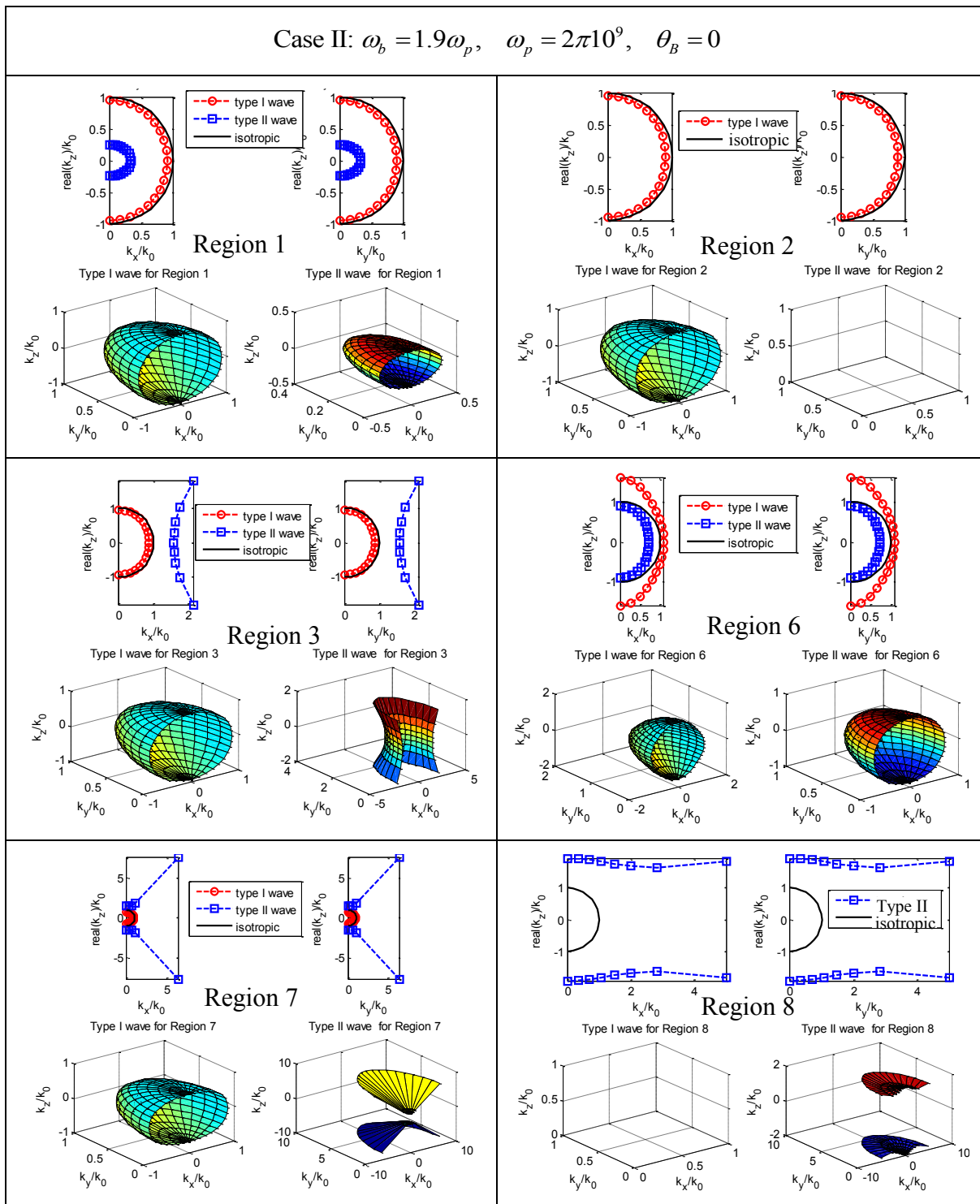


Table 5-4: Wave vector surfaces of all the frequency regions for Case II with the choice of $\omega_b = 1.9\omega_p$.

In Table 5-3 and Table 5-4, there are four subplots for each frequency region. The top left plot shows the real (k_z) versus k_x when $k_y = 0$, while the top right one shows real (k_z) versus k_y when $k_x = 0$. The 3D wave vector surfaces of Type I and Type II waves in the k_x - k_y plane are presented in the bottom left and bottom right subplots, respectively. Some observations from the wave vector surfaces shown in Table 5-3 and Table 5-4 are summarized here.

First, it is noted here that for the commonly existing frequency regions including Regions 1, 2, 3 and 8 for both Case I and Case II, there is no significant difference between the two cases observed for the wave vector surface corresponding to each frequency region. Secondly, both Type I and Type II characteristic waves exist along any propagation direction in Region 1 and Region 6 (which only exists for Case II). In Region 2, the only existing wave is the Type I wave and it can propagate along all directions. In Region 3 and Region 7 (which only exists for Case II), the Type I wave exists along any propagation direction while the Type II wave exists only for certain propagation directions with respect to the biasing magnetic field. In Region 4 (which only exists for Case I), the Type II wave exists for all the propagation directions. In Region 8, the Type II wave exists only for certain propagation directions with respect to the biasing magnetic field. There is no wave propagation in Region 5 (which only exists for Case I).

It is obvious to see from Table 5-3 and Table 5-4 that since the wave vector surfaces of both Type I and Type II waves for Region 1 is within that of the isotropic medium, no surface wave modes exist for a grounded gyroelectric slab in Frequency Region 1. Careful inspection indicates that Regions 3 and 8 for Case I and, Regions 3, 6, 7 and Region 8 for Case II are the only regions where the surface wave possibly exists. Referring to Table 4-1, it is observed that

the surface waves are restricted to the frequency region of $0 < \omega < \sqrt{\omega_b^2 + \omega_p^2}$. This result is consistent with what is obtained in [76].

In general, it is very sophisticated to get the complete surface wave loci for a grounded gyroelectric slab. For the purpose of illustration, the propagating constants of surface wave modes versus different thickness of a grounded gyroelectric slab are presented here for a specific frequency region. Particularly, Region 3 for Case I is considered here since the wave vector surface for frequency Region 3 is quite different from that of an isotropic medium. With the choice $\omega_b = 0.5\omega_p$, $\omega_p = 2\pi \times 10^9$, $\omega = 6.654 \times 10^9$, the permittivity matrices of gyroelectric slabs with the biasing magnetic field along y and z-directions are shown below.

$$\text{Biasing magnetic field along y-direction, } \bar{\varepsilon}_{1r} = \begin{bmatrix} -0.1474 & 0 & -0.5417i \\ 0 & 0.1084 & 0 \\ 0.5417i & 0 & -0.1474 \end{bmatrix}$$

$$\text{Biasing magnetic field along z-direction, } \bar{\varepsilon}_{1r} = \begin{bmatrix} -0.1474 & 0.5417i & 0 \\ -0.5417i & -0.1474 & 0 \\ 0 & 0 & 0.1084 \end{bmatrix}$$

It is seen in Fig. 5-20(a) that when the biasing magnetic field is along the y-direction, the propagation constants of the surface wave modes propagating along the x-direction are bounded within $1.3k_0$. However, there is no upper bound for the surface wave modes propagating along the x-direction when the biasing magnetic field is along the z-direction. This is a different phenomenon from the surface wave modes in grounded isotropic and grounded biaxial slabs. As the wave vector surfaces for the isotropic and biaxial media are closed surfaces, there exists the maximum magnitude of the wave vector along a certain direction. As it is known, propagation

constants of the surface wave modes k_p no longer exist for the region of k_p where it exceeds the maximum magnitude of the wave vector and are always bounded.

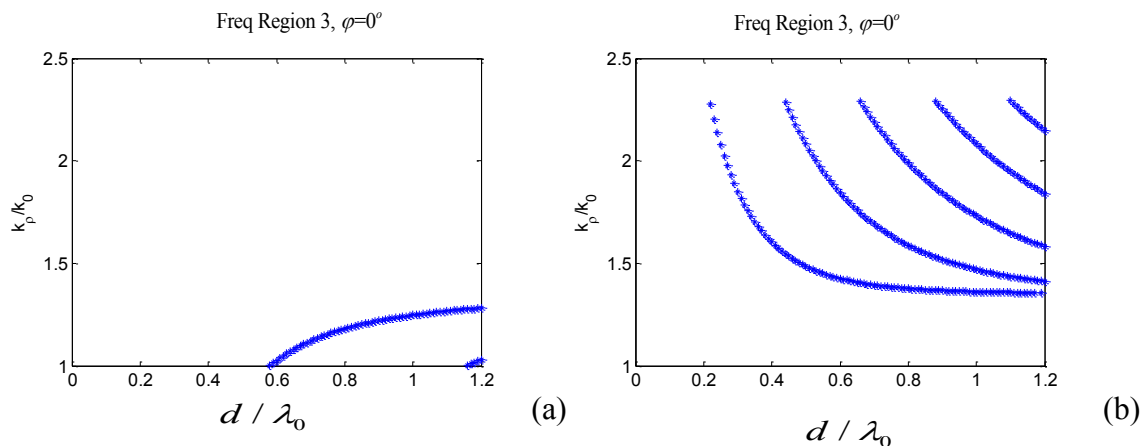


Fig. 5-20: $k_{x,sw}$ obtained with $k_y = 0$ versus the thickness of the gyroelectric slab for various surface wave modes present in a conductor backed gyroelectric slab with the biasing magnetic field along (a) y-direction, and (b) z-direction.

Fig. 5-21 displays the propagation constants of the surface wave modes along the y-direction.

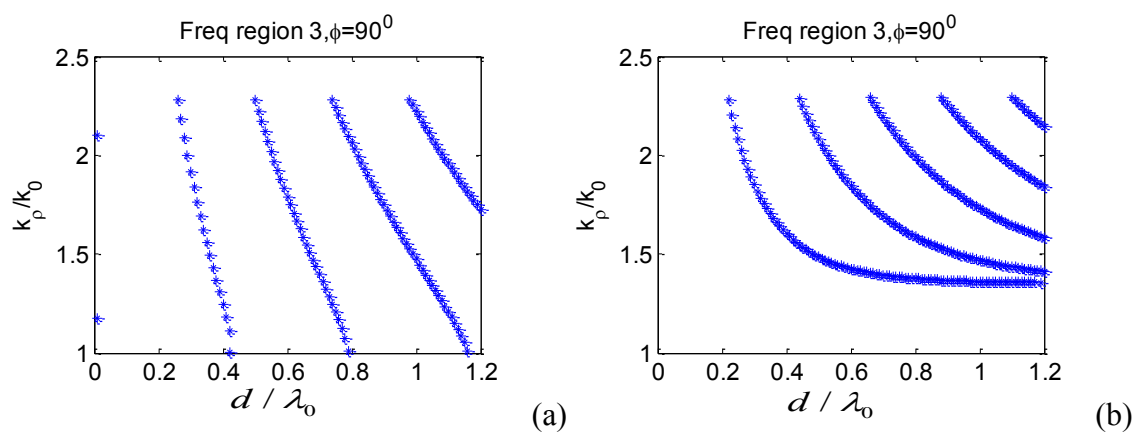


Fig. 5-21: $k_{y,sw}$ obtained with $k_x = 0$ versus the thickness of the gyroelectric slab for various surface wave modes present in a conductor backed gyroelectric slab with biasing magnetic field along (a) y-direction, and (b) z-direction.

As seen in Fig. 5-21, no upper bounds exist for the propagation constants of the surface wave modes for grounded gyroelectric slabs with both the y-directed and z-directed biasing magnetic fields. Another interesting thing noted here is that the y-propagating surface wave modes always exist even for the region of k_p when it is very close to k_0 if the grounded gyroelectric slab is y-directed biased, while y-propagating surface wave modes only exist in the region of k_p where it is larger than $1.6k_0$ if the grounded gyroelectric slab is z-directed biased.

5.3 Current Distribution of a Microstrip Dipole

5.3.1 Current Distribution of a Microstrip Dipole on a Grounded Biaxial Slab

The first numerical validation in this section is to check the current distribution of a printed dipole on a grounded biaxial medium, which were obtained by Pettis [37]. The current distribution can then be used to calculate the input impedance. The antenna is resonant when the reactance (imaginary part of the input impedance) is zero, and the corresponding antenna length is called as the resonant length. There usually exists more than one resonant length, which can be observed from impedance plot since the reactance crosses zeros many times. A half wavelength resonance ($\lambda / 2$) dipole is resonant at the length where the reactance crosses zero for the first time, while a full wavelength resonance (λ) dipole is resonant at the length where the reactance crosses zero for the second time. Since only the current distribution for a λ dipole is presented in [37], for the purpose of comparison, the same case is considered here. The thickness of the biaxial medium is $0.1\lambda_0$ and the width of the dipole is $0.01\lambda_0$.

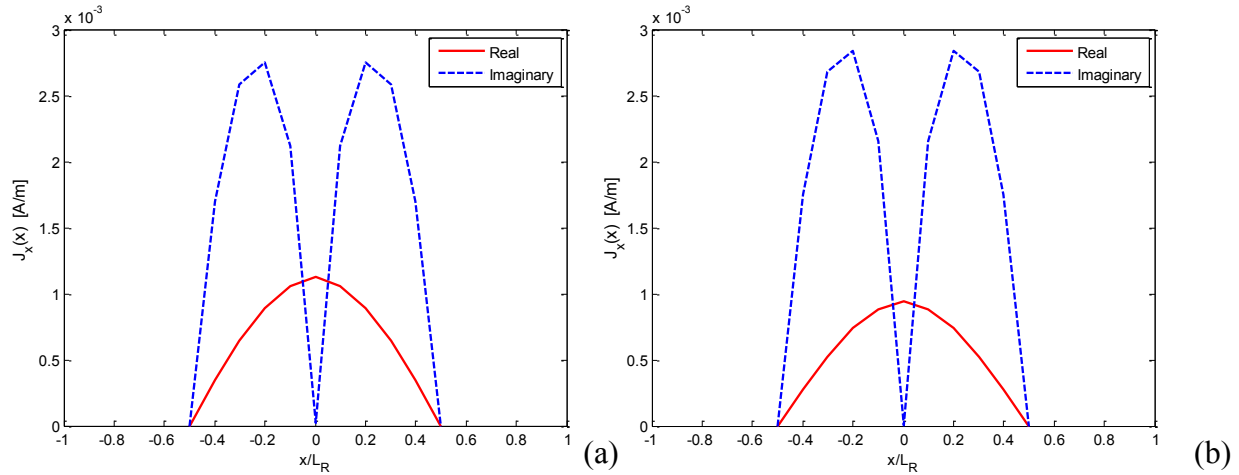


Fig. 5-22: Current distributions of a λ dipole on (a) a unrotated biaxial medium of $(\varepsilon_x, \varepsilon_y, \varepsilon_z) = (5, 3, 4)$ and (b) a rotated biaxial medium with $(\alpha, \beta, \gamma) = (10^\circ, 20^\circ, 30^\circ)$.

Fig. 5-22(a) presents the current distribution when the dipole is on an unrotated biaxial medium with principal permittivity of $(\varepsilon_x, \varepsilon_y, \varepsilon_z) = (5, 3, 4)$. Fig. 5-22(b) shows the current distribution for the λ dipole when the biaxial medium is rotated by $(\alpha, \beta, \gamma) = (10^\circ, 20^\circ, 30^\circ)$. It is shown in Fig. 5-22 that the current density is likely to be symmetric about the feeding point ($N/2$) regardless of the rotation of the medium. Meanwhile, the current density for a resonant dipole is complex along the dipole except at the feeding point. At the feeding point, the current is purely real. Hence, the input impedance is purely real. Also, the magnitudes for both the real and imaginary parts of the current density for a resonant dipole agree very well with the results in [37]. It has been found that the resonant lengths of the dipole on unrotated and rotated biaxial media are $0.4648\lambda_0$ and $0.4654\lambda_0$. Comparing with the resonant lengths of $0.4754\lambda_0$ and $0.4751\lambda_0$ obtained in [37], the relative difference is within 5%.

5.3.2 Current Distribution for a Microstrip Dipole on a Grounded Gyroelectric Slab

The current distribution of a $\lambda/2$ resonant length dipole on a grounded gyroelectric slab is shown in this section. For the purpose of illustration, plasma frequency and gyrofrequency are chosen as $\omega_p = 2\pi 10^9 \text{ rad/s}$, $\omega_b = 0.5\omega_p$ and the operating frequency is $\omega = 2\pi \times 1.059 \times 10^9 \text{ rad/s}$. Thus, the permittivity matrices are shown below.

Biassing magnetic field along x-direction gives

$$\begin{aligned} \theta_B &= 90^\circ, \quad \varphi_B = 0^\circ \\ \varepsilon_{1r} &= \begin{bmatrix} 0.1083 & 0 & 0 \\ 0 & -0.1475 & 0.5418i \\ 0 & -0.5418i & -0.1475 \end{bmatrix} \end{aligned} \quad (5.3-1)$$

Biassing magnetic field along z-direction gives

$$\begin{aligned} \theta_B &= 0^\circ \\ \varepsilon_{1r} &= \begin{bmatrix} -0.1475 & 0.5418i & 0 \\ -0.5418i & -0.1475 & 0 \\ 0 & 0 & 0.1083 \end{bmatrix} \end{aligned} \quad (5.3-2)$$

Biassing magnetic field along y-direction gives

$$\begin{aligned} \theta_B &= 90^\circ, \quad \varphi_B = 90^\circ \\ \varepsilon_{1r} &= \begin{bmatrix} -0.1475 & 0 & -0.5418i \\ 0 & 0.1083 & 0 \\ 0.5418i & 0 & -0.1475 \end{bmatrix} \end{aligned} \quad (5.3-3)$$

First, the current distribution along the thin dipole on a grounded gyroelectric medium with the x-directed biasing magnetic field is displayed in Fig. 5-23. The x-axis indicates the normalized coordinate along thin dipole with respect to the resonant length of $0.7992\lambda_0$, while the y-axis shows the real part of the current along the thin dipole. The curves with the square

marker, the circle marker, and the dashed line correspond to the cases when the subdivisions along the dipole are $N=6$, 12 , and 16 . It is observed that the peak current at the feeding point tends to converge with the increase of the subdivision along the thin dipole. It is seen that subdivisions of $N=12$ are a good estimate and will be used in the following numerical calculation.

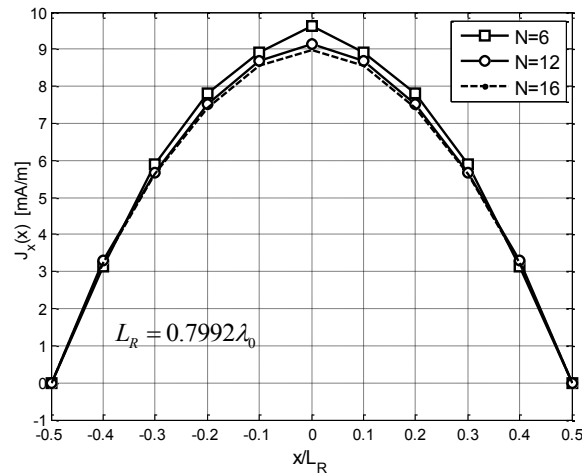


Fig. 5-23: Current distribution of $\text{Re}(J(x))$ for a $\lambda/2$ dipole on gyroelectric medium with $\omega = 2\pi \times 1.059 \times 10^9 \text{ rad/s}$, $\omega_p = 2\pi 10^9 \text{ rad/s}$, $\omega_b = 0.5\omega_p$ and the biasing magnetic field along x-direction ($\theta_B = 90^\circ$, $\varphi_B = 0^\circ$). $h = 0.1\lambda_0$, $W = 0.01\lambda_0$. $N=6$, $N=12$ and $N=16$.

The current distributions for a dipole on gyroelectric substrates with the biasing magnetic field along z-direction and y-direction are shown in Fig. 5-24(a) and (b), respectively. The solid line indicates the real part, and the dashed line indicates the imaginary part of the current distribution. It is interesting to note here that for both the x- and z- oriented biasing magnetic fields, the $\text{Re}(J(x))$ and $\text{Im}(J(x))$ are always symmetric. Specifically, similar phenomenon is observed for the current distribution of the dipole on biaxial medium when $M=1$ [37, p. 374].

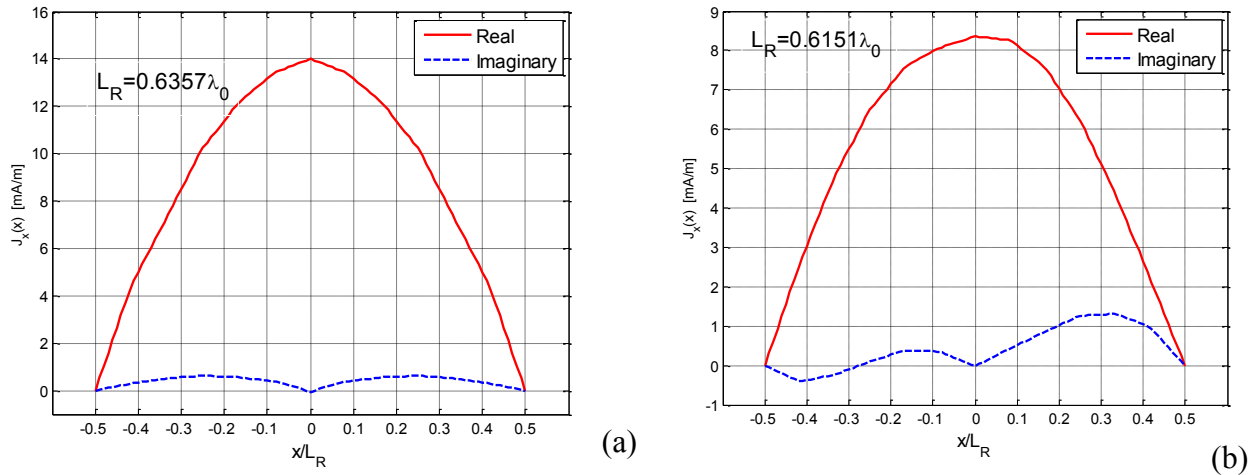


Fig. 5-24: Current distribution of $\text{Re}(J(x))$ and $\text{Im}(J(x))$ for a $\lambda/2$ dipole on a gyroelectric medium with $\omega = 2\pi \times 1.059 \times 10^9 \text{ rad/s}$, $\omega_p = 2\pi 10^9 \text{ rad/s}$, $\omega_b = 0.5\omega_p$ and the biasing magnetic field along (a) the z-direction ($\theta_B = 0^\circ$) and (b) the y-direction ($\theta_B = 90^\circ, \varphi_B = 90^\circ$). $h = 0.1\lambda_0$, $W = 0.01\lambda_0$. $N=12$.

However, when the biasing magnetic field is along the y-direction, the current distribution is no longer symmetric with respect to the feeding point as shown in Fig. 5-24(b). Asymmetric current distribution along the dipole may occur due to the non-reciprocal nature of the gyroelectric medium, which is not observed for a microstrip dipole on isotropic and biaxial media. Asymmetry in the current of a guided wave structure on a multilayered medium, including a ferrite material layer, has been reported in [77]. Another interesting phenomenon observed here is that the resonant length of a microstrip dipole is larger than half of the free space wavelength, and the resonant length of a microstrip dipole varies with the direction of the biasing magnetic field. The largest resonant length occurs at $0.7992\lambda_0$ when the biasing magnetic field is along the direction of the current distribution (x-direction). With the biasing magnetic field along both the y- and z-directions, the resonant lengths are $0.6151\lambda_0$ and

$0.6357\lambda_0$, respectively. With the current distribution calculated, other antenna parameters such as input impedance and directive gain can be obtained, correspondingly. Detailed discussion on the antenna parameters will be shown in the next section.

5.4 Antenna Parameters

With calculated current distribution of a printed dipole, the input impedance, resonant length and radiation pattern can easily be obtained and the formulations can be found in the extensive literature [4, 8, and 37]. In Section 5.4.1, the formulations of the input impedance and radiation pattern obtained from the current distribution are first presented. Then, Section 5.4.2 shows the numerical validation of antenna parameters for printed dipoles on various grounded substrates including isotropic, biaxial and ferrite media. Finally, a detailed parametric analysis is presented to study the effect of biasing field and operating frequency on the radiation of a microstrip dipole printed on a grounded gyroelectric substrate.

5.4.1 Formulations of Input Impedance and Radiated field

5.4.1.1 Input Impedance

The input impedance of a network can be calculated using

$$Z_{in} = \frac{P_s}{I_{in}I_{in}^*} \quad (5.4-1)$$

where P_s is the input power and I_{in} is the total input current.

Two variables of P_s and I_{in} need to be calculated here to obtain the input impedance. The complex input power delivered to the antenna is defined as

$$P_s = -\iint_{S'} \bar{E}_s \cdot \bar{J}_s^* ds' \quad (5.4-2)$$

where \bar{E}_s is the electric field generated from the surface currents.

It is known from the boundary condition that the electric field generated from the surface currents is equal to and opposite of the impressed electric field vector at the impressed source location and is zero everywhere else as discussed in Eq. (5.1-10). Thus,

$$P_s = \iint_{S'} \bar{E}_{\tan}^{imp} \cdot \bar{J}_s^* ds' \quad (5.4-3)$$

\bar{E}_{\tan}^{imp} is the impressed electric field and \bar{J}_s is the induced current generated by the impressed electric field.

Substituting the impressed electric field Eq. (5.1-9) and the current distribution Eq. (5.1-12) into the above equation gives

$$P_s = \iint_{S'} ds' \left\{ \delta(x-x_f) \left[u\left(y - \left(y_f - \frac{W}{2}\right)\right) - u\left(y - \left(y_f + \frac{W}{2}\right)\right) \right] \hat{x} \cdot \hat{x} \sum_{m=1}^{M(N-1)} a_m^* J_x^{m*}(x') J_x^{m*}(y') \right\} \quad (5.4-4)$$

If N is even, then the above formula reduces to

$$P_s = \sum_{q=1}^M \left[a_{(q-1)(N-1)+N/2} J_x^{[(q-1)(N-1)]}(x_c) \right]^* \quad (5.4-5)$$

Furthermore, since triangular sub domain basis functions are used with $J_x(x_c) = 1$, the power delivered to the source can be further simplified as

$$P_s = \sum_{q=1}^M \left[a_{(q-1)(N-1)+N/2} \right]^* \quad (5.4-6)$$

The next step is to calculate the input current. As N is an even number, the input current I_{in} is given by integrating the surface current flowing in the longitudinal direction at $x = x_c$.

Hence,

$$I_{in} = \int_{-W/2}^{W/2} dy J_x(x_c) J_x(y) = \sum_{q=1}^M [a_{(q-1)(N-1)+N/2}] \quad (5.4-7)$$

Thus, the input impedance

$$Z_{in} = \frac{P_s}{I_{in} I_{in}^*} = \frac{1}{\sum_{q=1}^M [a_{(q-1)(N-1)+N/2}]} \quad (5.4-8)$$

In the simple case when $M=1$ and N is even,

$$Z_{in} = \frac{1}{a_{N/2}} \quad (5.4-9)$$

5.4.1.2 Radiation Behavior

Similar to the formulations for the far field of a Hertzian dipole shown in Chapter 4, the method of stationary phase can be applied to the integral for the radiated field of a microstrip dipole to determine the radiated power. With given Green's function and the current distribution of the printed dipole, the final expression of the far field is given in [37], which is repeated here for convenience.

$$\bar{E}_0(r) \approx \frac{i\omega\mu_0}{4\pi r} e^{ik_0 r} \left\{ \begin{array}{l} \hat{h}^+ \left[\hat{h}^+ e^{-ik_0 z'} + R_{hh} \hat{h}^- e^{ik_0 z'} + R_{vh} \hat{v}^- e^{ik_0 z'} \right] + \\ \hat{v}^+ \left[\hat{v}^+ e^{-ik_0 z'} + R_{hv} \hat{h}^- e^{ik_0 z'} + R_{vh} \hat{v}^- e^{ik_0 z'} \right] \end{array} \right\} \cdot \hat{J}_s(k_x, k_y) \quad (5.4-10)$$

$\tilde{\mathbf{J}}_s(k_x, k_y)$ is the Fourier transform of the current distribution $\bar{\mathbf{J}}_s$. It's noted here that if the current source is a delta source as for a Hertzian dipole, then $\tilde{\mathbf{J}}_s(k_x, k_y) = 1$. Eq. (5.4-10) reduces to Eq. (4.2-10), which is the radiated field of a Hertzian dipole in the presence of a layered reciprocal medium. Since the coordinate system for the microstrip dipole is chosen such that dipole is located at $z=0$, the expression above is reduced to the following form.

$$\bar{\mathbf{E}}_0(r) \approx \frac{i\omega\mu_0}{4\pi r} e^{ik_0 r} \left\{ \begin{array}{l} \hat{\mathbf{h}}^+ \left[\hat{\mathbf{h}}^+ + R_{hh} \hat{\mathbf{h}}^- + R_{vh} \hat{\mathbf{v}}^- \right] + \\ \hat{\mathbf{v}}^+ \left[\hat{\mathbf{v}}^+ + R_{hv} \hat{\mathbf{h}}^- + R_{vh} \hat{\mathbf{v}}^- \right] \end{array} \right\} \cdot \tilde{\mathbf{J}}_s(k_x, k_y) \quad (5.4-11)$$

where $k_x = k_0 \sin \theta \cos \varphi$, $k_y = k_0 \sin \theta \sin \varphi$.

According to the definitions of the field vectors for horizontally and vertically polarized waves,

$\hat{\mathbf{h}}^+$, $\hat{\mathbf{v}}^+$ can be related with unit vectors in the spherical coordinate system as follows.

$$\hat{\mathbf{h}}^\pm = -\hat{\mathbf{a}}_\varphi, \quad \hat{\mathbf{v}}^\pm = -\hat{\mathbf{a}}_\theta \quad (5.4-12)$$

So in the spherical coordinate system, the far field in Region 0 can be approximated as

$$\bar{\mathbf{E}}_0(r) \approx -\frac{i\eta_0}{4\pi r} e^{ik_0 r} \left\{ \hat{\mathbf{a}}_\varphi E_\varphi + \hat{\mathbf{a}}_\theta E_\theta \right\} \quad (5.4-13)$$

where

$$\begin{aligned} E_\varphi &= k_0 \left[\hat{\mathbf{h}}^+ + R_{hh} \hat{\mathbf{h}}^- + R_{vh} \hat{\mathbf{v}}^- \right] \cdot \tilde{\mathbf{J}}_s(k_x, k_y) \\ E_\theta &= k_0 \left[\hat{\mathbf{v}}^+ + R_{hv} \hat{\mathbf{h}}^- + R_{vh} \hat{\mathbf{v}}^- \right] \cdot \tilde{\mathbf{J}}_s(k_x, k_y) \end{aligned}$$

5.4.1.3 Antenna Gain

The directive gain of an antenna D is defined as the ratio of the radiation intensity in a particular direction to the radiation intensity of an isotropic antenna with the same amount of total radiated power. Mathematically, it is given by Balanis [78, p. 39]

$$D(\theta, \varphi) = 4\pi \frac{U(\theta, \varphi)}{\int_0^{2\pi} \int_0^{\pi/2} U(\theta, \varphi) \sin \theta d\theta d\varphi} \quad (5.4-14)$$

where $U(\theta, \varphi)$ is the radiation intensity, given as

$$U(\theta, \varphi) = \frac{1}{2} \frac{\eta_0}{(4\pi)^2} \left[|E_\theta|^2 + |E_\varphi|^2 \right] \quad (5.4-15)$$

The directivity of an antenna is then given by

$$D_g = 4\pi \frac{\left[|E_\theta|^2 + |E_\varphi|^2 \right]_{\max}}{\int_0^{2\pi} \int_0^{\pi/2} \left[|E_\theta|^2 + |E_\varphi|^2 \right] \sin \theta d\theta d\varphi} \quad (5.4-16)$$

5.4.2 Numerical Validation with Printed Dipoles on Various Media

5.4.2.1 A Printed Dipole on an Isotropic Slab

In order to validate our calculation of the input impedance, the results obtained here are compared with those in the published literature and from the commercial software – Ansoft Designer. Input impedances of the microstrip dipole on isotropic slabs of two different thicknesses are calculated here.

The first example is accomplished by calculating the input impedance of a $0.01\lambda_0$ wide microstrip dipole on substrate of $h_1 = 0.0796\lambda_0$ with dielectric constant 3.25. λ_0 is the free space

wavelength. The result of this example can be found in [37, p.421]. The second example is to calculate the input impedance of a $0.001\lambda_0$ wide microstrip dipole on a substrate of $h_1 = 0.2\lambda_0$ with dielectric constant 2.45. The numerical results for this example appear in Yang et al. [79]. As presented in detail in Chapter 2, the dyadic Green's function of an anisotropic medium is no longer valid if the medium reduces to an isotropic medium. Thus, the relative permittivity tensors were set to $(\epsilon_x, \epsilon_y, \epsilon_z) = (3.25, 3.25, 3.251)$ and $(\epsilon_x, \epsilon_y, \epsilon_z) = (2.45, 2.45, 2.451)$ in order to simulate a printed dipole on a grounded isotropic slab using the code developed here.

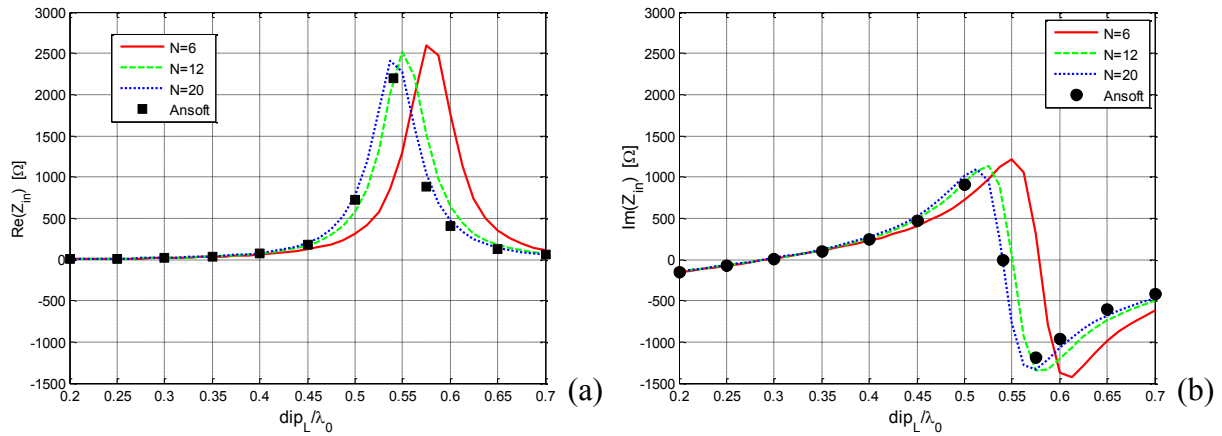


Fig. 5-25: (a) Real and (b) imaginary parts of the input impedance of a printed dipole on an isotropic substrate of $(\epsilon_x, \epsilon_y, \epsilon_z) = (3.25, 3.25, 3.251)$ with the dipole width of $0.01\lambda_0$. The height of the slab is $0.0796\lambda_0$.

For the first example, the input impedances of the microstrip dipole with various lengths are simulated and compared with the results obtained using Planar EM solver of Ansoft Designer. The real part of the input impedance is shown in Fig. 5-25(a) and the imaginary part of the input impedance is shown in Fig. 5-25(b). For the dipole width of $0.01\lambda_0$, it has been carefully checked that the integral of the matrix elements converges with integration range of k_x and k_y up

to $120k_0$. In addition to the integration range, different number of basis functions is also chosen to check the convergence of the integration. The solid line, dashed line, and dotted line in Fig. 5-25 correspond to the number of the basis functions $N=6$, $N=12$, and $N=20$. The results obtained using Ansoft Designer are plotted in Fig. 5-25 using the curve with square maker. It is noted here that $M=1$ for all cases. It is observed from the Fig. 5-25(b) that the resonant length is approximately $0.57\lambda_0$ for $N=6$. This matches closely with the result obtained in [37], which assumes the same number of the basis functions. When the number of the basis function is increased to $N=20$, the resonant length converges to $0.54\lambda_0$, which is almost at the resonant length obtained using the Ansoft Designer.

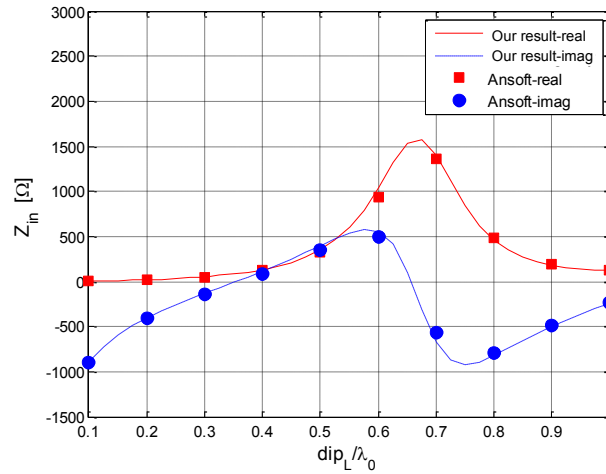


Fig. 5-26: Input impedance for gap-fed dipole with width of $0.001\lambda_0$ printed on an isotropic substrate with $(\epsilon_x, \epsilon_y, \epsilon_z) = (2.45, 2.45, 2.451)$. The height is $0.2\lambda_0$.

The second example considered here (Fig. 5-26) is for the dipole width of $0.001\lambda_0$. Due to a much narrower dipole width, the integration range for k_x and k_y is up to $340k_0$ to get the converged integral. The number of the basis functions is chosen as $N=12$ and $M=1$. Again, the

input impedances versus the different dipole length obtained using the method proposed here are compared with the results obtained from the Ansoft Designer, as shown in Fig. 5-26. It is seen from Fig. 5-25 and Fig. 5-26 that input impedances for various lengths obtained using the method developed here closely match the results obtained from the commercial software. Resonant length for this case is between $0.6\lambda_0$ and $0.7\lambda_0$, which also agrees very well with the published results in [80].

5.4.2.2 *A Printed Dipole on a Grounded Biaxial Slab*

The first example considered is the printed dipole on grounded biaxial medium. Previously, a good agreement with [37] has been observed for the current distribution of a λ dipole on an unrotated biaxial medium of $(\epsilon_x, \epsilon_y, \epsilon_z) = (5, 3, 4)$ as shown in Fig. 5-22. In this section, we present the results for the input impedance and the radiation pattern of the printed dipole on a biaxial anisotropic medium. The real part and imaginary parts of the input impedances versus different dipole lengths when the thickness of the grounded biaxial slab varies from $0.05\lambda_0$ to $0.15\lambda_0$ are displayed in in Fig. 5-27 (a) and (b). A careful comparison with what is obtained in Fig. 7-29 and Fig. 7-30 in [37] shows that for each different thickness of the slab, our results based on eigen-decomposition DGF are almost identical with the results obtained using transition-matrix DGF in [37] with a slight deviation around the second resonance point. Employing only five triangular subdomain basis functions yielded results that were within approximately 5% of the results in [37].

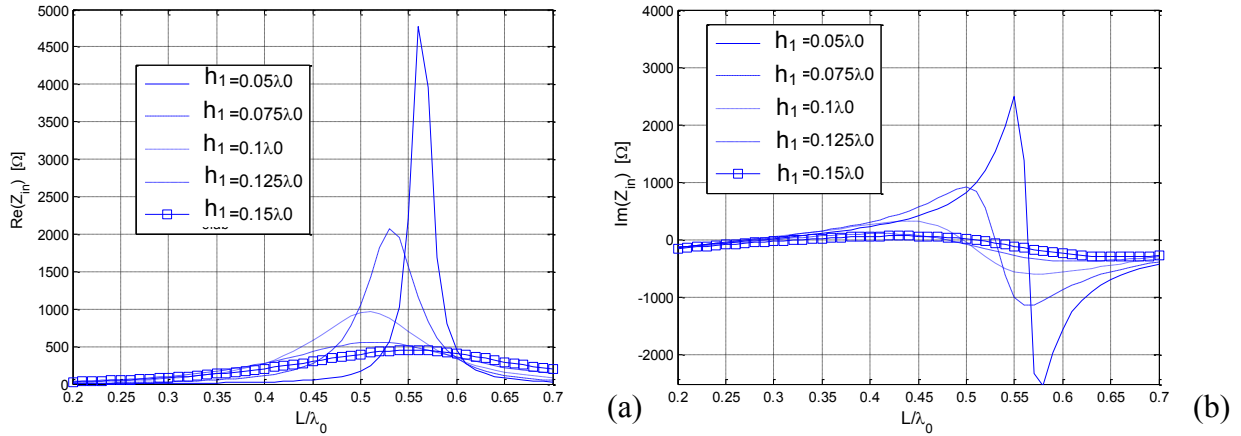


Fig. 5-27: (a) Real and (b) imaginary parts of the input impedance vs. dipole length of a microstrip dipole on an unrotated biaxially anisotropic medium of $(\epsilon_x, \epsilon_y, \epsilon_z) = (5, 3, 4)$. The dipole width is $0.01\lambda_0$.

Furthermore, the effect of rotation angles to the resonant length has been studied in detail in [37]. Similar results are presented here in Fig. 5-28 — Fig. 5-29 to verify with what is obtained in Fig. 7-31 — Fig. 7-38 of [37]. Good agreement is observed. With $\alpha = 0^\circ$ and $\gamma = 0^\circ$, the effects of the rotation angle β to the input impedance and resonant length are calculated and plotted in Fig. 5-28. Fig. 5-28(a1) and (b1) show the real part of the input impedance vs. the thickness of the biaxial slab with different rotation angles β of 0° , 30° , 60° , and 90° using the transition matrix method [37] and our method, respectively. Fig. 5-28(a2) and (b2) show the resonant length vs. the thickness of the biaxial slab with different rotation angle β of 0° , 30° , 60° , and 90° using the transition matrix method and our method, respectively. As indicated in the plots, the resonant length of the printed dipole decreases by around $0.01\lambda_0$ to $0.02\lambda_0$ depending on the thickness of the slab, while the real part of input impedance is almost kept constant.

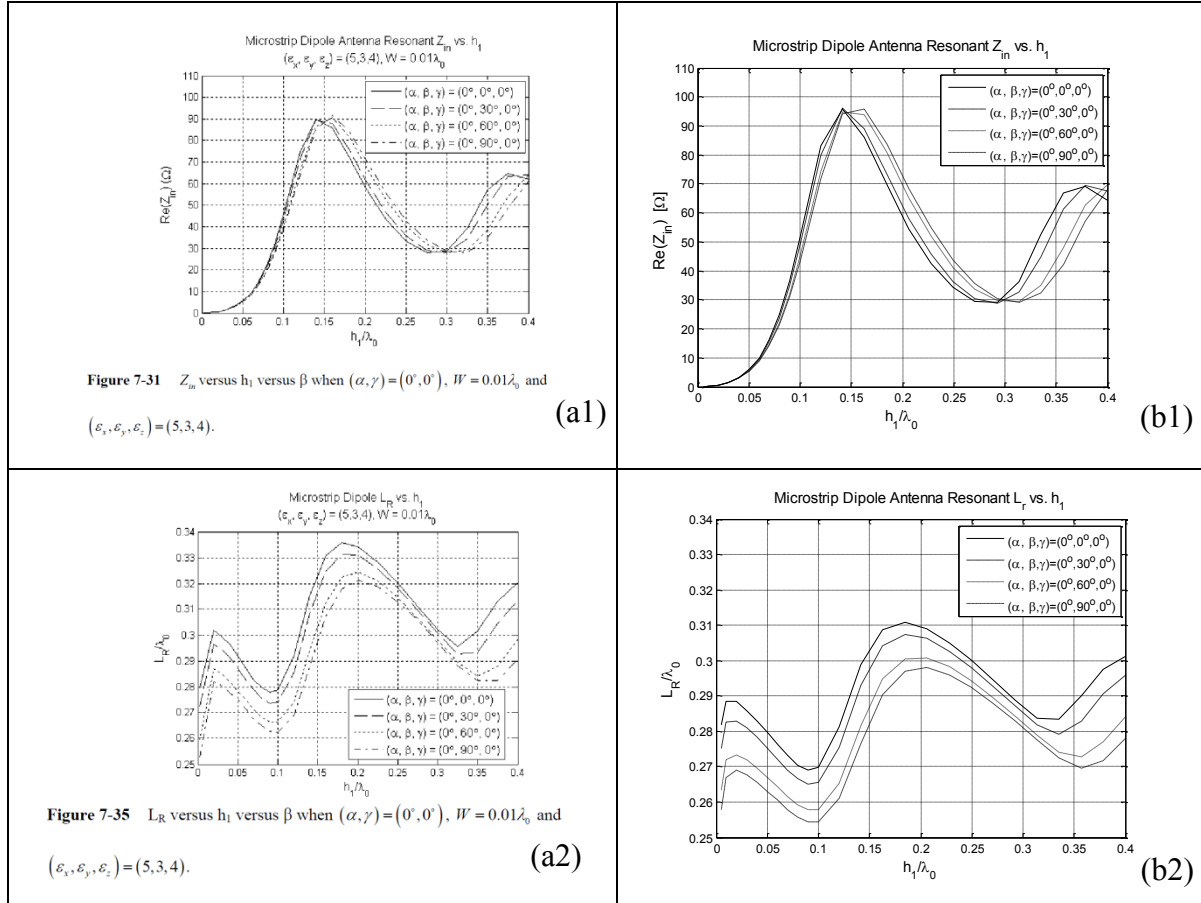


Fig. 5-28: Effect of rotation angle β to the input impedance and the resonant length with $\alpha = 0^\circ$ and $\gamma = 0^\circ$. (a1) and (a2) are from Pettis [37].

With $\beta = 0^\circ$ and $\gamma = 0^\circ$, the effects of the rotation angle α are calculated and plotted in Fig. 5-29. Fig. 5-29(a1) and (b1) show the real part of the input impedance vs. the thickness of the biaxial slab with different rotation angles α of $0^\circ, 30^\circ, 60^\circ$, and 90° using the transition matrix method and our method, respectively. Fig. 5-29(a2) and (b2) show the resonant length vs. the thickness of the biaxial slab with different rotation angles α of $0^\circ, 30^\circ, 60^\circ$, and 90° using the transition matrix method and our method, respectively. As indicated in the plots, the resonant length of the printed dipole decreases by around $0.02\lambda_0$ to $0.04\lambda_0$ depending on the thickness of the slab, while the real part of input impedance decreases.

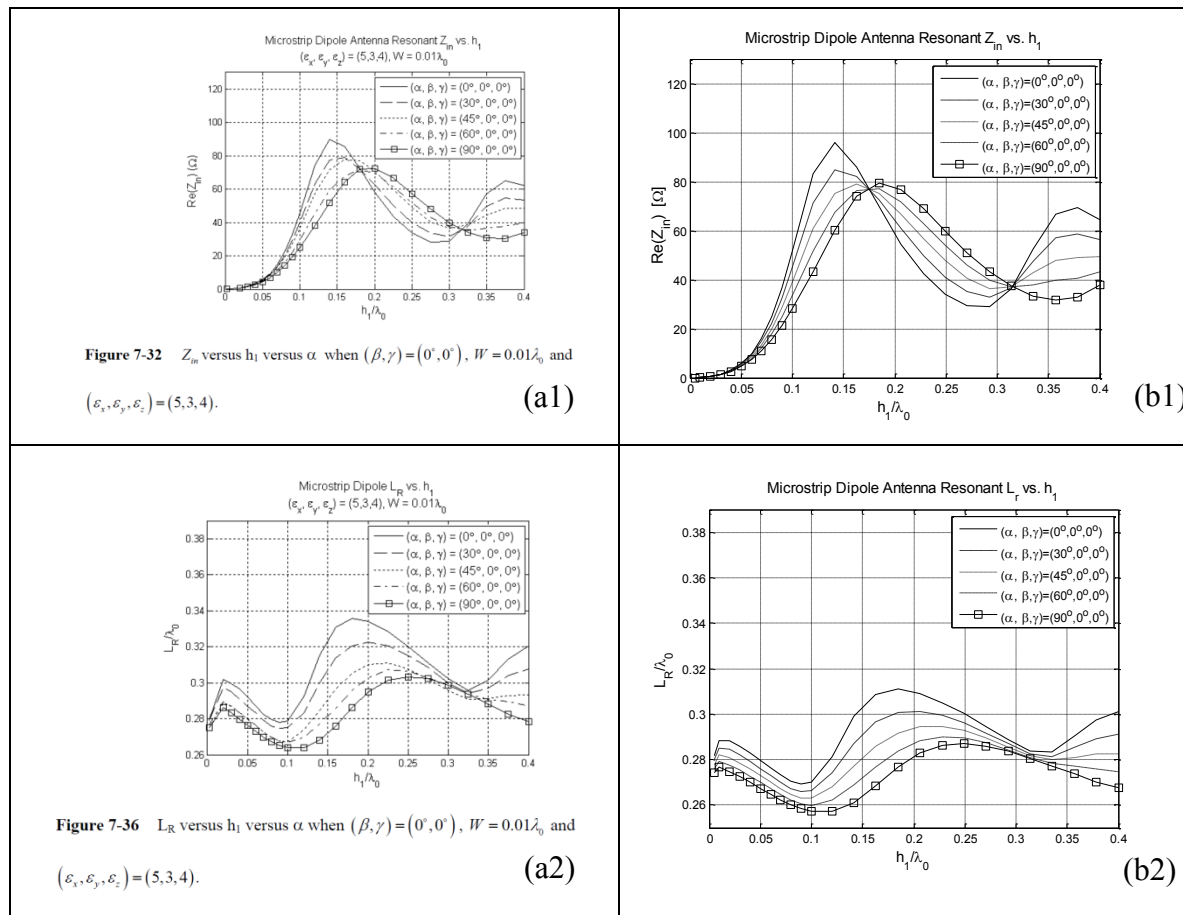


Fig. 5-29: Effect of rotation angle α to the input impedance and the resonant length with $\beta=0^\circ$ and $\gamma=0^\circ$. (a1) and (a2) are from Pettis [37].

The radiation pattern for a λ dipole (full wave resonant length) on a conductor backed slab filled with an unrotated biaxial medium is calculated and shown in Fig. 5-30. Fig. 5-30(a) shows the radiation pattern calculated in [37] and Fig. 5-30(b) shows the radiation pattern calculated using the method proposed here. It is observed that in Fig. 5-30(a), the maximum radiation is along the broad side direction ($\theta = 0^\circ$). The directive gain calculated here is 7.1dB. Compared with 7.5dB directive gain obtained in [37], the relative difference of the directive gain is less than 5%. The radiation patterns of a dipole on a ferrite substrate are calculated using the same set of code and are presented in the next section.

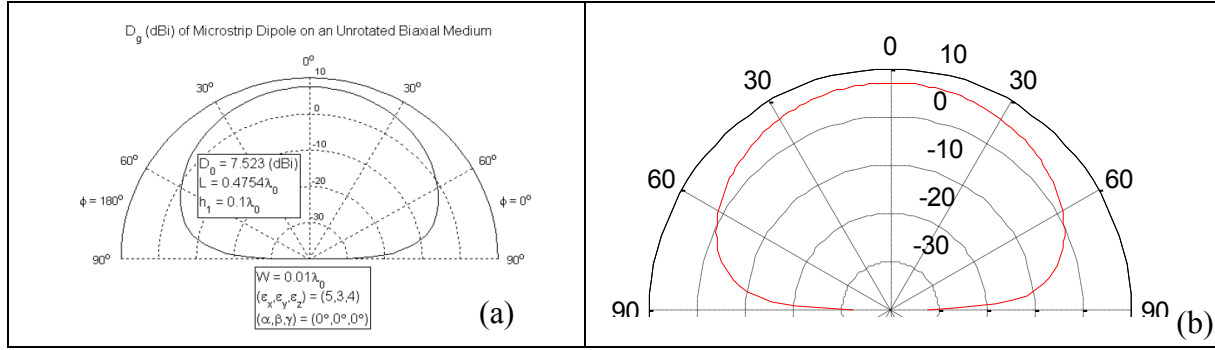


Fig. 5-30: Directive gain of a λ resonant dipole on a conductor backed slab filled with an unrotated biaxial medium of $(\epsilon_x, \epsilon_y, \epsilon_z) = (5, 3, 4)$. (a) from Pettis [37].

5.4.2.3 A Printed Dipole on a Grounded Ferrite Slab

As mentioned previously, the resonant length of the dipole can be found from the plots of the input impedance. The antenna is resonant when the reactance is zero. There usually exists more than one resonant length, which can be observed from impedance plot since the reactance crosses zeros multiple times. In this section, the resonant length of a printed dipole on top of the ferrite substrate is calculated and compared with Hsia et al. [81].

The principal permeability tensor of a ferrite material under a z-directed dc biasing field is given by

$$\underline{\mu}_p = \mu_0 \begin{bmatrix} \mu & -i\kappa & 0 \\ i\kappa & \mu & 0 \\ 0 & 0 & 1 \end{bmatrix} \quad (5.4-17)$$

where

$$\mu = 1 + \frac{\omega_0 \omega_m}{\omega_0^2 - \omega^2}, \quad \kappa = \frac{\omega \omega_m}{\omega_0^2 - \omega^2}$$

$$\omega_0 = \gamma \mu_0 H_0, \quad \omega_m = \gamma \mu_0 M_s, \quad \gamma = 1.759 \times 10^{11} \text{ kg / coul}$$

ω is the operating frequency, M_s is the material saturation magnetization, and H_0 is the dc biasing magnetic field. For an arbitrary direction of the biasing magnetic field (θ_B, φ_B) , the permeability tensor in the Cartesian coordinate system can be related with the principal permeability matrix $\bar{\bar{\mu}}_p$ through transformation matrix as follows.

$$\bar{\bar{\mu}} = \bar{\bar{T}}^{-1} \bar{\bar{\mu}}_p \bar{\bar{T}} \quad \bar{\bar{T}} = \begin{bmatrix} \sin \varphi_B & -\cos \varphi_B & 0 \\ \cos \theta_B \cos \varphi_B & \cos \theta_B \sin \varphi_B & -\sin \theta_B \\ \sin \theta_B \cos \varphi_B & \sin \theta_B \sin \varphi_B & \cos \theta_B \end{bmatrix} \quad (5.4-18)$$

For comparison purpose, the resonant length is chosen as the length where the reactance is zero and resistance is a maximum. Resonant lengths on an isotropic substrate and an x-directed biased ferrite substrate (along the direction of the dipole) are plotted in Fig. 5-31.

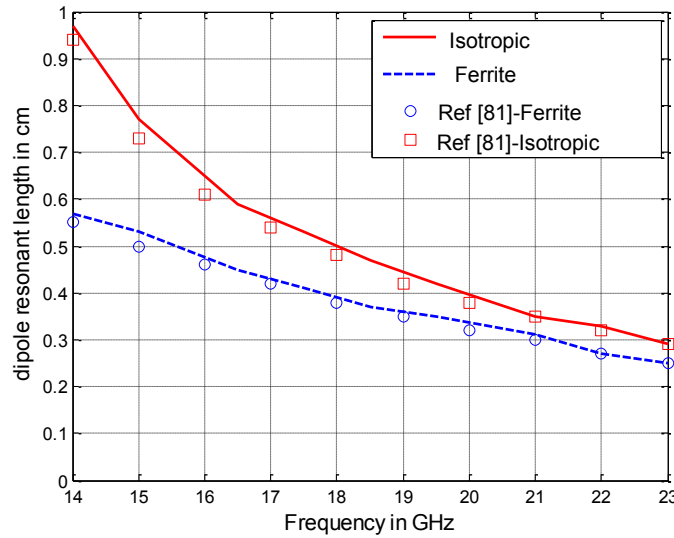


Fig. 5-31: Center-fed dipole resonant length versus frequency of printed dipole on a ferrite substrate of $\epsilon_r = 12.6$, $\mu_0 H_0 = 0.225$ [T], $\mu_0 M_s = 0.25$ [T] and an isotropic substrate of $\epsilon_r = 12.6$. The direction of the biasing magnetic field is along the direction of the dipole axis, i.e., x-direction ($\theta_B = 90^\circ, \varphi_B = 0^\circ$).

In Fig. 5-31, the solid line and dashed line show the resonant lengths obtained using the method developed in this chapter, while the square and circle markers correspond to the results obtained from [81]. As seen in Fig. 5-31, resonant lengths on an isotropic substrate and a gyromagnetic substrate agree very well with those of [81]. The slight difference might be due to the choice of a different number of basis functions and the different Green's functions used. In addition to validating the numerical comparisons for the input impedances and resonant lengths of a dipole on different substrates (isotropic, biaxial and ferrite media), the radiation patterns of a printed dipole on the grounded ferrite substrate are presented in Table 5-5 for the purpose of comparison. The permittivity and permeability are the same as those in [82]. The frequency is 30 GHz. The biasing field is parallel to the dipole with the length of 0.5 cm. The substrate thickness is 2.0 mm and $\epsilon_r = 12.6$, $\mu_0 H_0 = 0.715$ [T], $\mu_0 M_s = 0.3$ [T].

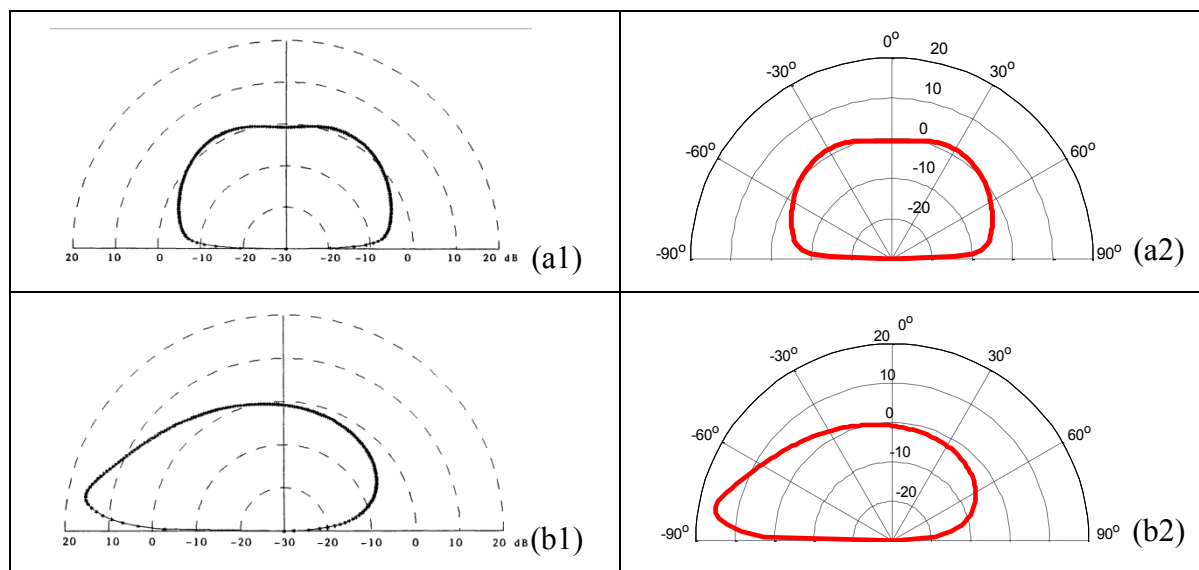


Table 5-5: (a) E-plane and (b) H-plane directivity for a center-fed dipole on a ferrite substrate. (a1) and (b1) from [82].

Table 5-5(a1) and (b1) display the E-plane and H-plane radiation patterns (Fig. 2.4 and Fig. 2.5 obtained in [82]). The same patterns are recalculated here again using the method

proposed in this chapter with E-DGFs involved and plotted in Table 5-5(a2) and (b2). Careful inspection of Table 5-5(a1) and (b1) with Table 5-5(a2) and (b2) indicates very good agreement. It is interesting to note that E-plane directivity is symmetric with respect to $\theta = 0^\circ$, while H-plane is not. The maximum radiation direction of E-plane is around $\theta = \pm 30^\circ$ with directive gain of 2 dB; and the maximum directive gain occurs around $\theta = -75^\circ$ in the H-plane with directivity gain more than 15 dB.

5.4.3 A Printed Dipole on a Grounded Gyroelectric Slab

The results of a microstrip dipole printed on isotropic, biaxial, and gyromagnetic substrates in the previous sections verified our method for modeling a printed dipole on top of a general anisotropic substrate using the E-DGFs. In this section, this method is used to model a printed dipole on a grounded gyroelectric slab, whose result has not been reported in the literature. Particularly, the input impedance, the resonant lengths and radiation patterns of a microstrip dipole on a grounded gyroelectric substrate are of primary interest.

5.4.3.1 Input Impedance and Resonant Length

The choice of plasma frequency and gyrofrequency is $\omega_p = 2\pi 10^9 \text{ rad/s}$, $\omega_b = 2\omega_p$, and $\varepsilon_{0r} = 1$. The operating frequency is chosen in Frequency Region 6 with $\omega = 2\pi \times 1.059 \times 10^9 \text{ rad/s}$. The dipole width is $0.01\lambda_0$. In the case of the biasing magnetic field along z-direction, the relative permittivity is written as

$$\underline{\underline{\varepsilon_{1r}}} = \begin{bmatrix} \varepsilon_{\perp} & -i\varepsilon_g & 0 \\ i\varepsilon_g & \varepsilon_{\perp} & 0 \\ 0 & 0 & \varepsilon_{//} \end{bmatrix} = \begin{bmatrix} 1.3474 & -i0.6561 & 0 \\ i0.6561 & 1.3474 & 0 \\ 0 & 0 & 0.1083 \end{bmatrix}$$

where ε_{\perp} , ε_g and $\varepsilon_{//}$ are defined in Eq. (2.3-3). When $\theta_B = 90^\circ, \varphi_B = 0^\circ$, corresponding to the x-directed biasing magnetic field for the gyroelectric substrate, the relative permittivity matrix of the substrate is given by

$$\varepsilon_{1r} = \begin{bmatrix} 0.1083 & 0 & 0 \\ 0 & 1.3474 & -0.6561i \\ 0 & 0.6561i & 1.3474 \end{bmatrix}, \quad (5.4-19)$$

In both cases, the wave vector surfaces of two characteristic waves in the gyroelectric medium are closed surfaces. The wave vector surface for the case of z-directed biasing magnetic field is shown in Fig. 5-32.

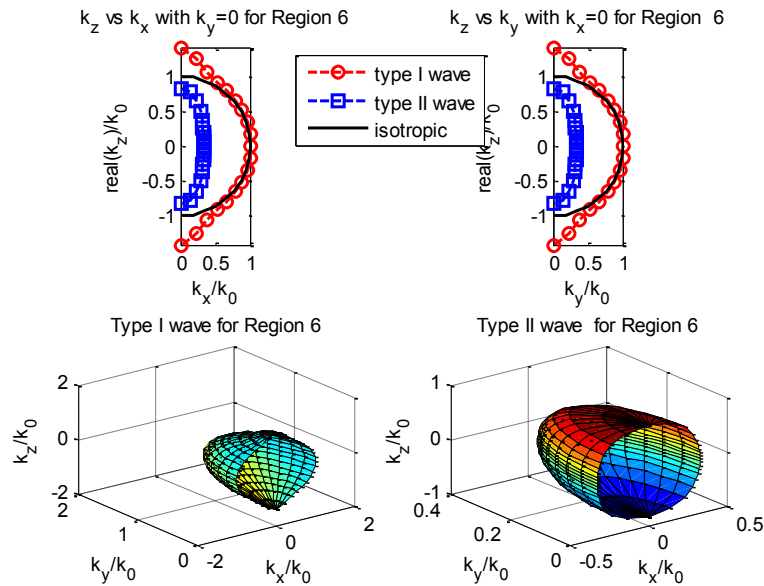


Fig. 5-32: Wave vector surfaces of Type I and Type II waves for the gyroelectric medium with $\omega = 2\pi \times 1.059 \times 10^9 \text{ rad/s}$, $\omega_p = 2\pi 10^9 \text{ rad/s}$, $\omega_b = 2\omega_p$, and the biasing magnetic field is along z-direction ($\theta_B = 0^\circ$).

A. Effect of Biasing Magnetic Field Direction

The first parameter investigated is the direction of the biasing magnetic field. Fig. 5-33 displays the variation of the input impedance of the antenna when the length of the dipole antenna changes from $0.1\lambda_0$ to $1.0\lambda_0$. The impedances for different directions of the biasing magnetic field are given. Specifically, Fig. 5-33 (a) presents the real part of the input impedance and Fig. 5-33 (b) shows the imaginary part of the input impedance.

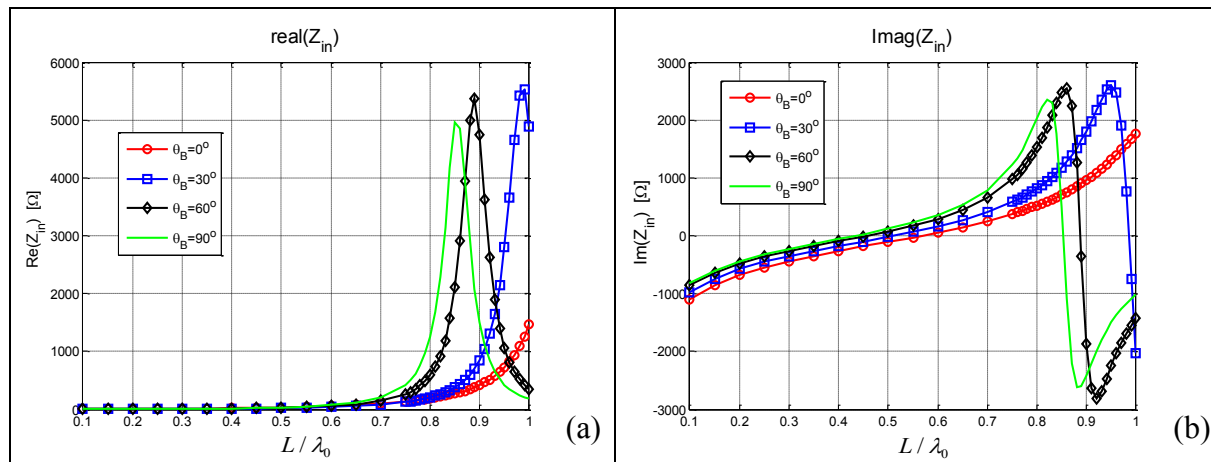


Fig. 5-33: (a) Real and (b) imaginary parts of the input impedance of the printed dipole on gyroelectric substrate with different directions of the biasing magnetic field. $\omega = 2\pi \times 1.059 \times 10^9 \text{ rad/s}$, $\omega_p = 2\pi 10^9 \text{ rad/s}$, $\omega_b = 2\omega_p$, the dipole width is $0.01\lambda_0$ and the substrate thickness is $0.1\lambda_0$.

A quick comparison of Fig. 5-33 with Fig. 5-25 shows that the input impedance of a microstrip dipole on a gyroelectric medium has resonant behavior similar to dipoles on an isotropic medium. It is interesting to note that the resonant length of the dipole varies with the direction of the biasing magnetic field. The resonant length decreases from $0.55\lambda_0$ to $0.45\lambda_0$ with the biasing magnetic field changing from z-direction ($\theta_B = 0^\circ$) to x-direction ($\theta_B = 90^\circ$, $\varphi_B = 0^\circ$).

Given the choice of the gyrofrequency $\omega_b = 2\omega_p$, it is calculated $\varepsilon_{\perp} = 1 - \frac{\omega_p^2}{\omega^2 - \omega_b^2} = 1.3474$.

Assuming the case for a printed dipole on top of an isotropic substrate of $0.1\lambda_0$ with relative permittivity of 1.3474, the resonant length is around $0.5\lambda_{eff} = 0.5\lambda_0 / \sqrt{\varepsilon_{eff}} = 0.4582\lambda_0$.

$\varepsilon_{eff} = 1.191$ is the effective permittivity, which can be obtained using the formula in [83],

$$\varepsilon_{eff} = \frac{\varepsilon_r + 1}{2} + \frac{\varepsilon_r - 1}{2} \frac{1}{\sqrt{1 + 12d/W}} \quad (5.4-20)$$

where d is the thickness of the substrate and W is the width of the dipole.

This estimated resonant length is very close to the resonant length of the dipole on a gyroelectric substrate with the biasing magnetic field along x-direction, as shown by the solid line of Fig. 5-33 (b). Thus, it may be concluded that, the dominant parameter of the permittivity tensor for a gyroelectric medium with permittivity tensor of Eq. (5.4-19) is

$\varepsilon_{\perp} = 1 - \frac{\omega_p^2}{\omega^2 - \omega_b^2} = 1.3474$ when the biasing magnetic field is oriented along the direction of the

dipole. If the biasing magnetic field changes from x-direction to z-direction, the resonant length increases from $0.45\lambda_0$ to $0.55\lambda_0$, indicating the decreased effect of the dominant term and increased effect of other terms in the permittivity tensor of Eq. (5.4-19).

B. Effect of Gyrofrequency or Magnitude of Biasing Magnetic Field

The next investigation is about the effect of the gyrofrequency (equivalently, the magnitude of the biasing field) on the resonant length when the direction of the biasing magnetic field is along the dipole orientation ($\theta_B = 90^\circ$, $\varphi_B = 0^\circ$). The parameters for the gyroelectric medium

are chosen as $\omega_p = 2\pi 10^9 \text{ rad/s}$, $\omega = 2\pi \times 1.059 \times 10^9 \text{ rad/s}$, and the thickness of the slab is $0.1\lambda_0$. Three different cases are considered here with $\omega_b = 0.5\omega_p$, $\omega_b = 1.5\omega_p$ and $\omega_b = 2\omega_p$.

The input impedances versus the length of a printed dipole on the substrate with the different values of gyrofrequency are plotted in Fig. 5-34. Fig. 5-34(a) shows the real part of the impedance while Fig. 5-34(b) shows the imaginary part of the impedance.

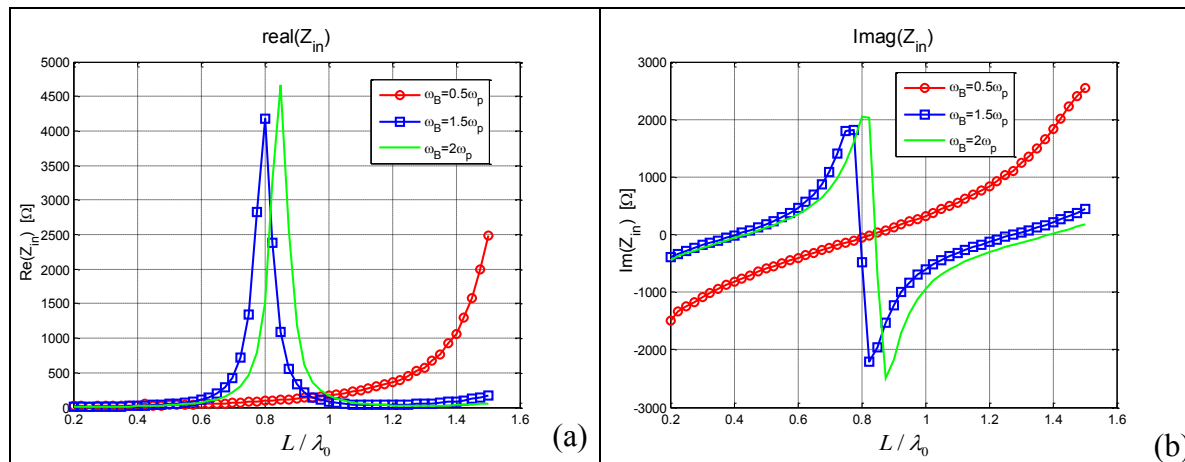


Fig. 5-34: (a) Real and (b) imaginary parts of input impedance vs. various dipole length for a microstrip dipole printed on a gyroelectric substrate with gyrofrequency $\omega_b = 0.5\omega_p$, $\omega_b = 1.5\omega_p$, and $\omega_b = 2\omega_p$.

Defining the resonant length as the length where the imaginary part of the impedance crosses zero for the first time, the resonant lengths for each case are summarized in Table 5-6. It is noted here that the dipole width is $0.01\lambda_0$. The relative permittivity of the gyroelectric medium and the resonant length are denoted as ϵ_{1r} and L_R . It is seen that for $\omega_b = 2\omega_p$ the resonant length is $0.42\lambda_0$, while for $\omega_b = 1.5\omega_p$, the resonant length is slightly decreased to $0.4\lambda_0$. According to the analysis in the previous section, the reason for the slight decrease of the

resonant length is the slight increase of the dominant term $\epsilon_{\perp} = 1 - \frac{\omega_p^2}{\omega^2 - \omega_b^2}$, which increases from 1.3474 to 1.8861 when ω_b decreases from $2\omega_p$ to $1.5\omega_p$. However, when $\omega_b = 0.5\omega_p$, ϵ_{\perp} becomes negative. In this case, the gyroelectric medium operates in Frequency Region 3. The wave vector surface as shown in Table 5-6 is no longer closed for Type II wave. The dominant term of the permittivity matrix in determining the resonant length is $\epsilon_{\parallel} = 1 - \frac{\omega_p^2}{\omega^2} = 0.1083$, which results in a significant increase of the resonant length from $0.42\lambda_0$ to $0.8\lambda_0$.

ω_b	Frequency Region 3: $\omega_b = 0.5\omega_p$	Frequency Region 6: $\omega_b = 1.5\omega_p$	Frequency Region 6: $\omega_b = 2\omega_p$
ϵ_{1r}	$\begin{bmatrix} 0.1083 & 0 & 0 \\ 0 & -0.1475 & 0.5418i \\ 0 & -0.5418i & -0.1475 \end{bmatrix}$	$\begin{bmatrix} 0.1083 & 0 & 0 \\ 0 & 1.8861 & -1.2551i \\ 0 & 1.2551i & 1.8861 \end{bmatrix}$	$\begin{bmatrix} 0.1083 & 0 & 0 \\ 0 & 1.3474 & -0.6561i \\ 0 & 0.6561i & 1.3474 \end{bmatrix}$
Wave vector surface			
L_R	$0.8\lambda_0$	$0.4\lambda_0$	$0.42\lambda_0$

Table 5-6: Resonant lengths for microstrip dipoles on a gyroelectric substrate.

From the discussion in this section, it is concluded that the variation of the resonant length is usually around 20% with a change in the direction of biasing magnetic field. However, more than 100% resonant length variation is possible depending on the ratio of gyrofrequency to the

plasma frequency, which is controlled by the magnitude of the biasing magnetic field. This additional parameter introduces more degrees of freedom to the antenna design and optimization.

5.4.3.2 Radiation Behavior

The radiation behavior of a printed dipole is also of interest. The radiation pattern of the printed dipole on the grounded biaxial substrate and ferrite was validated in Sections 5.4.2.2 and 5.4.2.3. We computed the fields in the same way using the method of the stationary phase here to study the effect of the biasing magnetic field as well as the ratio of the gyrofrequency to plasma frequency.

The first set of radiation patterns is obtained for the printed dipole on a gyroelectric substrate with different directions of biasing magnetic field. Fig. 5-35, Fig. 5-36 and Fig. 5-37 display the radiation patterns for both the E-plane ($\varphi = 0^\circ$) and the H-plane ($\varphi = 90^\circ$) with the biasing magnetic field along x-direction, y-direction and z-direction.

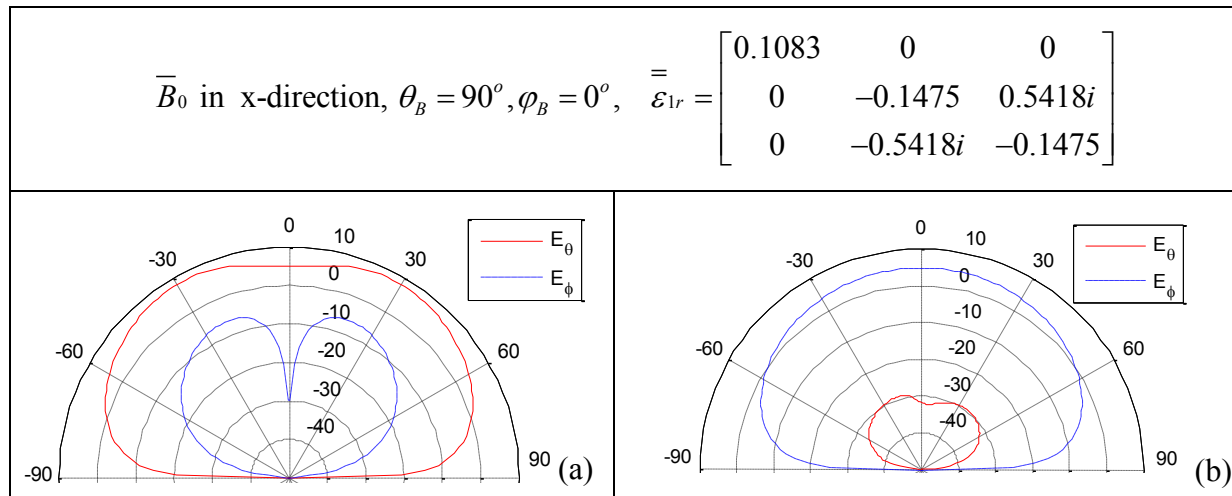


Fig. 5-35: Co-polarized and cross polarized radiation pattern of printed dipole for (a) E-plane and (b) H-plane with the direction of the biasing magnetic field along x-direction.

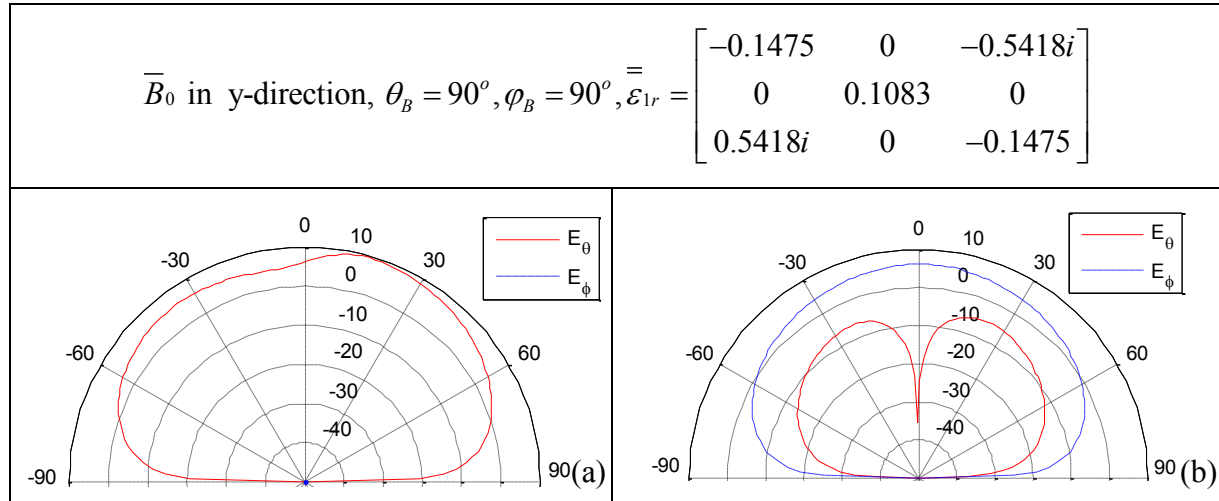


Fig. 5-36: Co-polarized and cross polarized radiation pattern of printed dipole for (a) E-plane and (b) H-plane with the direction of the biasing magnetic field along y-direction.

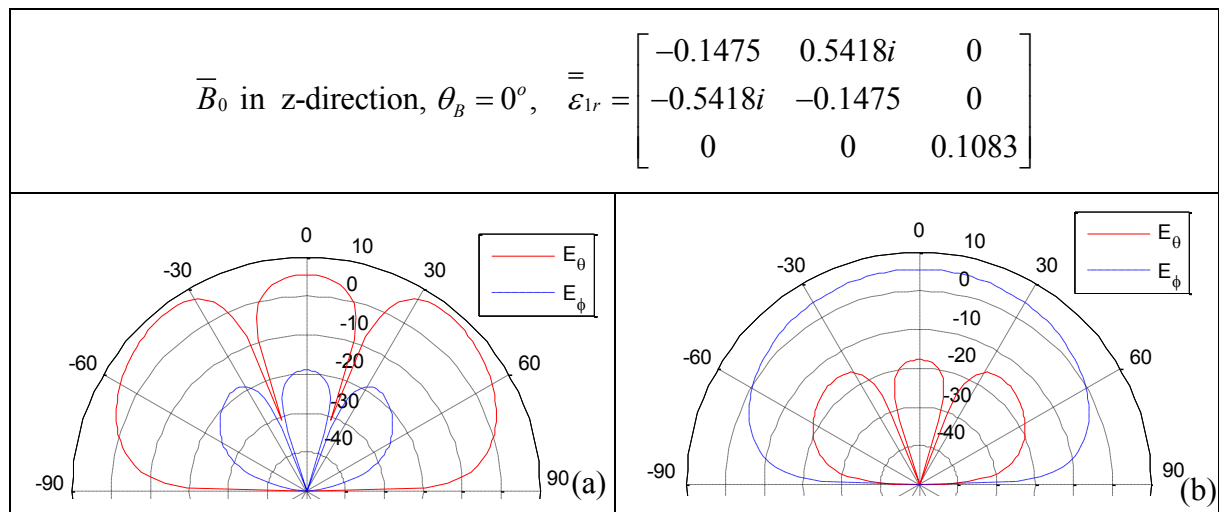


Fig. 5-37: Co-polarized and cross polarized radiation pattern of printed dipole for (a) E-plane and (b) H-plane with the direction of the biasing magnetic field along z-direction.

The parameters are chosen as $\omega = 2\pi \times 1.05910^9 \text{ rad/s}$, $\omega_p = 2\pi 10^9 \text{ rad/s}$, $\omega_b = 0.5\omega_p$ and the dipole width is $0.01\lambda_0$. It's noted here that in the E-plane, the co-polarized and cross-polarized components are E_θ and E_ϕ , while in the H-plane, the co-polarized and cross-polarized components are E_ϕ and E_θ . The first thing observed here is that the cross-polarized

radiated field always exists in both E-plane and H-plane for all three different directions of the biasing magnetic field with only one exception – that is, for the E-plane radiation pattern when the direction of the biasing magnetic field is along y-direction. When the biasing magnetic field is along x-direction, the cross-polarized field is much higher in the E-plane than in the H-plane. The cross-polarized field (E_ϕ) is almost 10 dB lower than the co-polarized field (E_θ) in the E-plane and almost 30 dB lower than the co-polarized field in the H-plane. When the biasing magnetic field is along y-direction, the cross-polarized field exists only in the H-plane, and it is around 10 dB lower than the co-polarized field component. When the biasing magnetic field is along z-direction, the cross-polarized field exists in both the E-plane and H-plane and they are around the same level, which is almost 10 dB lower than the co-polarized field component in both planes.

Another interesting thing noted here is that the radiation pattern is no longer always symmetric as is the case when a microstrip dipole is printed on a substrate filled with a biaxial medium. Only when the direction of the biasing magnetic field is along z-direction are both the co-polarized and cross-polarized field components symmetric with respect to $\theta = 0^\circ$ in both E-plane and H-plane. Asymmetry is introduced for the co-polarized pattern in the E-plane when the biasing magnetic field is along y-direction. This asymmetric co-polarized radiation pattern actually corresponds to the asymmetric current distribution when the biasing magnetic field is along y-direction, as shown in Fig. 5-24(b). The maximum directive gain is around 10 dB along 10° in E-plane when the biasing magnetic field is along y-direction.

The second set of radiation patterns is calculated for a printed dipole on a gyroelectric substrate with the different choice of the gyrofrequency when the direction of the biasing

magnetic field is along x-direction. The parameters are chosen as $\omega = 2\pi \times 1.059 \times 10^9 \text{ rad/s}$, $\omega_p = 2\pi 10^9 \text{ rad/s}$, $\omega_b = 2\omega_p$, $\omega_b = 1.5\omega_p$, $\omega_b = 0.5\omega_p$ and the dipole width is $0.01\lambda_0$.

Fig. 5-38(a) and (b) display the co-polarized and cross-polarized radiation patterns in the E-plane. Fig. 5-39(a) and (b) display the co-polarized and cross-polarized radiation patterns in the H-plane, respectively. Though the resonant length changes from $0.42\lambda_0$ to $0.8\lambda_0$ with ω_b decreasing from $2\omega_p$ to $0.5\omega_p$, as shown in Table 5-6, the radiation pattern is quite similar for each different case of gyrofrequency. However, as seen in both Fig. 5-38 (a) and Fig. 5-39 (a), the broadside gain is decreased by almost 3 dB with ω_b decreasing from $2\omega_p$ to $0.5\omega_p$. Also, the cross-polarized level is significantly larger in the E-plane for the choice of $0.5\omega_p$ than in the H-plane, as seen in Fig. 5-38(b) and Fig. 5-39(b). The cross-polarized component is 10 dB higher for $0.5\omega_p$ than the other two cases. Thus, special attention needs to be paid to the choice of the different parameters of a gyroelectric medium when it is used as a substrate for the antenna design and optimization process.

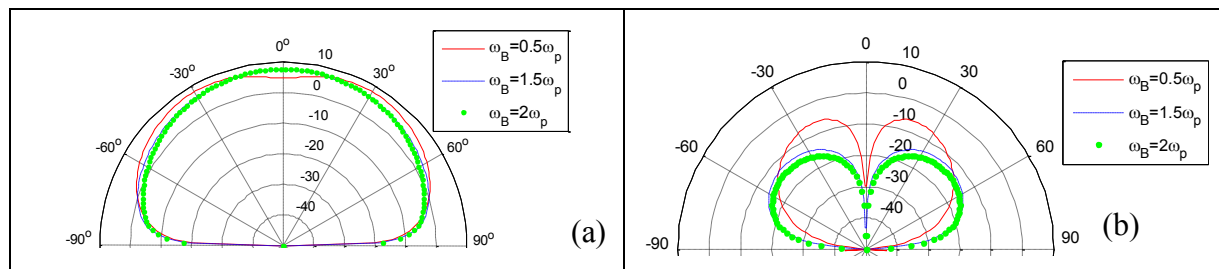


Fig. 5-38: (a) Co-polarized field pattern and (b) cross-polarized field pattern in E-plane with gyrofrequency $\omega_b = 0.5\omega_p$, $\omega_b = 1.5\omega_p$, $\omega_b = 2\omega_p$, when the biasing magnetic field is along x direction.

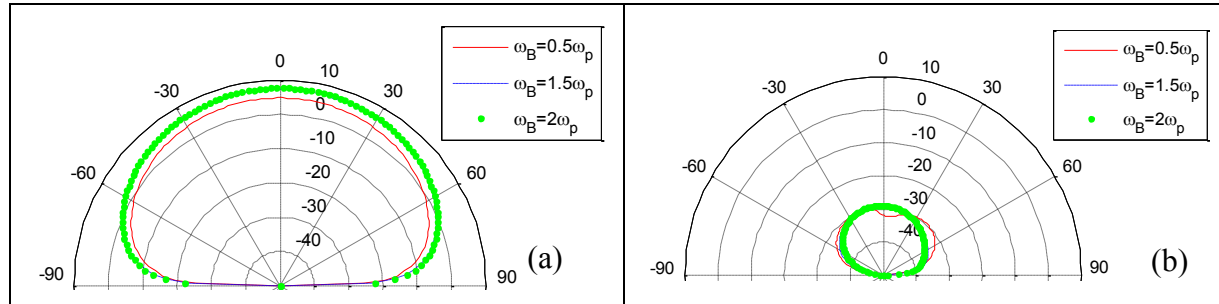


Fig. 5-39: (a) Co-polarized field pattern and (b) cross-polarized field pattern in H-plane with gyrofrequency $\omega_b = 0.5\omega_p$, $\omega_b = 1.5\omega_p$, $\omega_b = 2\omega_p$, when the biasing magnetic field is along x direction.

In this chapter, we have presented the formulation of a method of moment solution for a dipole antenna printed on a general anisotropic substrate. There is no restriction applied to the permittivity and permeability matrices of the medium. It can either be reciprocal media such as arbitrarily oriented uniaxial and biaxial media, or it can be non-reciprocal media such as a gyromagnetic medium (ferrite) or a gyroelectric medium.

Numerical examples of calculating current distribution, input impedance, resonant length and radiation pattern for the printed dipole on various media, including isotropic, biaxial, and ferrite media, are given. We observed very good agreement between the results obtained using our method and other methods from previous work. This validates the feasibility of the method proposed here applicable to solving for the radiation problems with a general anisotropic medium involved.

Furthermore, a more detailed analysis is given when the printed dipole is on a gyroelectric substrate. Numerous simulations were given to show the effect of the direction and magnitude of the biasing magnetic field.

6 CONCLUSIONS

In this dissertation, the eigenvector dyadic Green's functions (E-DGF) for unbounded and layered anisotropic geometry are derived and applications to the radiation problems are presented. It is demonstrated in the research that the proposed E-DGFs have no restriction imposed on the property of the anisotropic medium and may lead to broad numerical applications utilizing these E-DGFs to solve for practical problems with anisotropic media involved.

Using the eigen-decomposition method, the E-DGFs for an unbounded general anisotropic medium are derived in Chapter 2. The analytic expressions for E-DGFs for the unbounded uniaxial and gyrotropic media are presented. It is discovered that to fully represent the non-reciprocal behavior, E-DGFs of an unbounded non-reciprocal medium take a slightly different form from that of an unbounded reciprocal medium.

With the E-DGFs for the unbounded medium available, we proceed to derive the E-DGFs for a layered problem when the source is located either inside the isotropic region or anisotropic region in Chapter 3. The major contribution in this chapter includes two parts. The first part is to modify and generalize the symmetrical property so it accommodates with the problem when the anisotropic medium involved in the layered geometry is non-reciprocal. The second part is to propose the direct construction method to obtain the E-DGFs for layered geometry with a source inside the anisotropic region. This new method constructs the E-DGFs of a layered general anisotropic medium directly from the characteristic waves in each region using the eigen-decomposition and the matrix method. The advantages and disadvantages of both methods are briefly reviewed. Modified symmetrical property of DGF simplifies the process to obtain the DGF. However, applying the modified symmetrical property cannot provide the complete set of

DGFs for all the regions when the source is located inside the anisotropic slab. Also, the available symmetrical property doesn't apply to the medium with magnetic anisotropy. On the other hand, the direct construction method provides the complete DGFs of all regions, and can be extended to calculate the DGFs for a multilayered geometry filled with a general anisotropic (electric or magnetic) medium with a source located in any region.

To demonstrate the power of the E-DGFs obtained in Chapter 3, the radiated field of an arbitrarily oriented Hertzian dipole located either above or inside the layered anisotropic medium is solved in Chapter 4. By applying the method of stationary phase to the E-DGFs of layered anisotropic medium, the radiated field is formulated in a concise form with the straightforward physical interpretation. Numerical analysis for the radiation of a Hertzian dipole is discussed for three different cases including the dipole located over a half-space anisotropic medium, the dipole above a grounded layered gyroelectric slab, and the dipole immersed inside the gyroelectric slab. It is shown that a grounded gyroelectric slab may be used to achieve the directive radiation using two different mechanisms. One is through the reflection when the dipole is above the slab, and the other is through the transmission when the dipole is inside the slab. The analysis in this chapter may lead to a method whereby the volume of the radiator can be reduced with the utilization of a gyroelectric medium. This size reduction may make it possible to create a miniaturized antenna, which often is the goal of most antenna manufacturers.

In Chapter 5, application of the E-DGFs is further extended to a more practical problem – the radiation of a microstrip dipole antenna printed on a general anisotropic substrate. The formulation of a method of moment solution using the E-DGF with Galerkin's method is presented. The singularity of the integrand associated with the E-DGFs is discussed and integration path is carefully chosen. Since the E-DGFs derived for the layered geometry impose

no restriction to the permittivity and permeability matrices of the medium, the algorithm developed in this dissertation can solve for radiation problem of the microstrip dipole antenna printed either on a reciprocal medium (arbitrarily oriented uniaxial and biaxial media) or on a non-reciprocal medium (gyromagnetic medium (ferrite) or gyroelectric medium). To validate the general feasibility of the method proposed here, numerical examples for the printed dipole on isotropic, biaxial, and ferrite media are given. Particularly, current distribution, input impedance, resonant length and radiation pattern are calculated. Very good agreement with the results obtained in previous work using other methods is observed.

Furthermore, a detailed analysis is presented for the dipole printed on a gyroelectric substrate. Numerous simulations are presented to show the effect of the direction and magnitude of the biasing magnetic field. In our studies, we have found that gyrotropic anisotropy of y -directed biasing magnetic field perpendicular to the dipole axis results in the asymmetric current distribution and asymmetric radiation pattern with respect to $\theta = 0^\circ$. This is not observed for the dipole on an isotropic or a biaxial substrate. We have found that the resonant length of the dipole depends on the direction as well as the magnitude of the biasing field. Finally, we have studied in detail the radiation behavior of the printed dipole, and found that the existence of the cross-polarized field is dependent on the gyrofrequency and the direction of the biasing magnetic field.

Though the algorithm developed in this dissertation has a broad scope applicable to a general anisotropic medium, it is not recommended to apply the approach blindly without considering the medium property first. From the singularity analysis of the surface wave pole in Section 5.2.2, it is known that the surface wave poles are bounded in the region of k_0 and k_{\max}^{s2s} for the anisotropic medium with closed wave vector surface including the uniaxial and biaxial media. However, for a gyroelectric medium, there exists the case when the wave vector surfaces

for one or both of two characteristic waves are not closed. In this case, k_{\max}^{s2s} is an infinite number and indenting the integration path along the real axis in the region where surface wave singularity exists is not well defined. To overcome this problem, slight loss is added to a gyroelectric medium when calculating a dipole on a gyroelectric medium. With slight loss applied to the medium, we fail to get converged results when the wave vector surfaces of both characteristic waves are not closed. Thus, in the numerical analysis for the dipole printed on a gyroelectric substrate, the numerical results are presented only for Frequency Region 3 and Frequency Region 6 as listed in Table 5-6. When utilizing the numerical approach developed in this dissertation, special attention needs to be paid to a medium for which the wave vector surface of the characteristic waves is not closed.

Future work may include the following topics.

- (1) Applying the E-DGFs obtained in this dissertation to the propagation problem such as the transmission line on anisotropic substrates.
- (2) Applying the E-DGFs obtained in this dissertation to the radiation problem of a patch antenna.
- (3) Applying the E-DGFs obtained in this dissertation to the scattering problem with an arbitrarily shaped object embedded inside an anisotropic medium.
- (4) Numerical comparison of the E-DGF obtained in this dissertation with the T-DGF to investigate the benefits and drawback of the E-DGFs including the stability of the DGF when k_x and k_y are large numbers, and the computation time.

BIBLIOGRAPHY

- [1] N. G. Alexopoulos, "Integrated-circuit structures on anisotropic substrates," *IEEE Trans. Microwave Theory Tech.*, vol. 33, no. 10, pp. 847-881, Oct. 1985.
- [2] M. Geshiro, S. Yagi, and S. Sawa, "Analysis of slotlines and microstrip lines on anisotropic substrates," *IEEE Trans. Microwave Theory Tech.*, vol. 39, no. 1, pp. 64-69, Jan. 1991.
- [3] J. L. Tsalamengas, N. K. Uzunoglu, and N. G. Alexopoulos, "Propagation characteristics of a microstrip line printed on a general anisotropic substrate," *IEEE Trans. Microwave Theory Tech.*, vol. 33, no. 10, pp. 941-945, Oct. 1985.
- [4] D. M. Pozar, "Radiation and scattering from a microstrip patch on a uniaxial substrate," *IEEE. Trans. Antennas and Propag.*, vol. 35, no. 6, pp. 613-621, June. 1987.
- [5] T. Q. Ho and B. Becker, "Spectral-domain analysis of shielded microstrip lines on biaxially anisotropic substrates," *IEEE Trans. Microwave Theory Tech.*, vol. 39, no. 6, pp. 1017-1021, June. 1991.
- [6] F. J. Harackiewicz, *Electromagnetic Radiation and Scattering from Microstrip Antennas on Anisotropic Substrates*, PhD Dissertation, University of Massachusetts, Feb. 1990.
- [7] W. J. Wang, *Multilayer Printed Antennas with Biaxial Anisotropic Dielectric Substrates: General Analysis and Case Studies*, PhD Dissertation, Polytechnique University, Jan. 2002.
- [8] D. M. Pozar, "Radiation and scattering characteristics of microstrip antennas on normally biased ferrite substrate." *IEEE. Trans. Antennas and Propag.*, vol. 40, no. 9, pp. 1084-1092, Sep. 1992.

- [9] D. M. Pozar, "RCS reduction for a microstrip antenna using a normally biased ferrite substrate," *IEEE Microwave Guided Wave Lett.*, vol. 2, pp. 196-198, May. 1992.
- [10] A. D. Brown, J. L. Volakis, L. C. Kempel, and Y. Y. Botros, "Patch antennas on ferromagnetic substrate," *IEEE Trans. Antennas and Propag.*, vol. 47, no. 1, pp. 26-32, Jan. 1999.
- [11] J. Helszajn, *Ferrite Phase Shifters and Control Devices*, McGraw-Hill, San Francisco, CA, 1989.
- [12] R. F. Soohoo, *Microwave Magnetics*, Harper & Row, San Francisco, CA, 1985, Chapter 9.
- [13] B. Lax and K. J. Button, *Microwave Ferrites and Ferrimagnetics*, McGraw-Hill, New York, 1962, Chapter 12.
- [14] J. D. Adam, L. E. Davis, G. F. Dionne, E. F. Schloemann, and S. N. Stitzer, "Ferrite devices and materials," *IEEE Trans. Microwave Theory Tech.*, vol. 50, no. 3, pp. 721-737, Mar. 2002.
- [15] S. I. Sheikh, "Novel semiconductor phase shifter for millimeter-wave device", *Microwave and Optical Technology Letters*, vol. 39, no. 4, pp. 300-303, Nov. 2003.
- [16] Y. T. Lian and L. E. Davis, "Gyroelectric properties of indium antimonide at terahertz frequencies", *6th IEEE High Frequency Postgraduate Student Colloquium*, Cardiff, pp. 65-70, Sep. 9-10, 2001.
- [17] D. M. Bolle and S. H. Talisa, "Fundamental consideration in millimeter and near-millimeter component design employing magnetoplasmons," *IEEE Trans. Microwave Theory Tech.*, vol. 29, no. 9, pp. 916-923, Sep. 1981.

- [18] C. M. Krowne, "Waveguiding structure employing the solid state magnetoplasma effect for microwave and millimeter wave propagation," *IEE proceedings*, vol. 140, no. 3, pp. 148-165, June 1993.
- [19] L. E. Davis and R. Sloan, "Semiconductor junction circulator," *IEEE MTT-S International Microwave Symposium Dig.*, pp.483-486, June 1993.
- [20] L. E. Davis and R. Sloan, "Predicted performance of semiconductor junction circulator with losses," *IEEE Trans. Microwave Theory Tech.*, vol. 41, no. 12, pp. 2243-2247, Dec. 1993.
- [21] R. Sloan, C. K. Yong, and L. E. Davis, "Broadband theoretical gyroelectric junction circulator tracking behavior at 77K," *IEEE Trans. Microwave Theory Tech.*, vol. 44, no. 12, pp. 260-266, Dec. 1996.
- [22] C. K. Yong, R. Sloan, and L. E. Davis, "A Ka-band indium antimonide junction circulator", *IEEE Trans. Microwave Theory Tech.*, vol. 49, no. 6, pp. 1101-1106, Jun. 2001.
- [23] Z. M. Ng, L. E. Davis, and R. Sloan, "Differential isolation of a gyroelectric InSb disc", *Microwave and Optical Technology Letters*, vol. 41, no. 6, pp. 433-434, 2004.
- [24] Z. M. Ng and L. E. Davis, "Measurements of V -band n-type InSb junction circulators", *IEEE Trans. Microwave Theory Tech.*, vol. 52, no. 2, pp. 482-488, Feb. 2004.
- [25] S. I. Sheikh, A. A. P. Gibson, and B. M. Dillon, "Split frequencies in planar axisymmetric gyroelectric resonators", *IEEE Trans. Microwave Theory Tech.*, vol. 46, no. 1, pp. 62-69, Jan. 1998.

- [26] V. H. Mok and L. E. Davis, "Nonreciprocal wave propagation in multilayer semiconductor films at frequencies up to 200 GHz", *IEEE Trans. Microwave Theory Tech*, vol. 51, no. 12, pp. 2453-2460, Dec. 2003.
- [27] H. Mosallaei and K. Sarabandi, "Magneto-dielectrics in electromagnetics: concept and applications," *IEEE. Trans. Antennas and Propag.*, vol. 52, no. 6, pp. 1558-1567, Jun. 2004.
- [28] S. Hrabar, J. Bartolic, and Z. Sipus, "Waveguide miniaturization using uniaxial negative permeability metamaterial," *IEEE. Trans. Antennas and Propag.*, vol. 53, no. 1, pp. 110-119, Jan. 2005.
- [29] C. M. Krowne, "Electromagnetic-field theory and numerically generated results for propagation in left-handed guided-wave single microstrip structures," *IEEE Trans. Microwave Theory Tech.*, vol. 51, no. 12, pp. 2269-2283, Dec. 2003.
- [30] D. Sounas, T. Kodera, and C. Caloz, "Non-reciprocal gyrotropic electrically biased ring metasurface", *IEEE International Symposium on Antenna and Propagation*, Spokane, WA, July 3-8, 2011.
- [31] A. V. Rogacheva, V. A. Fedotov, A. S. Schwanecke, and N. I. Zheludev, "Giant gyrotropy due to electromagnetic-field coupling in a bilayered chiral structure," *Physical Review Letters*, vol. 97, pp. 177401-1-177401-4, Oct. 2006.
- [32] A. Boardman, P. Egan, R. M. Thomas, L. Velasco, and Y. Rapoport, "Modelling and theory of nonlinear or gyroelectric nanoscale metamaterials", *3rd International Congress on Advanced Electromagnetic Materials in Microwaves and Optics*, London, Aug. 30- Sep. 4, 2009.

- [33] E. Plum, V. A. Fedotov, A. S. Schwanecke, and N. I. Zheludev, "Giant optical gyrotropy due to electromagnetic coupling", *Applied Physics letters*, vol. 90, no. 2, pp. 223113-1-223113-3, 2007.
- [34] C. T. Tai., *Dyadic Green Functions in Electromagnetic Theory*, 2nd Ed., IEEE Press, NY, 1994.
- [35] J. K. Lee and J. A. Kong, "Dyadic Green's functions for layered anisotropic medium," *Electromagnetics*, vol. 3, pp. 111- 130, 1983.
- [36] S. Mudaliar and J. K. Lee, "Dyadic Green's function for two-layered biaxially anisotropic medium," *Journal of Electromagnetic Waves and Applications*, vol. 10, pp. 90-92, 1996.
- [37] G. Pettis, *Hertzian Dipoles and Microstrip Circuits on Arbitrarily Oriented Biaxially Anisotropic Media*, PhD Dissertation, Syracuse University, Syracuse, NY, 2008.
- [38] A. Eroglu and J. K. Lee, "Dyadic Green's functions for an electrically gyrotropic medium," *Progress in Electromagnetics Research*, vol. 58, pp. 223-241, 2006.
- [39] A. Eroglu and J. K. Lee, "Simplified formulation of dyadic Green's functions and their duality relations for general anisotropic media," *Progress in Electromagnetics Research*, vol. 77, pp. 391-408, 2007.
- [40] E. Park, *Propagation and Radiation of Electromagnetic Waves in the Presence of a Gyromagnetic Medium*, PhD Dissertation, Syracuse University, Syracuse, NY, 2005.
- [41] C. M. Krowne, "Green's function in the spectral domain for biaxial and uniaxial anisotropic planar dielectric structures," *IEEE. Trans. Antennas and Propag.*, vol. 32, no. 12, pp. 1273-1281, Dec. 1984.

- [42] F. L. Mesa, R. Marques, and M. Horno, "A general algorithm for computing the bidimensional spectral Green's dyad in multilayered complex bianisotropic media: The equivalent boundary method," *IEEE Trans. Microwave Theory Tech.*, vol. 39, no. 9, pp. 1640-1649, Sep. 1991.
- [43] L. W. Li, P. S. Kooi, M. S. Leong, and T. S. Yeo, "On the eigenfunction expansion of dyadic Green's function in planarly stratified media", *Journal of Electromagnetic Waves and Applications*, vol. 8, no. 6, pp. 663-678, 1994.
- [44] L. W. Li, and N. H. Lim, "Eigen functional expansion of dyadic Green's functions in gyrotropic media using cylindrical vector wave functions," *Progress in Electromagnetics Research*, vol. 43, pp. 101-121, 2003.
- [45] L. Vegni, R. Cicchetti, and P. Capece, "Spectral dyadic Green's function formulation for planar integrated structures," *IEEE. Trans. Antennas and Propag.*, vol. 36, no. 8, pp. 1057-1065, Aug. 1988.
- [46] F. V. Bunkin, "On radiation in anisotropic media," *JETP Lett.*, vol. 5, no. 2, pp. 338-346, Sep. 1957.
- [47] C. P. Wu, "Radiation from dipoles in a magneto-ionic medium," *IEEE. Trans. Antennas and Propag.*, vol. 11, no. 6, pp. 681-689, Nov. 1963.
- [48] J. L. Tsalamengas and N. K. Uzunoglu, "Radiation from a dipole in the presence of a grounded gyromagnetic slab," *J. Appl. Phys*, vol. 53, pp. 7149-7161, Nov. 1982.
- [49] I. Y. Hsia and N. G. Alexopoulos, "Radiation characteristics of Hertzian dipole antennas in a nonreciprocal superstrate-substrate structure," *IEEE. Trans. Antennas and Propag.*, vol. 40, no. 7, pp. 782-790, July. 1992.

- [50] J. A. Kong, "Electromagnetic fields due to dipole antennas over stratified anisotropic media," *Geophys.*, vol. 37, pp. 958-966, Dec. 1972.
- [51] Y. S. Kwon and J. J. H. Wang, "Computation of Hertzian dipole in stratified uniaxial media," *Radio Sci.*, vol. 21, pp. 91-902, Nov. 1982.
- [52] C. M. Tang, "Electromagnetic fields due to dipole antennas embedded in stratified anisotropic media," *IEEE. Trans. Antennas and Propag.*, vol. 27, no. 5, pp. 665-670, Sep. 1979.
- [53] S. M. Ali and S. F. Mahmoud, "Electromagnetic field of buried sources in stratified anisotropic media," *IEEE. Trans. Antennas and Propag.*, vol. 27, no. 5, pp. 671-678, Sep. 1979.
- [54] A. Eroglu and J. K. Lee, "Far field radiation from an arbitrarily oriented Hertzian dipole in the presence of a layered anisotropic medium," *IEEE. Trans. Antennas and Propag.*, vol. 53, no. 12, pp. 3963-3973, Dec. 2005.
- [55] J. L. Tsalamengas and N. K. Uzunoglu, "Radiation from a dipole in the proximity of a general anisotropic grounded layer," *IEEE. Trans. Antennas and Propag.*, vol. 33, no. 2, pp. 165-172, Feb. 1985.
- [56] J. L. Tsalamengas and N. K. Uzunoglu, "Radiation from a dipole near a general anisotropic layer," *IEEE. Trans. Antennas and Propag.*, vol. 38, no. 1, pp. 9-16, Jan. 1990.
- [57] J. L. Tsalamengas, "Electromagnetic fields of elementary dipole antennas embedded in stratified general anisotropic media," *IEEE. Trans. Antennas and Propag.*, vol. 37, no. 3, pp. 399-403, Mar. 1989.

- [58] N. K. Uzunoglu, N. G. Alexopoulos and J. G. Fikoris, "Radiation properties of microstrip dipoles," *IEEE. Trans. Antennas and Propag.*, vol. 27, no. 6, pp. 853- 858, Nov. 1979.
- [59] P. B. Kathei and N. G. Alexopoulos, "On the effect of substrate thickness and permittivity on printed circuit dipole properties," *IEEE. Trans. Antennas and Propag.*, vol. 31, no. 5, pp. 34-39, Jan. 1983.
- [60] E. Rana and N. G. Alexopoulos, "Current distribution and input impedance of printed dipoles," *IEEE. Trans. Antennas and Propag.*, vol. 9, no. 1, pp. 99-105, Jan. 1981.
- [61] M. D. Deshpande and M. C. Bailey, "Input impedance of microstrip antennas," *IEEE. Trans. Antennas and Propag.*, vol. 30, no. 4, pp. 645-650, July. 1982.
- [62] T. Itoh and W. Menzel, "A full wave analysis method for open microstrip structure," *IEEE. Trans. Antennas and Propag.*, vol. 29, no. 1, pp. 63-68, Jan. 1981.
- [63] D. M. Pozar, "Input impedance and mutual coupling of rectangular microstrip antennas," *IEEE. Trans. Antennas and Propag.*, vol. 30, no. 6, pp. 1191-1196, Nov. 1982.
- [64] D. M. Pozar, "Considerations for millimeter wave printed antennas," *IEEE. Trans. Antennas and Propag.*, vol. 31, no. 5, pp. 740- 747, Sep. 1983.
- [65] J. W. Graham, *Arbitrarily Oriented Biaxially Anisotropic Media: Wave Behavior and Microstrip Antennas*, PhD Dissertation, Syracuse University, Syracuse, NY, May 2012.
- [66] Hollis Chen, *Theory of Electromagnetic Waves—A Coordinate Free Approach*, McGraw-Hill, NY, 1983.
- [67] R. Courant and D. Hilbert, *Methods of Mathematical Physics*, vol. 1, Interscience Publisher, New York, Second Printing, 1955.

- [68] A. Eroglu, *Electromagnetic Wave Propagation and Radiation in Gyrotropic Medium*, PhD Dissertation, Syracuse University, Syracuse, NY, 2004.
- [69] L. Tsang, E. Njoku, and J. A. Kong, "Microwave thermal emission from a stratified medium with nonuniform temperature distribution," *J. Appl. Phys.*, vol. 46, pp. 5127-5133, 1975.
- [70] R. F. Harrington and A. T. Villeneuve, "Reciprocity relationships for gyrotropic media", *IRE Trans. Microwave Theory and Techniques*, vol. 6, no. 3, pp. 308-310, Jul. 1958.
- [71] L. Mandel and E. Wolf, *Optical Coherence and Quantum Optics*, Cambridge University Press, New York, 1995.
- [72] A. Eroglu and J. K. Lee, "Wave propagation and dispersion characteristics for a nonreciprocal electrically gyrotropic medium," *Progress in Electromagnetics Research*, vol. 62, pp. 237-260, 2006.
- [73] P. Baccarelli, P. Burghignoli, F. Frezza, A. Galli, P. Lampariello, G. Lovat, and S. Paulotto, "Effects of leaky-wave propagation in metamaterial grounded slabs excited by a dipole source", *IEEE Trans. Microwave Theory Tech.*, vol. 53, no.1, pp. 32-44, Jan. 2005.
- [74] G. Lovat, P. Burghignoli, F. Capolino, D. R. Jackson, and D. R. Wilton, "Analysis of directive radiation from a line source in a metamaterial slab with low permittivity", *IEEE Trans. Antennas and Propag.*, vol. 54, no. 3, pp. 1017-1030, Mar. 2006.
- [75] P. Burghignoli, G. Lovat, F. Capolino, D. R. Jackson, and D. R. Wilton, "Directive leaky-wave radiation from a dipole source in a wire medium slab", *IEEE Trans. Antennas and Propag.*, vol. 56, no. 5, pp. 1329-1339, May. 2008.

- [76] S. R. Seshadri and W. F. Pickard, "Surface waves on an anisotropic plasma sheath," *IEEE Trans. Microwave Theory Tech.*, vol. 12, pp. 529-541, Sep. 1964.
- [77] C.M. Krowne, "Electromagnetic distributions demonstrating asymmetry using a spectral-domain dyadic Green's function for ferrite microstrip guided-wave structures," *IEEE Trans. Microwave Theory Tech.*, vol. 53, pp. 1345-1361, Apr. 2005.
- [78] C. A. Balanis, *Antenna Theory Analysis and Design, 2nd Ed.*, John Wiley and Sons Inc., New York, 1997.
- [79] H. Y. Yang, A. Nakatani, and J. A. Castaneda, "Efficient evaluation of spectral integrals in the moment method solution of microstrip antennas and circuits," *IEEE Trans. Antennas Propagat.*, vol. 38, pp. 1127-1130, July. 1990.
- [80] J.R. James and P.S. Hall, *Handbook of Microstrip Antennas*, Vol. 1, Peter Peregrinus Ltd., London, UK, 1989.
- [81] I. Hsia, H Y. Yang, and N. G. Alexopoulos, "Microstrip antennas on ferrite substrate", *IEEE Antennas and Propagation Society International Symposium*, Dallas, TX, USA, May 7- 11, 1990.
- [82] H. Y. Yang, J. A. Castaneda, and A. Nakatani, "Microstrip Antennas on/in Anisotropic Material Layers," Technical Report, Nov. 1992.
- [83] D.M. Pozar, *Microwave Engineering*, 3rd Ed., John Wiley and Sons, Inc., 2005.

VITA

Name of Author: Ying Huang

Date and Place of Birth: July 8, 1983, Jiangsu, China

Positions

Academic Appointments

2008- 2010	Graduate Teaching Assistant, Syracuse University, Department of Electrical Engineering and Computer Science. Syracuse, NY, United States.
2007- 2008	Graduate Research Assistant, Syracuse University, Department of Electrical Engineering and Computer Science. Syracuse, NY, United States.
2005- 2007	Graduate Research Assistant, Nanjing University, School of Electronic Science and Engineering. Nanjing, China.

Other Employment

2010 – present	Microwave Engineer, Anaren Microwave, Inc. East Syracuse, NY, United States.
----------------	---

Degrees

2005 – 2008	M.S., Nanjing University, Electronic Science and Engineering Electrical Engineering.
2001 – 2005	B.S., Nanjing University, Electronic Science and Engineering Electrical Engineering.

Selected Honors & Awards

2010	Second Best Paper Award, IEEE Workshop on Microwave Passive Circuits and Filters.
2010	Nunan Research Grand Award, Syracuse University.

Publications

Journal Articles

- J1. **Y. Huang** and Jay K. Lee, "Radiation from an arbitrarily oriented Hertzian dipole in the presence of a gyroelectric slab", to be published in *IEEE. Trans. Antennas and Propagation*, vol. 62, no. 4, Apr. 2014.
- J2. **Y. Huang** and J. K. Lee, "Dyadic Green's functions for unbounded and two-layered general anisotropic media", *PIER B*, vol. 30, pp. 27-46, 2011.
- J3. **Y. Huang**, A. De, Y. Zhang, T. K. Sarkar, and J. Carlo, "Enhancement of radiation along the ground plane from a horizontal dipole located close to it," *IEEE Antennas and Wireless Propagation Letters*, vol.7, pp. 294 - 297, 2008.
- J4. **Y. Huang**, Y. Feng, and T. Jiang, "Electromagnetic cloaking by layered structure of homogeneous isotropic materials," *Optics Express*, vol. 15, no. 18, pp. 11133-11141, 2007.
- J5. Y. Chen, X. Teng, **Y. Huang**, and Y. Feng, "Loss and retardation effect on sub-wavelength imaging by compensated bilayer of anisotropic metamaterials," *Journal of Applied Physics*, vol.100, Dec. 2006.

Conference Presentations

- C1. **Y. Huang** and Jay K. Lee, "Analysis of a printed dipole antenna on a general anisotropic substrate with the method of moment employing eigenvector dyadic Green's functions", 31st URSI General Assembly and Scientific Symposium (31st URSI GASS), Beijing, China, August 16-23, 2014.
- C2. **Y. Huang** and Jay K. Lee, "symmetrical property of dyadic Green's functions for layered non-reciprocal medium", *IEEE International Symposium on Antenna and Propagation (APS/URSI)*, Orlando, Florida, USA, July 7-13, 2013.
- C3. **Y. Huang** and J. K. Lee, "Far field radiation from an arbitrarily oriented Hertzian dipole over layered gyroelectric medium", *IEEE International Symposium on Antenna and Propagation*, Spokane, WA, July 3-8, 2011.
- C4. **Y. Huang** and Jay K. Lee, "Dyadic Green's functions for general two-layer anisotropic geometry with source embedded inside the anisotropic layer," *IEEE International Symposium on Antenna and Propagation (APS/URSI)*, Toronto, Ontario, Canada, July 11-17, 2010.

- C5. **Y. Huang**, A. De, E. Arvas, and H. Partal, "Design of ultra-wideband (UWB) band-pass filter (BPF) satisfying the FCC Frequency Mask," *IEEE Workshop on Microwave Passive Circuits and Filters*, Syracuse, NY, April 20, 2010.
- C6. **Y. Huang**, A. De, and E. Arvas, "Novel design of a compact UWB bowtie antenna for GPR applications," presented at Graduate student poster competition, Syracuse University. This poster was selected as the best poster and won the grand award among all the Engineering Departments, held during the Nunan Research day on April 9th, 2010.
- C7. **Y. Huang**, A. De, and E. Arvas, "A novel design of ultra-wideband bowtie antenna for ground penetrating radar (GPR) applications," *25th International Review of Progress in Applied Computational Electromagnetics*, Monterey, CA, March 8-12, 2009.
- C8. **Y. Huang**, A. De, Y. Zhang, T. K. Sarkar, and J. Carlo, "Design of a low profile end-fire antenna using split-ring resonators," *IEEE International Symposium on Antenna and Propagation (APS/URSI)*, San Diego, CA, July 5-11, 2008.
- C9. Y. Feng, X. Xu, **Y. Huang**, and T. Jiang, "Optimization of the optical invisibility cloak constructed of concentric layered nanostructure," *Progress in Electromagnetics Research Symposium*, Hangzhou, China, March 24-28, 2008.
- C10. T. Jiang, **Y. Huang**, Y. Feng, "Sub-wavelength parallel plate resonator filled with bilayer of anisotropic metamaterials," *IEEE International Symposium on Antenna and Propagation (APS/URSI)*, Albuquerque, New Mexico, pp. 4531-4534, July 9-14, 2006.

Patents

- P1. Chong Mei and Ying Huang, A compact broadband impedance transformer, Application ID 13782279, 2013. (Pending)